A Controlled-Brake Orthosis for FES-Aided Gait

by

Michael Goldfarb

Submitted to the Department of Mechanical Engineering
in partial fulfillment of the requirements for the degree of

Doctor of Philosophy in Mechanical Engineering

at the

MASSACHUSETTS INSTITUTE OF TECHNOLOGY

May 1994

Author . . . .
Department of Mechanical Engineering
May 13, 1994

Certified by . . . .
William K. Durfee
Associate Professor
Thesis Supervisor

Accepted by . . . .
Ain A. Sonin
Chairman, Departmental Committee on Graduate Students

A Controlled-Brake Orthosis for FES-Aided Gait

by

Michael Goldfarb

Abstract

Functional electrical stimulation (FES) is a means of restoring gait to spinal cord injured (SCI) individuals. Two fundamental problems limit the ability of currently implemented FES-aided gait systems. The first is the rapid muscle fatigue that results from stimulated muscle contraction, and the second is the inadequate control of joint torques necessary to produce desired limb trajectories. Rapid muscle fatigue limits standing time and walking distance, and poor movement control results in non-repeatable steps. The controlled-brake orthosis (CBO) system was designed to address these limitations by utilizing FES in combination with a long-leg brace that contains controllable friction brakes at both knees and both hips. The system achieves desirable limb trajectories by utilizing the stimulated muscles as a source of coarsely regulated power and regulating the power at each joint by computer control of the friction brakes. The system also reduces the effect of muscle fatigue by locking the controllable brakes to provide the isometric joint torques necessary during stance. The CBO was evaluated and compared to conventional four channel FES-aided gait on a single T6 level paraplegic. Results show significant reduction in muscle fatigue and improvement in trajectory control when using the CBO.

Thesis Committee: Professor William K. Durfee
Professor Woodie C. Flowers
Professor Robert W. Mann
Professor Thomas A. McMahon

Thesis Supervisor: William K. Durfee
Title: Associate Professor

Acknowledgments

Many people helped make this thesis possible, and much of the credit for this work belongs to those both listed and unlisted who contributed their time, thought, and encouragement.

I have been very fortunate during the course of this thesis to have worked under the guidance of an excellent thesis committee. Professor Tom McMahon from Harvard University has provided many very interesting insights and intriguing ideas. I am very grateful for his participation.

Professor Robert Mann provided excellent advice and encouragement. I am grateful to Professor Mann for serving on my committee, and especially for creating the Newman Lab, in which I have conducted both my masters and doctoral research. Professor Mann is in many ways responsible for shaping the valuable graduate experience that I have had at MIT.

Professor Woodie Flowers has been a significant influence during my years at MIT. Woodie is an outstanding designer, a thoughtful intellect, an average actor, and a wonderful person.

Professor Neville Hogan was very generous with his time and was always willing to offer his keen insight and admirable breadth of knowledge.

I was very fortunate to work under the guidance and leadership of Professor Will Durfee. I hope to someday be as good an advisor and educator as Will has been to me and to many other students in the Department.

My fellow labmates have made my experience at MIT much more enjoyable and valuable than it otherwise would have been. Pat Lord, Justin Won, and Joe Doerringer provided deluxe computing facilities, many airport shuttles, good conversation, and most of all, friendship. Benji Sun, though a relatively recent addition to the lab, has been a good friend, too.

Zoher Karu, Elaine Chen, Jeff Chiou, and Heather Beck, collectively the FES group, provided wonderful company in which to work. There's not a research group at MIT that can parallel their culinary expertise.

Manuel Jaime, Aaron Barzalia, Peter Kassakian, Chin Chin Gan, and Angela Hsieh collectively contributed many hours of work.

Norm Berube, who can precisely remove metal faster than anyone I know, was instrumental in maintaining an aggressive project schedule.

Leslie Regan has made life at MIT immensely easier than it otherwise would have been. Leslie is always there when you need her and undoubtedly knows the answer to any question.

The clinical contigent of the research group at the VA hospital was very tolerant of the many bugs that we eventually worked out of the system. I am indebted to Kelli Keefe, who showed incredible courage and determination throughout the project. I could not have wished for a better person to work with. I hope that she and other people will eventually benefit from her effort and from this work. Nancy Walsh provided more expertise than she gives herself credit. Her involvement was vital to the entire project. Allen Wiegner was also instrumental in the development and especially in the testing and evaluation of the system.

My Grandma Bess has provided me with valuable opportunities that made this work possible, and has always been a role model for me and for all of her children and grandchildren.

My Grandma Ruth has always been a source of great encouragement. I am sorry that she is no longer here to read this.

My mother and father have always encouraged me to pursue my own interests and have constantly supported me in that pursuit.

Finally, I would like to thank Sally Eyles for being my best friend, an excellent nurse, and my lifelong companion.

Contents

Chapter 1

Introduction

There are currently about 250,000 spinal cord injured (SCI) individuals in the United States with roughly 7000 to 8000 new injuries sustained each year, about one half of which result in paraplegia [49, 73]. One of the major impairments resulting from paraplegia is the loss of mobility. The loss of lower limb function and the inability to walk or to stand significantly reduces a disabled individual's quality of life and carries with it severe psychological and physiological effects. Some of the documented physiological effects resulting from immobility include muscular atrophy, loss of bone mineral content, frequent skin breakdown problems, increased incidence of urinary tract infection, muscle spasticity, impaired lymphatic and vascular circulation, impaired digestive operation, and reduced respiratory and cardiovascular capacities [82, 87]. Partial restoration of gait, though by no means a panacea, has been shown to alleviate some of the effects resulting from immobility [4, 47, 74].

1.1 Restoring Gait to SCI

Considerable effort has been invested in the development of technology to restore gait to spinal cord injured persons. Several approaches to gait restoration have been established, including passive and powered orthoses, functional electrical stimulation (FES), and hybrid approaches which combine the two.

1.1.1 Passive Orthotics

Lower limb orthotics are one means of restoring gait to SCI individuals. These devices provide support at the ankle joint and utilize a locking mechanism to lock the knee joints during stance. Postural stability is provided by the upper body through the use of a stability aid, such as a walker or Canadian crutches. Hip flexion is typically driven by gravity with some help from the upper body. With a considerable energy contribution from the upper body, these devices can provide the user with a rudimentary form of gait.

The simplest form of passive orthotics are long-leg braces that incorporate an ankle-foot orthosis (AFO) to provide support at the ankle and ring locks to lock the knee joints. The hips are stabilized by arching the back so that the center of gravity of the torso falls posterior to the hip joints. In this position, called the C-posture, the torso is supported by the tension in the ligaments and musculature on the anterior aspect of the pelvis. Since almost all energy for movement is provided by the upper body, these orthoses require a high level of physical exertion and provide very slow walking speeds.

The Oswestry Parawalker provides a more effective orthosis design by incorporating hip joints that rigidly resist hip adduction and abduction, and a rigid shoe plate that provides increased center of gravity elevation at toe-off, thus enabling a greater degree of forward progression per stride [18, 60, 88, 95]. The Parawalker enables SCI individuals to walk short distances, is reasonably simple to use, and is also relatively easy to don and doff [103].

A reciprocating gait orthosis (RGO) is a passive device that incorporates a kinematic constraint that links hip flexion of one leg with hip extension of the other, typically by means of a push-pull cable assembly. As with other passive orthoses, the SCI individual leans forward against the stability aid, utilizing gravity to provide hip flexion. Since motion of the hip joints are reciprocally coupled, the gravity-induced hip flexion also provides contralateral hip extension, so that the stride length of gait is increased. Examples of this type of orthosis are the Louisiana State University RGO (LSURGO) [26] and the Steeper Advanced RGO (ARGO) [56]. In a compar-

12

ative trial, Whittle found that twelve of sixteen subjects preferred the LSURGO to the Oswestry Parawalker, though he cited cosmesis as one of the primary reasons.

Though mechanically locking the knee joints provides the knee stability necessary for stance, mechanical locks also mandate a stiff-legged gait that offers poor stability and typically requires lifting with the upper body to provide the swing leg with sufficient ground clearance, which requires a considerable amount of upper body energy expenditure [102]. The Vannini-Rizzoli Stabilizing Limb Orthosis (V-RSLO) incorporates a different approach to locking the knee joints for postural stability and stance phase. The V-RSLO is not a brace, but rather a high boot that incorporates a rigid ankle and an angled insole that tilts the SCI individual forward approximately 10–15 degrees so that his or her center of gravity falls anterior to the axis of knee flexion. This forces the knee joint into hyperextension, where it is stabilized against the posterior ligaments of the knee. As with the passive braces, stability of the trunk is provided by the C-posture, though the trunk can also be held up by pushing against a stability aid with the arms if necessary. The compact design of the V-RSLO however, compromises the effectiveness of the knee lock. Since locking the knee relies on the postural control of the SCI individual, occasional imbalance or a disturbance can move the center of gravity posterior to the axis of knee flexion, and thus place the individual in a highly unstable state that will likely result in a backwards fall. The dependence of the V-RSLO on the angle of the gravity vector with respect to ground also makes them unsuitable for ambulation on angled or uneven surfaces. Despite these drawbacks, clinical evaluations of the V-RSLO have shown that the orthosis successfully provides a means of ambulation for a select group of SCI individuals [50, 58].

1.1.2 Powered Orthotics

In order to decrease the high level of exertion associated with passive orthoses, some researchers have investigated the use of powered orthoses, which incorporate actuators to provide the torques necessary for gait. One of the first devices of this sort was developed by Vukobratovic [100]. This orthosis consists of a complete lower body

exoskeleton with shoe plates and bilateral uprights. Each leg of the exoskeleton incorporates three hydraulic cylinders which power flexion and extension of the ankle, knee, and hip joints, respectively. The resulting six degree-of-freedom hydraulically-actuated orthosis is massive, and relies on a similarly large umbilical for hydraulic supply.

Townsend constructed a "powered walking machine" which consists of a walker mounted on a wheeled platform [97]. The SCI individual stands on foot plates which are mounted to the platform on sliding tracks and are kinematically coupled to the drive wheel. An electric motor powers the drive wheel which simultaneously provides propulsion and drives reciprocal motion of the foot plates. Steering is provided by a separate electric motor and drive wheel. Though this device achieves a reciprocal gait of sorts, leg movement is a byproduct of motion, not the cause.

A more recent powered orthosis is the device being developed by Beard [11]. This orthosis incorporates a linkage that kinematically couples ipsilateral hip and knee motion, so that each leg exhibits only one independent degree of freedom. An electric motor operating through a large transmission ratio drives each leg to enable a reciprocating gait. The kinematic constraints imposed by the linkages reduce bipedal gait to two independent degrees freedom, and thus similarly reduce the orthosis actuator requirements to only two motors.

1.1.3   FES-Aided Gait

Another means of restoring mobility that has been given considerable attention is via the use of functional electrical stimulation (FES). FES utilizes electrical stimulation of peripheral motor nerves, using either skin surface or implanted electrodes, to elicit muscular contractions. FES actively involves the musculature of the lower as well as the upper body, and thus provides a means of total body exercise that has been shown to alleviate some of the physiological maladies resulting from immobility [37, 68, 75, 76, 87, 96, 99]. Because the FES system need only provide signal power to the muscles, external power requirements are modest. Like orthotic-based gait systems, FES-based systems do not provide postural stability, and must therefore be used with

14

a stability aid, such as a walker or Canadian crutches.

Several research groups have investigated various approaches to FES-aided gait. Their approaches can be divided into one of two categories: those that utilize skin surface electrodes for stimulation, and those that surgically implant electrodes into the muscle. One of the most active in the implanted category is the group led by Marsolais, who implants as many as 32 electrodes in each leg [61, 62, 63, 64]. Utilizing this system, some subjects have been able to achieve reciprocal gait speeds as high as 1.0 m/sec and can perform limited stair climbing function. Other research groups developing implanted FES-aided gait systems include those by Holle [40, 41] and Meadows [66].

The surface electrode approach to FES-aided gait is characterized by the protocol initially developed by Bajd and Kralj [5, 51, 52]. In contrast to the large number of electrodes utilized by Marsolais, the protocol of Bajd and Kralj incorporates only two channels of stimulation per leg. A quadricep channel is used to provide knee extension, and stimulation of the common peroneal nerve is utilized to elicit the flexion withdrawal reflex, which provides simultaneous hip and knee flexion. As with passive orthotic-based gait, hip stability is provided by the C-posture. The quadriceps and common peroneal stimulation channels are sometimes supplemented with a gluteal stimulation channel, which can provide additional stability to the hips and increase stride length by providing hip extension. FES-aided gait with surface electrodes is therefore provided with as few as four to six channels of stimulation. Variations and advances incorporating this flexion withdrawal reflex-based surface electrode protocol have been developed and evaluated by several other groups [25, 33, 34, 35, 45, 67, 77]. In 1990, Sigmedics Incorporated introduced the first (and currently only) flexion withdrawal reflex-based surface stimulation system to the commercial market [91]. The system, called Parastep, has undergone extensive clinical testing, and received approval of the United States Food and Drug Administration in early 1994.

Though both surface electrode and implanted electrode systems have been shown to provide an effective means of standing and walking for short distances, performance is limited by the rapid muscle fatigue that results from stimulated muscle contraction

and the inadequate control of joint torques necessary to produce desired limb trajectories. Muscle fatigue limits standing time and walking distance, and poor movement control results in non-repeatable steps.

1.1.4   Hybrid FES Systems

Several researchers have responded to the shortcomings of FES-aided gait by incorporating a hybrid-FES system that combines electrical stimulation with an orthotic device. Stallard incorporated FES with use of the Oswestry Parawalker [95]. Surface stimulation of the quadriceps was used to aid in standing, and stimulation of the gluteal group was utilized to aid in hip extension during gait. The addition of electrical stimulation was found to increase walking speed by an average of 33 percent and decrease oxygen cost by an average of 27 percent across subjects [6, 65, 72].

Petrofsky conducted a study comparing two hybrid systems, one incorporating a modified long-leg orthosis, and the other incorporating the LSURGO [78]. The long-leg orthosis was modified by adding joint position sensors for closed-loop control of muscle stimulation, and by incorporating computer-controlled servomotor actuated locks at each knee. The controllable knee locks were utilized to lock the knee joint to eliminate unnecessary muscle stimulation during standing. Instead of incorporating the flexion withdrawal reflex-based protocol of Bajd and Kralj, Petrofsky utilized ten channels of surface stimulation with the modified long-leg orthosis. The five channels utilized for each leg included the quadriceps for knee extension, hamstrings for knee flexion, gluteal group for hip extension, and simultaneous stimulation of the tensor fascia latae and the pectineus for hip flexion. This system was compared to an RGO-based hybrid system. The RGO was incorporated to reduce the complexity of gait by imposing kinematic constraints, provide a mounting platform for sensors that afford some degree of closed-loop control of the electrical stimulation, and help reduce fatigue by mechanically locking the knee joint and thus reducing the duty cycle of the stimulated muscle. The RGO-based system incorporated only six channels of stimulation: quadriceps, hamstrings, and gluteal groups for each leg. Since hip extension provides contralateral hip flexion with the RGO, hip flexion channels were

16

not necessary. Petrofsky found that the RGO provided better support and was less susceptible to muscular fatigue than the modified long-leg brace system. Although the long-leg brace offered the swing phase knee flexion of able-bodied gait, the weak hip flexors that are directly accessible with surface stimulation were quickly fatigued by the excessive weight and joint friction of the long-leg brace.

Solomonow also investigated the utility of combining surface stimulation with the LSURGO [93, 94] and showed that incorporation of the electrical stimulation reduced energy consumption [39]. Phillips demonstrated similar results in an RGO-based hybrid system [79, 80, 81].

Andrews developed a hybrid-FES system that incorporates the four stimulation channels of Kralj and a Floor Reaction Ankle-Foot Orthosis (FRO) [1, 2]. The FRO, which is a modified Knee-Ankle-Foot Orthosis (KAFO), provides rigid ankle support that tilts the SCI individual forward so that the knee joint is stabilized by hyperextension. The system utilizes strain gage sensors on the FRO to detect hyperextensive knee torque and stimulates the quadriceps muscles when the SCI individual's center of gravity falls posterior to the knee. This system was shown to reduce the duty cycle of quadricep stimulation to around 20 percent when standing, but showed only modest reductions of duty cycle during walking [2].

Others have developed orthoses with controllable knee joint locks. Chen designed a general purpose long-leg orthosis with solonoid actuated ring locks to lock and release the knee between stance and swing phase [20]. Jaeger utilized a long-leg orthosis with electrically-controlled knee joint locking in conjunction with quadricep stimulation to enable standing [46]. Schoenberg designed a lightweight orthosis for use with FES that also incorporates electrically-controlled knee joint locks [89].

Popovic has developed a system that combines electrical stimulation with a powered orthosis. The orthosis, called the Self-Fitting Modular Orthosis (SFMO), incorporates knee joints that are actuated with DC motors and can be locked with specially-designed drum brakes [54, 83, 84, 85, 86]. The system utilizes six channel flexion withdrawal reflex-based surface stimulation: quadriceps, peroneal, and gluteal channels for each leg. The DC motors are used to supplement knee flexion, while the

drum brakes lock the knee during stance to reduce excessive quadricep stimulation. Incorporation of the SFMO has enabled faster walking speeds for some subjects and has been used successfully on subjects that exhibit poor response to FES [84].

1.2   FES-Aided Gait in Perspective

Despite these efforts, the wheelchair remains the most prevalent form of SCI mobility. This is probably due to its proven reliability, energetic efficiency, and safety [19]. FES-aided gait technology of today is not intended to replace the wheelchair as a means of mobility. FES-aided gait does, however, provide many benefits that a wheelchair cannot. Among the greatest of these are the psychological benefits that result from the freedom to stand and walk short distances independently. Clinical studies have documented increases in morale, self-image, and self-esteem when using FES-aided gait systems [25, 99]. In addition to the psychological impact, several studies have indicated that FES-aided gait can provide important physiological benefits, such as retarding osteoporosis, reducing incidence of decubitus ulcers, improving cardiovascular health, aiding bowel and bladder function, and reducing the amount of spasticity in some individuals [4, 37, 47, 74, 75, 76, 87, 99]. In addition to offering psychological and physiological benefits, FES-aided gait enables upright bipedal locomotion, thus providing the SCI individual with the ability to interact with others eye-to-eye, and can enable access to rooms and places not easily gained by a wheelchair.

Chapter 2

FES-Aided Gait

2.1 The Physiology of FES

2.1.1 Able-Bodied Muscle Activation

The hardware that consitutes the human motor control system can be segmented into three parts: the central nervous system (CNS), the peripheral nervous system, and the musculoskeletal system. For purposes of muscle activation, the central nervous system functions principally as the controller, the peripheral nerves as the wiring, and the skeletal muscles as the actuators of the motor control system. The functional core of this control system is the motor unit, which consists of a single peripheral neuron that innervates multiple muscle fibers within the same muscle. Each muscle typically consists of hundreds or thousands of these motor units, each one independently controlled by the CNS through a single neuron. One reason that the CNS maintains such a large number of inputs into a single muscle is that the motor unit is a binary actuator, and is therefore either on or off. Since the muscle force output is the sum of the motor unit forces, the CNS can obtain proportional control of muscle force by activating a variable number of motor units.

The CNS actuates a motor unit by initiating a self-propagating voltage pulse, called an action potential, in a peripheral neuron. The action potential travels down the neuron and induces a "twitch" in the muscle fibers of the respective motor unit.

The twitch duration for a typical skeletal muscle is on the order of 200 ms. By sending several of these action potentials in close succession, the CNS can take advantage of the nonlinear characteristics of muscle activation to produce a fused contraction and thus obtain a constant and smooth muscle force.

2.1.2 Muscle Activation with FES

A spinal cord injury essentially severes the connection between the CNS and the peripheral system. Though all three components of the motor control hardware remain separately intact and alive, there are no means of relaying the action potentials necessary for movement from the CNS to the peripheral nerves. As illustrated in Figure 2-1, functional electrical stimulation takes advantage of the still operational peripheral neuromuscular system by artificially initiating action potentials in the peripheral nerves. An action potential is initiated by passing a current pulse through the nerve, using either skin surface or implanted electrodes, as described in the following sections.

Excitatory Properties of Nervous Tissue

The ability of nervous tissue to transmit an action potential is due to the presence of electrically charged ions and the capacity of the nerve cell membrane to control the flow of these ions between the intra- and extracellular fluids. The primary ions involved in nerve cell electrical dynamics are a sodium (Na^+) and potassium (K^+). The cell membrane contains active ion pumps that pump sodium out of the cell and potassium into the cell, creating high concentrations of extracellular sodium and intracellular potassium. These concentration gradients give rise to diffusion, which acts in opposition to the efforts of the pump. The nerve cell, however, can influence the rate of ion diffusion into and out of the cell by selectively altering the permeability of the membrane with voltage controlled ion gates. Under resting conditions, the nerve cell membrane is much more permeable to potassium than to sodium. Potassium is therefore permitted to diffuse across the cell membrane to the extracellular space, but sodium is prevented from diffusing in the opposite direction. The difference in
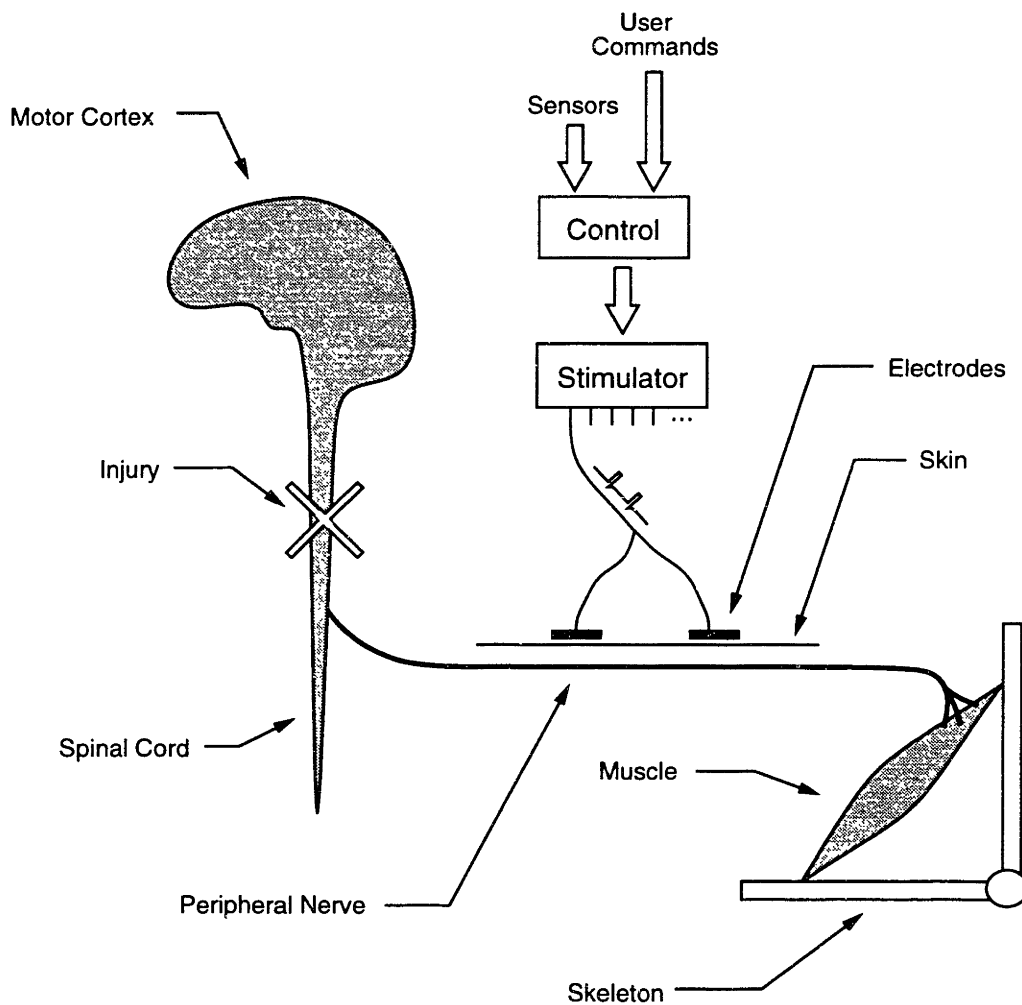
Figure 2-1: Schematic illustrating the basic concept of restoring function with functional electrical stimulation.
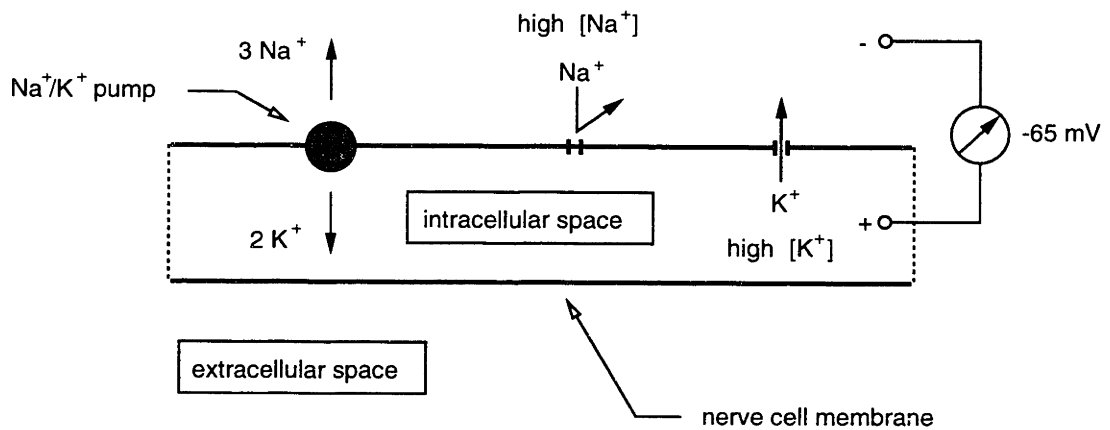
Figure 2-2: Schematic illustrating the mechanisms of active and passive sodium and potassium transport across nerve cell membranes. The resulting difference in ion concentrations inside and outside the cell creates a voltage potential across the resting membrane.

membrane permeability results in a larger number of positive ions outside the cell than inside, and thus creates a voltage difference across the resting membrane. This is illustrated in Figure 2-2.

The nerve cell membrane potential is defined as the intracellular voltage with respect to the extracellular voltage. The resting potential of the nerve cell membrane, which is typically at about -65 mV, can be altered primarily by either neurotransmitter release or the introduction of an external electrical current. Depolarizing the membrane potential opens the voltage controlled sodium ion gates and thus increases the cell membrane permeability to sodium ions, allowing some sodium to enter the cell. Further depolarization results in greater sodium permeability. When the membrane is depolarized to a threshold level of about -45 mV, the influx of sodium ions is large enough to contribute significantly to further depolarization, thus increasing the membrane permeability to sodium. This positive feedback loop continues until the membrane permeability to sodium is much greater than the permeability to potassium. Once the membrane potential reaches about +35 mV, the sodium channels suddenly shut off. The renewed impermeability to sodium, along with a temporary

increase in potassium permeability, enables the sodium/potassium pump and the diffusion of potassium to restore the cell to its original resting state. The voltage "pulse" that results from the sodium influx depolarizes the adjacent resting membrane, and continues to do so down the entire length of the axon. This self-propagating pulse, called an action potential, is the basis of neuromuscular signal transmission.

Initiating an Action Potential with FES

An action potential is triggered in a neuron when the cell membrane potential is depolarized to a threshold level. Figure 2-3 shows a simplified model of a nerve fiber and a schematic representation of the path of electrode current. As the current enters the nerve cell across the resistance and capacitance of the cell membrane, the charge differential is increased and the membrane potential is made more negative (hyperpolarization). As the current exits the nerve, however, the charges begin to balance out and the membrane potential is driven towards zero (depolarization). For this case, while the membrane potential is still above threshold, the potential is given by:

$$V_m(t) = V_{rest} + i(t)R(1 - e^{-t/RC}) \,, \tag{2.1}$$

where V_{rest} is defined as the membrane resting potential. An action potential is initiated when the membrane potential is depolarized to the threshold level, which occurs when:

$$i(t)R(1 - e^{-t/RC}) = V_{thresh} - V_{rest} \approx 20 \text{ mV} \,. \tag{2.2}$$

An action potential will therefore be elicited when the current pulse is of sufficient amplitude and duration to depolarize the membrane to the threshold level.

Motor Unit Recruitment

A typical peripheral nerve consists of hundreds to thousands of motor neurons. Motor units are recruited by electrical stimulation primarily as a function of two variables:
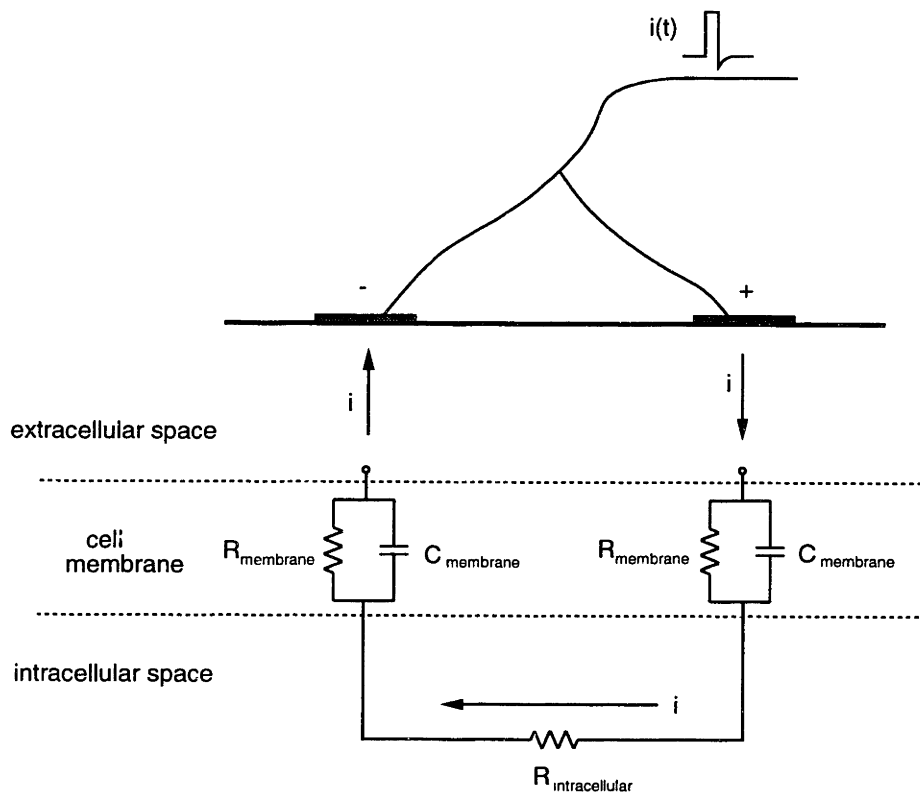
Figure 2-3: Diagram illustrating a simplified model of a nerve cell axon and a schematic representation of the path of electrode current.

the diameter of the nerve cell axon and the field strength of the stimulation current. As illustrated in Figure 2-3, the total resistance of the neuron path is

$$R_{neuron} = 2R_{membrane} + R_{intracellular} \cdot \tag{2.3}$$

The intracellular resistance can be modeled as

$$R_{intracellular} = \frac{\rho l}{A}, \tag{2.4}$$

where ρ is the resistivity of the intracellular fluid, l is approximately the length between electrodes, and A is the cross-sectional area of the nerve cell axon. Large diameter axons therefore have a smaller intracellular resistance than do smaller ones, and will therefore, under similar conditions, draw more current and reach threshold first [1].

Neuron recruitment is also influenced by electrical field strength. The field strength of the stimulation current decreases as the distance from the stimulation electrodes increases. The neurons that lie closest to the skin are therefore subjected to the strongest stimulation currents. Since cell membrane depolarization is a function of the current pulse duration and amplitude, a neuron that lies closest to the skin will reach threshold before a similar one that lies further away from the skin. These principals of motor unit recruitment are illustrated in Figure 2-4. Proportional forces are obtained by either increasing either the stimulation pulse width or pulse amplitude, which in turn uniformly increases the field energy, and subsequently excites a larger set of neurons, thus recruiting a larger number of motor units.

It should be noted that most peripheral nerves in the body are mixed nerves, i.e., they contain both sensory and motor components. Electrical stimulation therefore excites both the motor and sensory components of the nerve.

---

[1] Refer to [48] for a more thorough treatment of nerve cell axon models.

Current Pulse

Electrode

Skin Surface

section A-A
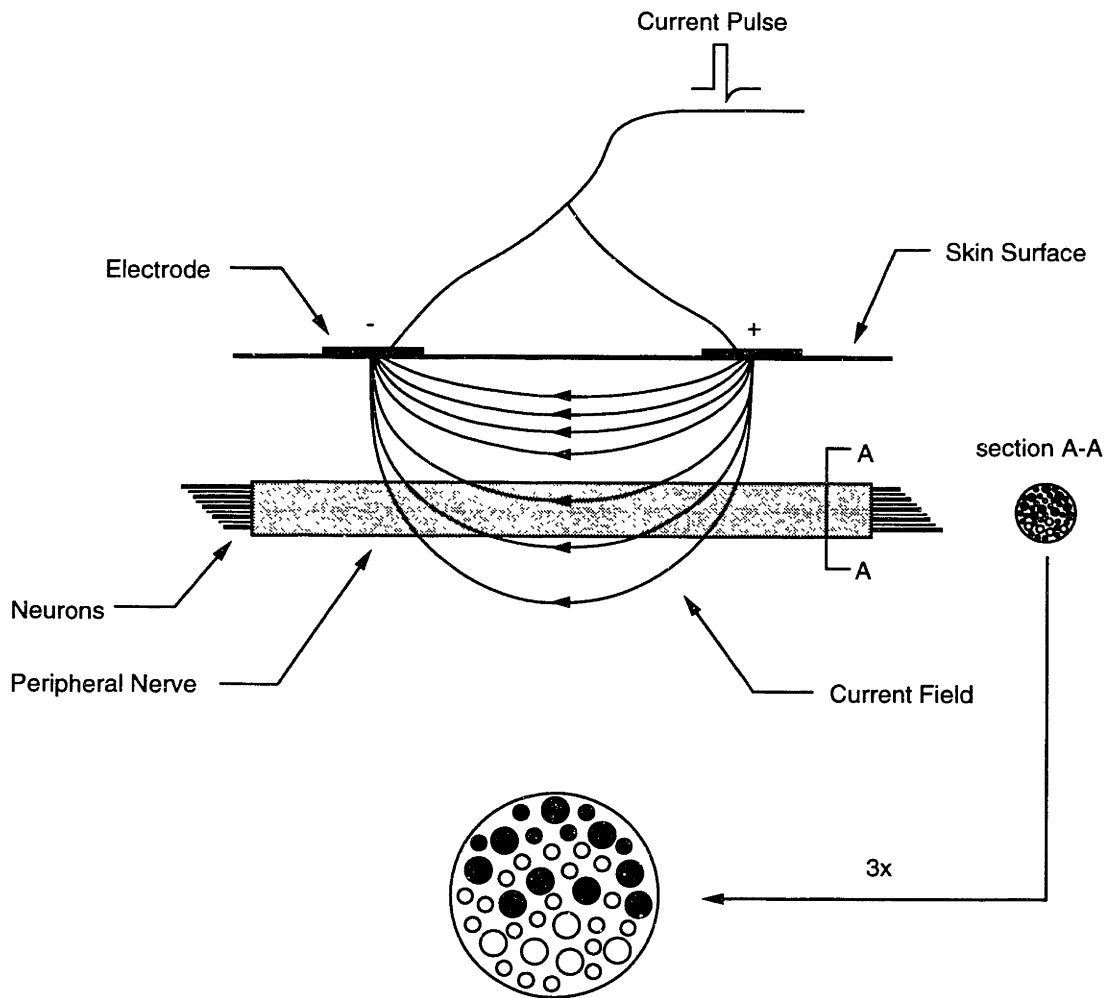
Neurons

Peripheral Nerve

Current Field

3x

Figure 2-4: Diagram illustrating the factors affecting the order of motor unit recruitment during functional electrical stimulation. In the enlarged cross section of the peripheral nerve, black axons indicate recruited motor units, white axons indicate those that have not yet reached threshold.

Electrodes

Electrodes for use in electrical stimulation can be classified as either implanted or non-implanted. Non-implanted electrodes are used on the surface of the skin. Surface electrodes are the least invasive, present little or no risk of infection or nerve damage, and can be used on a wide population of people. Surface electrodes, however, offer little muscular selectivity and do not enable stimulation of deep muscles.

Percutaneous electrodes are injected just under the skin. Wire leads from the injected electrodes emanate from the surface of the skin. These electrodes offer greater selectivity than do surface electrodes, but present a greater risk of infection and are susceptable to breakage.

Fully implanted electrodes offer even greater selectivity and the ability to stimulate muscles that lie deep in the body. Once implanted, these electrodes obviate the need for the careful maintenance of percutaneous electrodes and the frequency handling and application of surface electrodes. The major types of implanted electrodes, in order of increasing motor unit selectivity, are intramuscular, nerve cuff, intrafascicular, and very large scale integrated circuit (VLSI) types. Though the former two have been utilized in humans, the latter two remain in development stages. Implanted electrodes must be surgically inserted, require several electrodes to activate a large muscle mass, and present a higher risk of nerve or muscle damage than do surface electrodes.

The Stimulation Waveform

A typical electrical stimulation waveform, which consists of a series of short current pulses, is shown in Figure 2-5. Since the duty cycle of stimulation is typically about one percent, the average power dissipated in the body is quite low, typically not more than 1/10 watt. Each pulse is generated so that the net charge delivered to the body is zero, which corresponds to equal positive and negative areas in the current/time waveform, as shown in Figure 2-5. Neutralizing the net charge delivered to the body prevents charged electrolyte accumulation under the electrodes. The primary parameters determining the stimulation waveform are the stimulation amplitude, pulse width, and frequency. The stimulation amplitude and pulse width
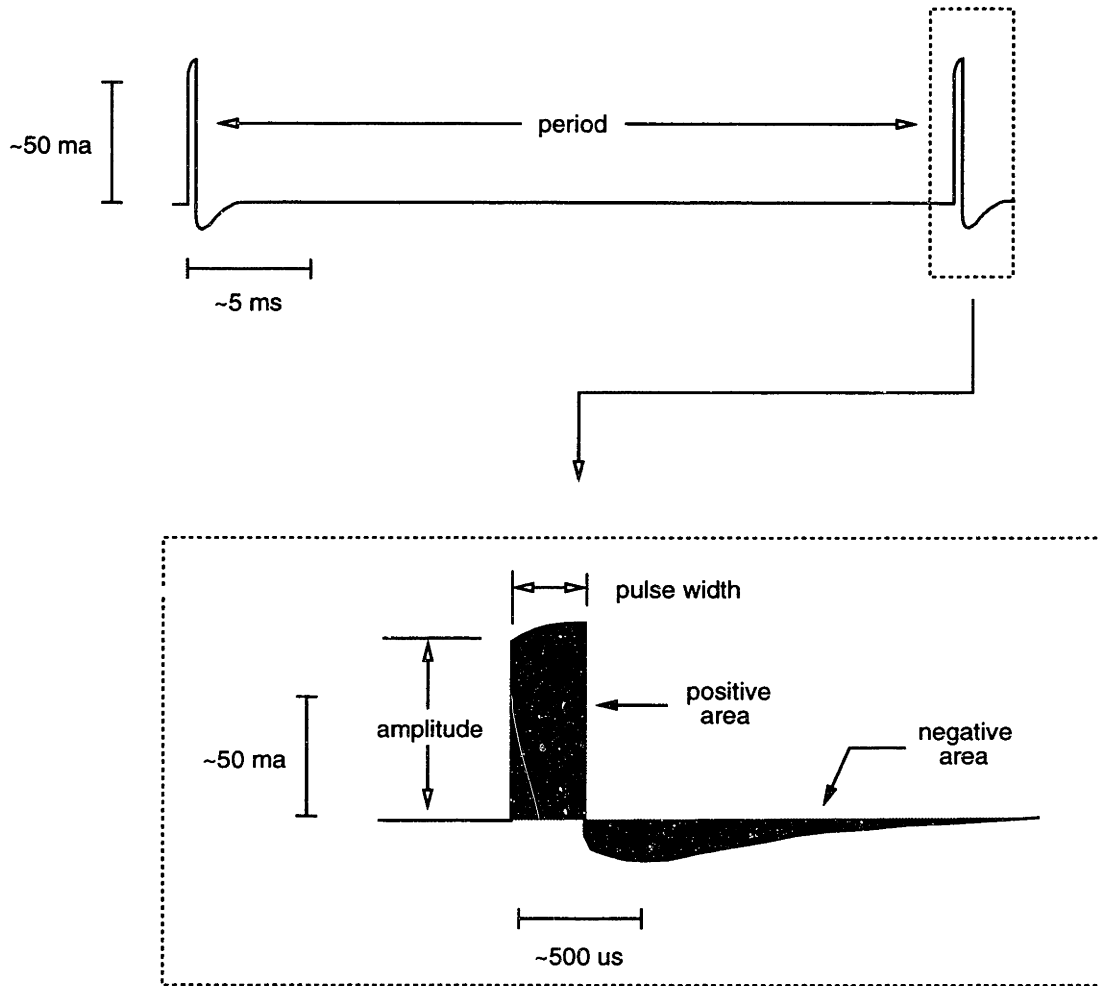
Figure 2-5: Diagram illustrating the stimulation waveform. The segment of the waveform enveloping the negative area results from the transformer-coupled output of the stimulator.

28

determine the energy of the current pulse delivered through the skin, thus determining the rate and duration at which the RC circuit that represents the neuron cell membrane is charged. If the combination is sufficent to depolarize the membrane to the level of threshold, the stimulus will elicit an action potential. Typical stimulation amplitudes range from 0 to approximately 100 milliamps, and typical stimulation pulse widths range from about 50 to 400 microseconds. The frequency of stimulation need only be high enough to provide a reasonably smooth muscle force output, which is typically at a rate of approximately 15–40 Hz.

2.2 FES-Aided Gait

2.2.1 FES-Aided vs. Able-Bodied Gait

FES-aided gait differs significantly from typical able-bodied gait. The able-bodied postural control system obtains information from several sensors and actuates control with sufficient bandwidth to reliably provide postural stability. FES gait systems do not have the sensors, the bandwidth, or the control performance necessary to reliably provide this function. FES-aided gait must therefore be conducted with a stability aid, such as a walker or a pair of Canadian crutches. Additionally, FES-aided gait does not exhibit the large angular accelerations or simultaneous multi-joint movement that characterizes typical able-bodied gait. Walking is instead generally conducted one step at a time, shifting from one double-support phase to the next.

2.2.2 Four Channel FES-Aided Gait

Four channel FES-aided gait, which utilizes a surface stimulation protocol that was originally developed by Kralj and Bajd in 1983, is the most common FES gait system. The four stimulation channels utilized in this protocol are the right and left quadriceps and the right and left peroneal. The quadriceps channels activate contraction of the quadriceps muscle group, which provides the knee extension torques necessary for gait. Hip flexion torques are more difficult to obtain with surface stimulation. Able-

bodied hip flexion torque is provided primarily by the iliacus and psoas major muscles (iliopsoas group), which lie deep in the body. Instead of stimulating the iliopsoas directly, the hip flexion torques, along with simultaneous knee flexion torques, are provided by eliciting the flexion withdrawal reflex via stimulation of the common peroneal nerve. The action potentials, which are initiated in afferent neurons, travel proximally to the spinal cord, where they synapse with interneurons which in turn transmit the efferent action potentials that induce hip and knee flexion.

The sequence of stimulation utilized in four channel FES-aided gait is illustrated in Figure 2-6. The system is run in an open-loop fashion. Since it does not attempt proportional control of muscle force, a given stimulation channel is either completely on or completely off. Standing and the double support phase of gait are sustained by stimulating both quadriceps channels, thereby locking the knees at full extension. The hip joints are stabilized by pushing the hips forward so that the center of gravity of the trunk is located behind the hip joints. In this position, called the C-posture, the hips are stabilized by the tension in the anterior hip ligaments. To take a step, the SCI individual incorporates upper body effort to shift his or her weight to the stance leg. A step then is initiated by turning off the quadricep stimulation, and after a short delay, stimulating the peroneal channel to elicit the flexion withdrawal reflex. The peroneal stimulation is maintained long enough to allow sufficient hip and knee flexion, at which point the quadricep stimulation is again turned on, extending the knee and once again bringing the individual to the double support phase, so that he or she can take a step with the contralateral leg. A typical time scale for a stimulation sequence is illustrated in Figure 2-7.

A sit-to-stand manuever is achieved by ramping the quadriceps muscles up from threshold to a maximum level. Since surface stimulation of the quadriceps cannot by itself provide enough knee torque for the sit-to-stand manuever, it must be supplemented by the upper body and use of a stability aid. Sitting is accomplished by ramping the quadricep stimulation down, and is again aided by work from the arms.

A typical stimulation waveform for the quadriceps channels consists of current pulses with an amplitude of approximately 80 milliamps and a pulse width of about
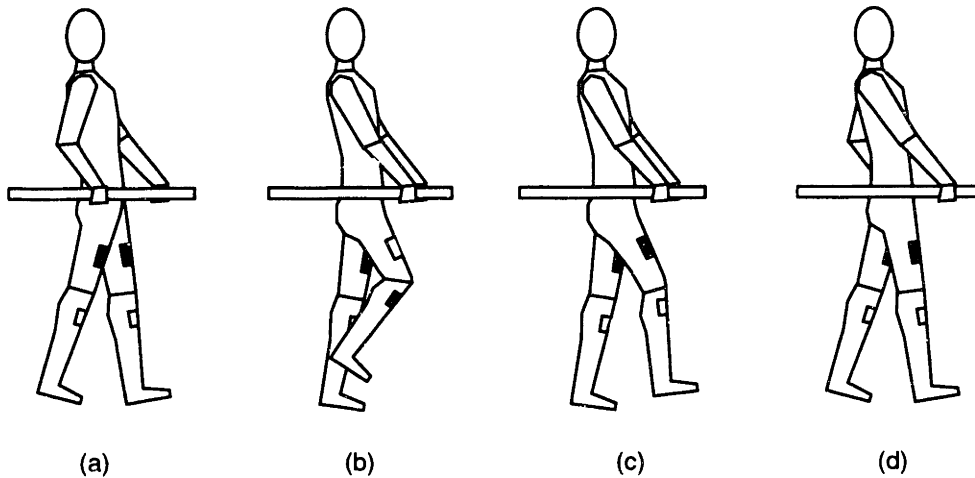
Figure 2-6: Diagram illustrating the sequence of stimulation during four channel FES-aided gait.

300 microseconds, delivered at a freqency of around 25 Hz. Current pulses for the peroneal channels have a typical amplitude of approximately 60 milliamps and a typical pulse width of about 350 microseconds and are delivered at a frequency of around 50 Hz. A larger muscle force is typically obtained by increasing stimulation amplitude (though increasing pulse width would work as well).

2.2.3   Problems with Four Channel Gait

Although the four channel FES protocol has been successful for a select population of SCI individuals [5, 25, 35, 45, 51, 67, 77], two major difficulties limit its ability to restore gait. The first is the rapid muscle fatigue that results from stimulated muscle contractions, and the second is the inadequate control of joint torques necessary to produce desired limb trajectories. Rapid muscle fatigue limits the standing time and walking distance of the SCI individual, and poor movement control results in non-repeatable steps.

Quadricep Stimulation

steady state
amplitude~80 ma

sub-threshold
amplitude~20 ma

quad off time~1000 ms

quad ramp
up interval ~100 ms

Peroneal Stimulation

peroneal burst
amplitude~60 ma

reflex start
time~250 ms

reflex duration~750 ms

*start
swing*
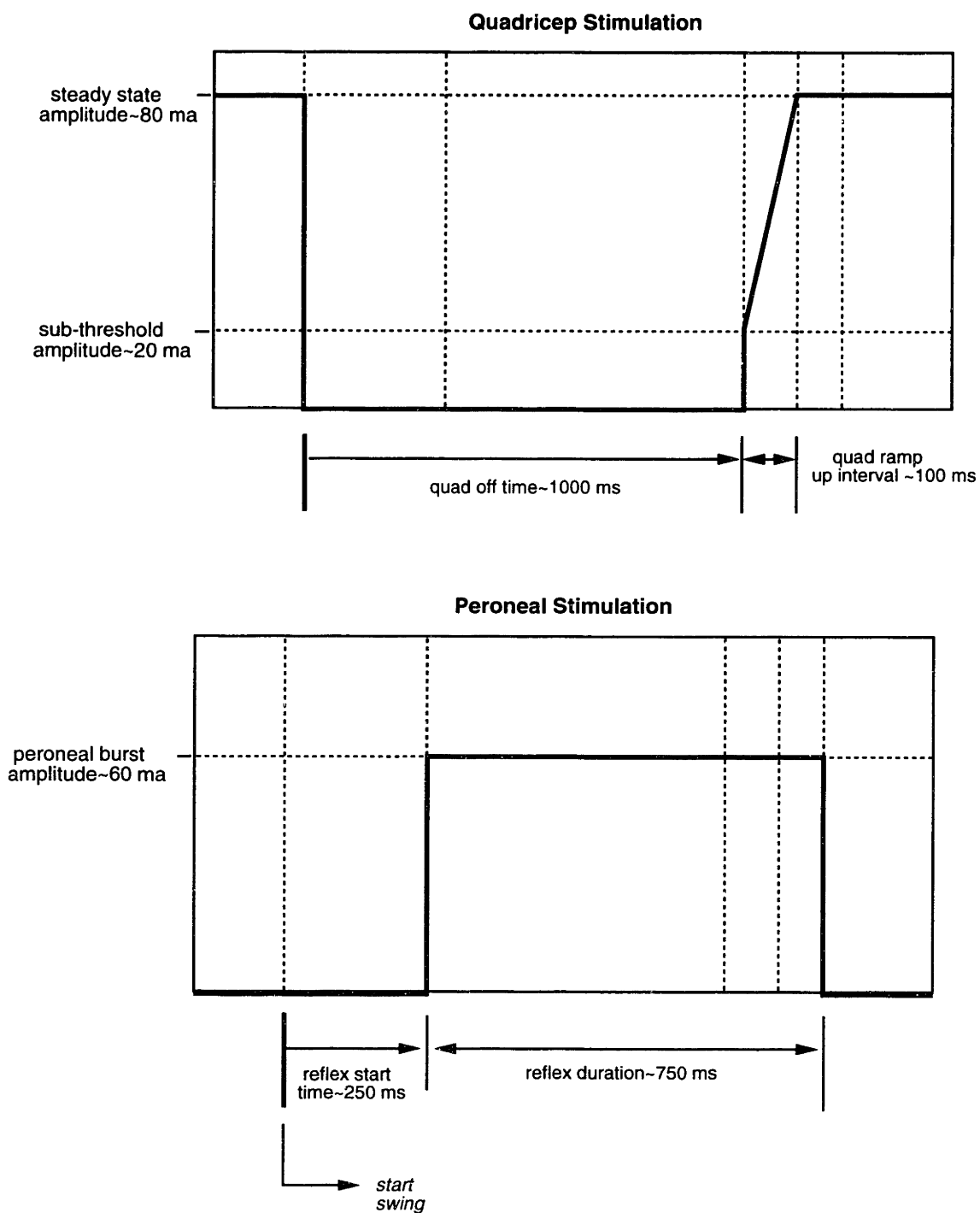
Figure 2-7: Diagrams representing the envelope of stimulation pulse amplitude as a function of time during a single swing phase of four channel FES-aided gait.

Muscular Fatigue

Muscle fatigue is manifested as the decrease in gain between muscle activation input and muscle force output. Muscles fatigue much faster with FES than when activated by the central nervous system, primarily due to the relatively high stimulation frequencies required for fused contractions, and the preference of electrical stimulation for exciting fast, fatigable muscle fibers.

The central nervous system utilizes two major strategies to increase muscular efficacy and delay the onset of muscular fatigue. The first is asynchronous recruitment of motor units, and the second is selective recruitment of motor unit fiber type. Since a muscle typically consists of a large number of motor units, the CNS can alternately recruit some units to provide the necessary force while allowing others to rest, cycling through the motor units in an asynchronous fashion. Asynchronous recruitment decreases the duty cycle of activation of each fiber. Since muscle fatigue is a highly non-linear function of duty cycle [14], a small amount of additional rest can significantly delay the onset of muscular fatigue.

In addition to asynchronous recruitment, the CNS further delays fatigue by efficient recruitment of motor unit fiber type. Each skeletal muscle consists of a mixture of muscle fibers that can be generally classified as either Type I or Type II. Type I fibers are less powerful and slower, but more fatigue-resistant than Type II fibers, which are generally fast and powerful, but fatigue quickly. A single motor unit consists of only one fiber type, and is thus either a fast, fatigable motor unit or a slow, fatigue-resistant one. The neurons innervating the fast muscle fibers have large diameter axons (for increased conduction velocity), while the axons innervating the slow fibers are of a smaller diameter. When activating a prolonged muscle force, the CNS will initially recruit slow, fatigue resistant motor units, eventually recruiting the faster units only to supplement the effort of the slow ones.

Though FES can obtain proportional forces by recruiting a variable number of motor units, it does not have the independent control of individual motor units that the CNS has. Motor units must therefore be recruited in a synchronous fashion, resulting in continuous fiber excitation at the duty cycle of stimulation, which in

turn results in a rapid rate of muscle fatigue. Fatigue due to synchronous motor unit recruitment is further exacerbated by the "inverse recruitment" behavior exhibited by FES. As described previously, electrical stimulation shows a preference for large diameter (lower resistance) axons, which in turn innervates fast, fatigable muscle fibers. FES therefore recruits motor units in a fashion opposite to that of the CNS, recruiting all the fatigue resistant fibers only at maximum levels of stimulation.

Muscle fatigue is a particularly dangerous problem in FES-aided gait. Stabilizing the hips with a C-posture generally places the center of mass of the trunk behind the knees, making them completely unstable in the absence of muscle contraction. The SCI subject therefore relies on the force produced by the quadriceps muscles to prevent the knee from buckling. Since FES-aided gait consists mostly of shifting between double support phases, the quadriceps are typically stimulated about eighty to ninety percent of the time. Deterioration of the quadriceps' ability to produce force due to the nearly continuous duty cycle required by FES-aided gait results in collapse of the individual, which is potentially hazardous. The problem is worsened by the lack of any ostensible warning indicating a state of severe muscle fatigue and imminent collapse [2].

Step Trajectory Control

Inadequate control of step trajectories with FES is due in part to the absence of a model that adequately describes the highly nonlinear and time-varying relationships between electrical stimulation input and muscle force output, and in part to the inability to measure the muscle output directly. Despite efforts by several researchers [7, 9, 10, 15, 22, 23, 24, 28, 42, 90, 106], there are no muscle models that adequately describe the highly nonlinear and time-varying relationships between electrical stimulation input and muscle force output. Attempts at system identification are severely hindered by the rapid and constant time-variation of muscle. Robust non-linear methods such as sliding-mode or adaptive-sliding mode control work well on reasonably unknown systems, but in general require powerful actuators and measurement of sys-

---

[2]Some research on this topic includes the work of [8, 17, 21, 29, 30, 31, 36].

tem output or states. Non-invasive FES systems, however, do not have access to direct measurement of muscle force or other muscle states. The control problem is compounded by poor muscular selectivity from stimulation electrodes and limited muscular bandwidth and power output.

2.3 Addressing the Problems of Four Channel Gait

The controlled-brake orthosis system addresses the limitations of FES-aided gait by utilizing FES in combination with a controllable passive orthosis. The controlled-brake orthosis (CBO) is a long-leg brace that contains controllable friction brakes at the knees and hips. During stance, the system reduces the effect of quadricep fatigue by locking the controllable brakes to provide the isometric torques necessary for knee stability. In this manner, the quadriceps are utilized only to provide knee extension during swing, thus reducing the duty cycle of stimulation and diminishing the problem of muscle fatigue. Since the brace provides knee stability, the CBO system eliminates all possibility of collapse due to fatigue, and thus provides SCI individuals with a much safer and more reliable gait system. Though the CBO provides the requisite isometric joint torques for stance, it relies on the skeleton to support axial loads, so that the orthosis need not be designed to withstand large compressive loads and the skeleton still derives the physiological benefits of weight bearing.

In addition to eliminating the problem of collapse due to fatigue, the CBO system also improves step control by utilizing the stimulated muscles as a source of coarsely regulated power and by regulating the power at each joint through computer control of the friction brakes. This approach to motion control builds upon work previously conducted by Durfee and Hausdorff [27, 38]. In contrast to uncontrolled passive orthoses, the CBO therefore enables direct dynamic control of the limb trajectories including the swing phase knee flexion that is characteristic of able-bodied gait. Unlike the actuators of a fully powered orthosis, the controlled brakes of the CBO are small, lightweight and energy efficient. Thus, a self-contained commercially-viable CBO is considerably more practical than a fully powered orthosis.

Chapter 3

Design of the Controlled-Brake Orthosis

3.1 Design Requirements

The present version of the orthosis was designed as a research tool. General design considerations included ensuring safety, providing comfort, minimizing bulk, and providing sufficient adjustability to fit a wide variety of body sizes. There are many important product-oriented design issues that have not been and will not be addressed until laboratory evaluation of the CBO system warrants product development. Some of these product-oriented issues include development in a self-contained battery-powered form, ease of donning and doffing, and cosmesis.

3.1.1 Gait Kinematics

The CBO should accommodate eight skeletal degrees of freedom, as illustrated in Figure 3-1. These are flexion and extension of the hip, knee, and ankle joints, which are necessary for forward progression, and the abduction and adduction of the hip joints, necessary in order to achieve static equilibrium in the frontal plane when in single stance phase. Additionally, implementing an adjustable limit stop on hip adduction will prevent the crossing of one leg in front of the other (scissoring) that
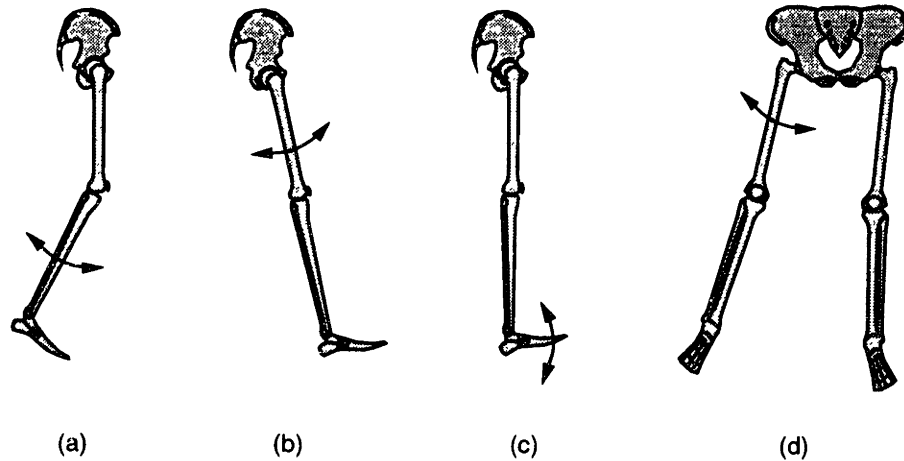
Figure 3-1: The CBO enables eight skeletal degrees of freedom (four for each leg). These are the flexion and extension of the hip, knee, and ankle joints (a, b, and c, respectively), and the abduction and adduction of the hip joints (d). The former three are necessary to enable forward progression during gait, the latter, to enable static equilibrium in the frontal plane in single support phase.

often occurs during FES-aided gait.

3.1.2   CBO Joint Kinematics

It is well known that the flexion and extension of the human knee joint consists not only of sagittal plane rotation, but sagittal plane sliding and horizontal plane rotation as well [69, 70]. Though reasonably effective polycentric joint designs have been developed to accommodate these additional components of knee motion [43, 44, 53, 98], accommodation in the CBO significantly complicates the objective of imposing controllable dissipation at the joint. In addition to necessitating stringent alignment with the anatomical joint, polycentric joints have several degrees of freedom which complicate the sensing of joint position and torque required for control. Since a revolute joint is a reasonably good approximation of knee motion [53, 55, 92], the knee joints were designed as simple revolute joints. Constructing the knees as revolute joints not only simplifies control, but also reduces the size, weight, and cost of each joint.

The human hip is well approximated as a ball-and-socket joint [57]. Hip flexion and extension can therefore be accommodated with a simple revolute joint. As in the knee joint of the orthosis, this results in a design that is well characterized and controlled with simple measurements. Hip ab- and adduction are also well characterized by a revolute joint. The axis of rotation, however, must pass through the hip, which is located internal to the pelvis. Since the hip joint of the orthosis is positioned on the lateral aspect of the pelvis, positioning a revolute joint "through" the hip would require a large gimbled joint, which would be both heavy and cumbersome. This difficulty is most easily addressed by locating a multiple degree of freedom linkage off-axis that allows skeletal hip ab- and adduction. Since the joint is not controlled and thus need not impose controlled external torques nor be dynamically characterized, a multiple degree of freedom solution does not significantly complicate the orthosis, and in fact, provides a more compact design. This linkage must be capable of withstanding the sagittal plane loads imposed by the flexion/extension hip and knee joints, while still providing for unimpaired hip ab- and adduction.

3.1.3   Joint Range of Motion

The range of motion for the joints was selected to accommodate normal gait and comfortable sitting. The hip joint should allow for 105 degrees of flexion and 25 degrees of extension. In the frontal plane, the orthosis should accommodate 15 degrees of hip abduction and 5 degrees of adduction, with an adjustable adduction lock to prevent scissoring. The knee joint should allow for 105 degrees of flexion and 0 degrees of extension.

3.1.4   Maximum Joint Torques

The brace must be capable of exerting controllable resistive torques on the flexion and extension degrees of freedom of the hip and knee joints. The ankle plantar- and dorsiflexion degrees of freedom should not be unrestricted, but rather should impose a stiffness sufficient to prevent foot drop during the swing phase of gait, yet compliant

enough to allow dorsiflexion during the stance phase. Since very little data exists regarding the mechanics of hybrid FES-aided gait, many of the design specifications for the CBO were established using model-based estimates. An important role of the completed laboratory-based orthosis is to help establish more specific, empirically-based design requirements for a consumer version.

Maximum joint torque specifications for the orthosis prototype were derived based on three desired capabilities. The orthosis should (1) be able to provide the dissipative torques observed in normal gait, (2) be capable of locking a joint against a stimulated muscle contraction, and (3) implement a controlled stand-to-sit maneuver without the aid of muscle activation. Calculations and existing data based on average-sized persons indicated that 50 Nm (450 in-lbs) of knee torque and 30 Nm (270 in-lbs) of hip torque would provide these capabilities For details of these calculations, refer Appendix D.

3.1.5   Minimizing Parasitic Losses

Since stimulated muscles have significant power and energy limitations, and because the brace is assisting rather than replacing existing limbs, minimizing orthosis weight, rotational inertia, and residual friction are paramount. Unlike an actively powered device, the added joint rotational inertia and residual friction of the brace cannot be negated by torque feedback from the actuators. Any increase in limb weight or rotational inertia, or any added joint friction, requires more muscle force for a given acceleration and more energy for a given motion. Intelligent distribution of the orthosis mass can minimize the effects of this added weight and inertia. For example, since the pelvis is not subjected to significant accelerations or to large vertical displacements, it is advantageous to locate as much of the orthosis weight as possible above the hip joint.
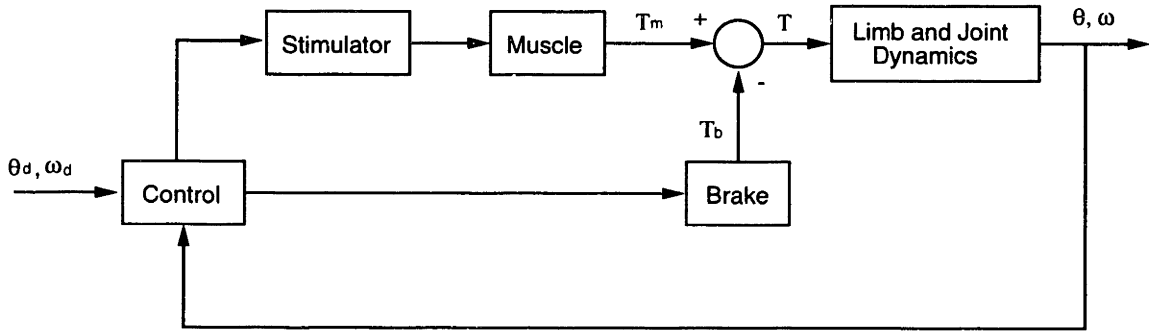
Figure 3-2: CBO system control strategy. During swing phase, the muscle is activated at a fixed stimulation level while the brake is modulated to control motion. During stance phase, the brakes are locked and stimulation is turned off. The controller adjusts the fixed stimulation level to compensate for muscle fatigue.

3.1.6 Design for Control

One of the primary functions of the controlled-brake orthosis is to improve the trajectory control of the lower limbs during gait. The CBO system circumvents the inadequacies of FES control by utilizing stimulated muscle as a source of unregulated power and regulating the motion of each joint by control of the modulated dissipators on the brace. An understanding of this approach to control is essential for establishing a viable orthosis design.

Figure 3-2 is a block diagram depicting the modulated dissipation control strategy for one degree of freedom (i.e., a single joint). The controller modulates the behavior of the dissipator based upon the joint angle and angular velocity in order to regulate the motion of the joint. Given that the muscle torque is large enough to provide the desired angular accelerations and that the brake has no significant power limitations, this strategy would provide an effective means of controlling limb motion. The controller performance is significantly influenced by the muscle torque level and by two important aspects of orthosis design. The first is the rigidity of the coupling between the brace joint and the skeletal joint; the second, the bandwidth of the modulated dissipator. A poor coupling or a slow dissipator will introduce dynamics into the feedback loop that will restrict the controller bandwidth and limit

41
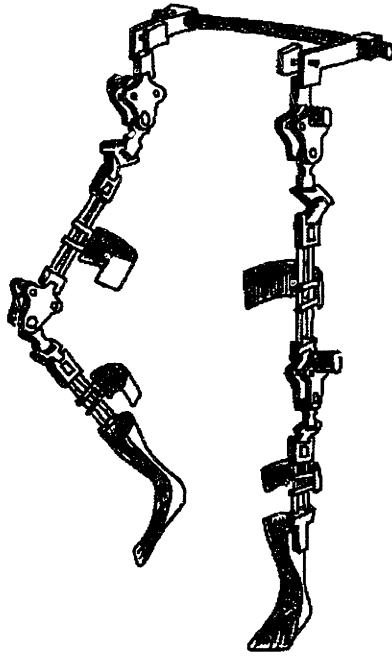
Figure 3-3: Illustration depicting the controlled-brake orthosis.

system performance.

3.2   Design Description

The completed CBO is depicted in the illustration of Figures 3-3, and shown in the photographs of Figures 3-4 and 3-5. The total orthosis weight configured for an averaged sized person is 6 kg (13 lbs). Over one half of the orthosis weight is located on the pelvis, and thus does not add significantly to the rotational inertia or gravitational loads of the lower limbs. The rotational inertia of the distal link of the orthosis about the knee joint is about 5 percent of a typical shank inertia, while the inertia of the proximal link about the hip joint is about 10 percent of a typical thigh inertia.

Figure 3-4: The CBO shown from the side as worn by an able-bodied subject.
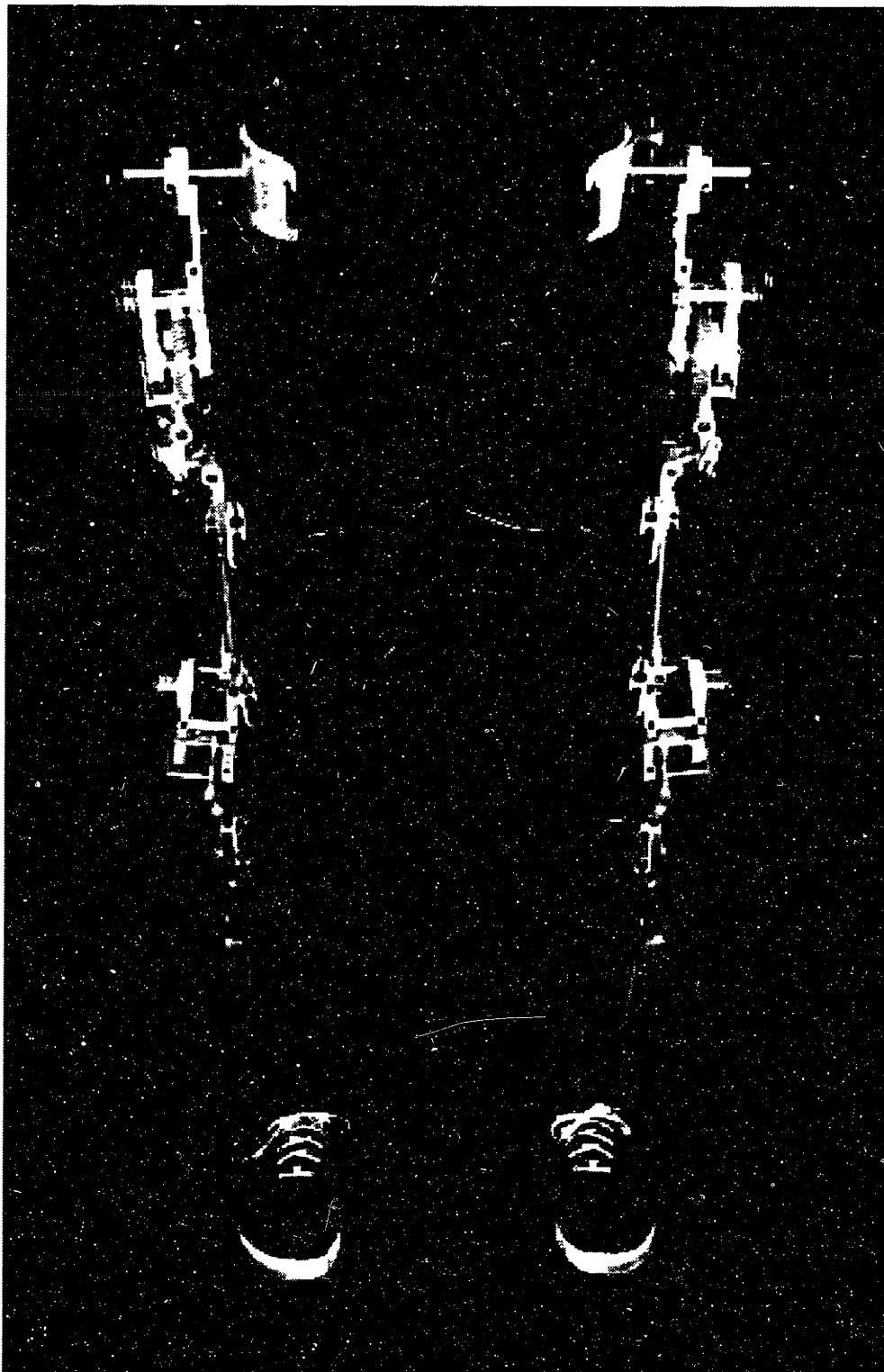
Figure 3-5: The CBO shown from the front as worn by an able-bodied subject.

3.2.1 Structure

The orthosis structure consists primarily of 2024-T3 aluminum alloy and 4130 chromium-molybdenum (chromoly) steel alloy, both chosen for their high strength-to-weight ratios. The aluminum alloy was utilized where a higher strength-to-weight was most important, the steel alloy where greater strength-to-size was desired. The two alloys have roughly equal stiffness-to-weight ratios.

The orthosis utilizes unilateral uprights. Bilateral uprights can obstruct gait by adding bulk to the medial aspect of the legs. Since the joint torques are applied only to the lateral upright, bilateral uprights also do not offer any significant stiffness benefits. The brace links, which extend the length of each limb segment and connect the orthosis joints, were designed as tubular I-beams. This configuration maximizes the orthosis stiffness and strength in the sagittal plane, where most of the major bending stresses are generated. The I-beams are constructed of 4130 steel tubes, which were chosen over carbon fiber tubes for purposes of safety, since the chromoly exhibits ductile failure, while the carbon fiber exhibits brittle failure. The hollow tubes of the beams conveniently function as electrical conduits for the routing of wires between joints. The orthosis design allows for small variations in the size of subject limbs. Larger variations in limb size are accommodated by interchanging the links, which enables fitting the brace to a wide range of male and female subjects.

3.2.2 Attachment Points

Applying controlled resistive torques to the musculoskeletal system requires a rigid coupling between the CBO and the lower limb segments. The CBO applies resistive joint torques to the lateral side of the limb only. As illustrated in Figure 3-6, this configuration exhibits a moment arm between the plane in which skeletal torques are applied and the plane of CBO joint torques. Brake torques acting across this moment arm subject the CBO to structural deformation, and any lateral compliance in the brace/body attachment results in the brace's twisting around the leg. The structural deformation is reduced by minimizing the forces acting on the attachments

and by making these attachments as rigid as possible. Since the CBO joint torques are transmitted to the limb segments through the attachment points by force couples, the forces transmitted are decreased by increasing the spacing between these points. Maximizing this spacing therefore decreases the structural deformation of the CBO, effectively creating a more rigid coupling between the brace and body.

Given these considerations, the orthosis is attached to each leg segment with stiff cuffs located at the proximal and distal ends of the respective segments. Velcro straps are used to tighten the leg against the cuffs. The orthosis is attached to the distal end of each shank by a conventional polyethylene ankle-foot orthosis (AFO), which is worn inside a subject's normal footwear. Coupling the orthosis to the pelvis is more difficult. The only viable option for a reasonably rigid attachment to the pelvis is to "c-clamp" onto the iliac crests, since all other parts of the pelvis lie deep within the body. This attachment is augmented by Velcro straps. The brace/body attachment points are shown schematically in the diagram of Figure 3-6, and on the orthosis in the photograph of Figure 3-7.

3.2.3 Controllable Dissipators

Selection of the dissipator is of great importance in the design of the orthosis. Considerations for selection of the dissipator include maximizing peak holding torque and bandwidth and minimizing weight and residual friction. Since the future commercial version of the CBO will be battery-powered, an additional design criteria is to minimize the electrical power consumption. The controllable dissipators considered for use in the CBO application included hydraulic cylinder-based fluid circuits, DC servomotors, and magnetic particle brakes.

A diagram of a hydraulic cylinder-based circuit is shown in Figure 3-8. A hydraulic system would offer the great advantage of supporting static loads without any electrical power consumption. Electrical power must be used to turn the flow valve off, but once off, no additional power would be necessary to support a static load. Such a system however provides a host of design and implementation difficulties. The specified maximum joint torque and range of motion requirements translate

46
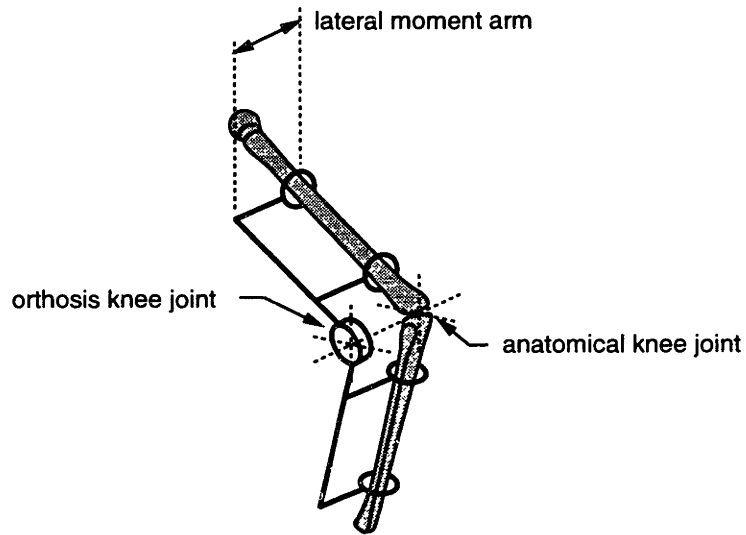
(a)
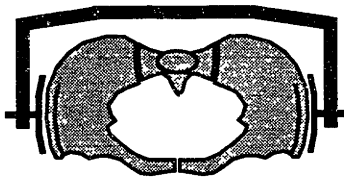
(b)

Figure 3-6: CBO attachment to (a) long bones and (b) pelvis. The moment arm between the orthosis knee joint and the anatomical knee joint subjects the CBO to structural deformation when brake torques are applied. Any lateral compliance in the brace/body attachment results in the brace's twisting around the leg.
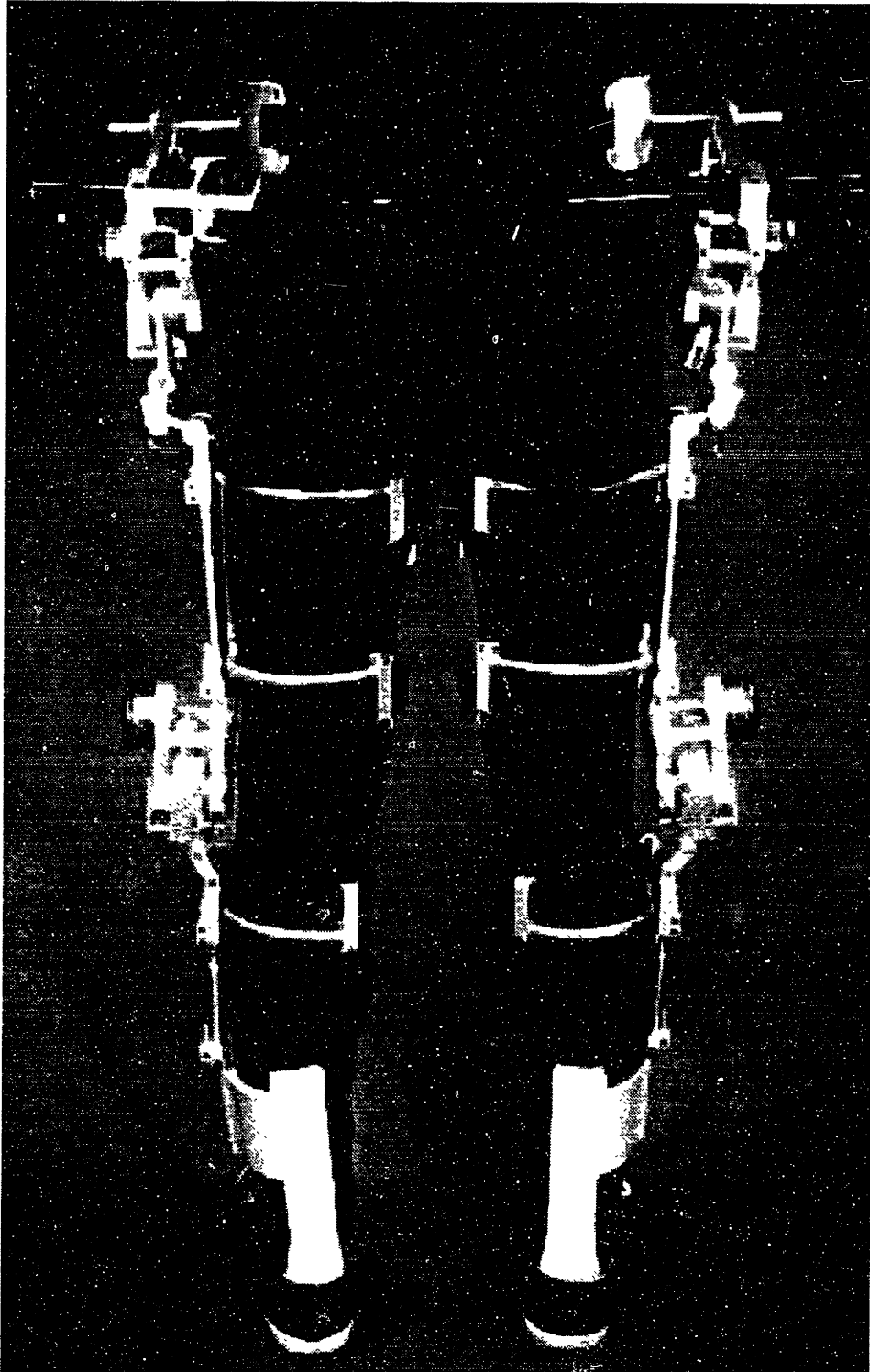
Figure 3-7: Photograph of the CBO from the back showing the brace/body attachment points, including the AFO, the rigid cuffs which wrap around the posterior surface of the leg, and the pelvis clamp.

into specifications for hydraulic cylinder piston travel, piston diameter, and maximum pressure, which result in large, relatively heavy hydraulic cylinders. Since the fluid is incompressible (the fluid must be incompressible to provide the necessary output stiffness), the cylinder must be of the double rod type, which requires a linear space almost three times the length of the body of the cylinder (the cylinder in Figure 3-8 is shown as a single rod cylinder for purposes of diagramatic simplicity). The fixed-volume problem can be addressed with a reservoir system, but incorporation of such a system without a large reduction in system output stiffness is a difficult design problem. Additionally, closed-circuit hydraulic systems are susceptible to air entrainment which results in a significant decrease in output stiffness. Hydraulic cylinders also exhibit considerable stiction due to the high pressure fluid seals around the piston and piston rods. Motion of the hydraulic fluid through the circuit imposes additional friction and inertia, both of which may be increased significantly by the rotary-to-linear transmission, since the inertia and friction of the hydraulic system will be multiplied by the square of the transmission ratio when reflected to the joint space. Another significant problem in designing a hydraulic system is the design of a small electrically-controlled proportional hydraulic valve. Such a valve must have a large bandwidth as well as the ability to operate while subject to the forces imposed by high pressure fluid. The combination of these capabilities favor the use of a high-powered servovalve, which is, in general, a device of considerable size and weight. Additionally, since the fluid is incompressible, the valve cannot introduce volume into the system, which excludes the use of needle valves and other similar types of proportional flow valves. Hydraulic systems also complicate the control problem, since the applied joint torque would not be independently controllable, but rather would be a function of the joint velocity. Imposing a constant resistive torque at the joint would therefore necessitate measurement of joint velocity or torque and appropriate real-time adjustment of the electrically-controlled proportional valve.

Direct current motors offer the advantage of straightforward control of joint torque, sufficient bandwidth, and the ability to add power to the system, if desired. The relatively low holding torque-to-weight ratio of these devices, however, would necessitate
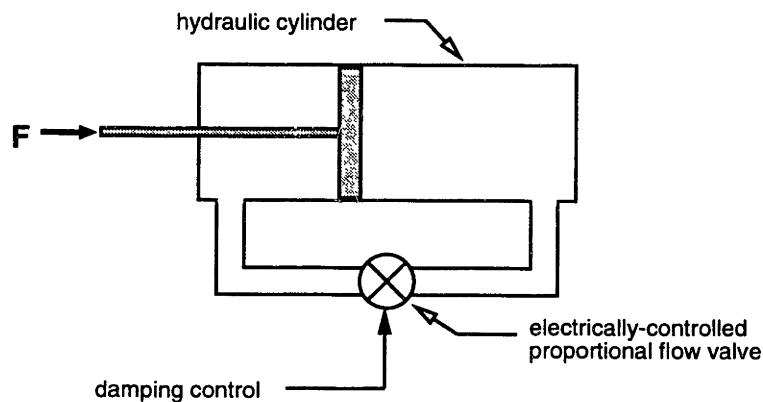
Figure 3-8: Concept for a controlled brake based on a hydraulic cylinder. By modulating the valve, resistance to motion of the cylinder piston can be controlled.

a large, back-drivable mechanical transmission. Since the inertia and residual friction of the motor would be multiplied by the square of the transmission ratio when reflected to the joint, a transmission of the size required would likely result in very significant parasitic joint inertia and friction. These problems could be eliminated using torque feedback, but implementation of this type of feedback through a large transmission is a difficult control problem that can result in instability. Another disadvantage is that utilizing a motor (or any actively-powered device) as a dissipator requires accurate measurement of velocity. Noise or dynamic distortion of the velocity signal can result in poor performance or instability. Motors are also relatively inefficient in their conversion of electrical power to static holding torque, which would make a battery-powered CBO infeasible. Finally, because motors are active power sources which can drive the limbs beyond their normal range of motion, significant safety concerns arise when motors interact with human subjects.

Magnetic particle brakes offer the advantage of simple control of joint torque over a bandwidth suitable for controlling the events involved in human gait. Unlike a DC motor, particle brakes are mechanically passive devices with no possibility of human injury resulting from unstable behavior, and thus are well suited for uses involving human interaction. Additionally, magnetic particle brakes offer a resistive torque to

weight ratio more than an order of magnitude greater than a typical high performance DC torque motor. A particle brake of roughly the same size and weight as a DC motor therefore would require a transmission ratio about one tenth that of the motor, thus making size and weight of the (back-drivable) transmission significantly smaller. Additionally, the smaller transmission ratio significantly reduces the effective inertia and friction reflected from the dissipator to the joint. Particle brakes also consume significantly less power for a given holding torque than do comparable DC torque motors. For a given peak torque, a magnetic particle brake offers a peak holding torque to power ratio at least 50 times greater than a high performance DC torque motor. For these reasons, magnetic particle brakes were chosen as the controlled brakes for the orthosis.

Magnetic particle brakes produce a steady-state resistive torque roughly proportional to the input current. DC current applied to the brake coil induces a magnetic field which links fine ferrite particles to the rotating brake shaft. The amount of current determines the strength of the magnetic field, which in turn determines the resistive torque imposed on the brake shaft. Since the brake resistance is imposed by fine ferrite particles, the engagement is smooth and quiet. These devices provide a relatively compact and light-weight means of exerting dissipative mechanical torques using an electrical control signal.

The primary dynamic behavior associated with a magnetic particle brake involves the electrical energy domain first-order dynamics of the brake inductance and the mechanical energy domain (approximately second-order) dynamics of the ferrite particle motion. The first-order electrical dynamics can be controlled with a standard voltage-to-current servoamplifier to force a current through the brake windings which is proportional to the command voltage. The second-order dynamics associated with the particle motion responding to the current are significantly faster than those of typical human gait and thus can be ignored in the CBO application. If necessary, faster dynamics can be achieved by closing a torque feedback loop around the brake.

Particle brakes were selected from Force Limited (Santa Monica, CA). The brakes for the knee joint (Model B20SF15) weigh 335 g (0.738 lb_m) and output a continuous

maximum torque of 2.8 Nm (25 in-lbs). The brakes for the hip joint (Model B20SF14) weigh 235 g (0.518 lb_m) and can output 1.8 Nm (16 in-lbs).

3.2.4 Transmission Selection

Magnetic particle brakes are primarily high angular velocity, low torque devices. Human gait however consists of relatively low angular velocity and high torque motion. Utilizing the full mechanical power range of the brakes therefore requires a mechanical transmission. The transmission must provide at least a 16:1 speed reduction from the brake to the joint to provide the specified maximum joint torques from the selected particle brakes. Since power flow is from the joint to the brakes, the transmission must be easily back-drivable (i.e., must provide the 1:16 speed increase from the joint to the brake). Additionally, in order to minimize parasitic dynamics, it should be stiff, light weight, and compact. Though cable drives offer the advantage of no backlash, their low stiffness makes them unsuitable for this application. The selected transmission is provided instead by an Evoloid gear set (ASI Technologies, Horsham, PA). Evoloid gears utilize a geometrical variation on the conventional involute-tooth helical gear profile that enables the use of a four tooth pinion without the associated undercut exhibited by conventional gearing. These gears can therefore provide a compact, back-drivable 16:1 transmission in a single stage capable of carrying large static loads. Evoloids are much smaller and lighter than comparable single stage spur or helical transmissions, and unlike hypoid and Spiroid (ITW Spiroid, Chicago, IL) gears, offer a parallel rather than a perpendicular shaft arrangement. Additionally, unlike multi-stage gear trains or a planetary set, the single stage Evoloids require only the housing and bearings necessary to support two shafts.

The large static loads characteristic of human gait require a very robust transmission. Each Evoloid gear therefore is machined from 4140 (chromium-molybdenum) steel alloy, and the pinion from 6100 series (chromium-vanadium) steel alloy. Both hip and knee joint gears have a 16:1 transmission ratio.

3.2.5 Joints

Each orthosis joint consists of a magnetic particle brake, an Evoloid gear set, and a gear housing, as shown in Figures 3-9 and 3-10. The gear housing is fabricated from two aluminum plates separated by the gear shaft and two smaller structural shafts. Mounting the Evoloid gear onto the gear shaft with a bearing allows a rigid connection between the housing plates and the shaft. The gear shaft therefore functions as a primary structural part of the housing. Mounting the gear directly on a bearing offers considerably less lateral stiffness than fixing the gear to the shaft and supporting each end of the shaft on bearings, however, the single bearing configuration offers the advantage of a significantly smaller and lighter gear housing and was therefore preferred.

Despite the efficient design of the Evoloid gear set, the mechanical transmission is still among the heaviest of the brace components. Careful effort was taken to minimize the size and weight of the Evoloid gear. Since the total range of motion of the joints are 135 degrees for the hips and 105 degrees for the knees, the Evoloid gears were cut so that only the section necessary for engagement remained. Thus the size and weight of the joint package were reduced. Weight was further reduced by cutting out sections to form a spoked gear. The combined mass of the spoked gear and pinion is 115 g (0.253 lb_m) for the hip joint and 182 g (0.400 lb_m) for the knee joint.

3.2.6 Hip Abduction and Adduction

As described previously, an off-axis, multiple degree of freedom hip ab- and adduction linkage provides a more compact package than a single degree of freedom gimbled joint. The linkage designed for the controlled-brake orthosis is a three degree of freedom linkage that utilizes revolute joints to accommodate the skeletal degree of freedom, as illustrated in Figure 3-11 and shown in the photograph of Figure 3-12. The limit stop which blocks the motion of the middle joint of the linkage results in a structurally determined brace/skeletal system, which provides the adduction lock

necessary to prevent scissoring during gait [1].

3.2.7 Sensors

The hip and knee joints are instrumented with angle and torque sensors. Potentiometers (CP-2FK, Midori America, Corona, CA) are located inside the tubular gear shafts to measure joint position. This mounting configuration enables a direct-drive coupling of the potentiometer shaft to the rotating member, thus obviating the need for belts and pulleys or other forms of transmission. Joint velocity is derived by off-board analog differentiation of the position signal. Strain gages (EA-13-060PB-350, Micro-Measurements, Raleigh, NC), shown in Figure 3-9, are fixed to a load bearing member to measure joint torque. The electronic circuitry for strain gage and potentiometer signal conditioning is located inside the gear shaft to minimize signal noise and provide for compact design.

---

[1]The adduction lock is described in more detail in Appendix D.
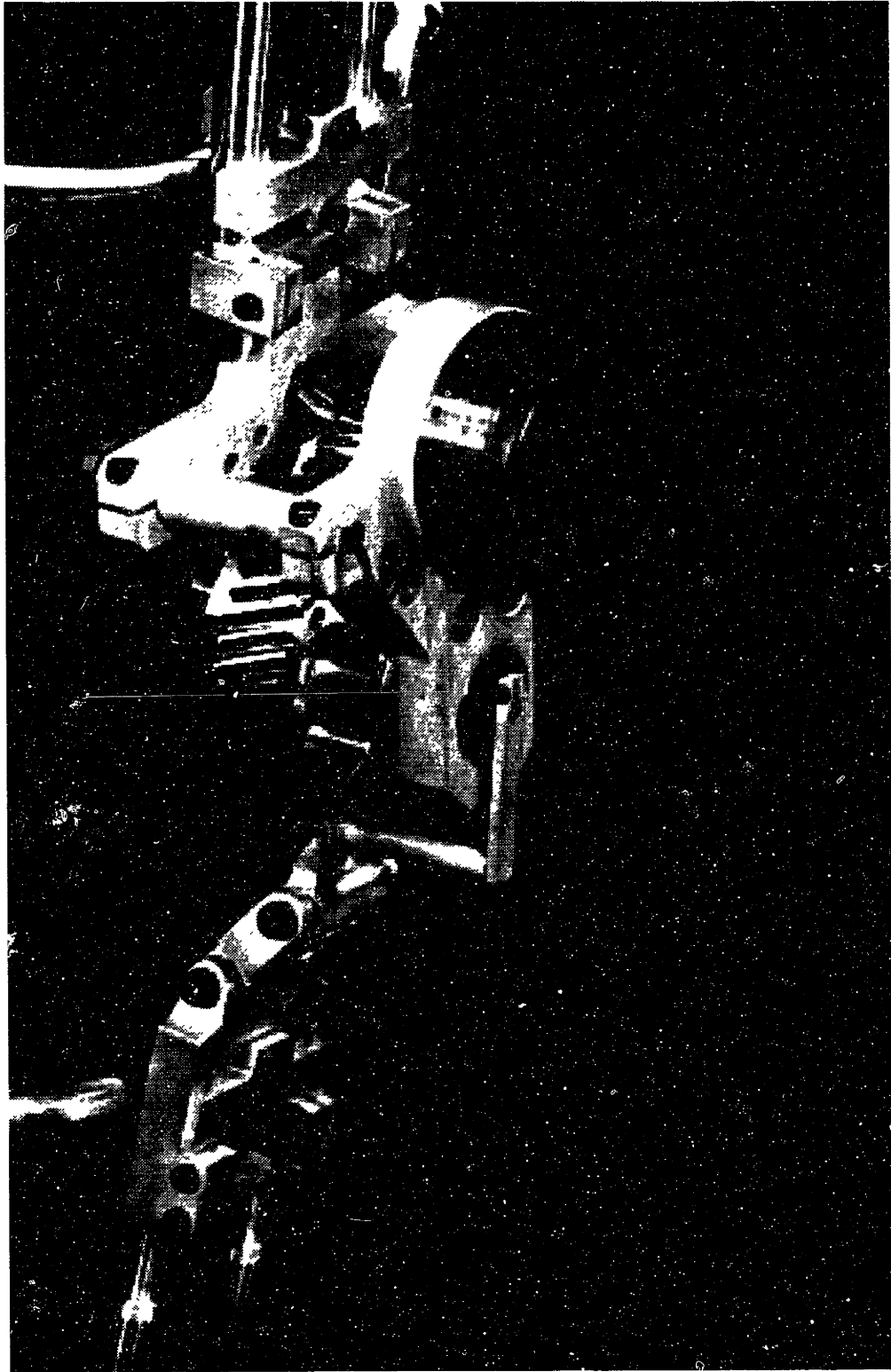
Figure 3-9: CBO knee joint showing the magnetic particle brake, transmission and posit: n sensor.
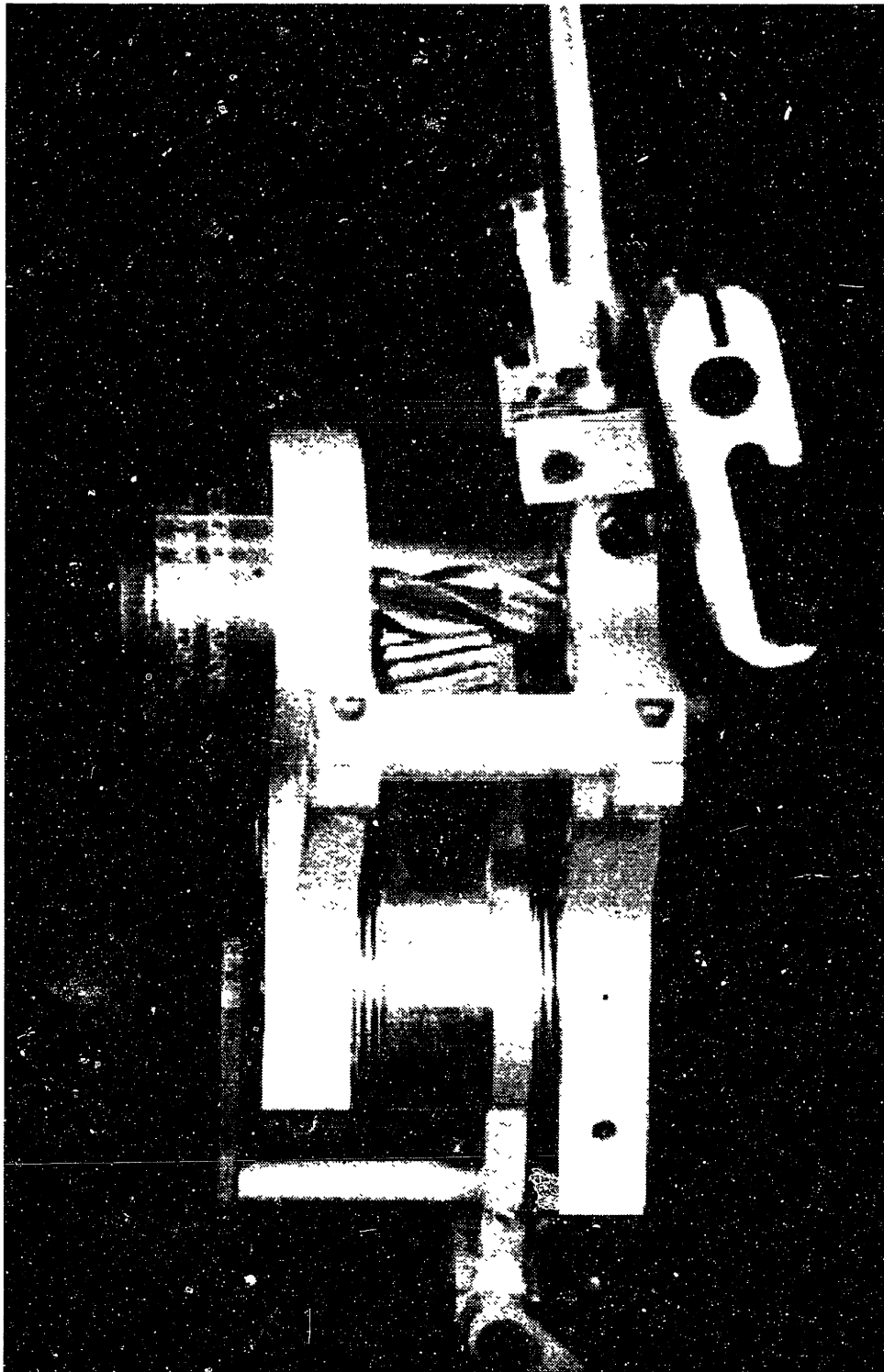
Figure 3-10: CBO knee joint showing the magnetic particle brake and Evoloid gear and pinion.
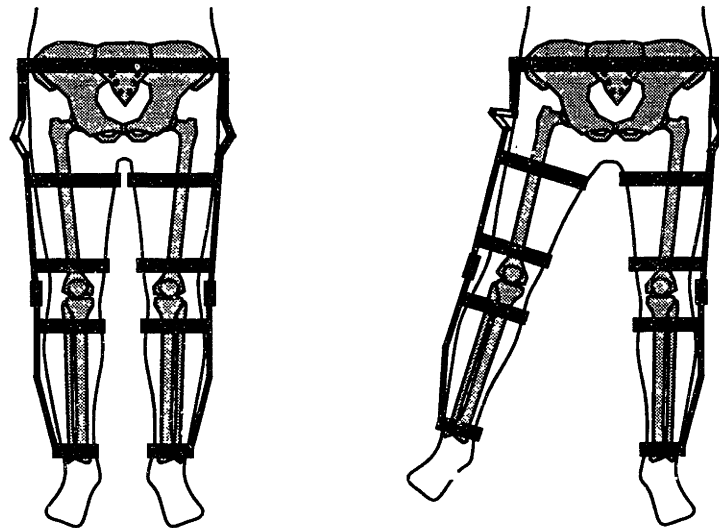
Figure 3-11: Linkage enabling hip abduction and adduction.
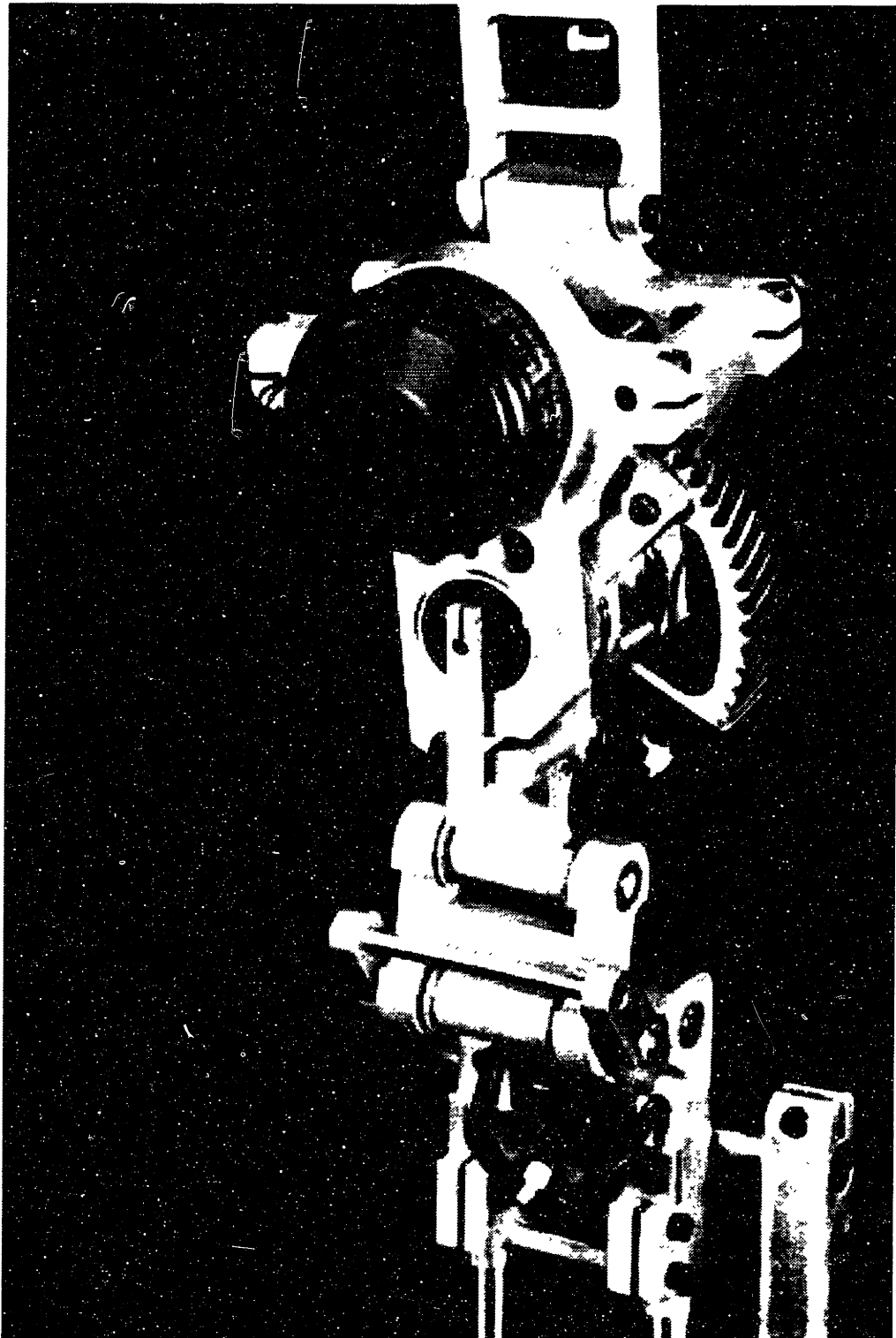
Figure 3-12: CBO hip joint showing the ab/adduction linkage.

Chapter 4

Orthosis Control

4.1 Joint Angle Trajectory Control

4.1.1 Introduction

The primary problem associated with utilizing FES alone to control joint motions during gait is the absence of a muscle model that adequately describes the highly nonlinear and time-varying relationships between electrical stimulation input and muscle force output. Additionally, since the output torque generated by the muscle cannot be directly measured, closed-loop control of the torque is not possible. The problem is compounded by poor muscular selectivity from stimulation electrodes, limited muscular bandwidth and power output, and inability to measure many of the muscle states. The basic idea underlying the controlled-brake orthosis approach is to achieve desirable position tracking by utilizing the muscles only as a source of coarsely regulated power, and regulating the power at each joint with the controllable dissipators on the brace.

4.1.2 A Dissipative Control System

A principle feature of the orthosis control system is that it is fundamentally dissipative. A typical control system effects control commands through an actuator, which can both add and remove power from the plant. The CBO system, however, effects

59

control commands through a dissipator, and therefore can only control the amount of power removed from the plant.

4.1.3   Controller Description

A block diagram of the trajectory controller for a single joint is shown in Figure 4-1. In the figure, θ is the joint angle and ω is the joint angular velocity. The tracking error e is the weighted sum of the position and velocity errors. The net torque acting on the joint T is the sum of the muscle torque T_m and the brake torque T_b. The brake torque is the control command torque T_c, filtered by the dynamics of the particle brake. The control output T_c is proportional to the tracking error, and therefore contains a viscous torque component based on the velocity error and a component based on the position error. The control action is analogous to a spring and damper, except that the spring cannot return any energy to the moving limb.

A requisite condition for effective control is that the muscle provide sufficient joint power to maintain the desired trajectory. The decision of when to use the brake is made by the half wave rectification of the tracking error. This rectification defines the two regions of the controller. When the tracking error is positive, the joint power from muscle stimulation is sufficient to maintain the desired trajectory, and the system is in the region of control. In this region, the controller can regulate joint motion by removing power from the moving limb. When the tracking error is negative, the joint power from muscle stimulation is inadequate. Since the controller can only remove power from the plant, the best it can do in this situation is shut off completely.

Utilizing tracking error instead of position error to effect when the joint power is sufficient provides a more energy-based measure than does using position error alone, since the kinetic energy of the limb is a function of its angular velocity. Take, for example, the case when the limb is behind the desired position trajectory, but moving faster than the desired velocity trajectory. The additional velocity information enables the controller to start dissipating energy before the limb reaches the desired position trajectory, slowing it down so that it joins the desired path in a smooth fashion.
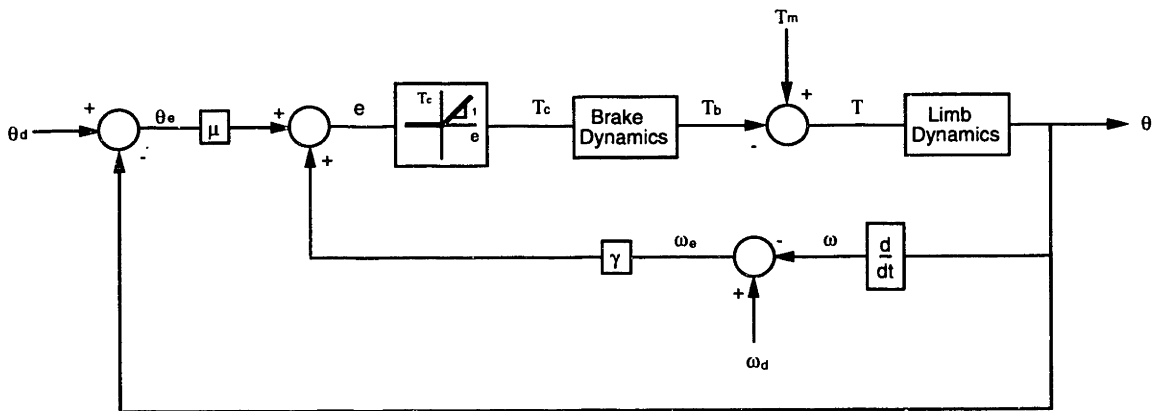
Figure 4-1: Joint angle control using the controlled brake for trajectory regulation.

4.1.4 Hip versus Knee Trajectory Control

Since both knee flexors (peroneal channels) and knee extensors (quadriceps channels) are stimulated, the knee controller can regulates both knee flexion and extension, and thus controls knee position for the entire gait cycle. The hip controller regulates hip flexion through stimulation of the peroneal channels, but does not have direct control over hip extension. Extension of the hip is effected primarily by the individual's upper body. Since the hip controller regulates hip motion for only half of the gait cycle, nearly every swing phase hip trajectory begins with an initial tracking error. Since the controller can only remove power from the joint, it is limited in its ability to quickly eliminate this error, and instead must wait for the system to arrive in the region of the trajectory before it can impose effective control.

4.1.5 Error Sign Conventions

Due to the nonlinear nature of the controller, the sign conventions associated with the tracking error depend on whether the joint is in flexion or extension. The block diagram shown in Figure 4-1 represents the proper sign convention for flexion, given that θ and ω are positive in this direction. The tracking error during flexion control is

$$e = -\mu\left(\theta_d - \theta\right) - \gamma\left(\omega_d - \omega\right) \tag{4.1}$$

Since the direction of muscle torque changes in extension, the sign of the tracking error must be reversed (positive feedback in the block diagram), and is therefore

$$e = \mu\left(\theta_d - \theta\right) + \gamma\left(\omega_d - \omega\right) \tag{4.2}$$

4.2 Trajectory Control Simulations

Experiments on spinal cord injured persons are significantly more restricted than those on able-bodied subjects. Since serious injury can result from a fall, the CBO system must provide consistent and reliable control. As a result, experiments on SCI subjects therefore provide limited opportunity for investigating controller behavior. Exploring controller behavior on able-bodied subjects is not a viable option due to the unavoidable voluntary suppression of the flexion withdrawal reflex. Numerical simulations therefore provide a valuable tool for investigating controller performance and for selecting appropriate feedback gains.

4.2.1 Modelling the Brace/Musculoskeletal System

The model utilized for the numerical simulations, which represents knee joint behavior during the swing phase of gait, was constructed with the objective of describing the salient features of the system with minimal model complexity. A block diagram representing the structure of the brace/musculoskeletal system for a single degree of freedom is shown in Figure 4-2.

Limb Dynamics

The dynamics of typical able-bodied gait utilize a significant amount of inertial coupling as a means of transferring mechanical energy between limb segments. Inertial coupling however is much less essential to FES-aided gait, and for the purposes of the
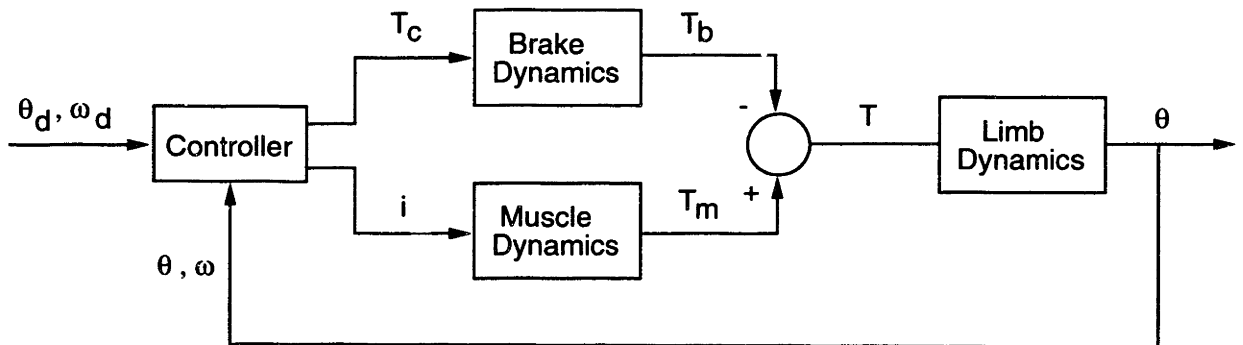
Figure 4-2: Block diagram representing the structure of the brace/musculoskeletal system for a single degree of freedom.
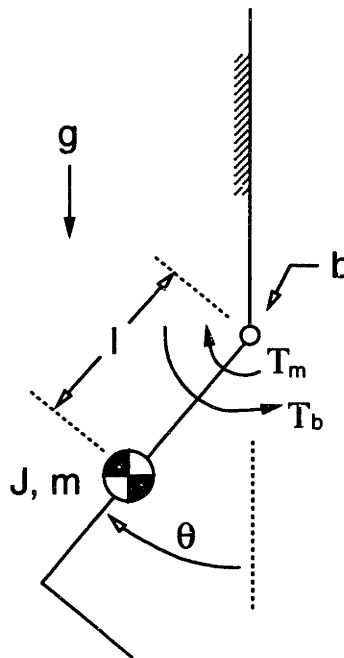
Figure 4-3: Free body diagram illustrating the model of limb dynamics.

model, was considered negligible. As a further simplification, the thigh segment was assumed to remain stationary and vertical for the duration of knee movement. The shank and foot were modeled as one rigid segment with a lumped mass m positioned at a distance l from the joint and a radius of gyration a distance r from the joint. The segment rotational inertia is thus

$$J = mr^2 \tag{4.3}$$

The joint damping due to the muscle and soft tissue were assumed to be viscous with a damping constant b. The brace was assumed to have negligible mass, rotational inertia, and joint friction. As shown in Figure 4-2, the torque acting on the limb is the difference between the torque produced by the muscle and the torque imposed by the brake. The dynamics of the limb are

$$J\ddot{\theta} + b\dot{\theta} + mgl\sin(\theta) = T_m - T_b sgn(\dot{\theta}) \tag{4.4}$$

where θ is the angle of knee flexion. Note that the brake torque term must include $sgn(\dot{\theta})$ and that $T_b \geq 0$ to ensure dissipative behavior. A diagram illustrating the model of limb dynamics is shown in Figure 4-3.

Muscle Dynamics

The muscle dynamics were modeled as a critically-damped second-order linear system. Several researchers have demonstrated that this approximation captures the essential dynamic behavior of stimulated muscle [10, 16, 22, 28, 59]. This linear description of muscle dynamics is typically coupled with a static nonlinear gain between stimulus level input and muscle force output, which accounts for the nonlinear character of neuromuscular recruitment. Since the muscle is used in a bang-bang fashion, however, the nonlinear gain need not be included in the model. Fatigue can also be neglected, since the short duration of swing phase movement does not allow for any significant muscle time variation. Though the active and passive force–length and force–velocity properties of the muscle and a characterization of joint geometry

are important elements for accurate description of non-isometric muscle behavior, they were not considered essential for this muscle model. The primary purpose of the simulations was to characterize the interaction between the limb moving under muscular stimulation and the magnetic particle brake under the influence of position and velocity feedback control. Though including the details of muscular behavior would improve simulation accuracy, their ommission should not significantly alter the character of this interaction. The dynamics of the muscle are therefore given by:

$$\ddot{T}_m - 2\alpha \dot{T}_m - \alpha^2 T_m = ki \tag{4.5}$$

where T_m is the joint torque produced by the muscle, α represents the location of the real repeated poles, and i is the level of muscle stimulation [1]. In this model, a positive stimulation input ($i > 0$) represents knee flexion and a negative stimulation input ($i < 0$) represents knee extension.

Brake Dynamics

A schematic of a magnetic particle brake in cross-section is shown in Figure 4-4. The primary components of the particle brake are the coil and iron core assembly, the shaft and drag disk assembly, and the ferrite particles. When the coil is not energized, the iron particles are in a low density, powder-like state. In this state, the powder exerts very little friction on the drag disk, and the shaft spins relatively freely. When the coil is energized, a magnetic flux is created in the core and across the gap, as illustrated in Figure 4-4. The magnetic flux links the particles to other particles, to the iron core, and to the drag disk, which acts to retard motion of the shaft. Increasing the coil current increases the strength of the magnetic field and thus increases the resistance imposed on the shaft. De-energizing the coil removes the flux and subsequently decouples the particles, iron core, and drag disk so the brake shaft can rotate freely.

The primary dynamic behavior exhibited by a magnetic particle brake is associated

---

[1]Note that the variable i is the envelope of stimulation amplitude. The stimulation pulse width and frequency are fixed.
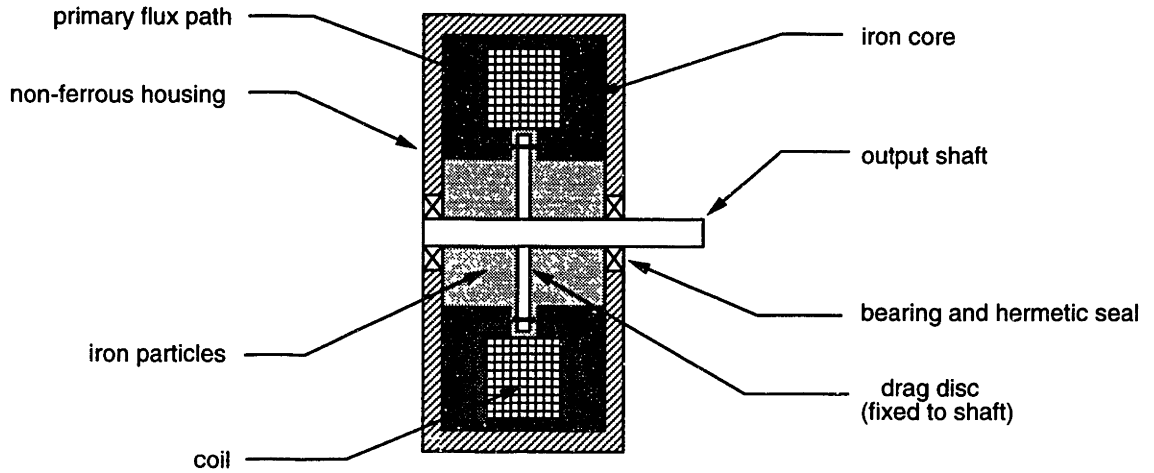
Figure 4-4: Schematic diagram of a magnetic particle brake in cross-section.

with the electrical energy domain dynamics of the brake coil inductance and the mechanical energy domain dynamics of the ferrite particle motion. Since the CBO brake input current is forced through the coil by a high bandwidth servo-amplifier, the inductance of the coil does not significantly contribute to the brake dynamics. The ferrite particle behavior can be approximated reasonably well by second-order linear dynamics [32]. Figure 4-5 shows the measured pulse response of the particle brake, along with a linear, second-order, critically-damped approximation. The irregular oscillations that appear at the tail end of the pulse response are most likely due to measurement artifact. Ideally, torque should be measured by rotating the brake shaft at a constant velocity, using a motor with a constant-velocity controller or a similar device. For this measurement, however, the brace link was rotated manually. Though attempts were made to move the joint at constant velocity, small aberrations in the torque data may be present due to the presence of small angular accelerations.

Unity gain between controller torque command T_c and actual brake torque T_b and real repeated poles at β result in a model of brake dynamics given by:

$$\ddot{T_b} - 2\beta \dot{T_b} - \beta^2 T_b = \beta^2 T_c \tag{4.6}$$

66

Actual and Simulated Particle Brake Pulse Response
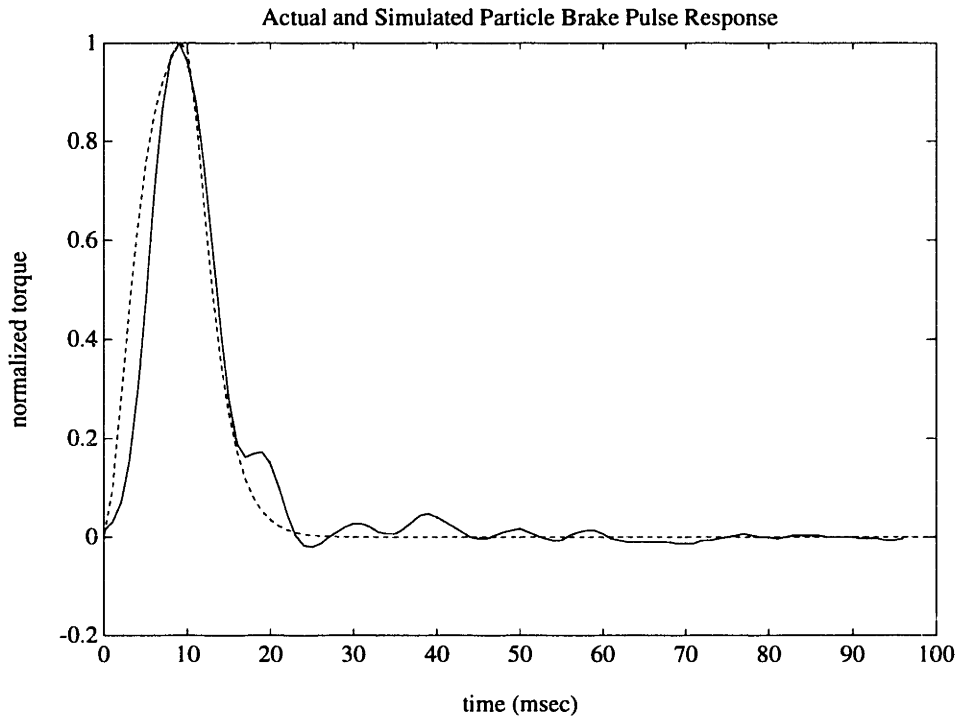
Figure 4-5: Measured pulse response of the particle brake (solid line), along with a linear second-order critically-damped approximation (dashed line). This response was obtained by moving the knee joint of the CBO at approximately constant velocity and pulsing approximately 100 milliamps of current for 10 milliseconds. The irregular oscillations that appear at the tail end of the pulse response are most likely due to measurement artifact.

The Controller

The desired position and velocity trajectories, were chosen to approximate the motion of a typical able-bodied swing phase, and are given by

$$\theta_d = \frac{\theta_f}{2}\left(1 - \cos(\frac{2\pi t}{T})\right) \tag{4.7}$$

and

$$\omega_d = \frac{\theta_f \pi}{T}\left(\sin(\frac{2\pi t}{T})\right) \tag{4.8}$$

where θ_f is the specified angle of full flexion and T is the duration of swing phase. These trajectories are illustrated by the dashed lines in the upper two plots of the simulations in Figures 4-6 through 4-21.

Simple bang-bang control is utilized to provide the necessary muscle torque. The knee flexion channel is activated for $t = 0$ to $t \leq T/2$, followed by activation of the knee extension channel for $t > T/2$ to $t \leq T$.

From Figure 4-1, control of the particle brakes is based on the tracking error, which is

$$e = -\mu\left(\theta_d - \theta\right) - \gamma\left(\omega_d - \omega\right) \tag{4.9}$$

for knee flexion and

$$e = \mu\left(\theta_d - \theta\right) + \gamma\left(\omega_d - \omega\right) \tag{4.10}$$

for knee extension, where μ and γ are the position and velocity feedback gains, respectively. The control output is

$$T_c = \begin{cases} 0 & \text{if } e \leq 0 \\ e & \text{otherwise} \end{cases} \tag{4.11}$$

The simulated controller also provides limit stops for both flexion and extension by locking the brakes at full flexion and at full extension, respectively.

68

Model Parameter Selection

The mass, center of mass, and radius of gyration of the combined shank and foot segment were estimated based on published anthropometric data in Table $A.1$ of Appendix A in *Biomechanics of Human Movement* by David Winter [104]. According to the data, which is based upon work of several researchers, the shank/foot segment mass is approximately 0.061 × *total body mass*. The segment center of mass and radius of gyration are located 0.606 and 0.735 × *total segment length*, respectively, from the knee joint. The total segment length is defined as the distance from the femoral condyles of the femur to the medial malleolus of the tibia. For an average-sized person, these estimates yield the following limb parameters:

$$m = 3.9 \text{ kg}, \tag{4.12}$$

$$l = 0.25 \text{ m}, \tag{4.13}$$

and

$$J = 0.25 \text{ kg m}^2 \tag{4.14}$$

The passive knee joint damping constant was selected so that oscillations from a free fall with an initial displacement of 45 degrees from the vertical would subside after approximately 5 seconds, as was observed in an actual limb. This yielded a damping constant of

$$b = 0.5 \text{ kg m}^2/\text{sec} \tag{4.15}$$

The real repeated poles of the muscle model are at the inverse of the time-to-peak of the impulse response. The time-to-peak was estimated to be approximately 100 ms, which is typical of stimulated muscle [59]. The system gain was chosen so that the output muscle torque was .15 Nm for an stimulation pulse amplitude of 60 ma. The muscle model parameters are thus

$$\alpha = 10 \;\; \text{rad/sec} \tag{4.16}$$

and

$$k = 2.5 \times 10^4 \;\; \text{Nm/A s}^2 \tag{4.17}$$

The particle brake impulse response shown in Figure 4-5 was estimated to have a time-to-peak of about 10 ms. The poles of the brake dynamics were therefore placed at

$$\beta = 10 \;\; \text{rad/sec} \tag{4.18}$$

The desired joint angle and velocity trajectories were computed with a maximum angle of knee flexion

$$\theta_f = 65 \;\; \text{degrees} \tag{4.19}$$

and a total swing duration of

$$T = 1.5 \;\; \text{seconds} \tag{4.20}$$

4.2.2 Controller Simulations and the Selection of Feedback Gains

Selection of proper position and velocity feedback gains can significantly affect controller performance. Figure 4-6 illustrates the simulated open loop behavior of the knee joint during swing phase. In the simulation, swing phase duration is 1.5 seconds with a maximum knee flexion angle of 65 degrees. The peroneal channel is activated for flexion (initial 750 milliseconds), followed by activation of the quadriceps for extension (final 750 milliseconds). The controller activates limit stops at full flexion and full extension, but otherwise does not affect leg motion. The simulations show the desired (dashed line) and actual knee angle and angular velocity trajectories, the

position and velocity errors, the tracking error, and the commanded and actual brake torque. Notice that since gravity drives the limb in the direction of extension, the position and velocity errors are somewhat greater in this direction than in flexion. Note also that due to the dissipative nature of the controller, trajectory control would only be possible in the regions of positive position error in flexion and negative position error in extension. The region of negative position error during flexion and positive position error during extension is due to the relatively slow response time of the stimulated muscle. The flexion error could be minimized by activating the peroneal stimulation in advance of the trajectory, and similarly activating the quadriceps prior to the desired knee extension. For the purpose of this work, however, the muscles were treated as unmodeled sources of power, and no attempt was made to address these initial errors. Recall that tracking error is defined as

$$e = -\mu\left(\theta_d - \theta\right) - \gamma\left(\omega_d - \omega\right) \tag{4.21}$$

for knee flexion and

$$e = \mu\left(\theta_d - \theta\right) + \gamma\left(\omega_d - \omega\right) \tag{4.22}$$

for knee extension. Note also that the small discontinuities present in the position and velocity trajectories of the simulations are due to limitations on numerical precision (introduced to limit file size and computational load), and not to model dynamics.

Velocity Feedback

Now consider system behavior when utilizing only velocity feedback to control the brake. Figures 4-7 through 4-12 show simulated knee joint behavior for the system with velocity feedback gains of 10, 20, 30, 40, 50 and 100 Nm/rad/sec, respectively. As the velocity gain is increased, the velocity trajectory more faithfully follows the desired velocity trajectory, and as the velocity error is driven to zero, so is the position error. However, if the velocity gain is too high, oscillations begin to appear in the velocity trajectory and subsequently in the control command and brake output.

71
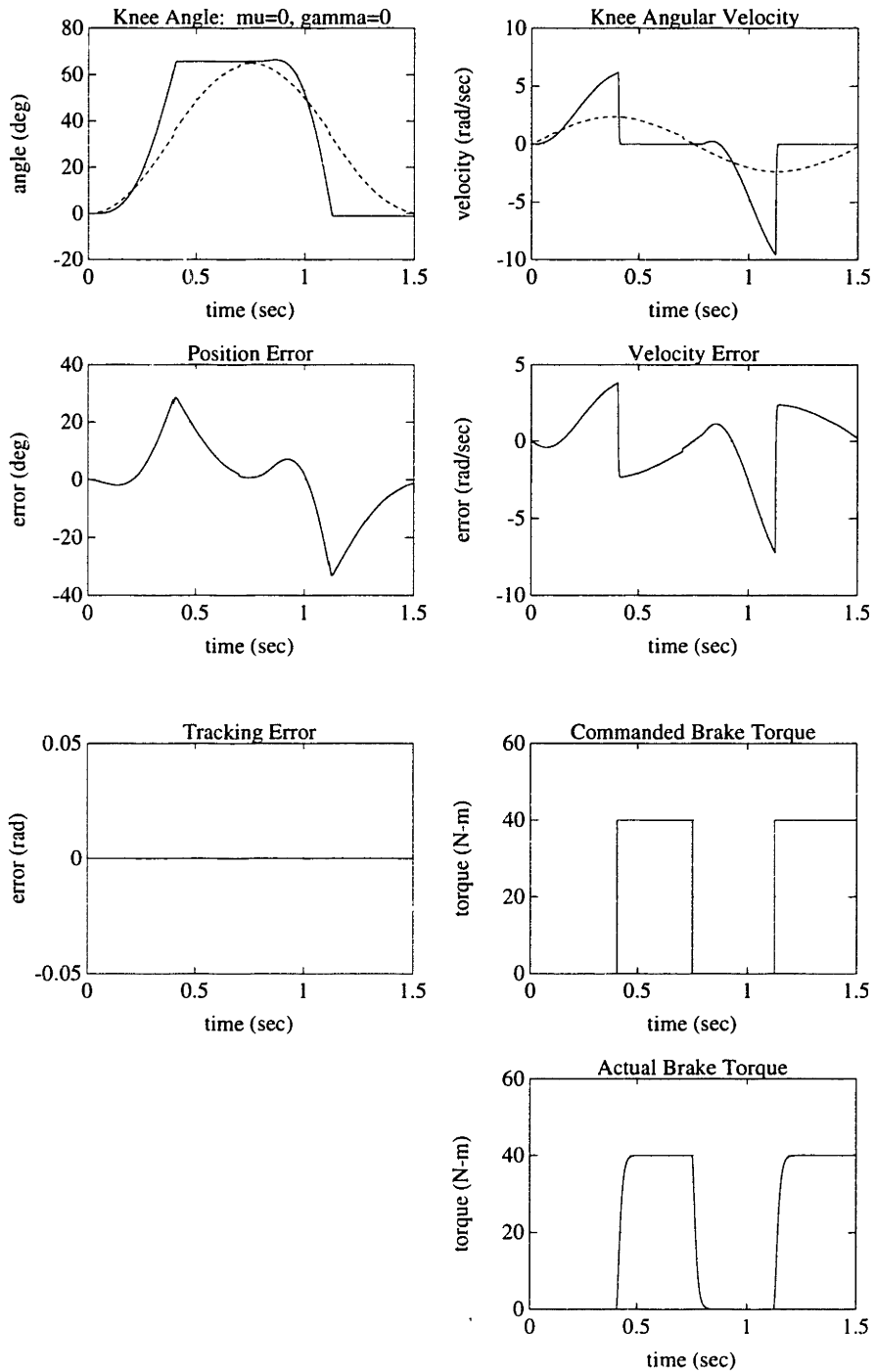
Figure 4-6: Simulation of open loop behavior of knee during swing phase. The CBO is utilized to effect limits stops at full flexion and extension.

These oscillations, which are manifest in the leg motion as chatter, become quite pronounced for the larger gains, as shown in Figures 4-10 and 4-11. As the loop gain increases, the unity gain crossover frequency increases until, as in Figure 4-12, the crossover corresponds to a particle brake phase lag of more than 180 degrees and the control system becomes unstable. These torque oscillations, therefore, are due solely to the phase lag of the particle brake, and would exist even in the absence of muscle stimulation. Note that the amplitude of oscillation in the simulation levels off because of particle brake torque output saturation, not because of metastable dynamics. Though the control command has become unstable, the plant remains stable, since the particle brake cannot add power to the limb. The instability does not result in increasingly large accelerations of the limb, but rather results in increasingly large decelerations, which results in increasing chatter. The velocity gain should therefore be set at a value that enables the system to follow the desired trajectory, but does not exceed the stable bandwidth of the particle brake.

Position Feedback

Figures 4-13 through 4-18 show simulated knee joint behavior for a closed-loop system with position feedback only for feedback gains of 100, 200, 300, 400, 500 and 1000 Nm/rad, respectively. The position trajectory shows an oscillatory component, though at a much lower frequency than the oscillations exhibited by the velocity feedback loop. These low frequency position trajectory oscillations give the limb motion a segmented character. This segmentation is illustrated by the distinct peaks in the joint velocity. Increasing the position feedback gain results in a subsequent increase in the observed frequency of oscillation. In the regions of positive velocity, the controller behaves like a spring, the stiffness of which is determined by the position feedback gain. The frequency of oscillation observed in the position trajectory reflects the natural frequency of the limb inertia interacting with the controller "stiffness." As the position feedback gain is increased and the controller stiffness increases, so does the natural frequency of the system and thus the frequency of oscillation. Therefore, while the velocity feedback loop reflects the dynamics of the particle brake, the
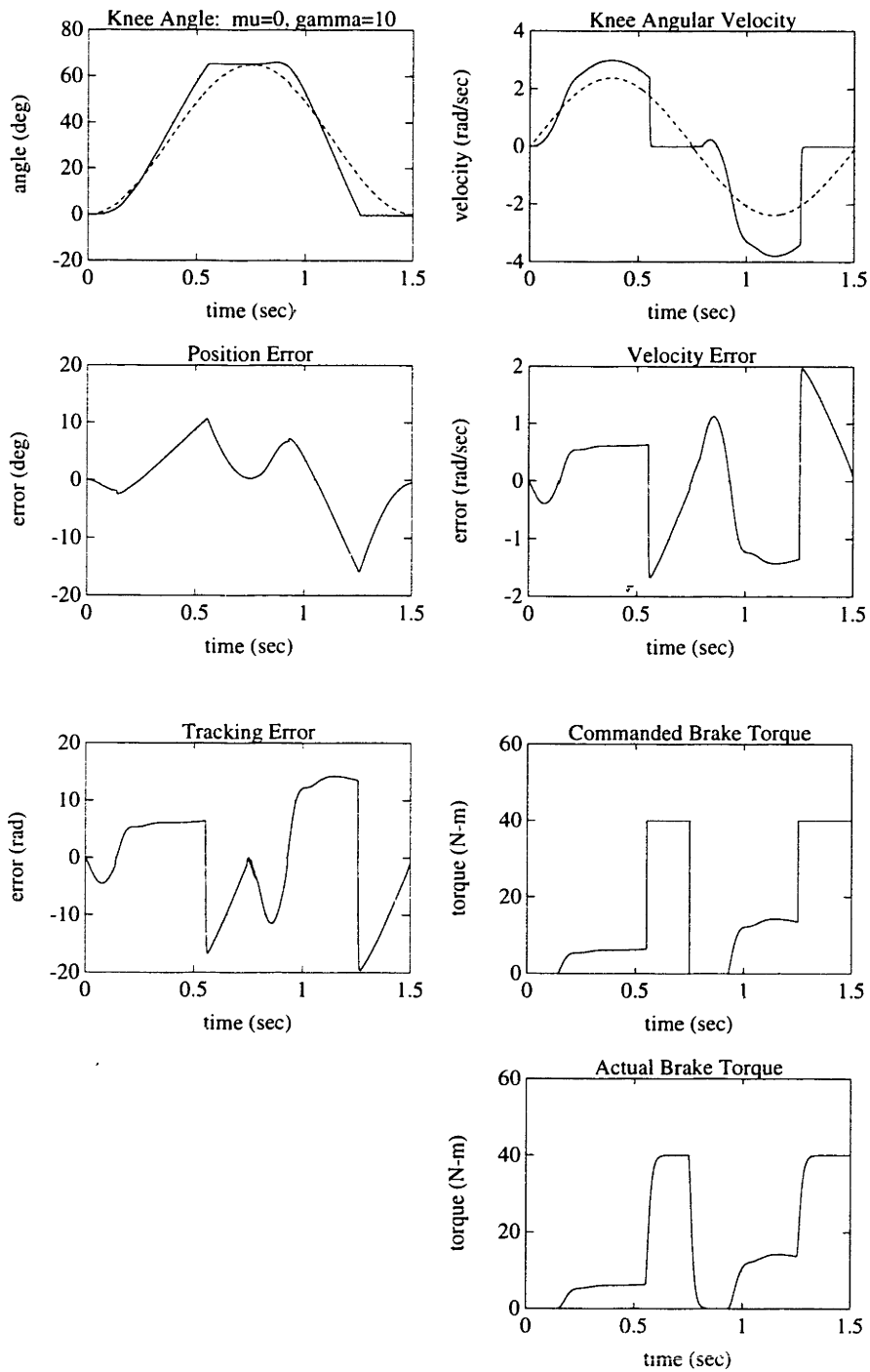
Figure 4-7: Simulation of knee joint behavior with a velocity feedback gain of 10 Nm/rad/sec and no position feedback. The CBO is also utilized to effect limits stops at full flexion and extension.
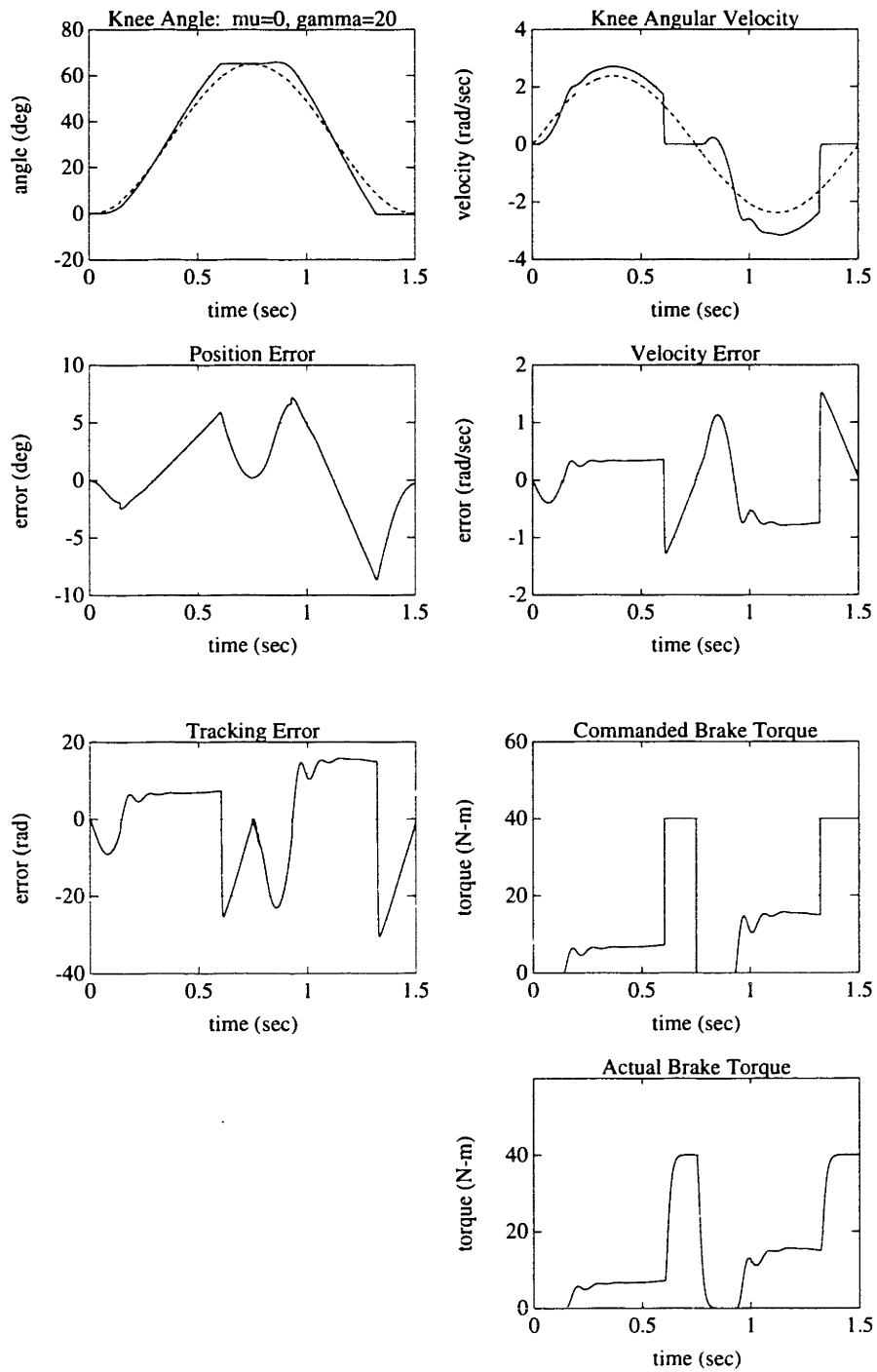
Figure 4-8: Simulation of knee joint behavior with a velocity feedback gain of 20 Nm/rad/sec and no position feedback.
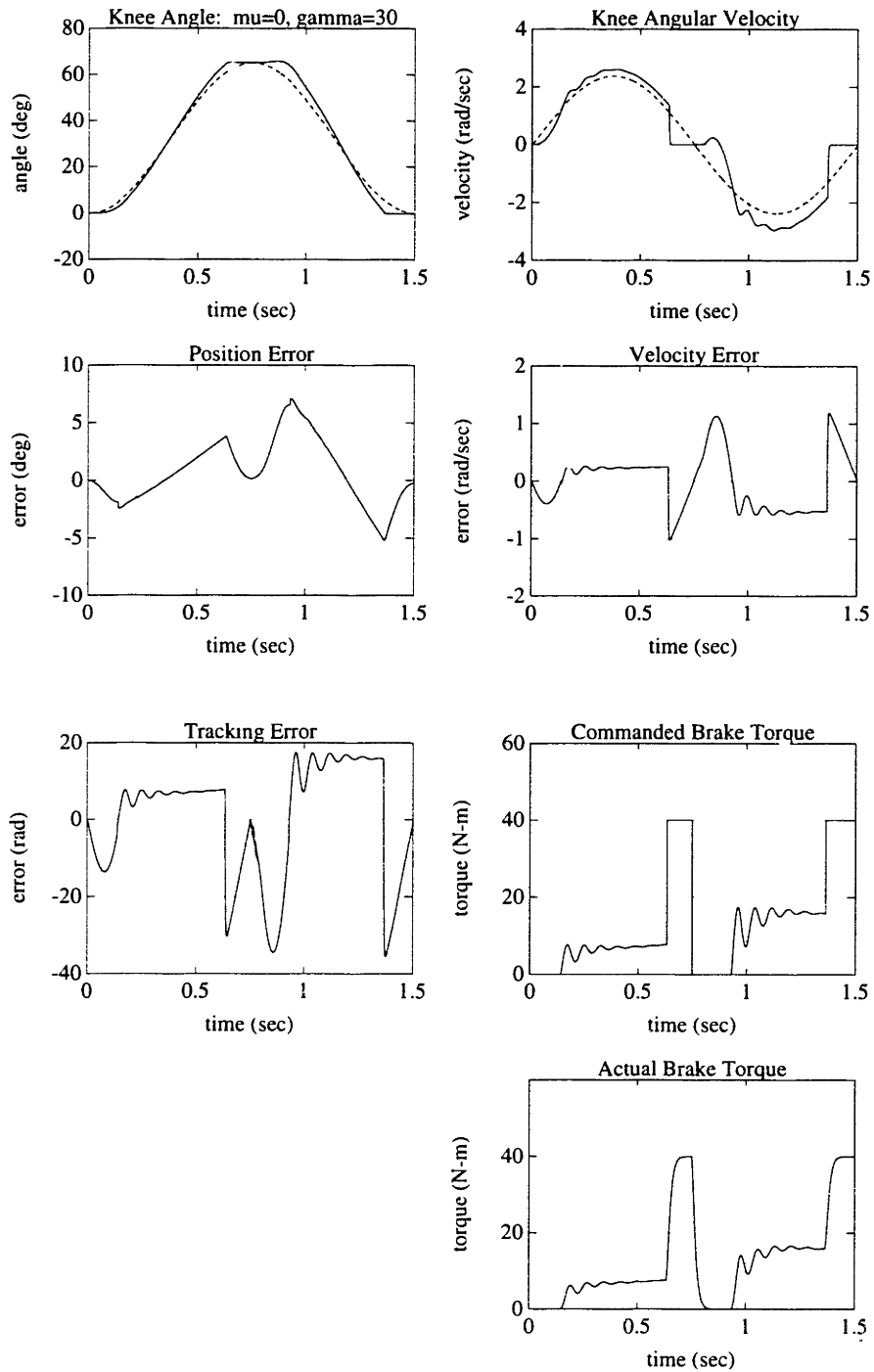
Figure 4-9: Simulation of knee joint behavior with a velocity feedback gain of 30 Nm/rad/sec and no position feedback.
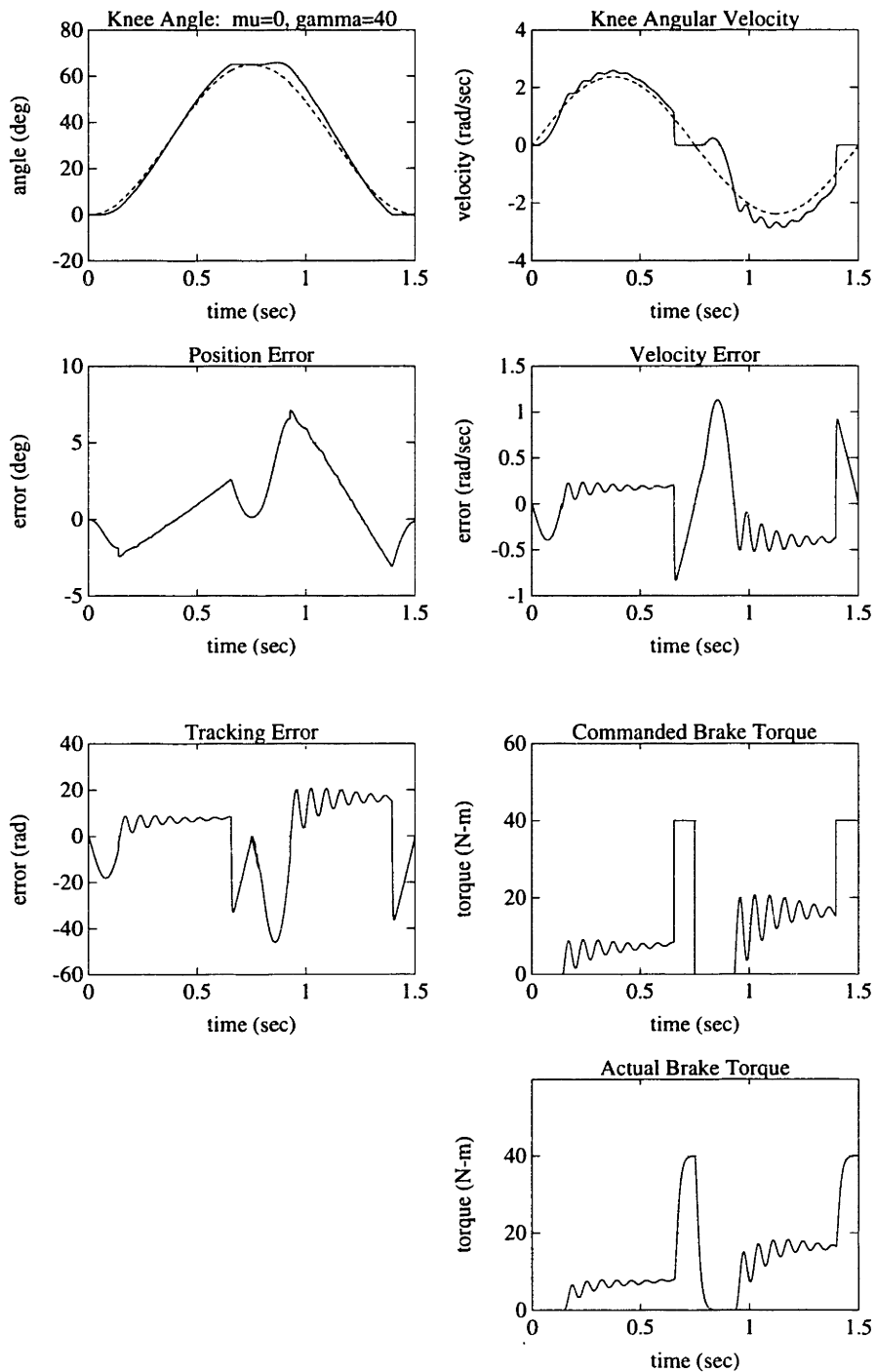
Figure 4-10: Simulation of knee joint behavior with a velocity feedback gain of 40 Nm/rad/sec and no position feedback.
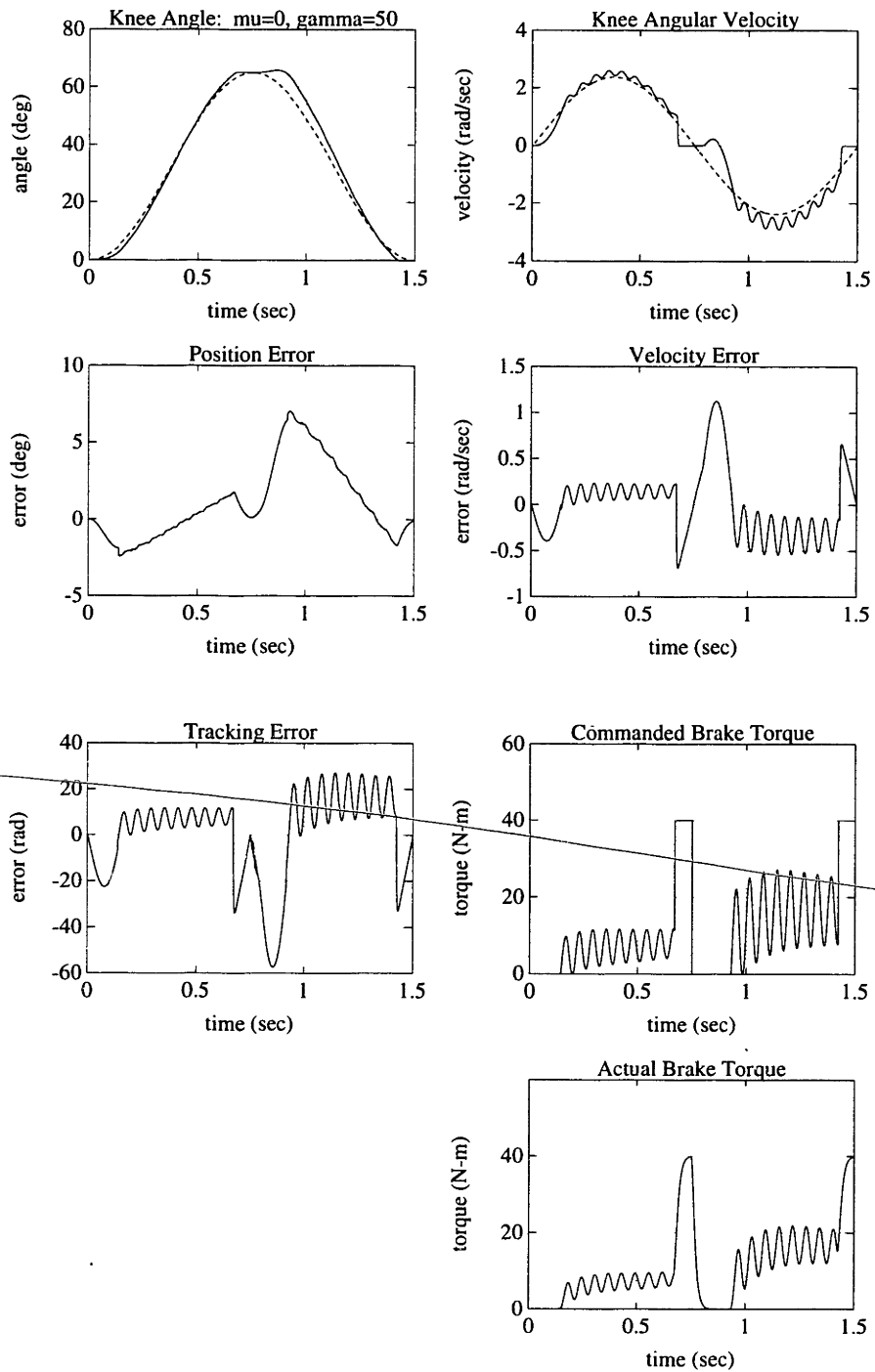
Figure 4-11: Simulation of knee joint behavior with a velocity feedback gain of 50 Nm/rad/sec and no position feedback.
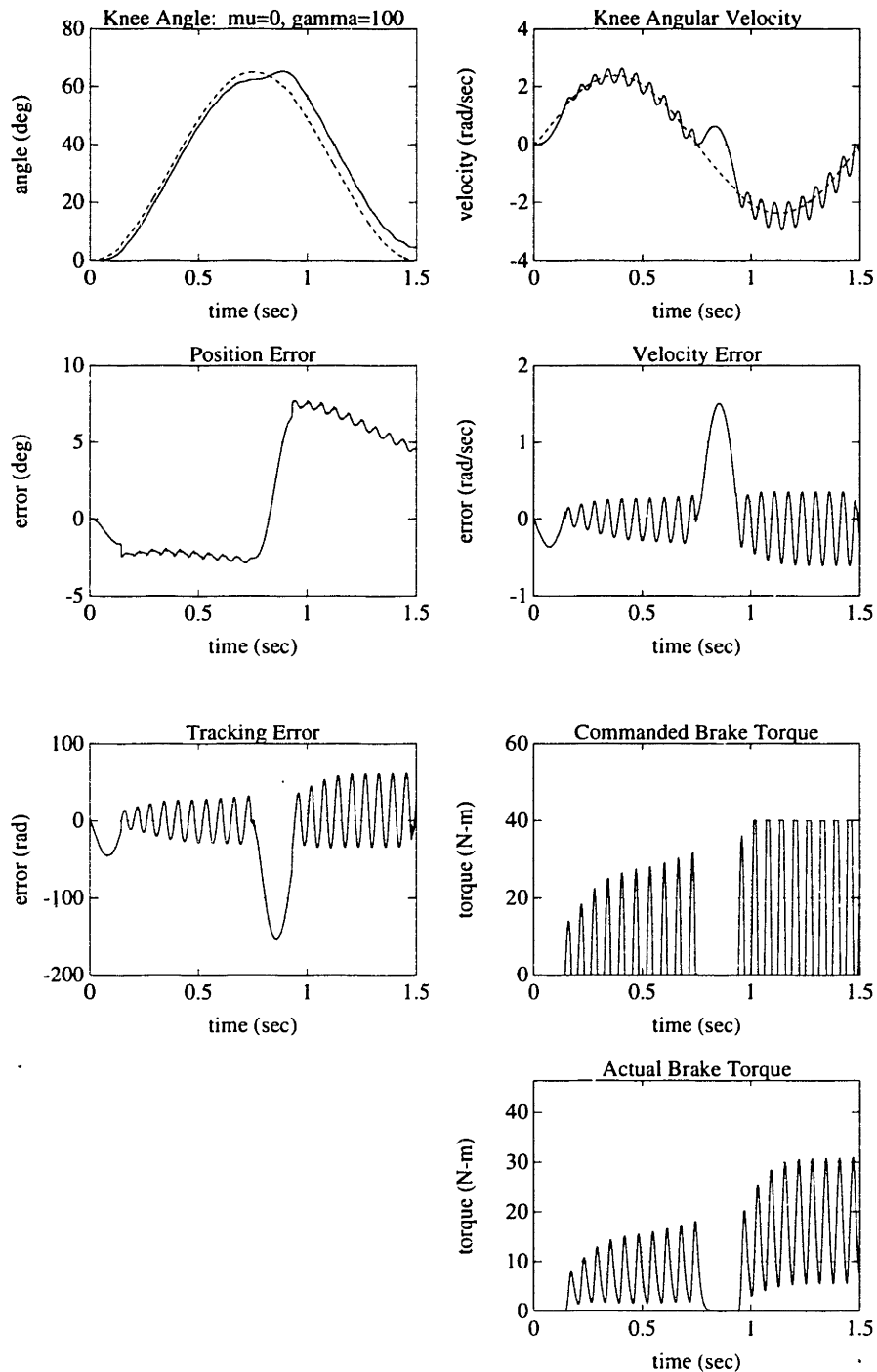
Figure 4-12: Simulation of illustrating unstable knee joint behavior when the velocity feedback gain is too large (100 Nm/rad/sec).

position feedback loop reflects the dynamics of the limb. As the feedback gain is increased further, the particle brake is continually driven into saturation, as shown in Figure 4-18. In this region, the brake controller essentially behaves like a bang-bang controller, or perhaps more appropriately, a bang controller. Though the magnitude of position error is decreased slightly with increased position feedback gain, controller performance is poor at any gain with position only feedback.

These results correspond well with the experimental results obtained by Durfee and Hausdorff [27]. In these experiments, a magnetic partical brake with position feedback was used in conjunction with electrical stimulation of the quadriceps and hamstrings muscle groups to control knee joint motion. As predicted by the simulations, the knee angle trajectories of their experiments exhibited a segmented character.

Combined Position and Velocity Feedback

Incorporating both the position and velocity components of feedback enables significantly better tracking performance. Figure 4-19 shows the simulated system performance for appropriately selected feedback gains. Notice that in the regions of trajectory control (approximately 200 to 500 milliseconds in flexion and approximately 1000 to 1500 milliseconds in extension), the tracking is both smooth and accurate. When utilized together, the position feedback loop acts to keep the limb on the desired trajectory and the velocity feedback loop acts to damp out the segmented motion of the position loop.

In the absence of particle brake dynamics, increasing the magnitude of the feedback gains would decrease the size of the tracking errors and thus improve performance. Since the controller does have limited bandwidth and output magnitude, large feedback gains result in motion that is neither smooth nor accurate. A large position feedback gain requires a similarly large velocity feedback gain to damp out low frequency oscillations in position that manifest as segmented motion. A large velocity gain, however, approaches the stability bandwidth of the particle brakes and results in the lightly damped high frequency oscillations that manifest as chatter.

80
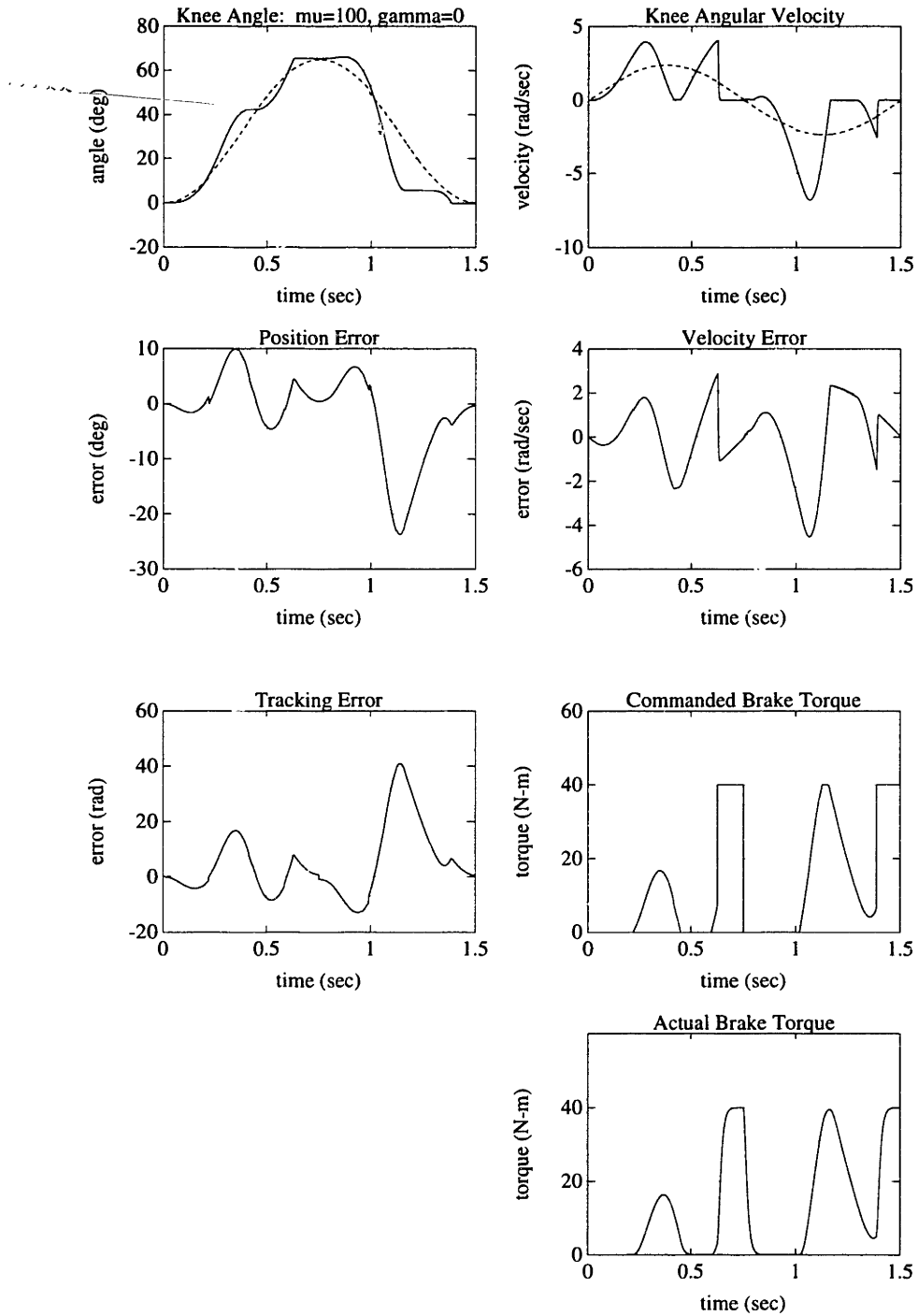
Figure 4-13: Simulation of knee joint behavior with a position feedback gain of 100 Nm/rad and no velocity feedback. The CBO is also utilized to effect limits stops at full flexion and extension.
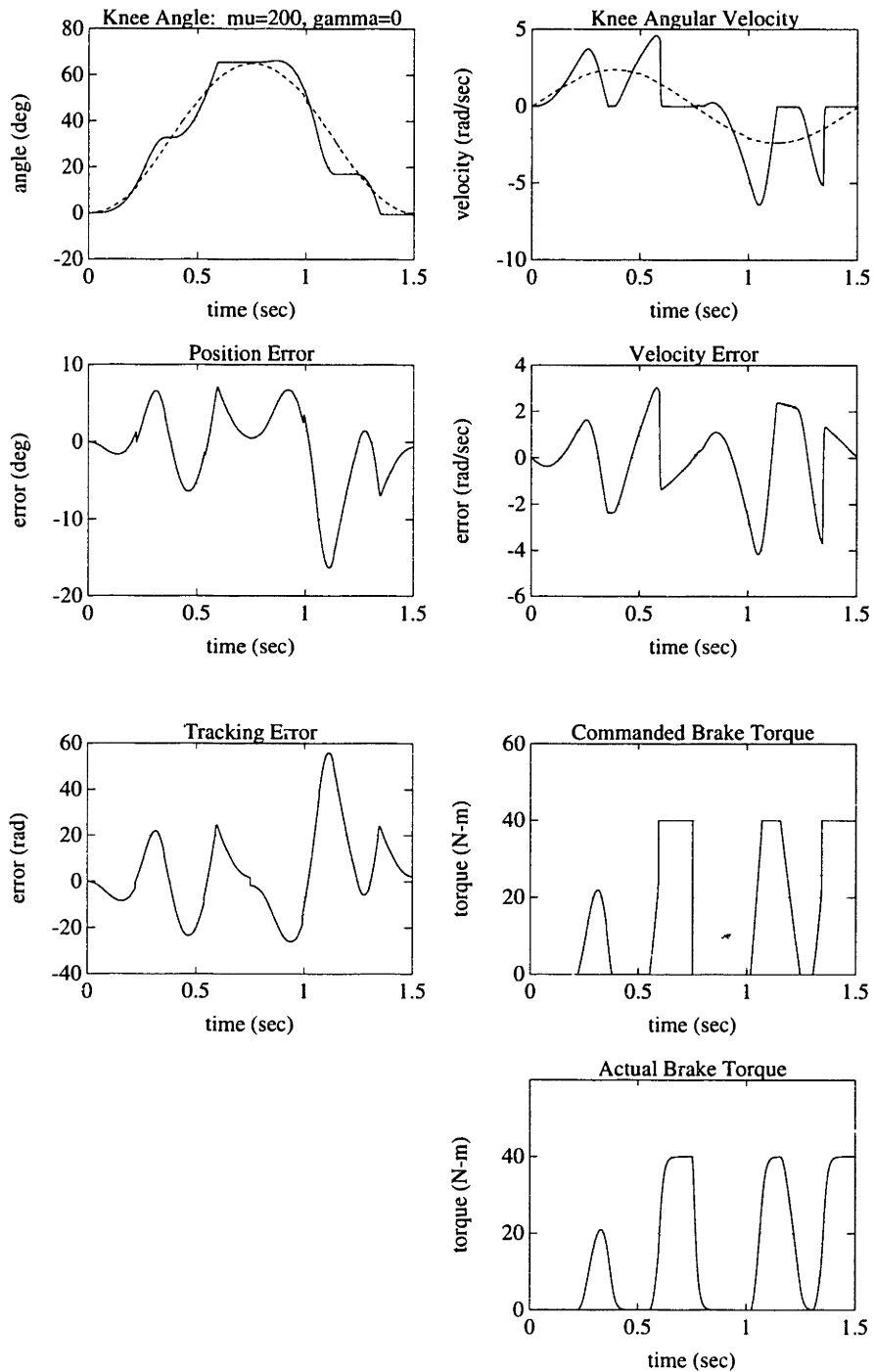
Figure 4-14: Simulation of knee joint behavior with a position feedback gain of 200 Nm/rad and no velocity feedback.
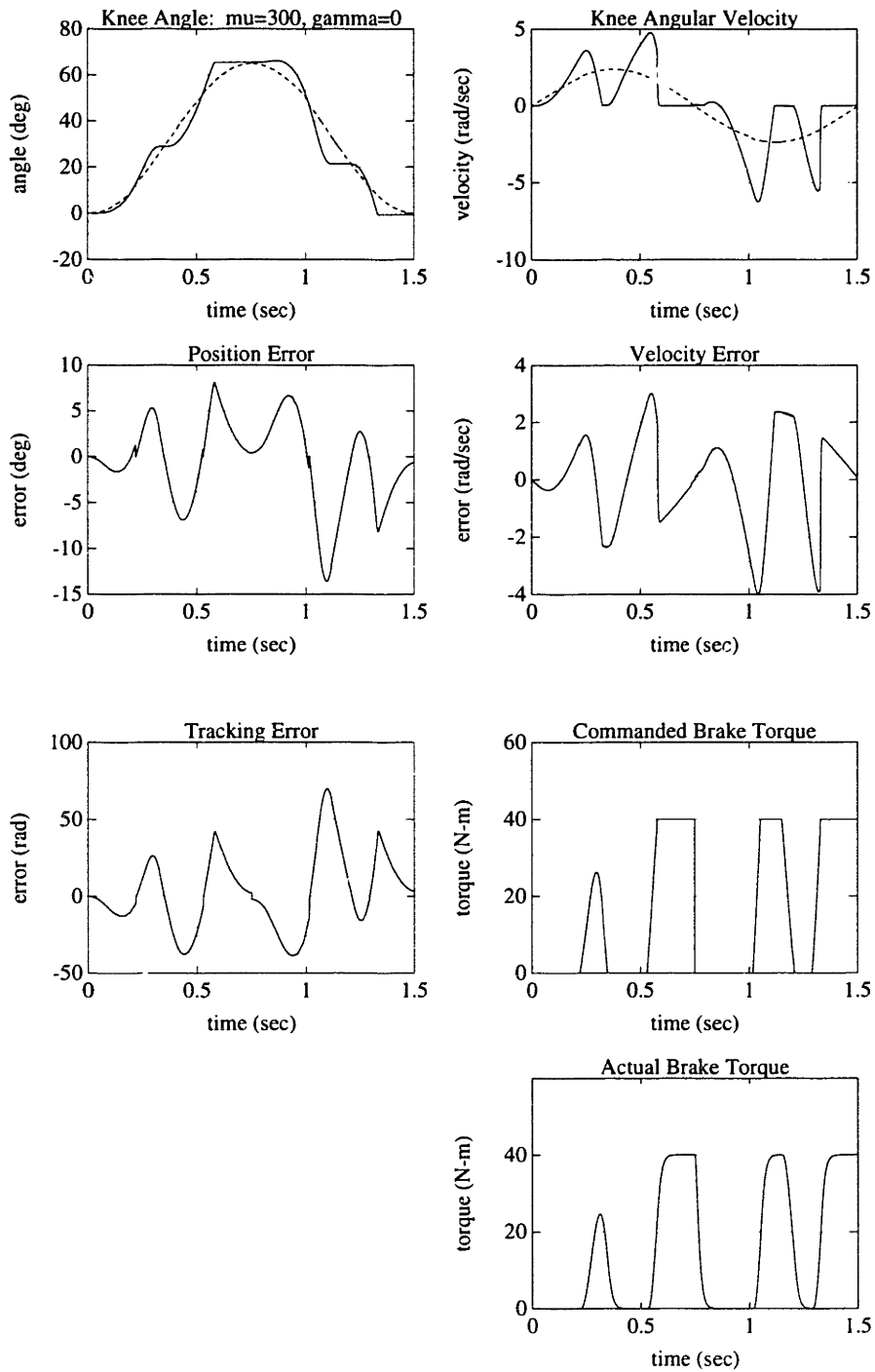
Figure 4-15: Simulation of knee joint behavior with a position feedback gain of 300 Nm/rad and no velocity feedback.
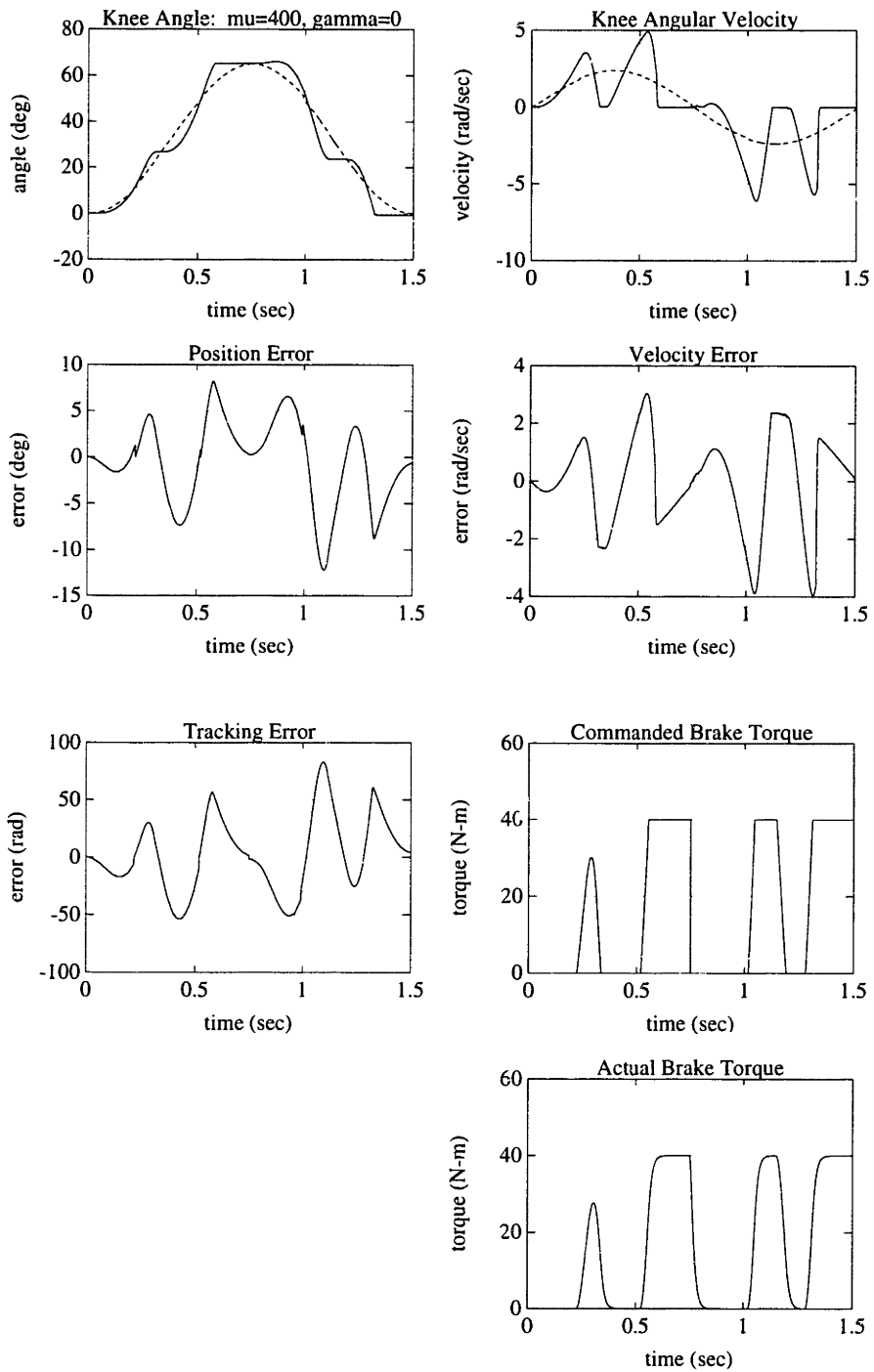
Figure 4-16: Simulation of knee joint behavior with a position feedback gain of 400 Nm/rad and no velocity feedback.
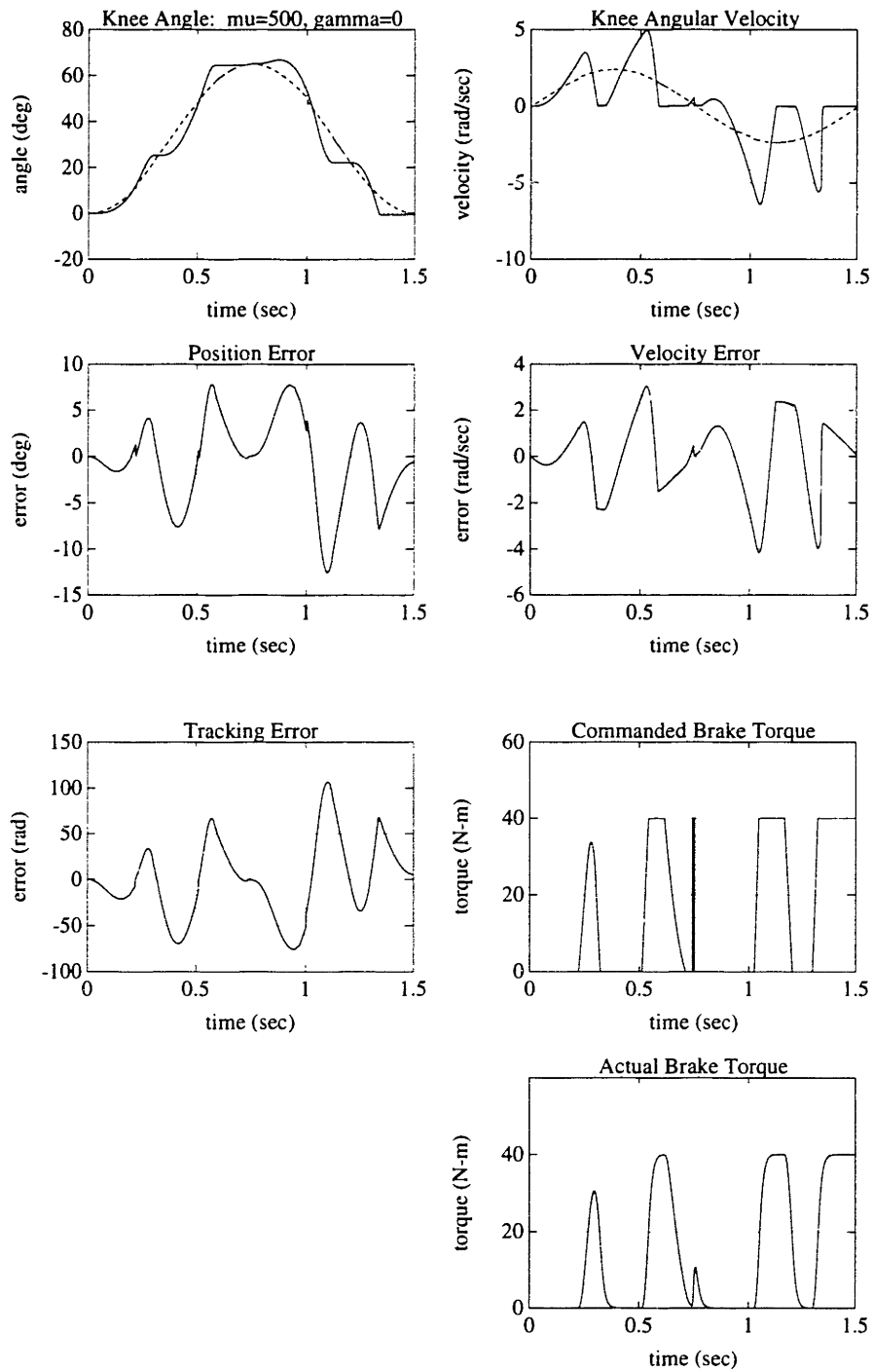
Figure 4-17: Simulation of knee joint behavior with a position feedback gain of 500 Nm/rad and no velocity feedback.
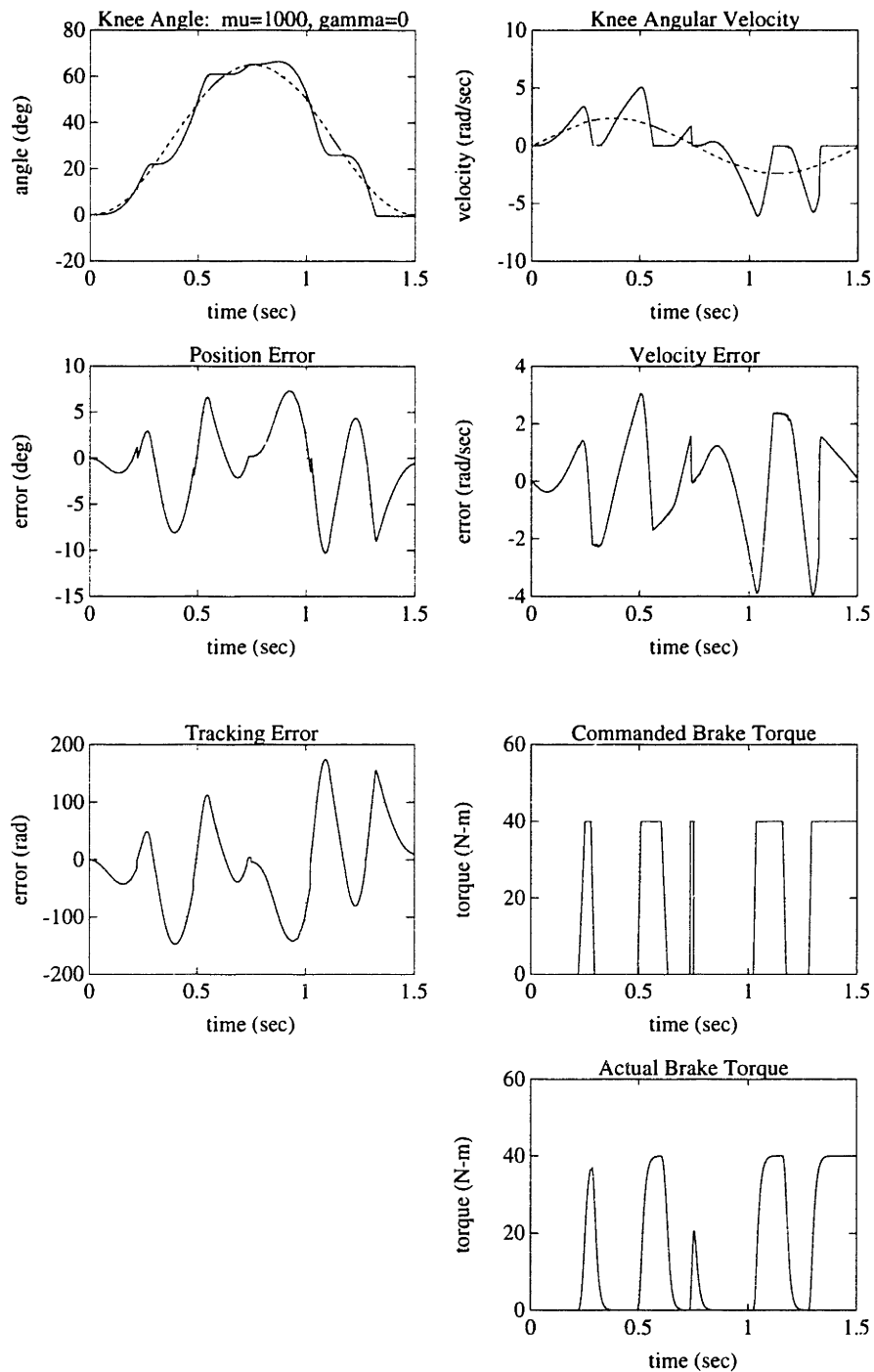
Figure 4-18: Simulation of knee joint behavior with a position feedback gain of 1000 Nm/rad and no velocity feedback. With this gain, the brake controller essentially behaves like a bang-bang controller, driving the particle brake into saturation at the smallest position error.
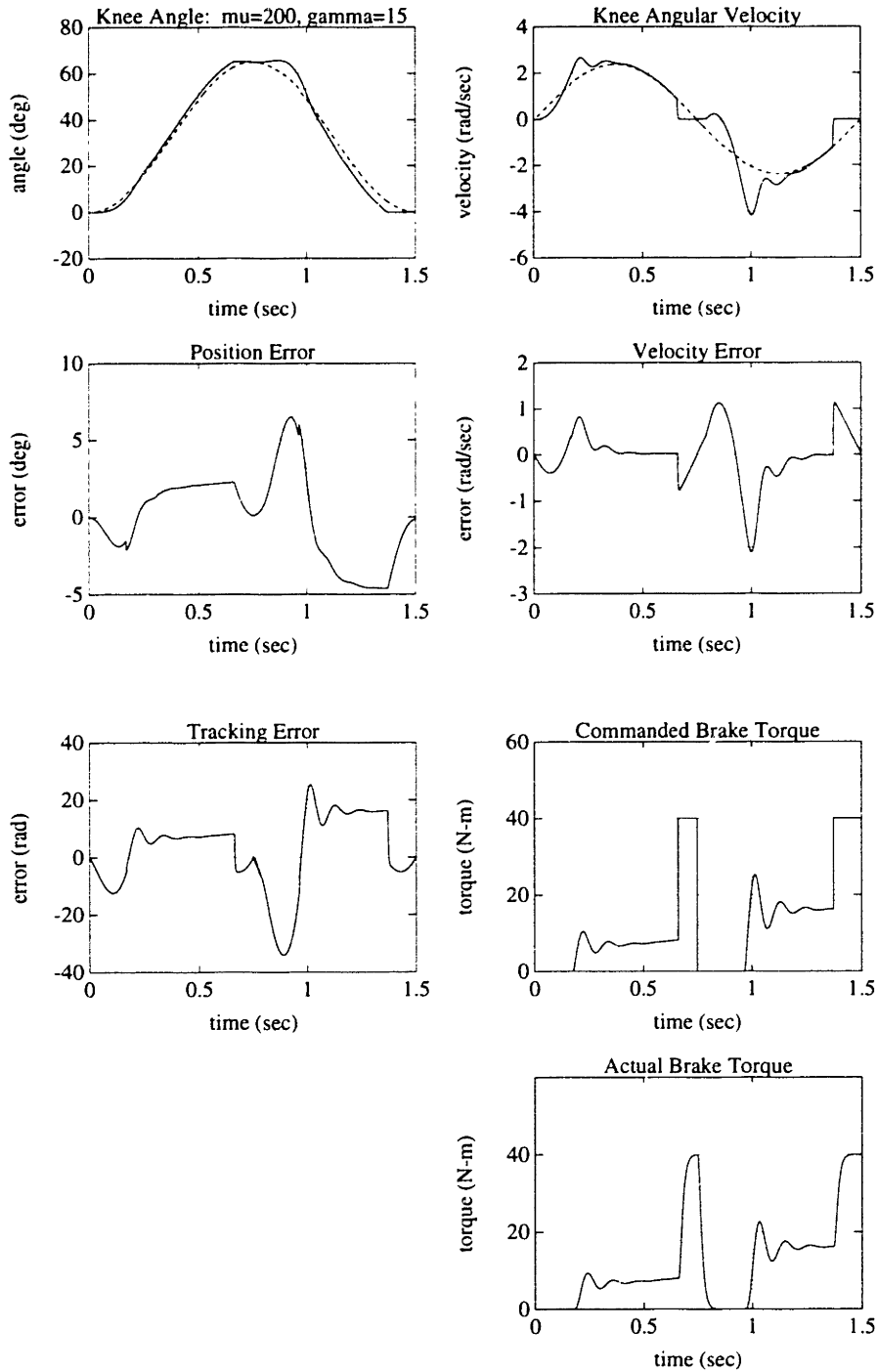
Figure 4-19: Simulation of knee joint behavior with appropriately selected position and velocity feedback gains (position is 200 Nm/rad and velocity is 15 Nm/rad/sec). Incorporating both the position and velocity components of feedback enables significantly better tracking performance.
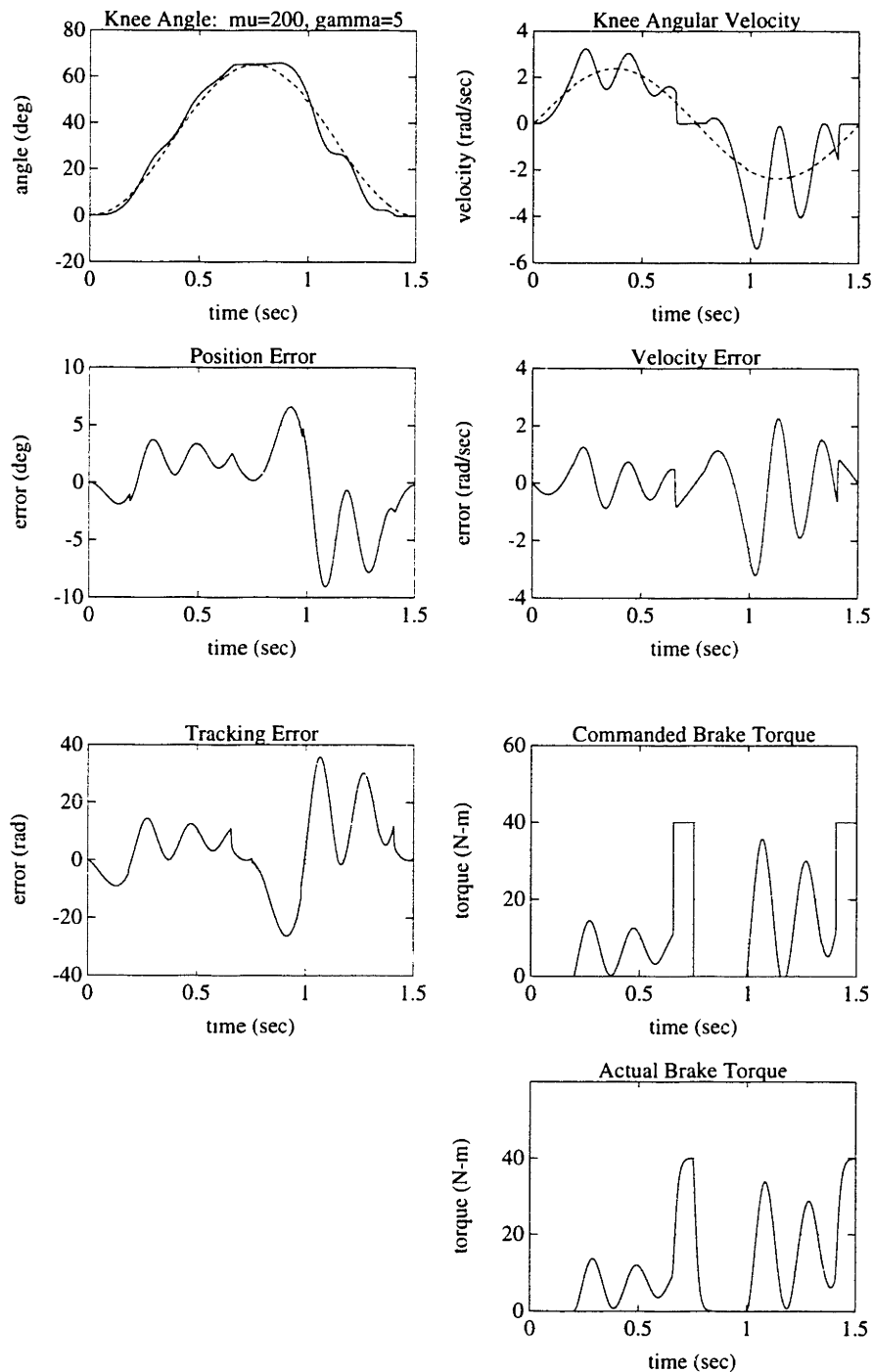
Figure 4-20: Simulation of knee joint behavior when the ratio of position gain to velocity gain is too low (position is 200 Nm/rad and velocity is 5 Nm/rad/sec). In this situation, the "spring-mass" dynamics of the limb and position loop dominate and the limb moves in a segmented fashion.
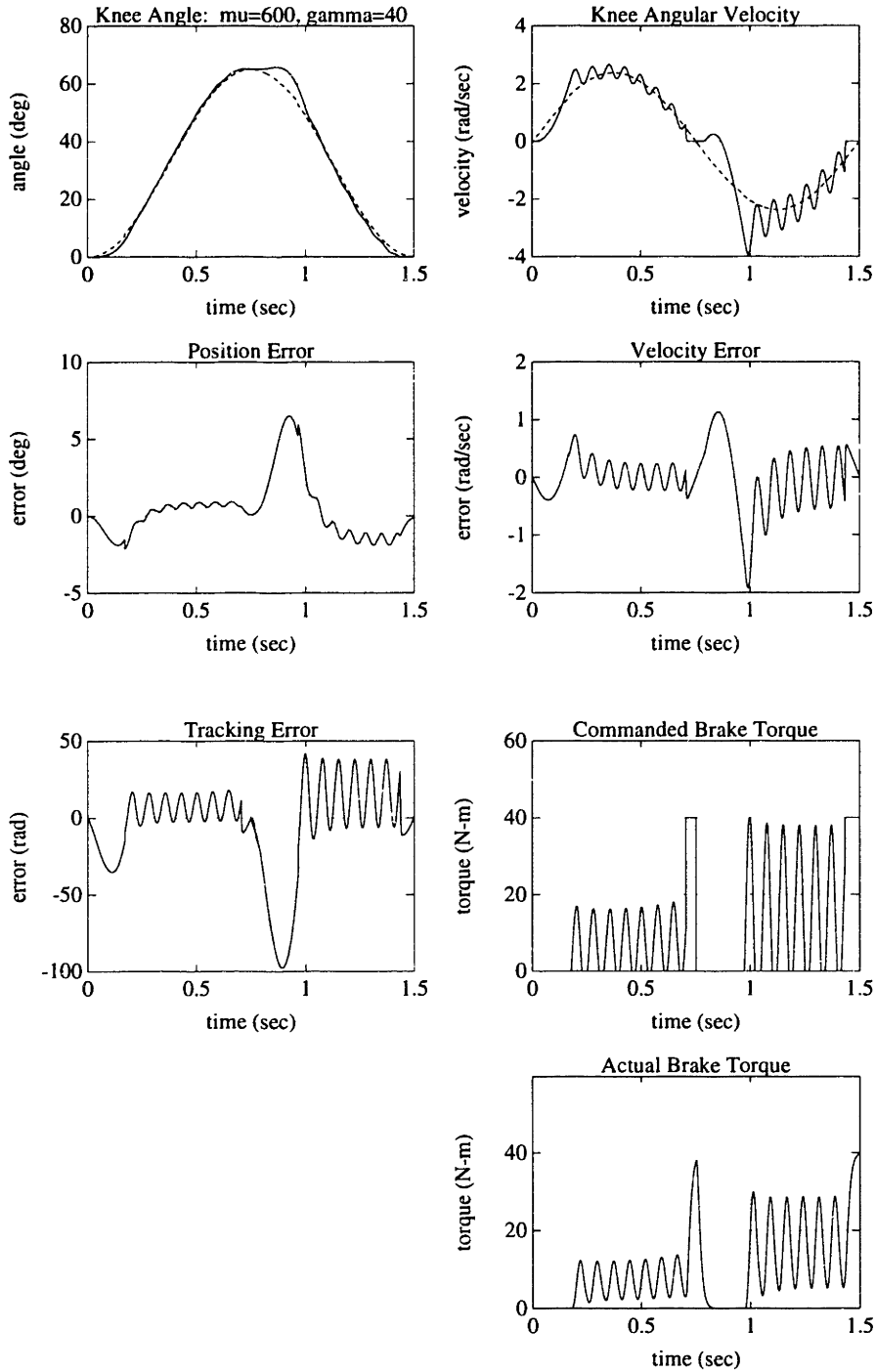
Figure 4-21: Simulation of knee joint behavior when the ratio of position gain to velocity gain is too high (position is 600 Nm/rad and velocity is 40 Nm/rad/sec). In this situation, the velocity gain cannot introduce enough damping to eliminate the low frequency oscillations without introducing high frequency chatter.

Figures 4-20 and 4-21 illustrate the trade-offs involved in selecting feedback gains. When the ratio of position gain to velocity gain is too low, the "spring-mass" dynamics of the limb and position loop dominate and the limb moves in a segmented fashion, as shown in Figure 4-20. When the position gain is too large, the velocity gain cannot introduce enough damping to eliminate the low frequency oscillations without introducing high frequency chatter, as shown in Figure 4-21.

When implementing the system on SCI individuals, gains are selected by first adjusting the position feedback gain to a level of moderate controller response. Then the velocity feedback gain is increased until the low frequency oscillations of the position trajectory are eliminated. If the magnitude of the velocity gain introduces chatter before the position segmentation is eliminated, the position gain must be decreased. If, on the other hand, the segmentation is easily smoothed and the particle brake is well out of the region of saturation, the position gain can be increased and the velocity gain adjusted accordingly.

4.3   Muscle Stimulation Level Control

4.3.1   Introduction

Though the controlled-brake system obviates the need for fine regulation of muscle torque, some level of coarse regulation is important for effective gait control. The joint angle trajectory control is only effective when the joint power provided by muscle stimulation is sufficient to maintain the desired trajectory. The purpose of the muscle stimulation level control is therefore to regulate muscle stimulation to provide adequate joint power. Though maintaining maximum stimulation would provide this function, needlessly high levels of stimulation would result in excessive joint torques that would entail unnecessary power dissipation and muscle fatigue. The appropriate level of stimulation will depend to a large extent on the state of muscle fatigue, which is an ill-known function of time and several other variables. The purpose of the stimulation level controller is to adjust the level of stimulation during gait so that the

90

muscle can provide adequate limb acceleration without enduring excessive fatigue.

4.3.2 Efferent vs. Afferent Pathways

The four stimulation channels utilized in conventional FES-aided gait are the right and left quadricep groups, which provide knee extension torques, and the right and left peroneal channels, which provide simultaneous knee and hip flexion torques. The quadriceps channels are activated through an efferent pathway. The stimulation current pulse excites action potentials in motor neurons which travel distally to induce a muscle contraction. The peroneal channels however are effected through an afferent pathway. Instead of reaching the target muscles directly through efferent neurons, the induced action potentials travel proximally through sensory neurons to the spinal cord, where they synapse with interneurons which in turn transmit motor neuron action potentials that induce muscle contraction. Regulation of the stimulation level for a given channel requires some knowledge of the relationship between muscle torque output and stimulation input. The fact that muscle torque output increases monotonically with stimulation pulse amplitude for efferent stimulation channels is sufficient information to control the quadriceps channel [38]. The input/output relationship for the peroneal channels however is not easily characterized. Although some efforts have been made to characterize the behaviour of the stimulated flexion withdrawal reflex, none has indicated a structure suitable for control [33, 34, 71].

4.3.3 Reflex Characterization

Figures 4-22, 4-23, and 4-24 show results for one subject from a cursory study of the flexion withdrawal reflex. In these tests, a T6 level paraplegic stood in place in parallel bars wearing the CBO. The CBO provided knee stability by locking the knee joint of the stance leg, so no quadriceps stimulation was necessary. The subject was instructed to place her weight on the stance leg, and a series of six flexion withdrawal reflexes were elicited through peroneal stimulation while standing in place, with 15 seconds rest between each. Joint position sensors on the CBO recorded the hip and

knee motion during each "step." The subject was then instructed to place her weight on the opposite leg, so that both legs could be tested. The subject alternated legs a total of six times, so that each leg received a total of 36 inputs. The inputs were of varying pulse widths, amplitudes, and freqencies, and were introduced in random order for a burst duration of 750 milliseconds.

The resulting data does not indicate any clear or consistent trends. Increasing the amplitude, pulse width, or frequency increases the response in some intervals and decreases it in others. A thorough characterization of the stimulated flexion withdrawal reflex would be quite involved and is not within the scope of this work. Without this characterization however the reflex stimulation level cannot be regulated. The peroneal stimulation is therefore set to a level that elicits a good response, then left unaltered. The stimulation level controller thus involves only the efferent (quadriceps) stimulation channels.

4.3.4 Controller Description

The stimulation controller is implemented on a step-by-step basis, with no attempt to regulate the level of stimulation within a single swing phase. Since muscle time variation is significantly slower than the duration of swing phase, and since the bandwidth of the magnetic particle brake is approximately an order of magnitude larger than that of stimulated muscle, real-time stimulation control is neither necessary nor effective. The stimulation level controller instead utilizes the integrated error filtered over a specified number of previous steps to adjust the level of muscle stimulation for the following step.

A block diagram of the stimulation level controller is shown in Figure 4-25. This controller utilizes two feedback components—one formed from the position tracking error and the other from torque command. The former component is utilized primarily to detect when stimulation level is too low, and the latter primarily when the level is too high. Both are necessary because of the nonlinear nature of the system. Position tracking error alone provides little information on excessive stimulation levels, while torque command information alone provides similarly little information
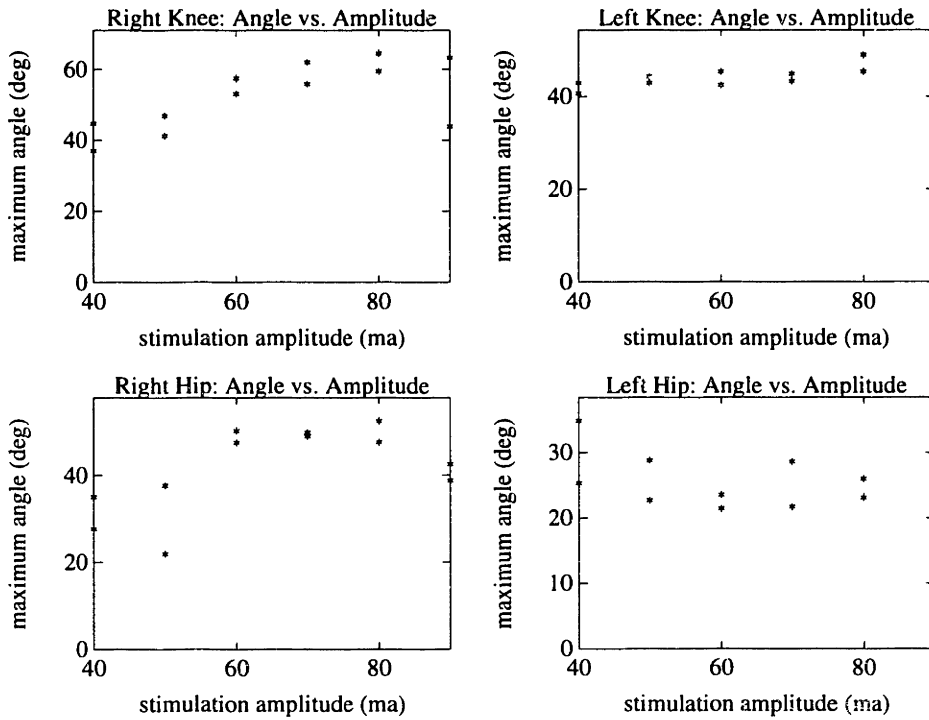
Figure 4-22: Effect of varying stimulation amplitude on the flexion withdrawal reflex. Each point represents the peak angle measured for a burst duration of 750 milliseconds, with stimulation pulses of varying amplitudes at a fixed pulse width of 350 microseconds and delivered at a frequency of 50 Hz.
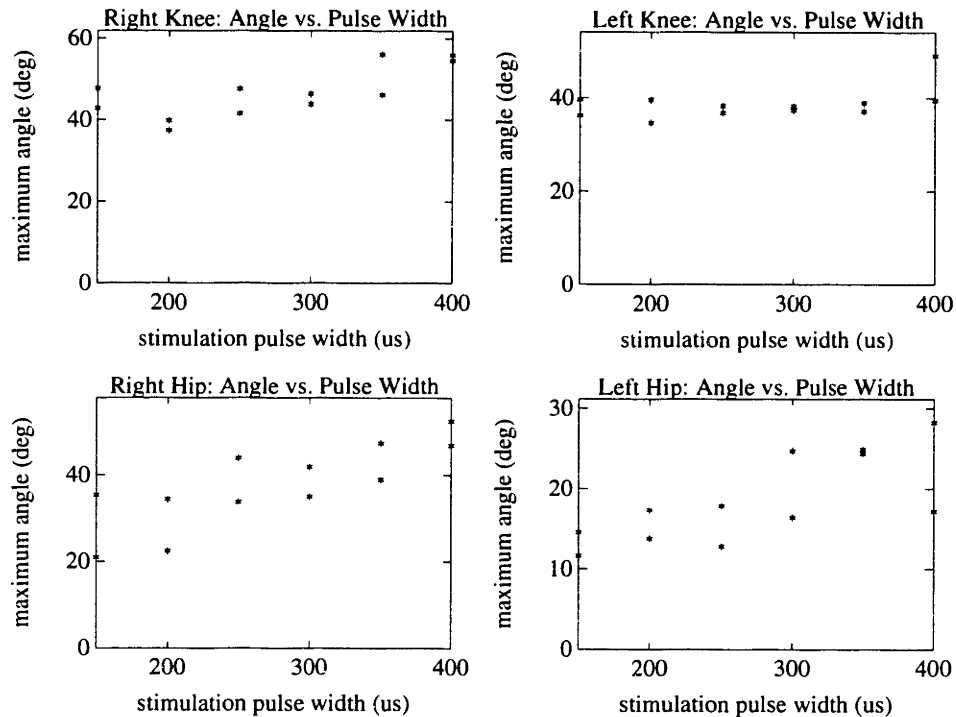
Figure 4-23: Effect of varying stimulation pulse width on the flexion withdrawal reflex. Each point represents the peak angle measured for a burst duration of 750 milliseconds, with stimulation pulses of varying widths at a fixed pulse amplitude of 60 milliamps and delivered at a frequency of 50 Hz.
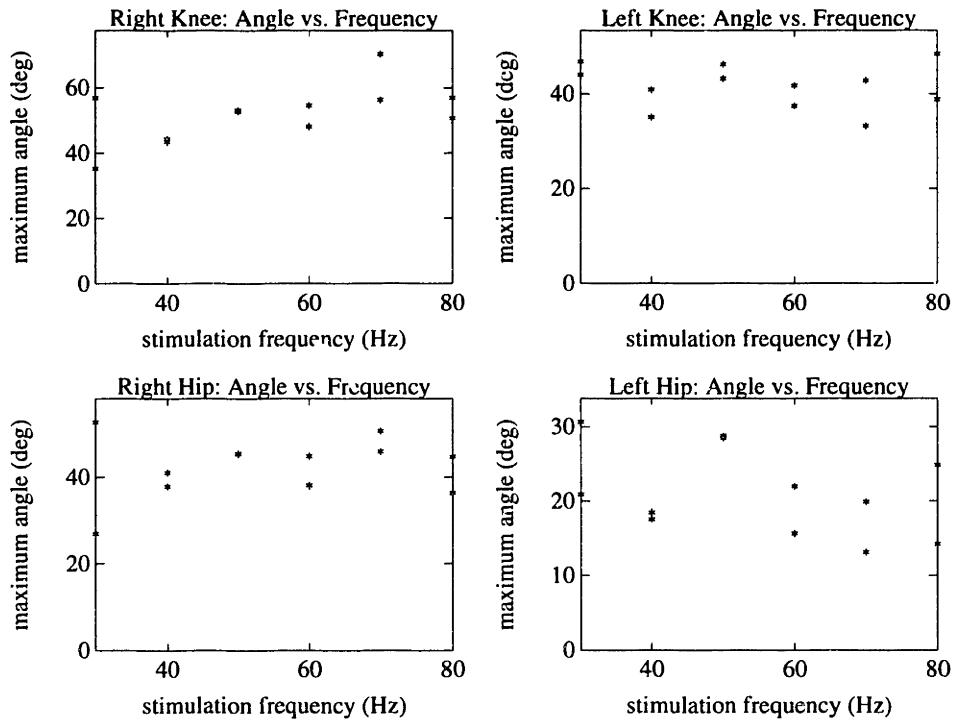
Figure 4-24: Effect of varying stimulation frequency on the flexion withdrawal reflex. Each point represents the peak angle measured for a burst duration of 750 milliseconds, with stimulation bursts delivered at varying frequencies at a fixed pulse amplitude of 60 milliamps and a fixed pulse width of 350 microseconds.
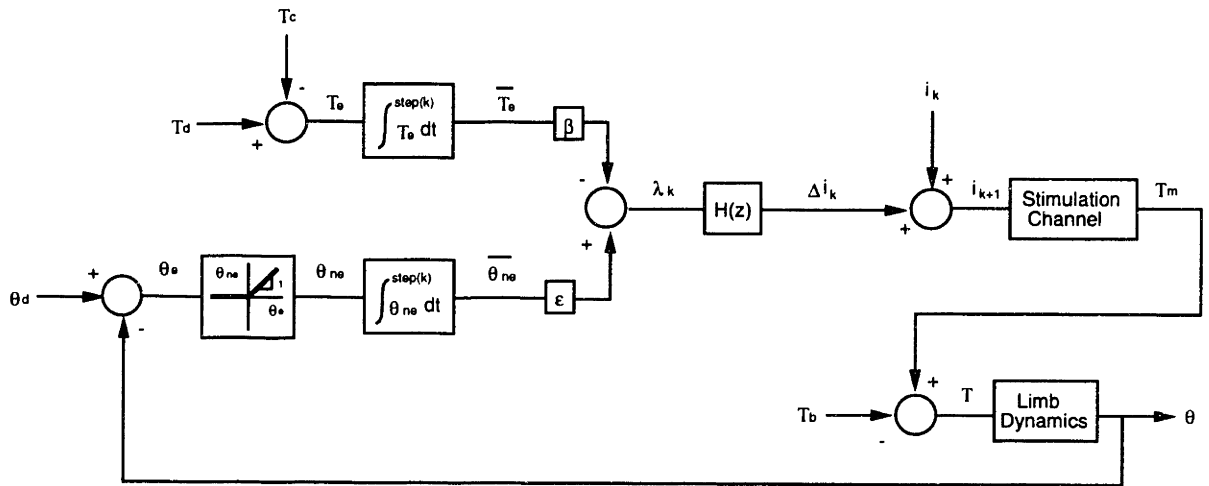
Figure 4-25: Block diagram illustrating muscle stimulation level control.

about insufficient levels of stimulation. The combination, however, constitutes an error signal that contains sufficient information to detect both regions of error.

The performance of the joint angle trajectory control is much more sensitive to errors in which the stimulation level is too low than to errors of excessive stimulation. When the stimulation level is too high, the system can maintain the desired trajectory by control of the brakes. When the stimulation level is too low the best the trajectory control system can do is turn off completely and let the uninhibited muscle torque accelerate the limb towards the desired trajectory. In order to isolate the region of error in which the stimulation level is too low, the position tracking error is half-wave rectified (represented in the block diagram by $\theta_{ne}(\theta_e)$). This "negative error" represents the region of motion during which the muscle torque is insufficient to produce an acceleration large enough to maintain the desired trajectory. The negative position error is averaged and discretized by integrating it over the duration of stimulated motion to form a signal representing the muscle torque insufficiency for each step.

The excessive muscle torque component of the error is represented by the torque command error. Maintaining the system in the region of brake control ($e > 0$)

requires that the brake maintain a non-zero torque for the duration of motion. The torque command "set point" is represented in the block diagram by the input T_d. The difference between this quantity and the actual torque command is the "torque command error," represented in the block diagram by T_e. A positive value indicates too little muscle torque; a negative value indicates too much. The positive values of torque command error saturate at the command set point (since command cannot be negative), and therefore this component has a limited ability to characterize low levels of muscle torque. Like the negative position error, this term is averaged and discretized by integrating it over the duration of motion of a step.

As shown in the block diagram, the total stimulation level error is a weighted difference of the position and torque error terms. If the integrated negative position error and the integrated torque command error for a given step are given by $\overline{\theta_{ne}}$ and $\overline{T_e}$ respectively, then the total stimulation level error for that step is

$$\lambda = \epsilon\,\overline{\theta_{ne}} - \beta\,\overline{T_e} \tag{4.23}$$

One limitation of the stimulation level controller is that it cannot explicitly detect disturbances. A foot scraping the ground or one leg rubbing against the other during swing phase can not be differentiated from a state of inadequate muscle torque. The disturbance provides an external dissipative torque about the joint, which results in an increase in negative position error and a corresponding decrease in brake command. Inadequate muscle torque due to insufficient muscle stimulation would provide a similar error condition. Since these disturbances occur relatively infrequently and at arbitary intervals, their effect can be diminished by low-pass filtering the stimulation level error to determine the desired change in stimulation level. The discrete-time low pass filter, represented in Figure 4-25 by the transfer function $H(z)$, weights the error terms from a specified number of previous steps with integer coefficients arranged in descending order. The transfer function of this discrete-time filter for n steps is given by

$$H\left(z\right) = \frac{\Delta I\left(z\right)}{\Lambda\left(z\right)} = \frac{A\left[n\,z^n + \left(n-1\right)z^{n-1} + \left(n-2\right)z^{n-2} + \cdots + z\right]}{0.5\,n\left(n+1\right)z^n}\,, \qquad (4.24)$$

which represents the difference equation

$$\Delta i_k = \left[\frac{A}{0.5\,n(n+1)}\right]\left[n\,\lambda_k + \left(n-1\right)\lambda_{k-1} + \left(n-2\right)\lambda_{k-2} + \cdots + \lambda_{k-n+1}\right] \qquad (4.25)$$

The stimulation level for the next step is the sum of the current level i_k and the computed change in stimulation Δi_k

$$i_{k+1} = i_k + \Delta i_k \qquad (4.26)$$

A feature not explicitly shown in the block diagram is the saturation of both the rate of change of stimulation, Δi_k, and the absolute stimulation level, i_k. Both are limited for purposes of safety.

4.3.5 Torque Command versus Brake Torque

Note that the stimulation controller utilizes the torque command, T_c, and not the brake torque, T_b, to compute the torque-based component of stimulation level error. Since the brake has a linear gain and a large bandwidth, and assuming the leg moves continuously for the duration of motion, the two signals should be approximately the same. Although the measured brake torque would provide the advantage of a more collocated control structure, it has the disadvantage of being corrupted by analog noise and distorted by sampling rate time delay and low-pass filtering. The torque command signal is preferred because it is discrete and does not possess the instrinsic noise or distortion associated with analog signals.
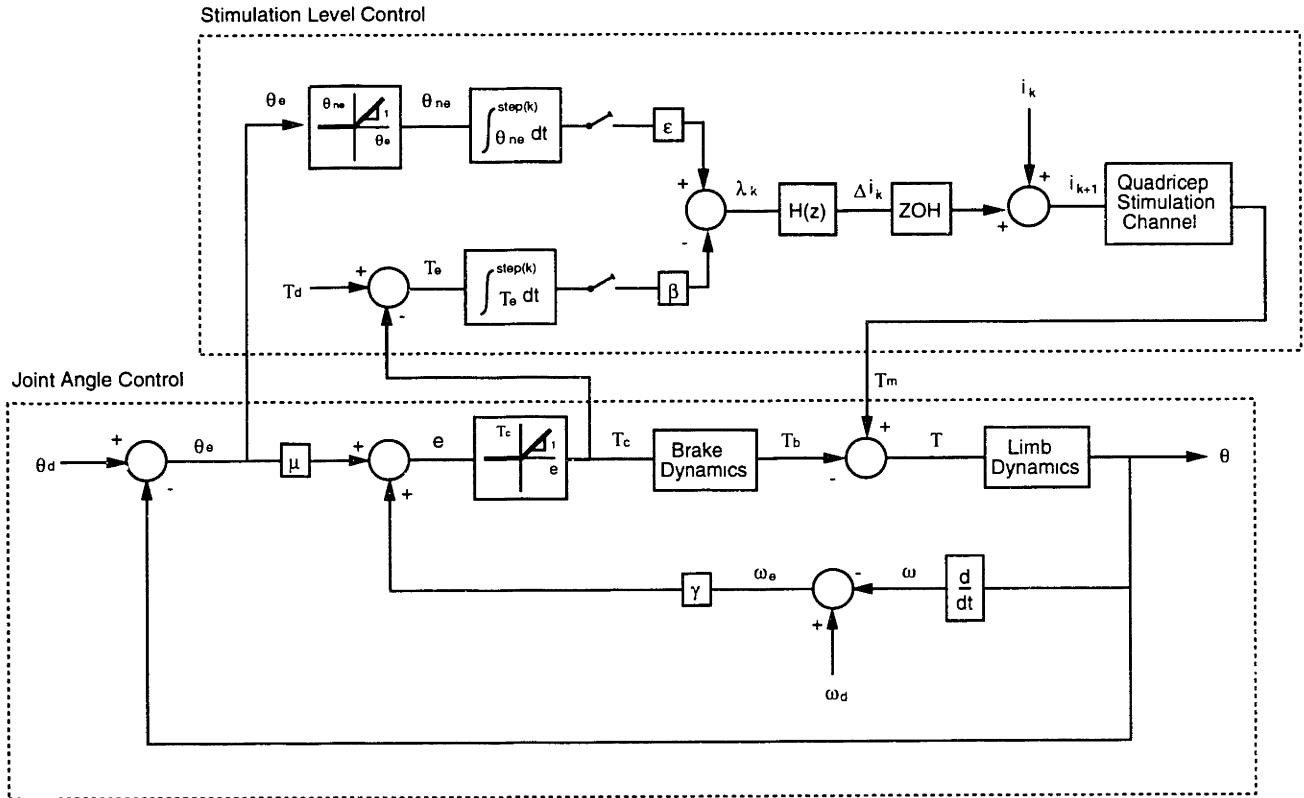
Figure 4-26: Block diagram illustrating the combined joint angle trajectory and muscle stimulation level control.

4.4 Coupling the Joint Angle and Stimulation Level Controllers

The combined joint angle trajectory control and muscle stimulation level control systems for knee extension are shown in Figure 4-26. Since the peroneal stimulation level is not regulated during flexion, control consists only of the joint angle trajectory control.

4.4.1 Movement Sequence

The function of the combined joint angle and stimulation level control is to regulate the motion of swing phase during CBO-controlled gait. The three controlled compo-

nents of the swing phase movement are knee flexion, knee extension, and hip flexion. Use of the flexion-withdrawal reflex via the peroneal stimulation channel elicits simultaneous hip and knee flexion, and therefore places constraints on the sequence of swing phase. Typical able-bodied swing phase movement consists of a phase of simultaneous hip and knee flexion, followed by a phase of continued hip flexion and simultaneous knee extension. Because hip and knee flexion are coupled in CBO-controlled gait, the hip cannot flex while the knee is extending. The resultant swing phase therefore begins with simultaneous hip and knee flexion, as in able-bodied swing phase, but cannot continue hip flexion during the knee extension phase. Instead, the controller behaves like a ratchet, locking the hip at full flexion while knee extension occurs.

4.5   Controller Hardware

The hardware for the CBO controller consists of a Northgate 33 MHz, 80386 computer, a four channel computer-controlled stimulator, CBO control electronics, and the CBO. A schematic of the system is shown in Figure 4-27. The computer, which functions as the system controller, is equipped with an Intel 80387 floating point numerical coprocessor, an Analog Devices RTI-815 I/O card for A/D conversion of brace sensors, and a Metrabyte DDA-06 I/O card, which has D/A conversion for particle brake control and digital output for stimulator control. The four channel computer-controlled stimulator was built specifically for the CBO system and is described and documented in Appendix C. The brace control electronics contain the servo-amplifiers utilized to drive the magnetic particle brakes and general signal processing for sensor inputs, including the analog differentiation circuits for deriving velocity and anti-aliasing filters. Documentation of the brace electronics, along with experimental data characterizing the major dynamic components, is provided in Appendix B.
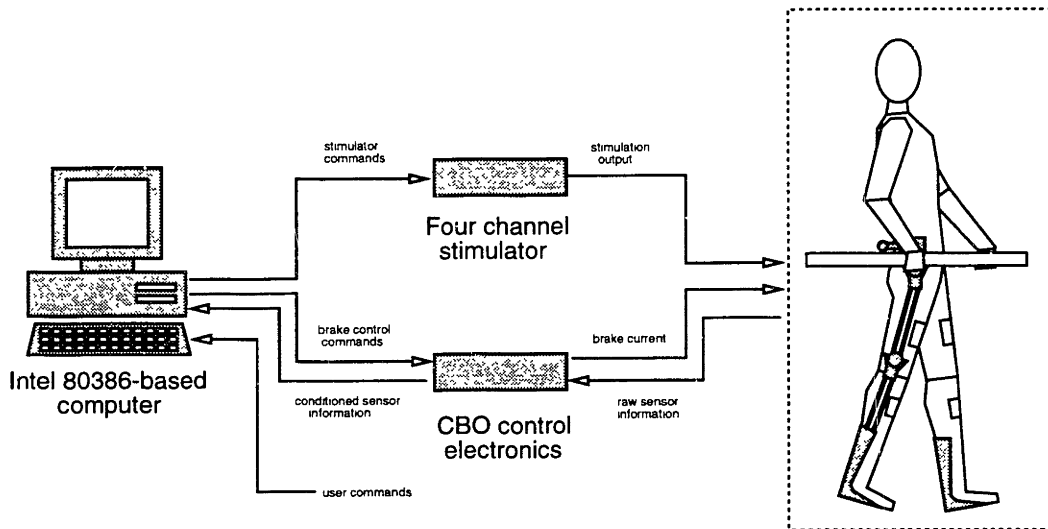
Figure 4-27: CBO control system hardware. A 386-based computer controls a four channel stimulator and interfaces with the CBO through controlling electronics. User commands such as left step, right step, stand, and sit are input through the computer keyboard.

Chapter 5

Clinical Evaluations

5.1 Experimental Methods

Clinical evaluations were conducted on a paraplegic subject to evaluate the performance of the CBO system with respect to conventional four channel FES-aided gait. The hybrid gait paradigm incorporating the CBO in conjunction with four channels of electrical stimulation is henceforth referred to as *CBO gait*. The conventional four channel FES paradigm is referred to as *FES gait*. So that the differences observed in the results of the evaluation could be accredited solely to the CBO, the CBO gait paradigm utilized the same four channels of stimulation used during FES gait.

All experiments were conducted in the Physical Therapy Clinic at the Brockton/West Roxbury Veterans Administration Medical Center. The clinic is equipped with a set of parallel bars approximately 6 meters (20 feet) in length. Experiments were conducted with three experimenters present: a physical therapist to record heart rate and blood pressure and to ensure medical safety, a computer operator to input system commands, and a data recorder for documenting information not collected by the computer. The subject was a 26 year old female, approximately two years post-injury, with a sensory and motor complete lesion. Photographs of the T6 level SCI subject walking in the controlled-brake orthosis and the experimental setup are shown in Figures 5-1 and 5-2.

The experimental protocol was designed to assess quadriceps muscle fatigue, swing
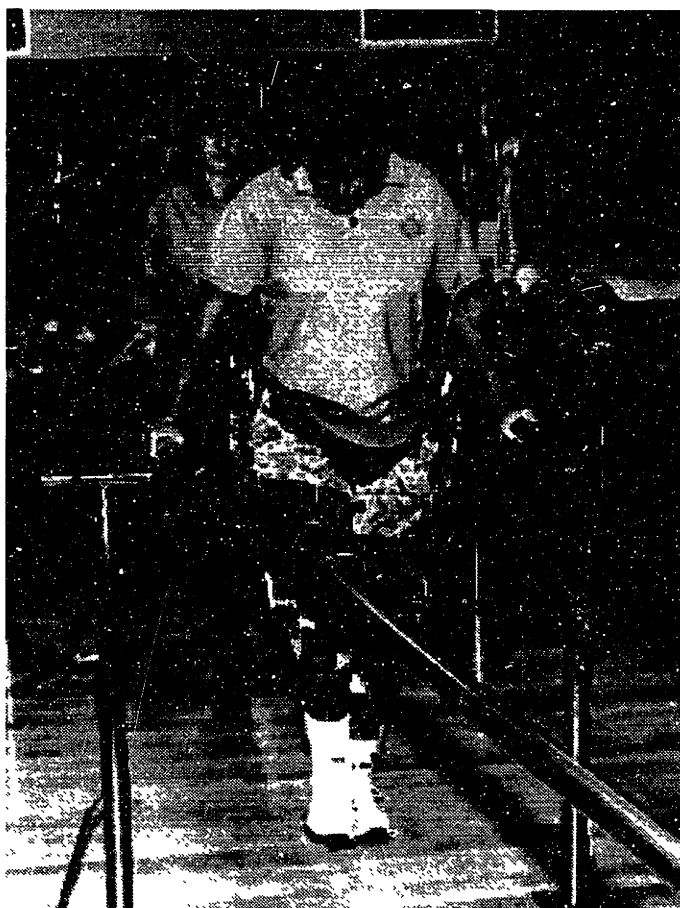
Figure 5-1: T6 level SCI subject walking in the CBO. A physical therapist, shown behind the subject, was always present at the experiments to monitor the subject and ensure safety.

Figure 5-2: The CBO experimental setup in the Physical Therapy Clinic of the Brockton/West Roxbury Veterans Administration Medical Center. The cart on the right side of the photograph is holding, from top to bottom, the computer-controlled four channel stimulator, the CBO control electronics, the Intel 386–based computer, the computer monitor and keyboard, and an uninterruptable power supply.

phase trajectory control, the general level of physical exertion, and typical gait speeds for both gait systems. Characterization of quadriceps muscle fatigue is based on the duty cycle of muscle stimulation and on measurement of isometric recruitment curves taken at discrete intervals, and the level of exertion is indicated by heart rate and blood pressure measurements, also taken at discrete intervals. The effectiveness of swing phase trajectory control is evaluated primarily by step-to-step variation in joint angle trajectories and in stride length.

The FES and CBO gait paradigms were presented on separate days to better isolate each system's performance. The experimental protocol was based on the subject's walking 10 meter (33 foot) increments, during which time the CBO would record information on joint angle trajectories, muscle stimulation, and particle brake control. The 10 meter distance consisted of one lap (two lengths) of the parallel bars, and thus was travelled in two 5 meter (16.5 foot) segments with a momentary pause to turn around between the two. Every 5 meter segment was timed to obtain average gait speeds. After every 10 meter increment, the subject would sit so that heart rate, blood pressure, and isometric recruitment curve measurements could be taken.

Standing, sitting, and right and left step commands were given vocally by the subject, which were in turn entered into the keyboard by the computer operator (see Figure 5-2). While walking, the subject would generally command the next step after she had shifted her weight from her trailing to her leading stance leg. After some practice trials, however, the subject chose to give control of step timing to the computer operator, since he could visually judge when she was ready for the next step.

5.1.1 The Isometric Recruitment Curve

The isometric recruitment curve (IRC), which was taken at regular distance increments during the gait sessions, represents the nonlinear static gain between stimulation level input and muscle force output. The simplest method of measuring the IRC is by administering a series of step inputs in muscle stimulation, and recording the steady state joint torque output for each (joint torque and muscle force are directly

proportional in the isometric case). This method, however, fatigues the muscles and typically requires several minutes for accurate measurement. A method for measuring the IRC which is significantly faster, non-fatiguing, repeatable, and computationally robust is the input-output cross-correlation technique developed by Beck and Durfee [12, 13]. In this method, the entire IRC is measured with a single stimulation input. The magnitude of this stimulation input varies as a single period of a low frequency cosine wave. The muscle force output has the same general shape, but lags the input due to the neuromuscular dynamics. Phase lag and time delay introduced by these dynamics are removed by cross-correlating the input and output, and shifting the output by the amount that corresponds to the peak of the correlation. The shifted output is then cross-plotted with the input and the rising and falling curves are averaged to obtain the IRC. Since the IRC is a function of muscle length, and since the rectus femoris (a major component of the quadriceps group) spans both the hip and knee joints, the joints must be positioned repeatably to obtain a repeatable measurement of the IRC.

The CBO conveniently provides all the necessary functions necessary for measuring the IRC. While the subject is sitting, the controller locks the brace joints at specified angles with the particle brakes, administers the appropriate stimulation input, and measures the resulting joint torques with the joint torque sensors. Specifically, the controller initially conditions the muscles with 5 seconds of stimulation at a moderate level, followed by a 5 second rest, then administers two separate cosine inputs, each with a period of 4 seconds, separated by 5 seconds of rest. The second cosine input, though redundant, is incorporated to ensure confidence in the measurement. The resulting IRC, which is an average of the two data sets, is thus measured in approximately 30 seconds, with only about 13 seconds of muscle stimulation.

Another condition for proper measurement is that the subject's legs must be unobstructed when recording torque. This function was provided during the clinical evaluations by a dentist's chair with a hydraulic lift that could easily and quickly be raised and lowered. The subject would sit in the chair, be hydraulically raised for IRC measurement, then lowered once again for standing.

5.1.2 Standing Time and Walking Distance

One of the primary motivations for design of the CBO system was to increase the standing time and walking distance capabilities of FES-aided gait. Although direct measurement of these quantities is scientifically attractive, measuring the limits of standing time and walking distance in a statistically meaningful manner presents significant safety issues. Placing an SCI subject in a situation of imminent collapse is unacceptable clinical practice. The distances chosen for gait evaluation were therefore set within a range that would avoid the possibility of collapse and so maintain the confidence and well-being of the subject.

5.1.3 The CBO and Data Collection

The orthosis was utilized in both CBO and FES gait as a data collection device to record joint angles during gait and measure the IRC at specified intervals. The brace was worn during both FES and CBO gait. The evaluation is slightly biased by hindering FES gait with what is effectively a substantial goniometer. Although the effect of the added inertia and friction of the brace was not quantified, visual observation of many trials indicated that the low rotational inertia and joint friction of the CBO had an insignificant effect on FES gait dynamics.

5.1.4 Heart Rate as a Measure of Work

The level of overall physical exertion was measured by monitoring the subject's heart rate during the gait sessions. There is generally a linear relationship between O_2 uptake and heart rate, so that heart rate may be used to reliably estimate work load[1] [3, 101].

---

[1] This linear relationship does not generally hold for diseased hearts, but physiological experiments have verified that the relationship between O_2 uptake and heart rate is still monotonic. Therefore, even in the case of a diseased heart, the heart rate is indicative of work load.

5.1.5 Evaluation Protocol

Appropriate distances for the SCI subject were determined to be 30 meters with FES gait and 50 meters with CBO gait (not including the 10 meter warm-up lap). Total sitting time between each 10 meter interval was 3 minutes, with the cardiovascular measurements occuring immediately after sitting and the IRC measurement occuring 1 minute and 30 seconds after sitting. The specific evaluation protocol was as follows:

Leg Lifts. Subject performs five leg lifts while sitting to warm up the quadricep muscles and loosen the knee joint.

Cardiovascular Measurements. Measure resting heart rate (ten second count) and resting systolic and diastolic blood pressure.

IRC Measurement. Raise hydraulic chair and take IRC.

Warm-up Lap. 10 meter warm-up walk. During this lap, the CBO locks the knee joints so that the quadriceps group need not be stimulated during stance, but does not impose trajectory control during swing. The warm-up lap has several purposes: to warm-up the muscles, test placement of the electrodes, test the quality of the reflex, and observe if the brace is obstructing motion. Upon completion of the warm-up lap, the subject sits to enable cardiovascular and IRC measurement.

Cardiovascular Measurements. Measure heart rate and blood pressure.

IRC Measurement. Raise hydraulic chair and take IRC. Since the quadriceps are warmed up but not fatigued, this measurement is considered the baseline IRC.

Gait Lap. Stand and walk 10 meters with either FES or CBO gait, depending on the selected paradigm. Each 5 meter segment is timed to obtain average gait speed. Upon completion of lap, the subject sits to enable cardiovascular and IRC measurement.

Cardiovascular Measurements. Measure heart rate and blood pressure.

IRC Measurement. Raise hydraulic chair and take IRC.

Repeat. Repeat the previous three steps for two more times for FES gait and four more times for CBO gait.

5.2 Evaluation Results

Three sets of data were taken for both FES and CBO gait. The complete data from these six days are included in Appendix A.

5.2.1 Muscle Fatigue

Figure 5-3 shows a typical record of stimulation for several steps taken with conventional four channel FES gait. The quadriceps muscle group, which is responsible for maintaining knee extension during stance, is stimulated approximately 87 percent of the time, as shown in the middle two plots of Figure 5-3. Figure 5-4 shows a typical record for similar steps taken while using the CBO. Since the CBO provides the isometric knee torques necessary to hold the body upright during stance, the quadriceps group need only be stimulated for knee extension during swing phase, and thus is stimulated only about 12 percent of the time. It should be noted that the stimulation duty cycles, though typical of the data for continuous walking, are a strong function of the ratio of stance phase to swing phase. For example, increasing the standing time between steps would significantly increase the quadricep duty cycle during FES gait, while decreasing the duty cycle during CBO gait.

Figure 5-5 shows a typical series of normalized quadricep isometric recruitment curves taken during a session of FES gait. (See Appendix A for data from other sessions). All IRC's in the plot are normalized to the reference IRC which was taken just after the warm-up lap. Every successive 10 meter lap results in muscle degeneration, until after 30 meters, the peak joint torque is approximately 30 percent of the original. In addition to the degeneration in peak torque, each successive IRC exhibits a small increase in stimulation threshold, which is also characteristic of fatiguing muscle. Figure 5-6 shows a typical series of normalized quadricep IRC's taken during a session of CBO gait, again normalized to the post warm-up IRC. (See Appendix A for data from other sessions.) Since the CBO provides the isometric torques necessary during stance, the quadriceps group remains strong, and even after 50 meters exhibits very little evidence of fatigue, both in the level of peak force and the consistency in

110
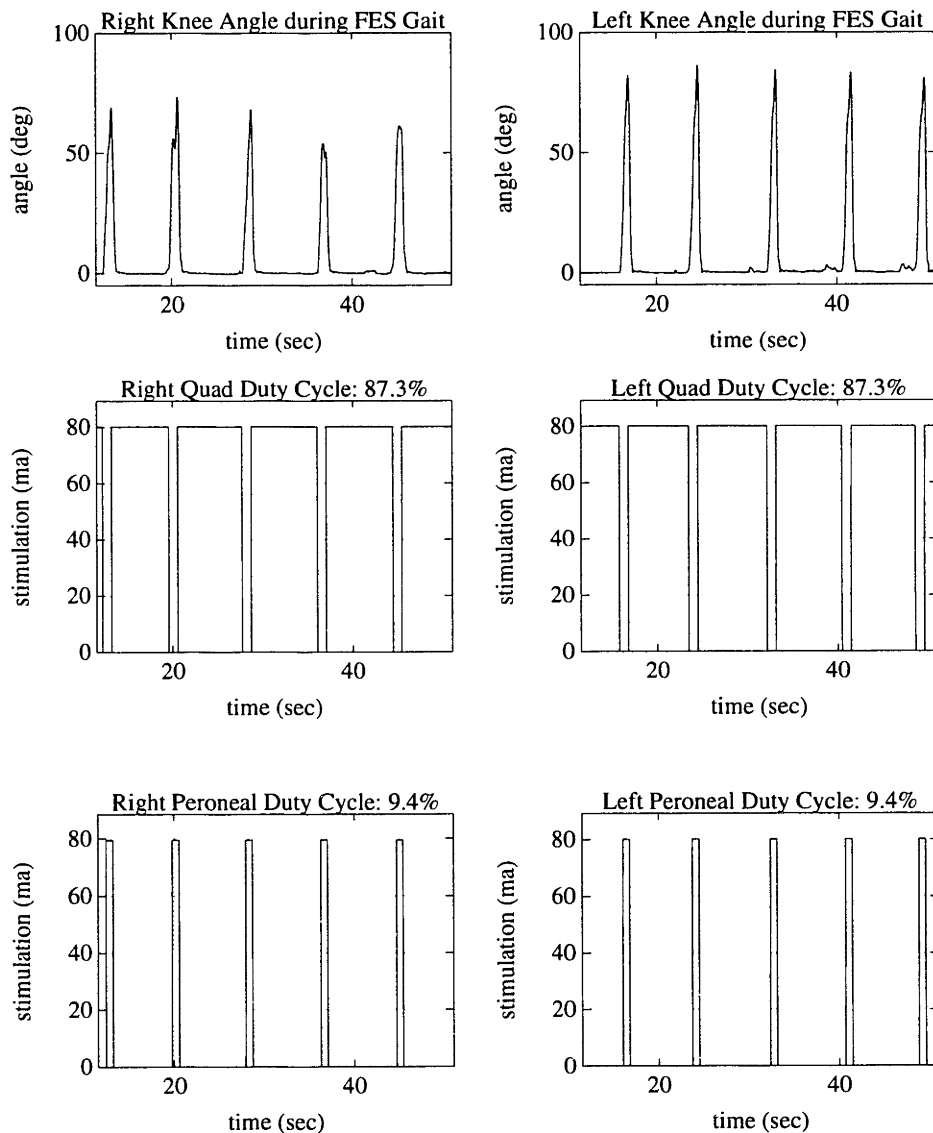
Figure 5-3: Typical record of stimulation duty cycle for continuous walking during FES gait. The plots show the knee angles, the quadricep stimulation duty cycles, and the peroneal stimulation duty cycles for the left and right legs for a total of ten steps (five for each leg). The stimulation plots represent the envelope of stimulation amplitude. (The actual stimulation waveform is not continuous). The quadriceps muscle group, responsible for maintaining knee extension during stance, is stimulated approximately 87 percent of the time.
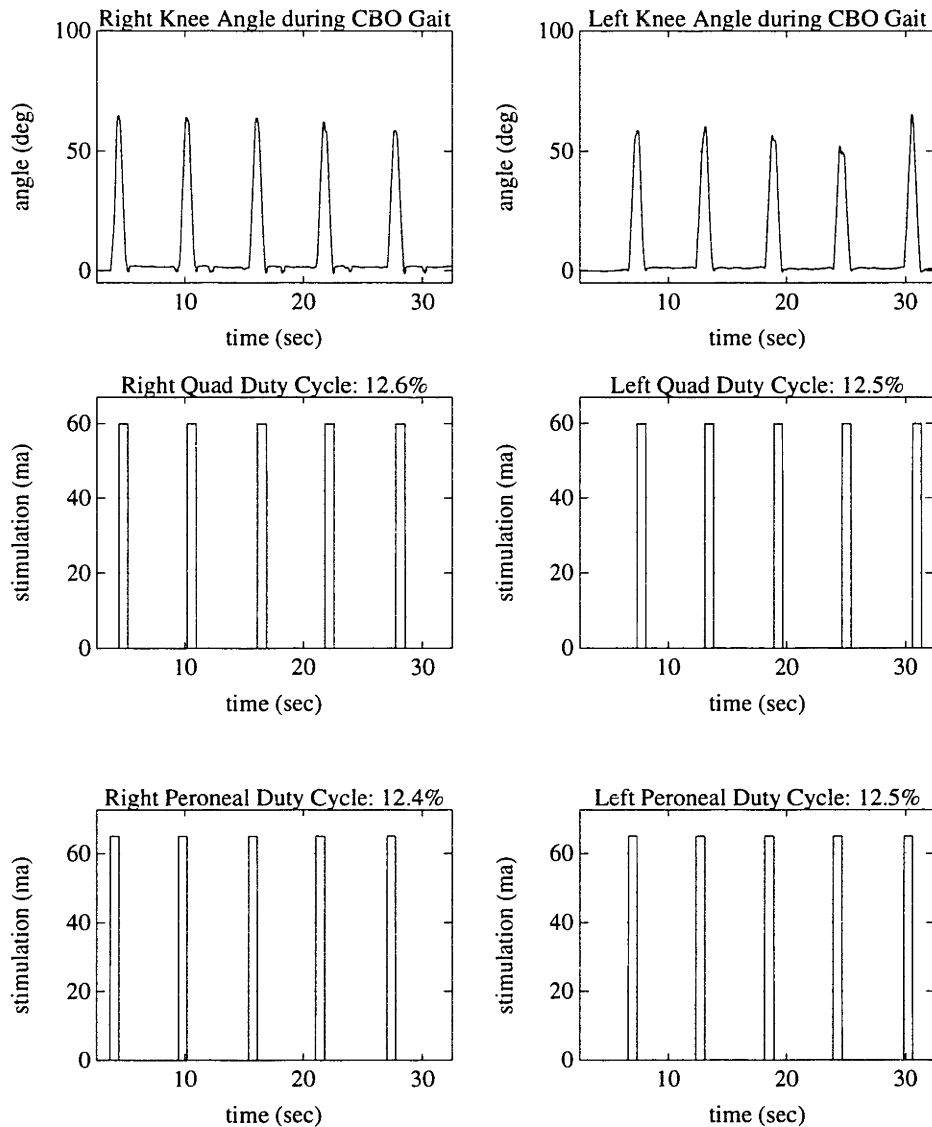
Figure 5-4: Typical record of stimulation duty cycle for continuous walking during CBO gait. The plots show the knee angles, the quadricep stimulation duty cycles, and the peroneal stimulation duty cycles for a total of ten steps. Since the CBO provides the isometric knee torques necessary to hold the body upright during stance, the quadriceps need only be stimulated for knee extension during swing phase, and thus are stimulated only about 12 percent of the time.

112
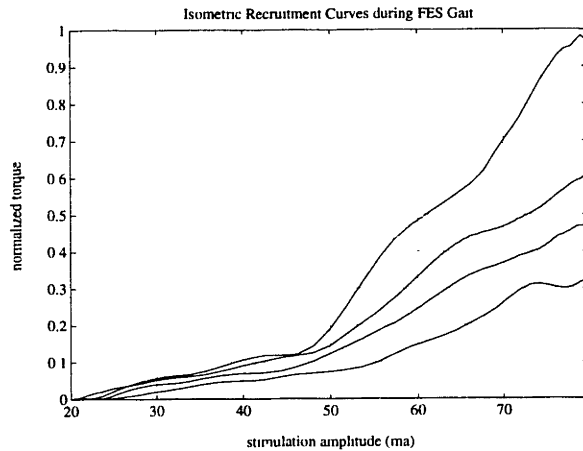
Figure 5-5: Typical set of isometric recruitment curves taken during an FES gait session. The curves, in order of descending slope, were taken after successive 10 meter intervals of walking with FES gait, for a total of 30 meters. The torque is normalized to the maximum torque measured just after the warm-up lap. Notice that after 30 meters, the peak quadricep torque has degenerated to 30 percent of the original.
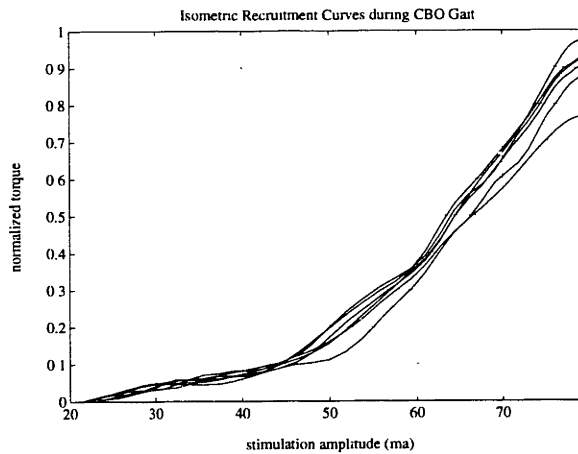
Figure 5-6: Typical set of isometric recruitment curves taken during a CBO gait session. The curves were taken after successive 10 meter intervals of walking with CBO gait, for a total of 50 meters. Since the CBO provides the isometric torques necessary during stance, the quadriceps group remains strong, and even after 50 meters exhibits very little deterioration.

threshold.

The contrast in muscle fatigue between with FES and CBO gait is illustrated in Figure 5-7, which compares the peak knee torque as a function of distance for the data shown in Figures 5-5 and 5-6.

5.2.2 Exertion

Figure 5-8 shows a typical record of heart rate as a function of distance during an FES gait session (other data given in Appendix A). Figure 5-9 shows similar data for a typical CBO gait session. The subject's resting heart rate across all data sessions was relatively constant, generally 66–72 beats per minute. During FES gait, the heart rate consistently climbed to 135–140 beats per minute, while during CBO gait the maximum heart rate rose to 110–115 beats per minute. The heart rate data indicates that CBO gait was less taxing than walking with FES alone.

Blood pressures were not significantly different between the FES and CBO gait sessions (see Appendix A for data).
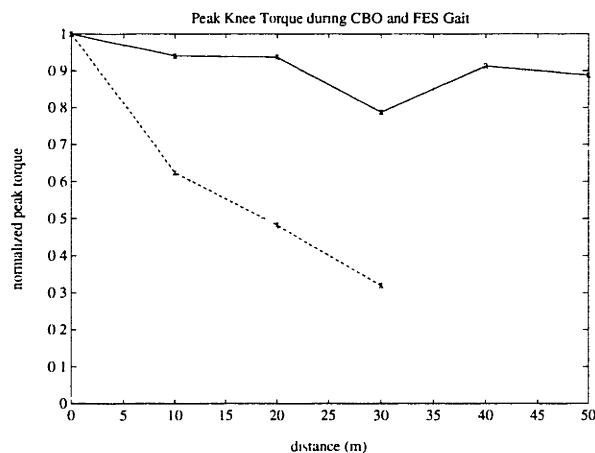
Figure 5-7: Peak knee torque as a function of distance walked for both CBO (solid line) and FES (dashed line) gait. The x-marks represent data points. The relatively high duty cycle required by FES gait results in rapid quadriceps fatigue. Since the CBO provides the isometric torques necessary during stance, the quadriceps group remains strong, and even after 50 meters of walking can produce almost 90 percent of the original knee torque.

Heart Rate during FES Gait
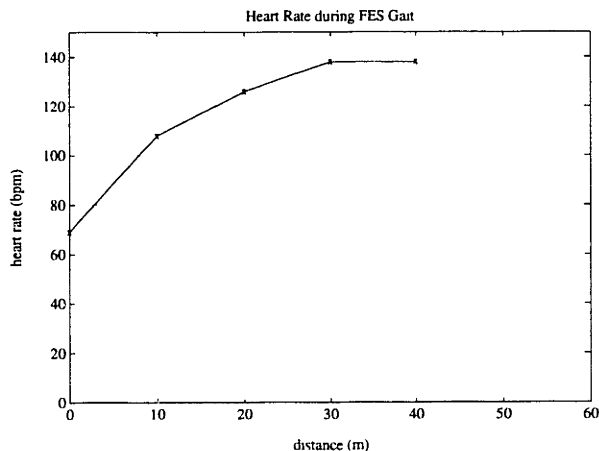
Figure 5-8: Typical heart rate data during an FES gait session. The x-marks represent data points. The subject's heart rate consistently climbed to approximately 135–140 beats per minute.

Heart Rate during CBO Gait
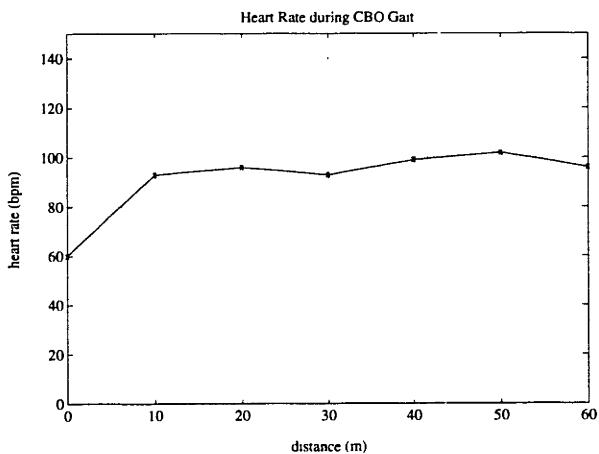
Figure 5-9: Typical heart rate data during a CBO gait session. The x-marks represent data points. The subject's heart rate consistently rose to approximately 110–115 beats per minute, indicating a significantly lower level of exertion than during FES gait.

5.2.3 Trajectory Control

Figures 5-10 and 5-12 show overlays of knee and hip joint angle trajectories for 50 steps taken from the three FES gait sessions. Figures 5-11 and 5-13 show the same for the three CBO gait sessions. The plots illustrate improvement in step trajectory repeatibility when using the brace. As indicated by the plots, the variation present in the CBO gait joint angle trajectories is due to cases in which the joint power provided by muscle stimulation was inadequate. Given sufficient power, the variation in the joint angle swing phase trajectories would be significantly smaller than those obtained. When the joint power is insufficient, however, the dissipative controller is ineffective. This lack of power is particularly apparent in the steps for which the flexion withdrawal reflex was too weak to achieve full knee flexion. In fact, the lack of power and the day-to-day inconsistency of the flexion withdrawal reflex is probably the primary weakness of both FES and CBO gait. Though the CBO can address many of the problems associated with FES gait, it cannot compensate for insufficient joint power.

As indicated by the relative variation between Figures 5-11 and 5-13, hip control with the CBO is a more difficult task than knee control. The knee controller regulates both knee flexion and extension, and thus can control knee position for the entire gait cycle. The hip controller, however, regulates hip flexion only. Hip extension, which occurs during stance phase, is effected primarily by the individual's upper body. Since the hip controller regulates hip motion for only half of the gait cycle, nearly every swing phase hip trajectory begins with an initial tracking error. Since the controller can only remove power from the joint, it is limited in its ability to drive the error to zero, and instead must wait for the system to arrive in a region of the trajectory where it can impose effective control.

Observe in Figure 5-12 that during FES gait the hip typically exhibits excessive flexion, then falls back as the leg drops due to gravity, resulting in a form of gait that resembles marching. As shown in Figure 5-13, the CBO locks the hip joint at full flexion, yielding larger step lengths and giving the SCI individual a more able-bodied gait appearance.
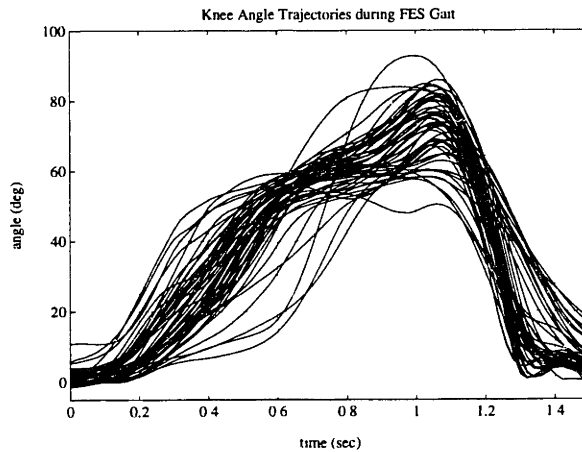
Figure 5-10: Knee angle during swing phase for 50 steps taken during the FES gait sessions.
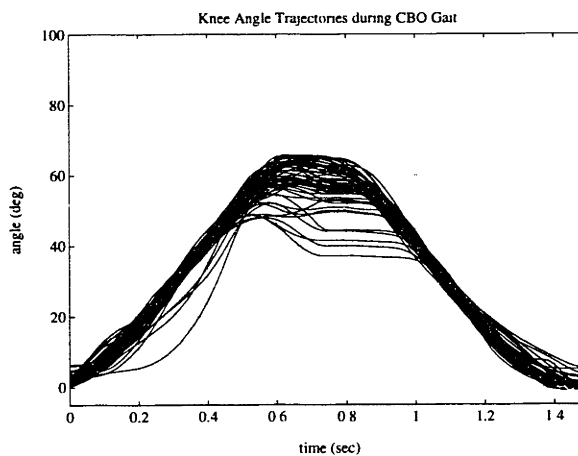
Figure 5-11: Knee angle during swing phase for 50 steps taken during the CBO gait sessions. Though trajectory repeatability is improved, the effectiveness of the CBO is limited to regions in which muscle stimulation provides sufficient joint torque.
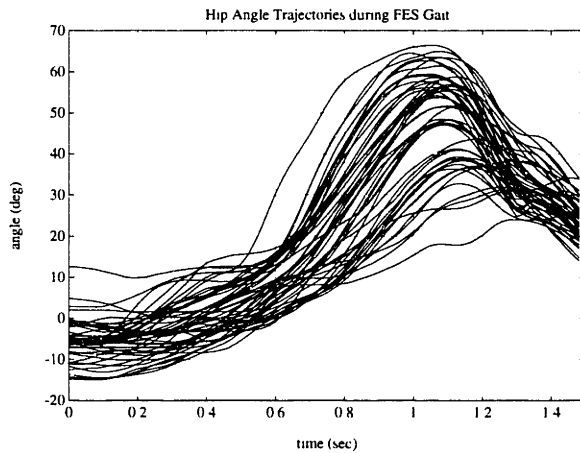
Figure 5-12: Hip angle during swing phase for 50 steps taken during the FES gait sessions. The hip typically exhibits excessive flexion, then falls back as the leg drops due to gravity, resulting in a form of gait that resembles marching.
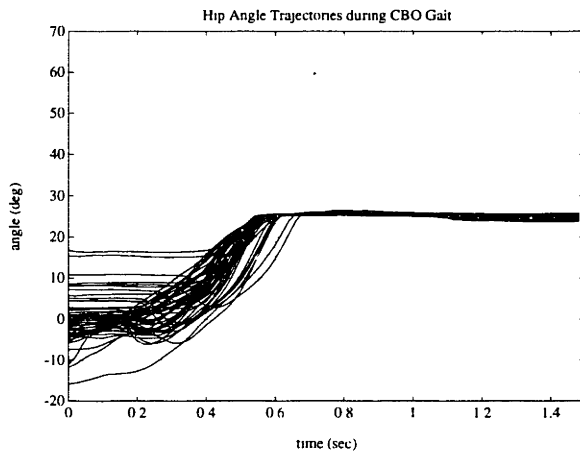
Figure 5-13: Hip angle during swing phase for 50 steps taken during the CBO gait sessions. Locking the hip at full flexion yields a larger step length and gives the SCI individual a more able-bodied gait appearance. Since the hip controller regulates hip motion for only half of the gait cycle, nearly every swing phase hip trajectory begins with an initial tracking error.
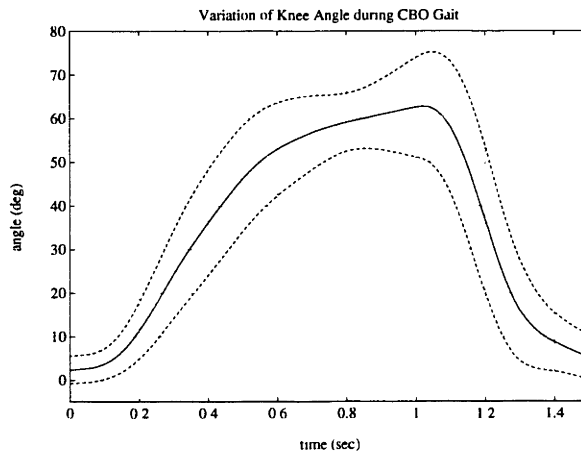
Figure 5-14: The mean trajectory (solid line) and one standard deviation on either side (dashed line) of the swing phase knee angle for all the steps taken during the FES gait sessions (a total of 235 steps).
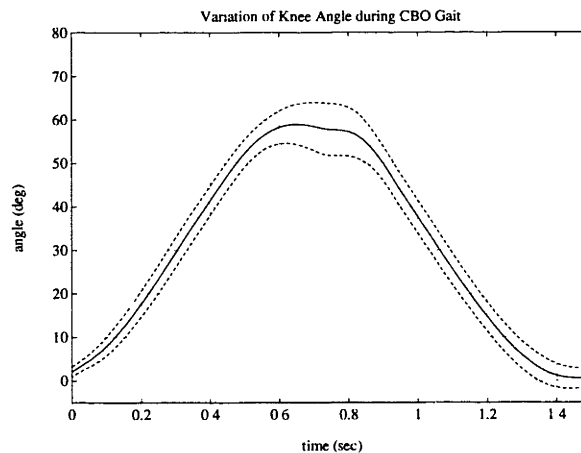
Figure 5-15: The mean trajectory (solid line) and one standard deviation on either side (dashed line) of the swing phase knee angle for all the steps taken during the CBO gait sessions (a total of 453 steps). Notice that the repeatability is quite good in the regions of sufficient joint power, but is noticeably worse in the region of maximum flexion where the joint power provided by the muscles is often inadequate.
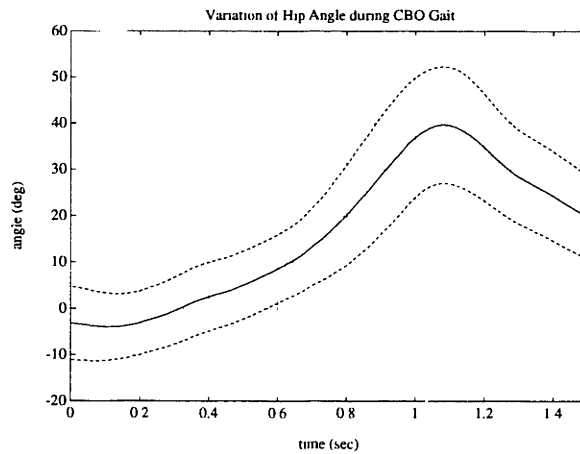
Figure 5-16: The mean trajectory (solid line) and one standard deviation on either side (dashed line) of the swing phase hip angle for all the steps taken during the FES gait sessions (a total of 235 steps).
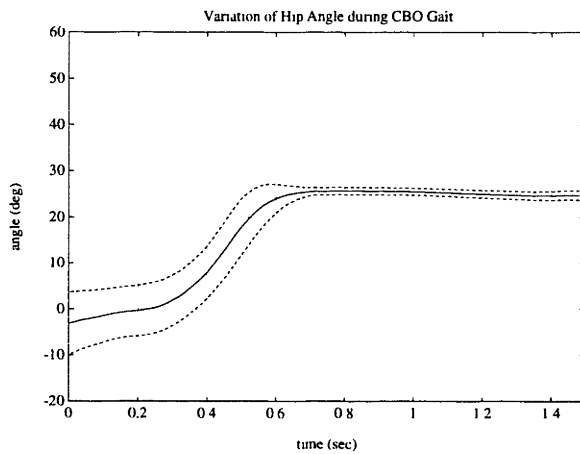
Figure 5-17: The mean trajectory (solid line) and one standard deviation on either side (dashed line) of the swing phase hip angle for all the steps taken during the CBO gait sessions (a total of 453 steps). Since the hip controller regulates hip motion for only half of the gait cycle, nearly every swing phase hip trajectory begins with an initial tracking error. Since the controller can only remove power from the joint, it is limited in its ability to quickly drive away this error, and instead must wait for the system to arrive in the region of the trajectory before it can impose effective control.

Figures 5-14 and 5-16 show the mean trajectory and a standard deviation on each side of the mean for the knee and hip angles of all the steps taken during the FES gait sessions (a total of 235 steps). Figures 5-15 and 5-17 show the same for all the steps taken during the CBO gait sessions (a total of 457 steps).

Stride length, which is formally defined as the distance travelled along the line of progression from initial contact of one foot to the next initial contact of the same, was computed for all strides taken during the gait sessions. Since the CBO can only record kinematic information about hip and knee flexion and extension, the computation is restricted to *approximate* stride length, subject to the assumptions that (1) pelvic rotation can be neglected and (2) ankle stiffness can be neglected. The resulting value represents the net change in hip angle for two successive steps and even without the stride length assumptions, is indicative of the step size. For the three days of FES gait in which the subject walked a total of 90 meters and took 60 successive strides [2], the mean (approximate) stride length was 70 centimeters (27.5 inches) with a standard deviation of 22 centimeters (8.5 inches). For the three days of CBO gait, the subject walked a total of 150 meters and took 141 successive strides, with a mean (approximate) stride length of 82 centimeters (32 inches) and a standard deviation of 19 centimeters (7.5 inches). The CBO therefore increases the average stride length by 17 percent. These stride length calculations are represented by the graph in Figure 5-18. As indicated by this data, the CBO serves to increase stride length by acting as a ratchet at the hip, thus preventing the reversal of hip motion that is characteristic of FES gait. The trajectory control imposed by the brace also helps decrease the stride length variation. Since the computed stride length is solely a function of hip angle, and since hip motion is controlled for only half the gait cycle, the CBO is limited in its ability to diminish stride length variability. Though hip motion is consistently locked at the specified angle of flexion, the fact that it starts every swing phase at a somewhat arbitrary position contributes significantly to stride length variation.

---

[2]For these calculations, a stride is defined as a right step following by a left step. Steps separated by turning around do not constitute a stride.

The average gait velocity was measured by timing each five meter increment. The subject was not given any instructions relating to gait speed, and thus proceeded at a comfortable pace. For the three days of FES gait in which the subject walked a total of 90 meters, the average gait speed was 0.092 m/s (18.1 ft/min) with a standard deviation of 0.016 m/s (3.15 ft/min). For the three days of CBO gait, the subject walked a total of 150 meters with an average gait velocity of 0.106 m/s (20.9 ft/min) and a standard deviation of 0.014 m/s (2.76 ft/min). This data is represented in the graph of Figure 5-19. As illustrated in the graph, the average velocity during CBO gait was 15 percent higher than during FES gait. Since the step frequency was roughly the same during both FES and CBO gait, the difference in gait speed is due primarily to the increase in stride length that result from CBO hip trajectory control.

5.2.4   External Power Requirements

Any commercially viable gait system must be self-contained and battery-powered. Since FES provides only signal power to the neuromuscular system, the external power requirements of using electrical stimulation are low. Given that a typical quadricep duty cycle during FES gait is approximately 87 percent and a typical peroneal duty cycle around 10 percent, and assuming typical pathway impedances and levels of stimulation, the average external power required for FES gait is about 0.14 Watts.

The power required for CBO gait is determined almost entirely by the power supplied to the particle brakes on the brace. Since the energy used by the brakes during swing phase is significantly less than during stance, the power requirements of CBO system are determined almost completely by the duty cycle of particle brake locking. During typical walking with the CBO, the knee brakes are locked approximately 76 percent of the time. The hip brakes are generally not locked. Locking each knee brake requires 350 milliamps of current across 80 Ohms of resistance, which for both brakes yields an average power over the gait cycle of approximately 15 Watts.
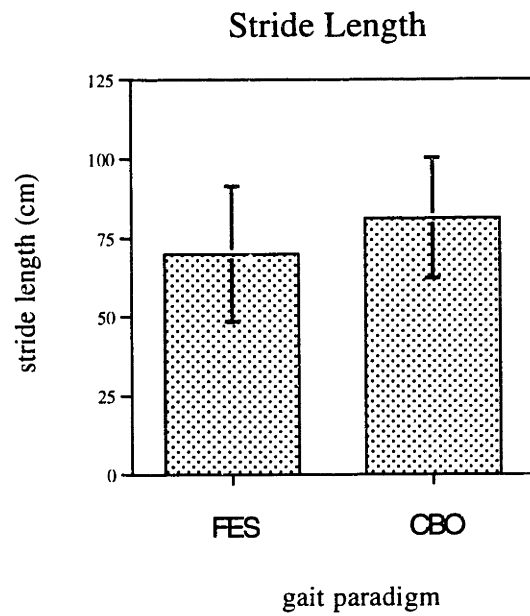
Stride Length

Figure 5-18: The mean and standard deviation of stride length during FES and CBO gait.

Average Gait Velocity
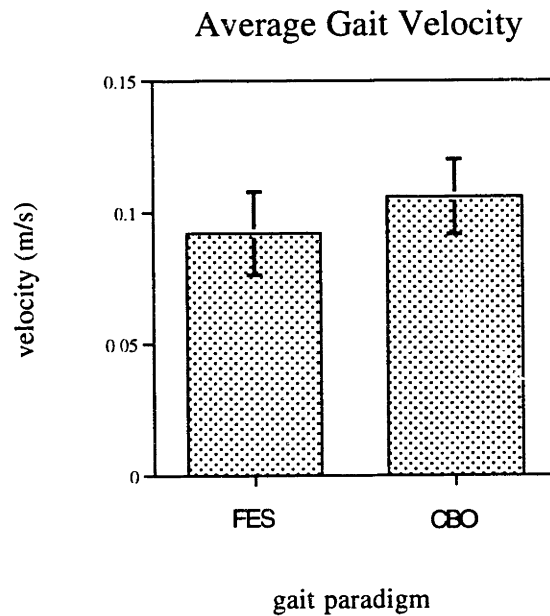
Figure 5-19: The mean and standard deviation of average gait velocity during FES and CBO gait.

Assuming the commercial electronics would be about 80 percent efficient, the average power required by the FES and CBO gait systems would be approximately 0.18 Watts and 18.0 Watts, respectively. Given that a NiCad (Nickel-Cadmium) battery can hold approximately 18 Watt-hours per pound, the FES gait system could sustain approximately 100 hours of use from one pound of NiCad batteries. The CBO gait system could provide approximately one hour of walking from a pound of NiCad batteries.

5.2.5 Knee Ligament Laxity

Although the CBO offers several advantages over conventional FES-aided gait, one potential problem exists in knee ligament laxity. Like several other joints in the body, the knee is stabilized by a combination of joint ligaments and muscle tension. When the knee joint is loaded, it is typically either supplemented structurally by tension in the patellar ligament imposed by contraction of the quadriceps muscle group, or by being in the "screwed home" position. The screwed home position is the configuration in which the joint is most stable, due primarily to tension in the joint ligaments. For the knee joint, this position occurs when the joint is fully extended and the tibia is rotated laterally with respect to the femur. When the quadriceps are not contracted and the joint is not in the screwed home position, the knee exhibits a relatively large degree of valgus/varus (side-to-side) mobility. During CBO gait, the orthosis provides the isometric knee torque in the flexion/extension plane, but relies on the skeleton and anatomical knee joint to bear all compressive loads. The knee joint is thus fully-loaded in the complete absense of any muscle contraction. In the case of a ligamentous lax joint, loading in this manner could cause buckling in the medio-lateral plane and thus damage the knee ligaments and other connective tissue. This joint instability is also present when walking with other gait orthotics, such as the Vannini-Rizzoli boots or a reciprocating gait orthosis. Joint instability due to lagmentous laxity is not a problem with FES gait, since contraction of the quadriceps group stabilizes the joint.

In the case of a ligamentous lax joint, stability problems can be significantly re-

duced by proper orientation of the ankle-foot orthoses (AFO) on the brace. Orienting the AFO in a "toe out" position helps tighten the knee ligaments and thus helps screw home the joint. Additionally, adjusting the amount of inversion or eversion of the foot can compensate for the valgus or varus laxity.

5.2.6 Subject Opinions

The subject was asked four questions at the conclusion of the study. The questions are listed and the subject's answers paraphrased below.

Question

Without regard to monetary cost, describe what criteria a hybrid-FES system must meet in order for you to use it?

Answer

- The orthosis must be easy to carry from a wheelchair and easy to handle, i.e., should be easy to put in the trunk of a car.

- The orthosis should be lighter and be less bulky than the existing prototype.

- The system should be battery-powered and self-contained, with a battery pack and electronics package each small enough to clip on a belt.

- The system should be used with a walker that contains step control buttons that are operable by the thumbs.

Question

How would you use such a system?

Answer

- I would use the system as a means of exercise, walking everyday for about a half hour a day.

- Standing in the kitchen and around the house. I would wear it in my wheelchair and stand when I need to access something on my feet.

- Standing at parties and in social situations, so I can look at and speak to others eye-to-eye.

Question

With regard to the two systems tested, how does walking without the brace (FES gait) compare to walking with the brace (CBO gait)?

Answer

- I like walking with the brace much better than walking without.

- Walking with the CBO feels more secure, since I'm not at risk of collapsing.

- My knees and ankles feel more stable with the CBO.

- My steps feel more consistent with the brace.

Question

How do you feel about implanted versus surface electrodes?

Answer

- I prefer surface electrodes. They are easy to use and very manageable.

- I don't want to deal with the surgery necessary for implanted electrodes or the associated possibilities of infection.

Chapter 6

Conclusions and

Recommendations

6.1 Summary of Results

A controlled-brake orthosis was designed and built to assess the effectiveness of augmenting FES-aided gait by utilizing FES in combination with a long-leg brace that contains controllable friction brakes at both knees and both hips. Clinical evaluations comparing gait with the CBO to conventional four channel FES-aided gait were conducted on a single T6 SCI subject. A summary of results from these evaluations is as follows:

- Quadricep muscle stimulation duty cycle is significantly lower when using the CBO than when walking with conventional FES-aided gait.

- Isometric recruitment curves indicate a significant reduction in quadriceps muscle fatigue when walking with the CBO.

- Since the burden of maintaining knee joint stability during stance has been assumed by the CBO, the most serious consequence of quadricep fatigue, collapse of the individual without warning, is eliminated.

- Heart rate data indicate that the CBO requires a lower level of physical exertion than does conventional FES-aided gait.

- The repeatability of swing phase joint angle trajectories is significantly improved with the use of the CBO.

- The ability of the brace to effect trajectory control is limited by its dissipative nature. Insufficient joint power, especially in the flexion withdrawal reflex, sometimes rendered the brace controller ineffective.

- Stride length was increased and stride length variation decreased with the use of the CBO. As with trajectory control, the brace effectiveness in reducing variation was limited by limitations in muscle power.

- The hip adduction lock prevented scissoring during gait.

6.2   Recommendations

6.2.1   Gait Control

The Flexion Withdrawal Reflex

The lack of hip and knee power in the flexion withdrawal reflex is the most limiting component of the swing phase trajectory control system. Though the reflex often provided adequate power, the response to peroneal stimulation was highly variable. Some of the factors that appeared to affect the quality of the flexion withdrawal reflex are

- The response was a strong function of active and reference (negative and positive) electrode placement.

- The response varied with the size of electrodes used.

- Less observable physiological conditions seemed to influence the magnitude of response. Physiological factors would change over a time span on the order of two weeks that would yield a significantly different response for what appeared to be a very similar input. For example, the subject would have a good reflex response for two weeks, and then exhibit a poor response for the following two weeks, for no obvious reason.

The cursory experimental examination of the flexion withdrawal reflex indicated that the reflex does not exhibit monotonically increasing response with increased stimulation amplitude, pulse width, or frequency, but rather exhibits a peak in one region and tapers off elsewhere. A thorough investigation of the flexion withdrawal

reflex would be of great utility for any FES-aided gait protocol incorporating this component. In particular, methods must be developed to enable reliable and sufficient joint power to obtain reliable and repeatable trajectory control.

Incorporating a Hip Motor

A primary reason that magnetic particle brakes were chosen as the controlled dissipators on the CBO is their large holding torque to weight ratio. Large holding torques are necessary at the knee joint for postural stability, but are not required at the hip joint, since the hip is stabilized by the C-posture. The hip only requires trajectory control torques, which are much smaller than the holding torques required during stance. Additionally, since the orthosis hip joint need not provides skeletal torques for stance, the consequences of hip joint torque saturation are benign. A lightweight motor, acting through a large back-drivable transmission, could be incorporated in place of a particle brake. The hip joint motor, in addition to effecting trajectory control, could supply additional hip power during swing phase when the power provided by the flexion withdrawal reflex is inadequate. This motor could also be used to help maintain hip extension during stance phase, and thus reduce the upper body work load as well as eliminate some of the position variation exhibited in the initial phase of the hip angle swing trajectory.

Gluteal Stimulation

Incorporating stimulation of the gluteal channels for hip extension offers several advantages. The C-posture that stabilizes the hip joints at all times during FES-aided gait is effected by the subject's maintaining the center of gravity of his or her torso posterior to the hip joints. Forward motion is effected by using the arms to pull the body forward. Pulling forward on the parallel bars or walker creates a destabilizing torque about the hips, which the subject must counteract by applying large torques with the arms through the walking aid. The addition of controlled gluteal stimulation would help to stabilize thet hip by (1) providing a stabilizing extensive hip torque during stance and (2) pushing the subject forward with the stance leg, decreasing

129

the necessity to pull with the upper body. Additionally, added hip extension would provide greater stride length.

The drawbacks to adding gluteal stimulation are (1) the need to add two more stimulation channels, and (2) the awkwardness of applying the electrodes, which are located in the gluteal region.

6.2.2 Orthosis Design

By nature of its function, the orthosis is subject to a fair amount of mechanical abuse. One of the most vulnerable components on the orthosis is the electrical wiring and related connectors. Any redesign of the orthosis should incorporate a mechanically robust wiring system, taking careful measures to mechanically protect the wiring to the extent possible.

The high level control commands (right step, left step, stand, and sit) were issued on the subject's voice command by a computer operator. Handswitches should be designed to enable the subject to control the system directly. These could be in the form of ring-like switches worn on the forefinger, or could be push buttons mounted on the grips of a walker.

The possibility of injury due to knee ligament laxity could be significantly diminished by designing more valgus/varus structural strength and stiffness into the orthosis. A large lateral stiffness, however, could also cause joint problems in the case where the orthosis joint is not properly aligned with the anatomical joint. Such a design would also probably add weight and bulk.

Bibliography

[1] B. Andrews et al. A hybrid orthosis for paraplegics incorporating feedback control. In *Advances in External Control of Human Extremities IX*, pages 297–311, 1987.

[2] B. Andrews et al. Hybrid FES orthosis incorporating closed loop control and sensory feedback. *J. Biomed. Eng.*, 10:189–195, 1988.

[3] Per-Olof Astrand and Kaare Rodahl. *Textbook of Work Physiology: Physiological Bases of Exercise.* McGraw-Hill Book Company, 1977.

[4] D. Gurski Axelson, P.W. and A. Lasko-Harvill. Standing and its importance in spinal cord injury management. In *Proceedings of the RESNA 10th Annual Conference*, pages 477–479, 1987.

[5] T. Bajd et al. The use of a four-channel electrical stimulator as an ambulatory aid for paralegic patients. *Phys. Ther.*, 63(7):116–1120, 1983.

[6] J.V. Banta, K.J. Bell, E.A. Muik, and J. Fezio. ParaWalker: energy cost of walking. *European Journal of Pediatric Surgery*, pages 7–10, December 1992.

[7] R. Baratta and M. Solomonow. The dynamic response model of nine different skeletal muscles. *IEEE Trans. Biomed. Eng.*, 37(3):243–251, 1990.

[8] D.T. Barry, S.R. Geiringer, and R.D. Ball. Acoustic myography: a non-invasive monitor of motor unit fatigue. *Muscle and Nerve*, 8:189–194, 1985.

[9] P. Bawa, A. Mannard, and R. Stein. Effects of elastic loads on the contractions of cat muscles. *Biol. Cybern.*, 22:129–137, 1976a.

[10] P. Bawa, A. Mannard, and R. Stein. Predictions and experimental tests of a visco-elastic muscle model using elastic and inertial loads. *Biol. Cybern.*, 22:139–145, 1976b.

[11] J.E. Beard, J.C. Conwell, D.S. Rogers, and H. Lamousin. Design of a powered orthotic device to aid individuals with a loss of bipedal locomotion. In *Proceedings of the Second National Applied Mechanisms and Robotics*, 1991.

[12] H. Beck and W. Durfee. A comparison of methods for estimating isometric recruitment curves in human quadriceps muscle. In *Proceedings of the Eighteenth Annual Northeast Bioengineering Conference*, pages 58–59, 1993.

[13] H. Beck and W.K. Durfee. Estimation of isometric recruitment curves in human quadriceps muscle. In *Proceedings of the Annual International Conference of the IEEE Engineering in Medicine and Biology Society*, volume 15, 1993.

[14] L. Benton, L. Baker, B. Bowman, and R. Waters. *Functional Electrical Stimulation: A Practical Guide, 2nd edition.* Professional Staff Association, Rancho Los Amigos Rehabilitation Engineering Center, Rancho Los Amigos Hospital, Downey CA, 1981.

[15] L. Bernotas, P. Crago, and H. Chizeck. A discrete-time model of electrically stimulated muscle. *IEEE Trans. Biomed. Eng.*, 33(9):829–838, 1986.

[16] L Bernotas, P. Crago, and H. Chizeck. Adaptive control of electrically stimulated muscle. *IEEE Trans. Biomed. Eng.*, 34(2):140–147, 1987.

[17] B. Bigland-Ritchie, D. Jones, and J. Woods. Excitation frequency and muscle fatigue: electrical responses during voluntary and stimulated contractions. *Expt. Neurol.*, 64:414–427, 1979.

[18] P.B. Butler, R.E. Major, and J.H. Patrick. The technique of reciprocal walking using the hip guidance orthosis (HGO) with crutches. *Prosthetics and Orthotics International*, 8(1):33–38, 1984.

[19] D. Cerny, R. Waters, H. Hislop, and J. Perry. Walking and wheelchair energetics in persons with paraplegia. *Physical Therapy*, 60(9):1133–1139, 1980.

[20] D. Chen, H. Hemami, I. MacLean, and R. McGhee. An electrically controlled knee joint for long leg braces. In *Advances in External Control of Human Extremities IV*, pages 496–503, 1973.

[21] N. Chesler. EMG as an indicator of fatigue during FES-aided standing of paraplegics. Master's thesis, Massachusetts Institute of Technology, May 1991.

[22] T. Chia, P. Chow, and H. Chizeck. Recursive parameter identification of constrained systems: an application to electrically stimulated muscle. *IEEE Trans. Biomed. Eng*, 38(5):429–442, 1991.

[23] P. Crago, P. Peckham, and G. Thrope. Modulation of muscle force by recruitment during intramuscular stimulation. *IEEE Trans. Biomed. Eng.*, 27(12):679–684, 1980b.

[24] P.E. Crago, M.A. Lemay, and L. Liu. External control of limb movements involving environmental interactions. In J.M. Winters and S.L. Woo, editors, *Multiple Muscle Systems*, chapter 21. Springer-Verlag, 1990.

[25] G. Cybulski, R. Penn, and R. Jaeger. Lower extremity functional neuromuscular stimulation in cases of spinal cord injury. *Neurosurgery*, 15(1):132–146, 1984.

[26] R. Douglas et al. LSU reciprocating gait orthosis. *Orthopedics*, 6:834–839, 1983.

[27] W.K. Durfee and J.M. Hausdorff. Regulating knee joint position by combining electrical stimulation with a controllable friction brake. *Annals of Biomedical Engineering*, 18:575–596, 1990.

[28] W.K. Durfee and K.E. MacLean. Methods for estimating isometric recruitment curves of electrically stimulated muscle. *IEEE Trans. Biomed. Eng.*, 36(7):654–667, 1989.

[29] B. Bigland-Ritchie et al. Contractile speed and EMG changes during fatigue of sustained maximum voluntary contractions. *Journal of Neurophysiology*, 50:313–324, 1983.

[30] C. Orizio et al. Spectral analysis of muscular sound during isometric contraction of biceps brachii. *American Journal of Physiology*, pages 508–512, 1990.

[31] M.S. Goldenberg et al. Acoustic myography as an indicator of force during sustained contractions of a small hand muscle. *American Journal of Physiology*, pages 87–91, 1991.

[32] M. Goldfarb. Modeling and simulation of a magnetic particle brake. Class project for 2.141: Advanced Systems Modeling, December 1992.

[33] M.H. Granat, B.W. Heller, D.J. Nicol, R.H Baxendale, and B.J. Andrews. Improving limb flexion in FES gait using the flexion withdrawal response for the spinal cord injured person. *Journal of Biomedical Engineering*, 15(1):51–56, 1993.

[34] M.H. Granat, D.J Nicol, R.H. Baxendale, and B.J. Andrews. Dishabituation of the flexion reflex in spinal cord-injured man and its application in the restoration of gait. *Brain Research*, 559(2):344–346, 1991.

[35] D. Graupe. EMG pattern analysis for patient-responsive control of FES in paraplegics for walker-supported walking. *IEEE Transactions in Biomedical Engineering*, 36(7):711–719, 1989.

[36] Y. Grierson. Standing system failure detection: A postural study of paraplegics standing through the use of functional electrical stimulation. BSME Thesis, Massachusetts Institute of Technology, May 1990.

[37] J. Gruner et al. A system for evaluation and exercise-conditioning of paralyzed leg muscles. *J. Rehabilitation R & D*, 20(1):21–30, 1983.

[38] J. Hausdorf. Gait orthosis combining controllable damping and muscle stimulation. Master's thesis, Massachusetts Institute of Technology, August 1988.

[39] S. Hirokawa, M. Grimm, T. Le, M. Solomonow, R.V. Baratta, H. Shoji, and R.D. D'Ambrosia. Energy consumption in paraplegic ambulation using the reciprocating gait orthosis and electric stimulation of the thigh muscles. *Archives of Physical Medicine and Rehabilitation*, 71(9):687–694, 1990.

[40] J. Holle et al. Walking with an implantable stimulation system for paraplegics. In *Proceedings of the 2nd Int'l. Conf. on Rehab. Eng.*, pages 551–552, 1984.

[41] J. Holle, M. Frey, H. Gruber, H. Kern, H. Stohr, and H. Thoma. Functional electrostimulation of paraplegics: experimental investigations and first clinical experience with an implantable stimulation device. *Orthopedics*, 17:1145–1156, 1984.

[42] I. Hunter and M. Korenberg. The identification of nonlinear biological systems: Wiener and Hammerstein cascade models. *Biological Cybernetics*, 55:135–144, 1986.

[43] Indiana Brace Company, 1815 North Capitol Avenue, Suite G-01. Indianapolis, Indiana 46202. *Indiana Knee Orthosis*.

[44] Innovation Sports, 7 Chrysler. Irvine, California 92718. *MVP Knee Orthosis*.

[45] E. Isakov, J. Mizrahi, and T Najenson. Biomechanical and physiological evaluation of FES-activated paraplegic patients. *J. Rehab. Res.*, 23(3):9–19, 1986.

[46] R. Jaeger, G. Yarkony, and E. Roth. Standing by a combined orthotic/electrical stimulation system in thoracic paraplegia. In *Proceedings of the International Conference of the Association for the Advancement of Rehabilitation Technology*, pages 336–337, 1988.

[47] P. Kaplan, B. Gandhavadi, L. Richards, and J. Goldschmidt. Calcium balance in paraplegic patients: Influence of injury duration and ambulation. *Archives of Physical Medicine and Rehabilitation*, 59:447–450, 1978.

[48] ZZ Karu. Optimization of force and fatigue properties of electrically stimulated human skeletal muscle. Master's thesis, Massachusetts Institute of Technology, Department of Electrical Engineering, May 1992.

[49] E.J. Kennedy. *Spinal Cord Injury: The Facts and Figures*. The University of Alabama at Birmingham Press, 1986.

[50] H.O. Kent. Vannini-Rizzoli stabilizing orthosis (boot): preliminary report on a new ambulatory aid for spinal cord injury. *Archives of Physical Medicine and Rehabilitation*, 73(3):302–307, 1992.

[51] A. Kralj et al. Gait restoration in paraplegic patients: A feasibility demonstration using multichannel surface electrode. *Journal of Rehabilitation Research and Development*, 20(1):3–20, 1983.

[52] Alojz Kralj and Tadej Bajd. *FES: standing and walking after Spinal Cord Injury*. CRC Press, 1989.

[53] H. Kurosawa, P.S. Walker, S. Abe, A. Garg, and T. Hunter. Geometry and motion of the knee for implant and orthotic design. *Journal of Biomechanics*, 18:487–499, 1985.

[54] Schwirtlich L. and D. Popovic. Hybrid orthosis for deficient locomotion. In *Advances in External Control of Human Extremities VIII*, pages 23–32, 1984.

[55] J.L. Lewis and W.D. Lew. A method for locating an optimal fixed axis of rotation for the human knee joint. *Journal of Biomechanical Engineering*, 100:187–193, 1978.

[56] Liberty Mutual Research Center, 71 Frankland Road, Hopkinton MA 01748. *Steeper Advanced Reciprocating Gait Orthosis*.

[57] P. J. Lord. *Computer Aided Intertrochanteric Osteotomy Planning and Surgery Simulation*. PhD thesis, Massachusetts Institute of Technology, 1994.

[58] M. Lyles and J. Munday. Report on the evaluation of the Vannini-Rizzoli stabilizing limb orthosis. *Journal of Rehabilitation Research and Development*, 29(2):77–104, 1992.

[59] K. MacLean. Estimation of isometric recruitment curves of electrically stimulated muscle. Master's thesis, Massachusetts Institute of Technology, August 1988.

[60] R.E. Major, J. Stallard, and G.K. Rose. The dynamics of walking using the hip guidance orthosis (HGO) with crutches. *Prosthetics and Orthotics International*, 5(1):19–22, 1981.

[61] E. Marsolais et al. Improved synthetic walking in the paraplegic patient using implanted electrodes. In *Proceedings of the 2nd Int'l. Conf. on Rehab. Eng.*, pages 439–440, 1984.

[62] E. Marsolais and R. Kobetic. Functional walking in paralyzed patients by means of electrical stimulation. *Clinical Orthopaedics*, 175:30–36, 1983.

[63] E.B. Marsolais and R. Kobetic. Development of a practical electrical stimulation system for restoring gait in the paralyzed patient. *Clinical Orthopaedics*, 233:64–74, 1988.

[64] R. Kobetic Marsolais, E and H. Chizeck. Basic problems in development of FNS-aided crutch walking in the paraplegic individual. In *Proceedings of the Annual International Conference of the IEEE Engineering in Medicine and Biology Society*, pages 1569–1570, 1988.

[65] M. McClelland et al. Augmentation of the Oswestry ParaWalker orthosis by means of surface electrical stimulation: gait analysis of three patients. *Paraplegia*, 25:32–38, 1987.

[66] P. Meadows et al. Implantable gait stimulation: a system overview. In *Proceedings of the RESNA 9th Annual Conference*, pages 457–459, 1986.

[67] J. Mizrahi, Z. Braun, T. Najenson, and D. Graupe. Quantitiative weightbearing and gait evaluation of paraplegics using functional electrical stimulation. *Med. & Biol. Eng. & Comput.*, 23:101–107, 1985.

[68] E.A. Muller. The influence of training and inactivity on muscle strength. *Archives of Physical Medicine and Rehabilitation*, 51:449, 1978.

[69] M. C. Murphy. *Geometry and the Kinematics of the Normal Human Knee*. PhD thesis, Massachusetts Institute of Technology, 1990.

[70] M.C. Murphy et al. In vivo measurement of the three-dimensional skeletal motion at the human knee. In R.L. Spilker, editor, *1984 Advances in Bioengineering*, pages 64–65. ASME, 1984.

[71] R. Nakai, D. McNeal, P. Meadows, and W. Tu. Characterization of the flexion-withdrawal reflex for use in stimulation-assisted SCI gait. In *Proceedings of the Annual International Conference of the IEEE Engineering in Medicine and Biology Society, Volume 11:1989*, pages 1490–1491, 1989.

[72] A.V. Nene. An assessment of the ORLAU ParaWalker electrical stimulation hybrid orthosis. In *Proceedings of the Annual International Conference of the IEEE Engineering in Medicine and Biology Society*, volume 11, pages 1016–1017, 1989.

[73] Spinal cord injury fact sheet, 1988. Publication of the National Spinal Cord Injury Statistics Center.

[74] I. Odeen and E. Knutsson. Evaluation of the effects of muscle stretch and weight load in patients with spastic paraplegia. *Scandinavian Journal of Rehabilitative Medicine¡*, 13:117–121, 1981.

[75] P.G. Pacy et al. Effect of anaerobic and aerobic exercise promoted by computer regulated functional electrical stimulation (FES) on muscle size, strength and histology in paraplegic males. *Prosthetics and Orthotics International*, 11(2):78, 1987.

[76] P.G. Pacy, R. Hesp, D. Halliday, D. Kath, G. Cameron, and J. Reeve. Muscle and bone in paraplegic patients, and the effect of functional electrical stimulation. *Clinical Science*, 75:481–487, 1988.

[77] R. Patterson, P. Garrett, and K. Wood. Functional electrical stimulation using external electrodes: Some problems and solutions. In *Advances in External Control of Human Extremities IX*, pages 153–159, 1987.

[78] J. Petrofsky, C. Phillips, P. Larson, and R. Douglas. Computer synthesized walking: an application of orthosis and functional electrical stimulation (FES). *J. Neurolog. Orthop. Med. Surg.*, 6(3):219–230, 1985.

[79] C.A. Phillips. Electrical muscle stimulation in combination with a reciprocating gait orthosis for ambulation by paraplegics. *Journal of Biomedical Engineering*, 11(4):338–344, 1989.

[80] C.A. Phillips and D.M. Hendershot. Functional electrical stimulation and reciprocating gait orthosis for ambulation exercise in a tetraplegic patient: a case study. *Paraplegia*, 29(4):268–276, 1991.

[81] C.N. Phillips and D. Hendershot. The EMS-RGO: A physician prescribable FES ambulation exercise system. In *Proceedings of the Annual International Conference of the IEEE Engineering in Medicine and Biology Society, Volume 10:1988*, pages 1573–1574, 1988.

[82] L. Phillips, M. Ozer, P. Axelson, and H. Chizek. *Spinal cord injury: A guide for patient and family*. Raven Press, 1987.

[83] D. Popovic. Final report: Technical and clinical evaluation of the self-fitting modular orthosis (SFMO). Technical report, Faculty of Electrical Engineering, University of Belgrade, 1986.

[84] D. Popovic and L. Schwirtlich. Hybrid powered orthoses. In *Advances in External Control of Human Extremities IX*, pages 95–104, 1987.

[85] D. Popovic, R. Tomovic, and L. Schwirtlich. Hybrid assistive system - the motor neuroprosthesis. *IEEE Trans. Biomed. Eng.*, 36(7):729–737, 1989.

[86] D.B. Popovic, L. Schwirtlich, and S. Radosavljevic. Powered hybrid assistive system. In D.B. Popovic, editor, *Advances in External Control of Human Extremities, X*, pages 177–186. NAUKA, 1990.

[87] K. Ragnarsson. Physiologic effects of functional electrical stimulation-induced exercises in spinal cord-injured individuals. *Clin. Orthop. Rel. Res.*, 233(August):53–63, 1988.

[88] G.K. Rose. The principles and practice of hip guidance articulations. *Prosthetics and Orthotics International*, 3:37–43, 1979.

[89] A. Schoenberg and J. Long. Design of a quickly-assembled, light-weight leg orthosis for FES assisted paraplegic mobility. In *Proceedings of the 10th Annual Conference on Rehabilitation Technology*, pages 633–635, 1987.

[90] G.H. Shue. Multiplicative model of stimulated muscle for FNS control. Master's thesis, Case Western Reserve University, 1990.

[91] Sigmedics, Incorporated, One Northfield Plaza, Suite 411, Northfield IL 60093. *Technological Advancements in Rehabilitation: Independent Standing and Short Distance Walking for the Spinal Cord Injured.*, 1991. An Overview of the Parastep System.

[92] G.L. Smidt. Biomechanical analysis of knee flexion and extension. *Journal of Biomechanics*, 6:79–92, 1973.

[93] M. Solomonow, R. Baratta, S. Hirokawa, N. Rightor, W. Walker, P. Beaudette, H. Shoji, and R. D'Ambrosia. The RGO Generation II: muscle stimulation powered orthosis as a practical walking system for thoracic paraplegics [published erratum appears in orthopedics 1989 dec:12(12):1522]. *Orthopedics*, 12(10):1309–1315, 1989.

[94] M. Solomonow et al. FES powered locomotion of paraplegics fitted with the LSU reciprocating gait orthoses (RGO). In *Proceedings of the Annual International Conference of the IEEE Engineering in Medicine and Biology Society, Volume 10:1988*, page 1672, 1988.

[95] J. Stallard et al. Engineering design considerations of the ORLAU ParaWalker and FES hybrid system. *Engineering in Medicine*, 15(3):123–129, 1986.

[96] M. Stefancic et al. Neurophysiological background of the use of functional electrical stimulation in paraplegia. *Electromyogr. Clin. Neurophysio.*, 26(5-6):433, 1986.

[97] M. Townsend and R. Lepofsky. Powered walking machine prosthesis for paraplegics. *Medical and Biological Engineering*, page 436, 1976.

[98] Townsend Design, 4630 Easton Drive, Suite 1. Bakerfield, California 93309. *Townsend Functional Knee Orthosis*.

[99] R. Turk and P. Obreza. Functional electrical stimulation as an orthotic means for the rehabiliation of paraplegic patients. *Paraplegia*, 23(6):345, 1985.

[100] M. Vukobratovic, D. Hristic, and Z. Stojiljkovic. Development of active anthropomorphic exoskeletons. In *Advances in External Control of Human Extremities IV*, pages 337–358, 1973.

[101] Karlman Wasserman, James E. Hansen, Darryl Y. Sue, and Brian J. Whipp. *Principles of Exercise Testing and Interpretation*. Lea and Febiger, 1987.

[102] R.L. Waters and B.R. Lunsford. Energy cost of paraplegic locomotion. *Journal of Bone and Joint Surgery*, 67(8):1245–1250, 1985.

[103] M.W. Whittle, G.M Cochrane, A.P. Chase, A.V. Copping, and R.J Jefferson. A comparative trial of two walking systems for paralysed people. *Paraplegia*, 29(2):97–102, 1991.

[104] D. Winter. *Biomechanics of Human Movement*. John Wiley and Sons, 1979.

[105] D. Winter. *The Biomechanics and Motor Control of Human Gait: Normal, Elderly, and Pathological, 2nd Edition.* University of Waterloo Press, 1991.

[106] F.E. Zajac. Muscle and tendon: properties, models, scaling, and application to biomechanics and motor control. *CRC Crit. Rev. Biomed. Eng.*, 17(4):359–411, 1989.

Appendix A

CBO Evaluation Data

A.1 Isometric Recruitment Curves

A.1.1 IRC's Recorded for FES Gait
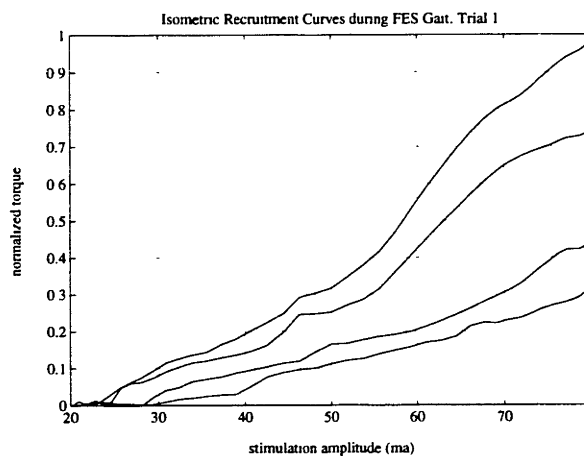
Figure A-1: Isometric recruitment curves taken during FES gait session 1. The curves were taken at the beginning of the session and at successive 10 meter intervals for a total of 30 meters of walking.
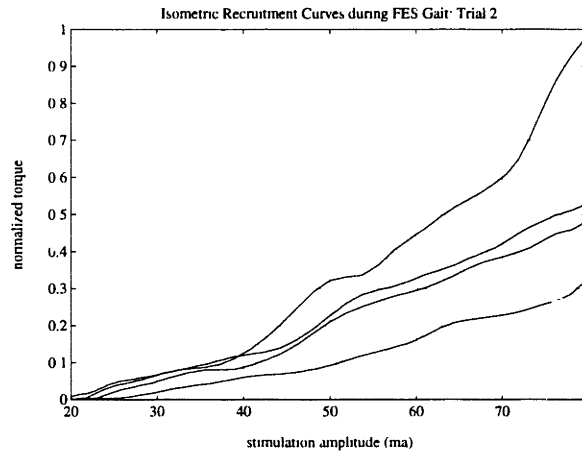
Figure A-2: Isometric recruitment curves taken during FES gait session 2. The curves were taken at the beginning of the session and at successive 10 meter intervals for a total of 30 meters of walking.
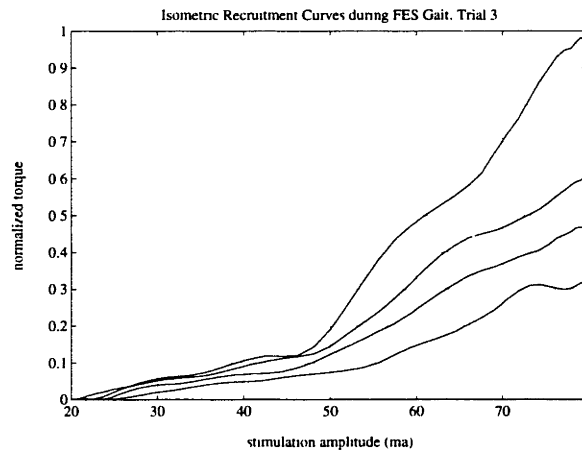
Figure A-3: Isometric recruitment curves taken during FES gait session 3. The curves were taken at the beginning of the session and at successive 10 meter intervals for a total of 30 meters of walking.

A.1.2 IRC's Recorded during CBO Gait
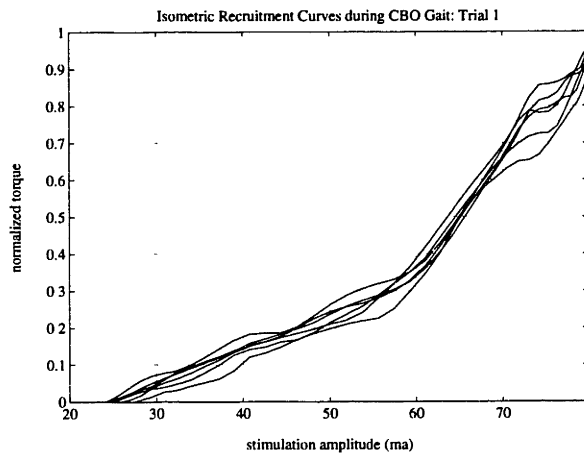
Figure A-4: Isometric recruitment curves taken during CBO gait session 1. The curves were taken at the beginning of the session and at successive 10 meter intervals for a total of 50 meters of walking.
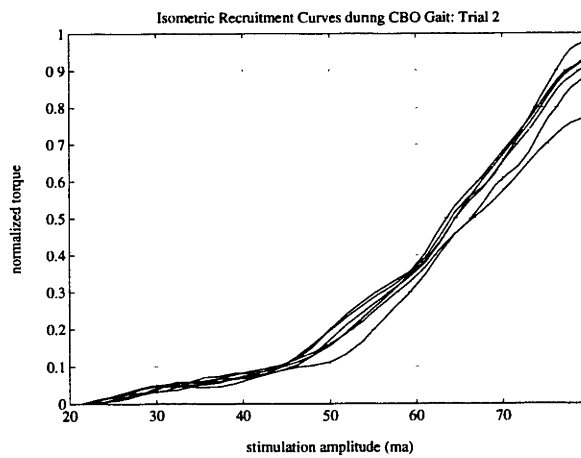
Figure A-5: Isometric recruitment curves taken during CBO gait session 2. The curves were taken at the beginning of the session and at successive 10 meter intervals for a total of 50 meters of walking.
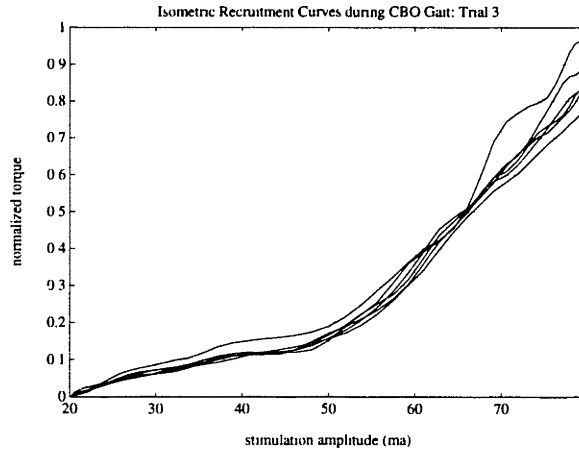
Figure A-6: Isometric recruitment curves taken during CBO gait session 3. The curves were taken at the beginning of the session and at successive 10 meter intervals for a total of 50 meters of walking.

A.2 Peak Torque vs. Distance
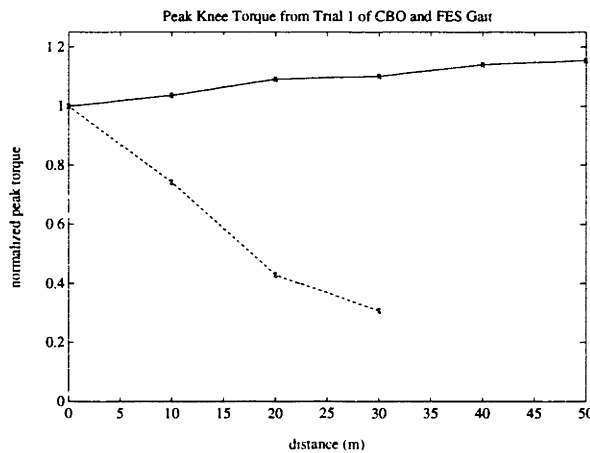
Figure A-7: Peak knee torque as a function of distance during session 1 of both CBO (solid line) and FES (dashed line) gait. The x-marks represent actual data points.
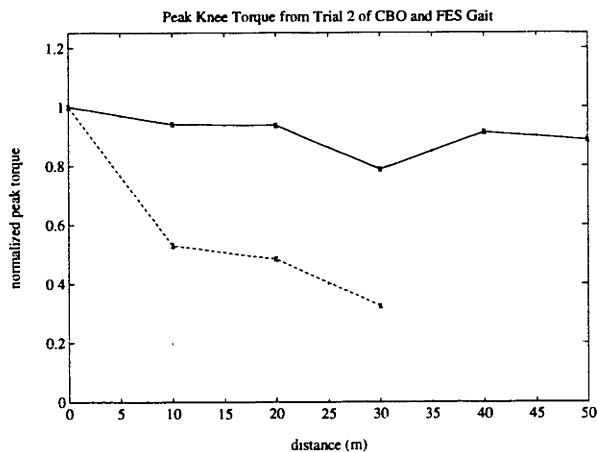
Figure A-8: Peak knee torque as a function of distance during session 2 of both CBO (solid line) and FES (dashed line) gait. The x-marks represent actual data points.
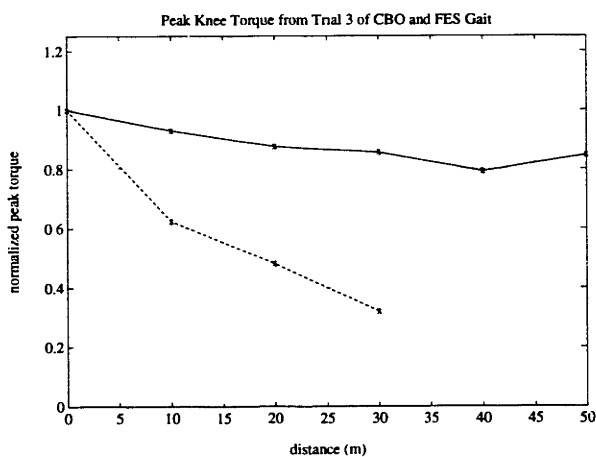
Figure A-9: Peak knee torque as a function of distance during session 3 of both CBO (solid line) and FES (dashed line) gait. The x-marks represent actual data points.

A.3 Heart Rate

A.3.1 Heart Rate Records for FES Gait
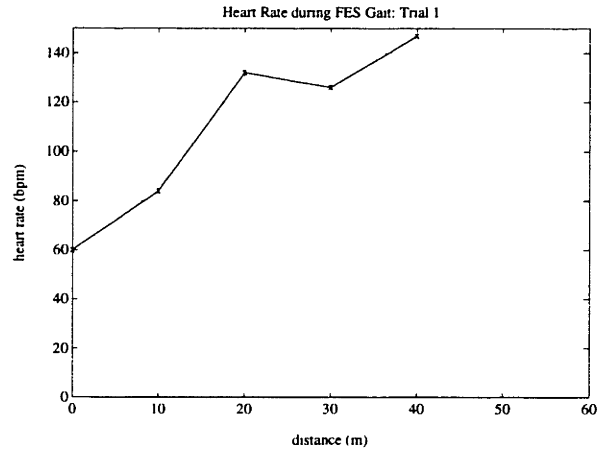
Figure A-10: Heart rate during FES gait session 1. The x-marks represent actual data points.
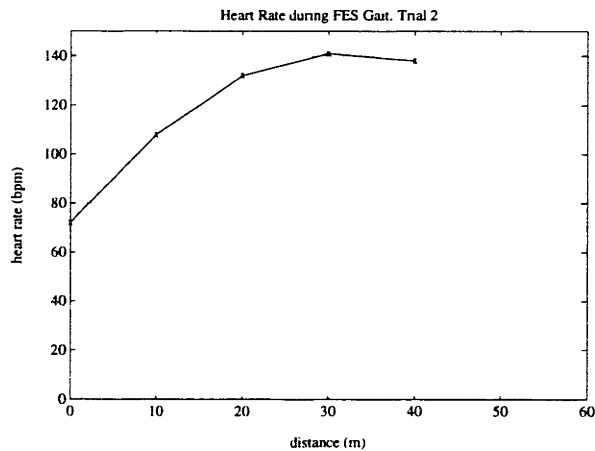
Figure A-11: Heart rate during FES gait session 2. The x-marks represent actual data points.
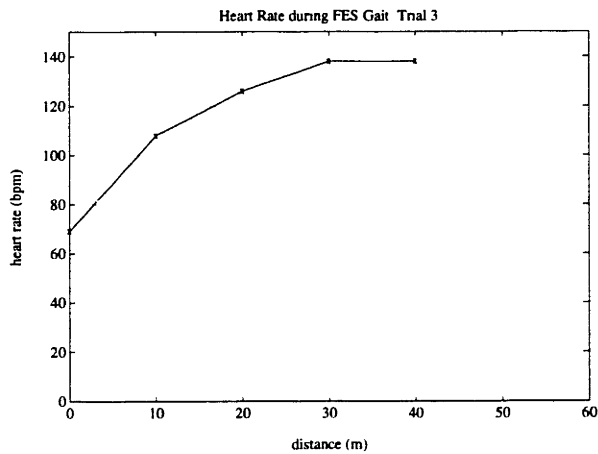
Figure A-12: Heart rate during FES gait session 3. The x-marks represent actual data points.

A.3.2 Heart Rate Records for CBO Gait
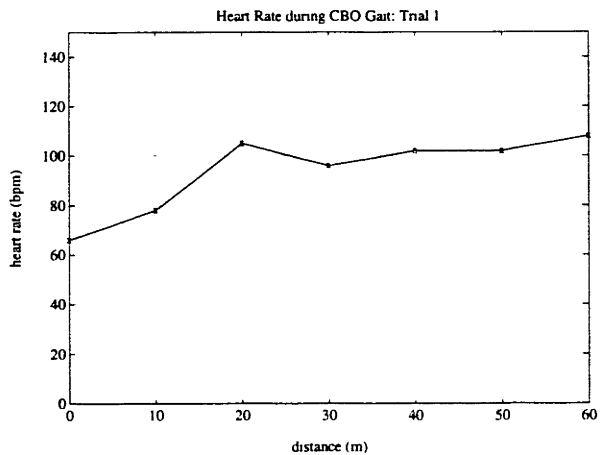
Figure A-13: Heart rate during CBO gait session 1. The x-marks represent actual data points.
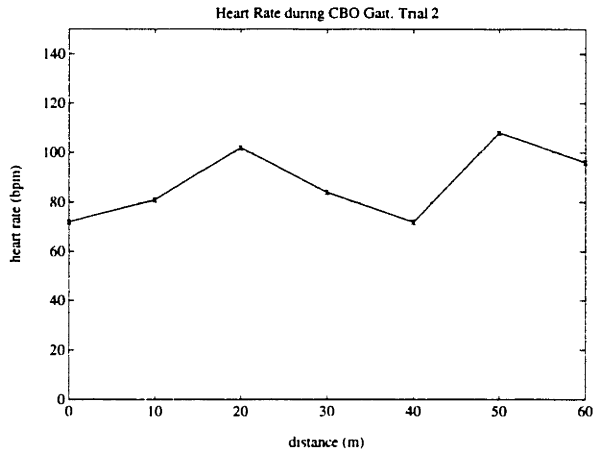
Figure A-14: Heart rate during CBO gait session 2. The x-marks represent actual data points.
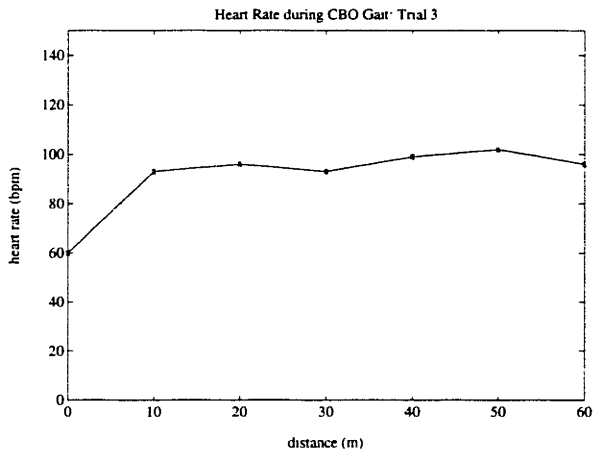
Figure A-15: Heart rate during CBO gait session 3. The x-marks represent actual data points.

150

A.4 Blood Pressure

A.4.1 Blood Pressure Records for FES Gait
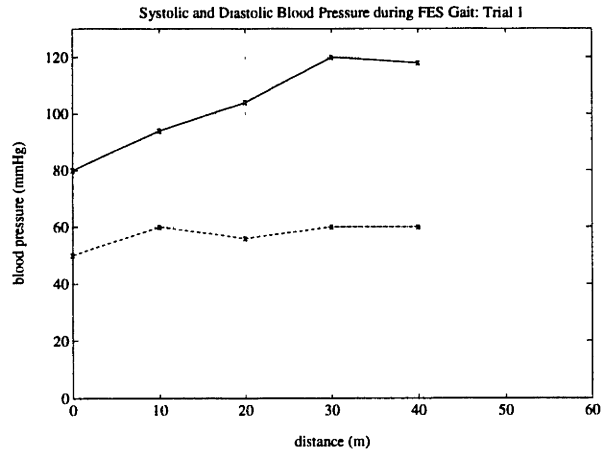
Figure A-16: Systolic (solid line) and diastolic (dashed line) blood pressure during FES gait session 1. The x-marks represent actual data points.
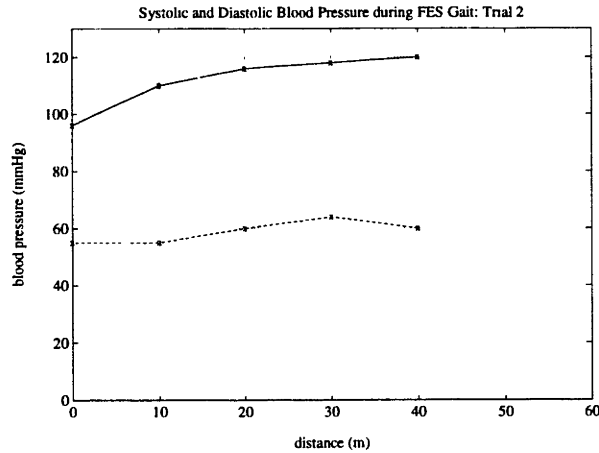
Figure A-17: Systolic (solid line) and diastolic (dashed line) blood pressure during FES gait session 2. The x-marks represent actual data points.

151

Systolic and Diastolic Blood Pressure during FES Gait: Trial 3
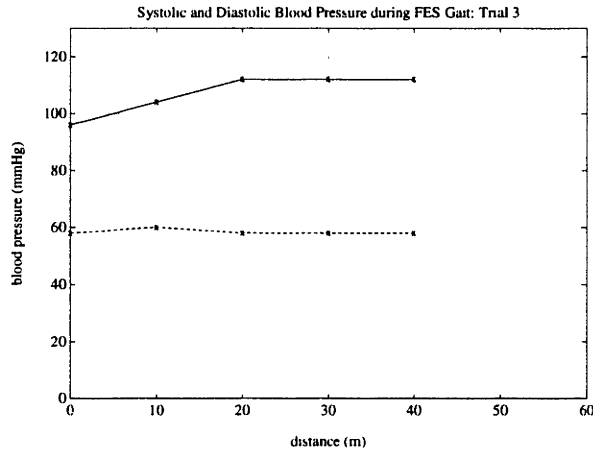
Figure A-18: Systolic (solid line) and diastolic (dashed line) blood pressure during FES gait session 3. The x-marks represent actual data points.

A.4.2 Blood Pressure Records for CBO Gait

Systolic and Diastolic Blood Pressure during CBO Gait: Trial 1
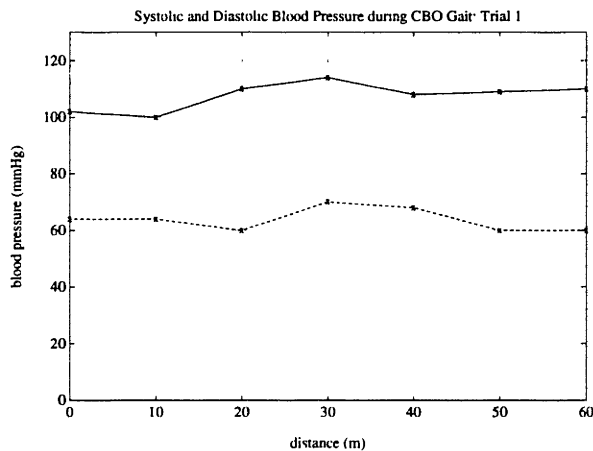
Figure A-19: Systolic (solid line) and diastolic (dashed line) blood pressure during CBO gait session 1. The x-marks represent actual data points.
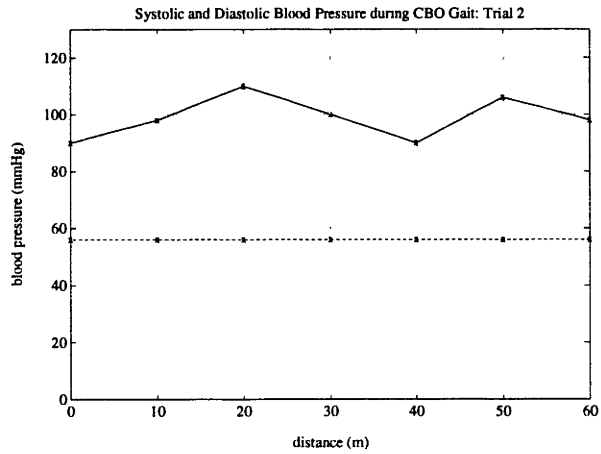
Figure A-20: Systolic (solid line) and diastolic (dashed line) blood pressure during CBO gait session 2. The x-marks represent actual data points.
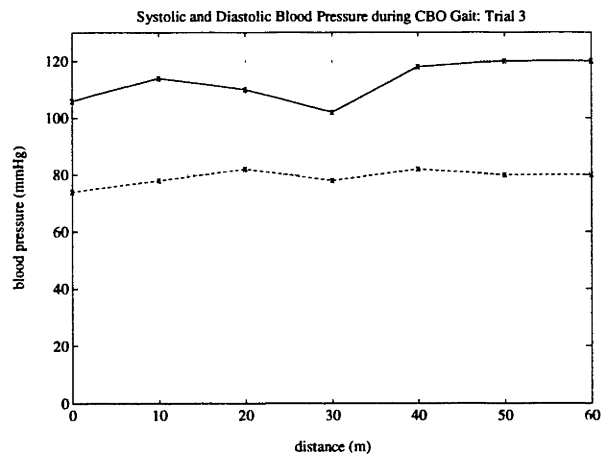
Figure A-21: Systolic (solid line) and diastolic (dashed line) blood pressure during CBO gait session 3. The x-marks represent actual data points.

A.5   Joint Angle Data

A.5.1   Joint Angle Records for FES Gait
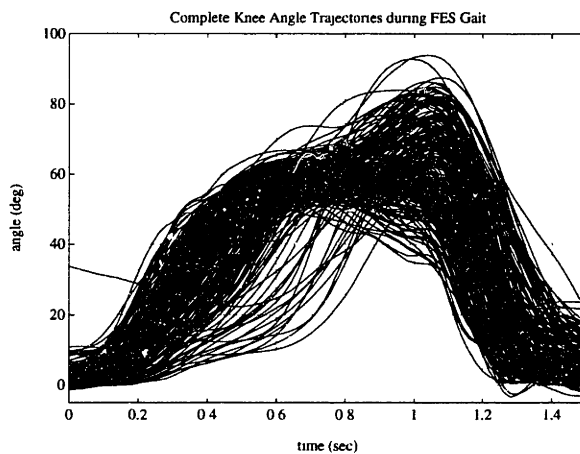
Figure A-22: Knee angle for all steps taken during the FES gait sessions 1, 2, and 3. The plot represents a total of 235 steps.
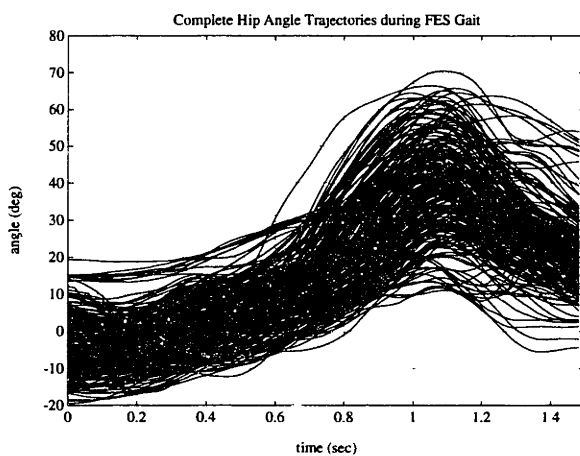
Figure A-23: Hip angle for all steps taken during the FES gait sessions 1, 2, and 3. The plot represents a total of 235 steps.

A.5.2 Joint Angle Records for CBO Gait
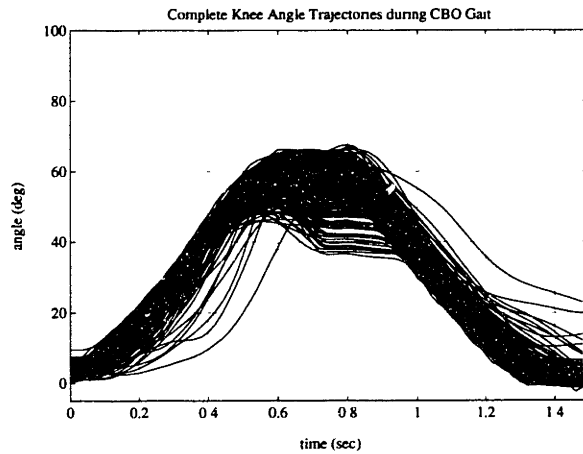
Figure A-24: Knee angle for all steps taken during the CBO gait sessions 1, 2, and 3. The plot represents a total of 453 steps.
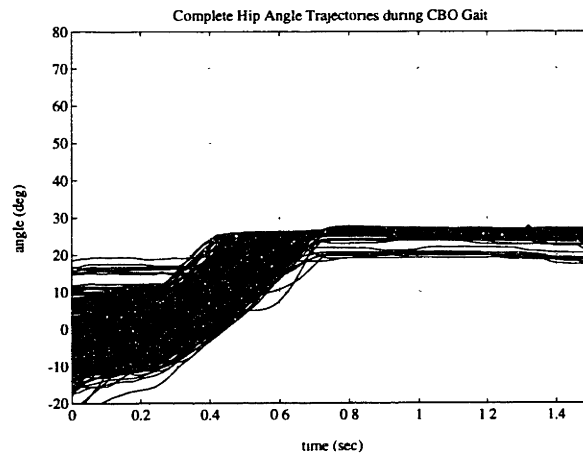
Figure A-25: Hip angle for all steps taken during the CBO gait sessions 1, 2, and 3. The plot represents a total of 453 steps.

Appendix B

Brace Electronics

B.1   Brace Electronics Schematics

B.1.1   Signal Processing
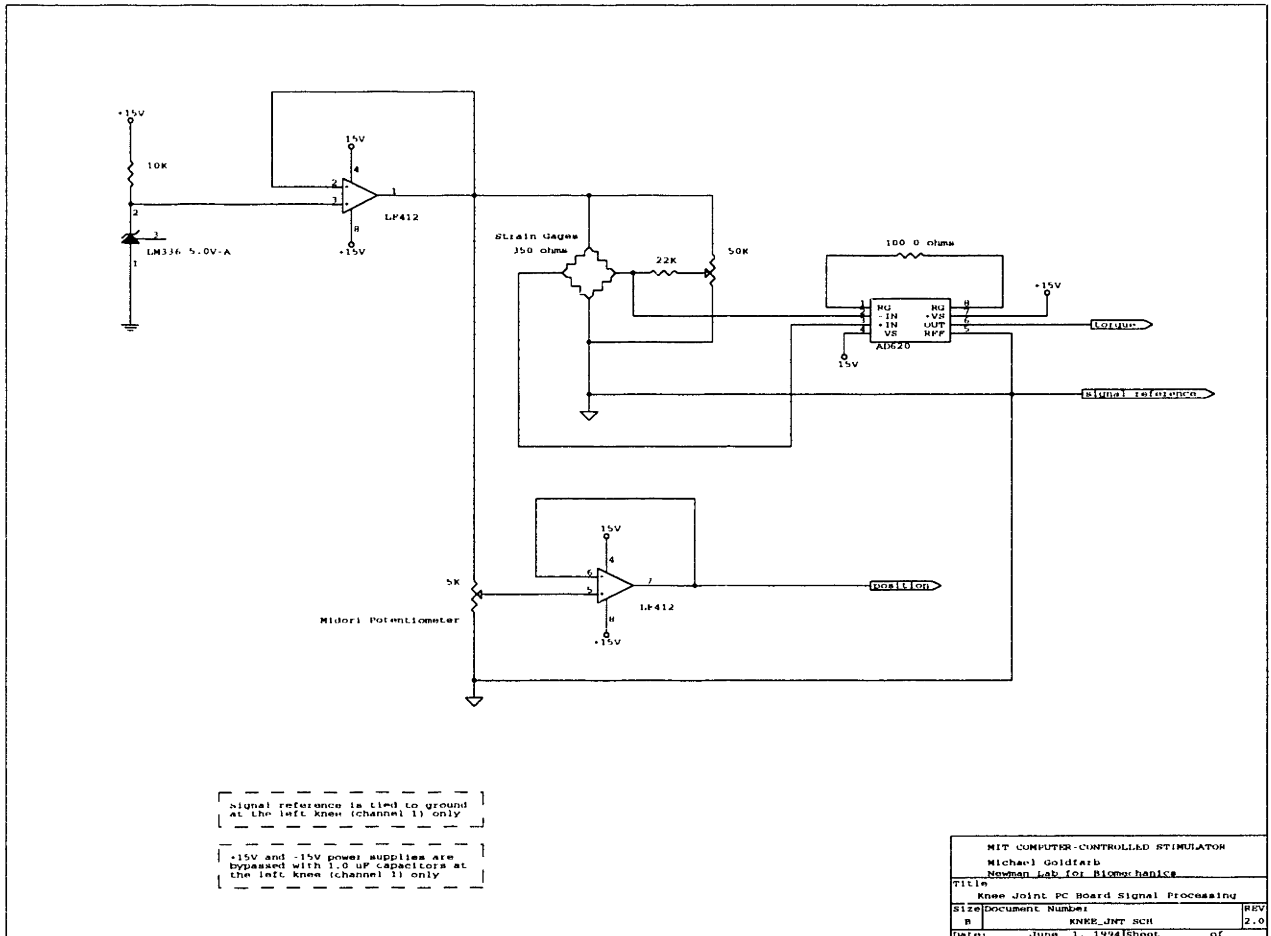
Figure B-1: Schematic of printed circuit board located inside the gear shafts of the right and left knee joints (channels 0 and 1, respectively). The two boards are identical except for the bypass capacitors and the signal reference–ground connection in the left knee circuit. The gain on the AD620 instrumentation amplifier is set at 500.
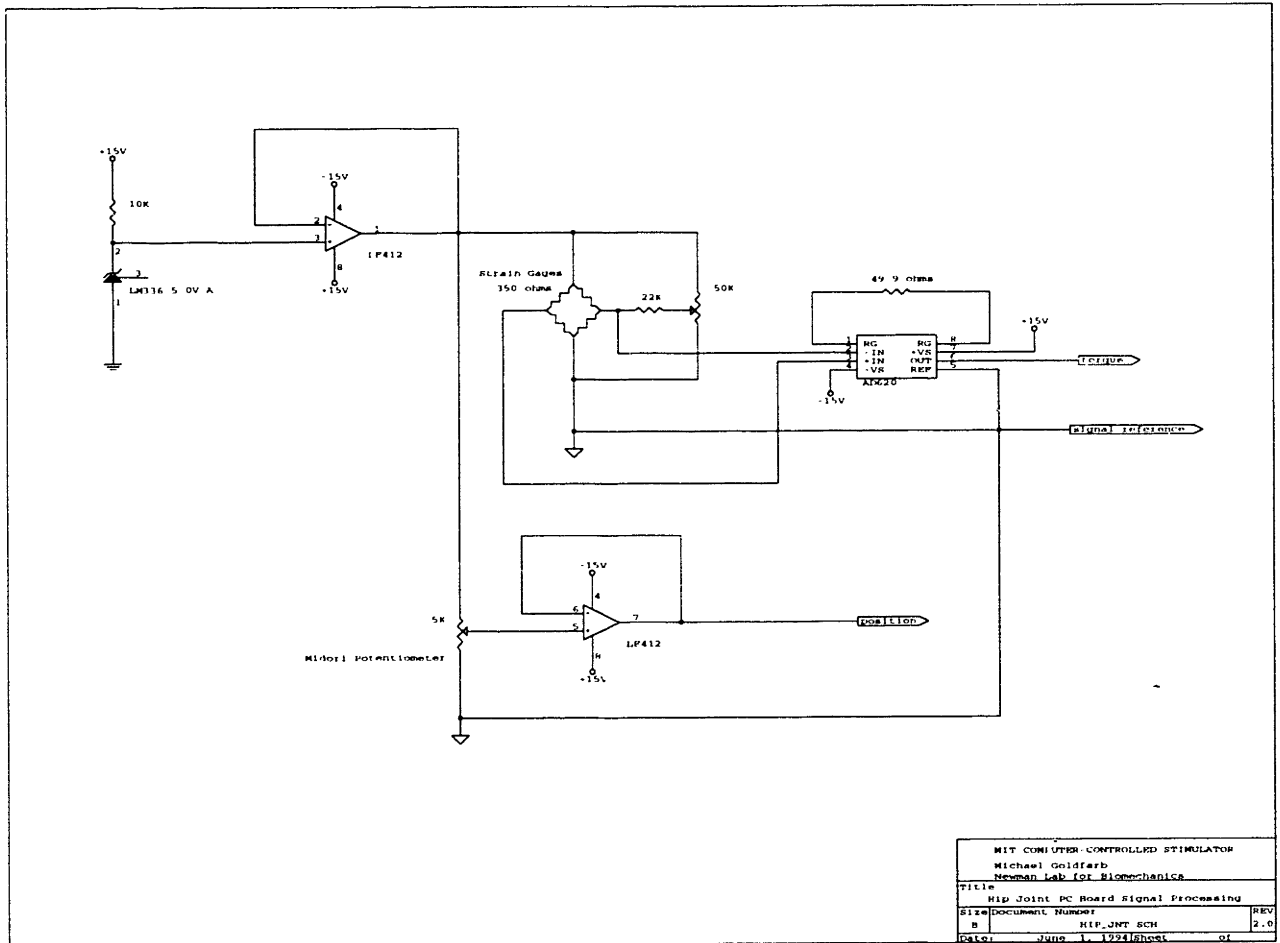
Figure B-2: Schematic of printed circuit board located inside the gear shafts of the right and left hip joints (channels 2 and 3, respectively). These boards differ from the knee boards only in the gain of the AD620 instrumentation amplifier, which is set at 1000.
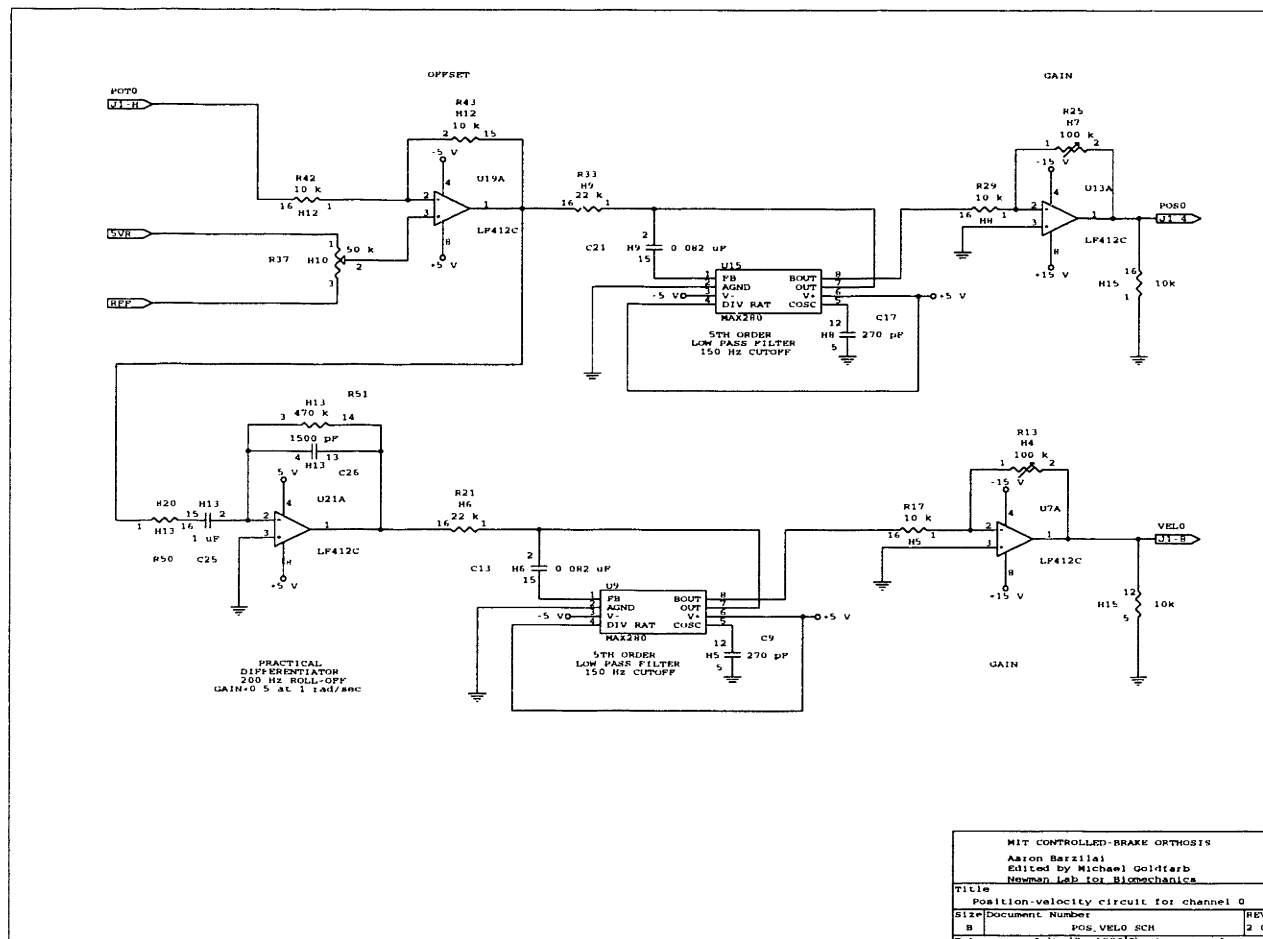
Figure B-3: Channel 0 joint angle and velocity signal processing. The joint angle processing includes an offset stage, a low-pass anti-aliasing filter with a 150 Hz cutoff, and an adjustable gain stage. The velocity segment includes a practical differentiator, a low-pass anti-aliasing filter, and a gain stage.
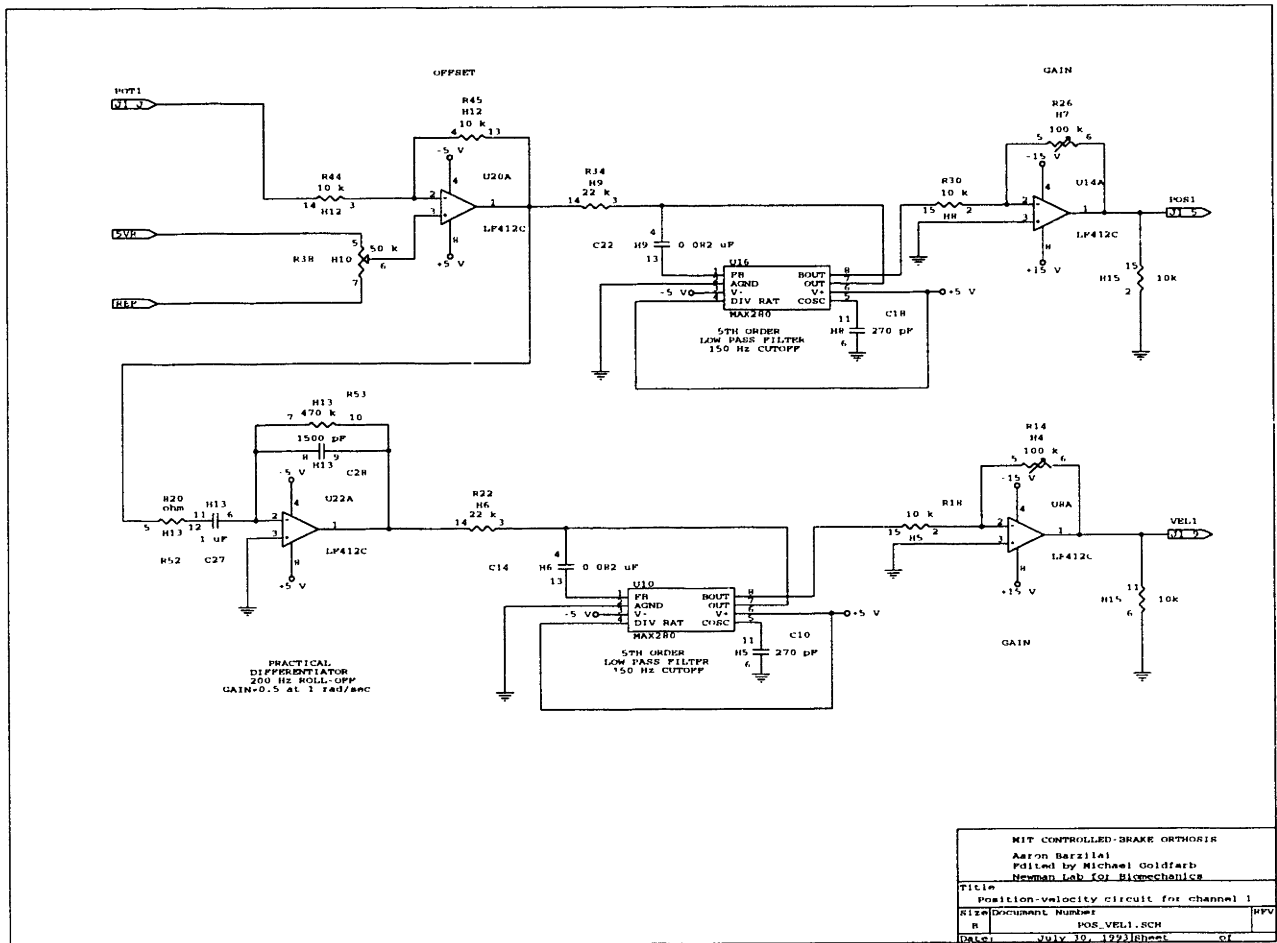
Figure B-4: Channel 1 joint angle and velocity signal processing. The joint angle processing includes an offset stage, a low-pass anti-aliasing filter with a 150 Hz cutoff, and an adjustable gain stage. The velocity segment includes a practical differentiator, a low-pass anti-aliasing filter, and a gain stage.

Figure B-5: Channel 2 joint angle and velocity signal processing. The joint angle processing includes an offset stage, a low-pass anti-aliasing filter with a 150 Hz cutoff, and an adjustable gain stage. The velocity segment includes a practical differentiator, a low-pass anti-aliasing filter, and a gain stage.

162
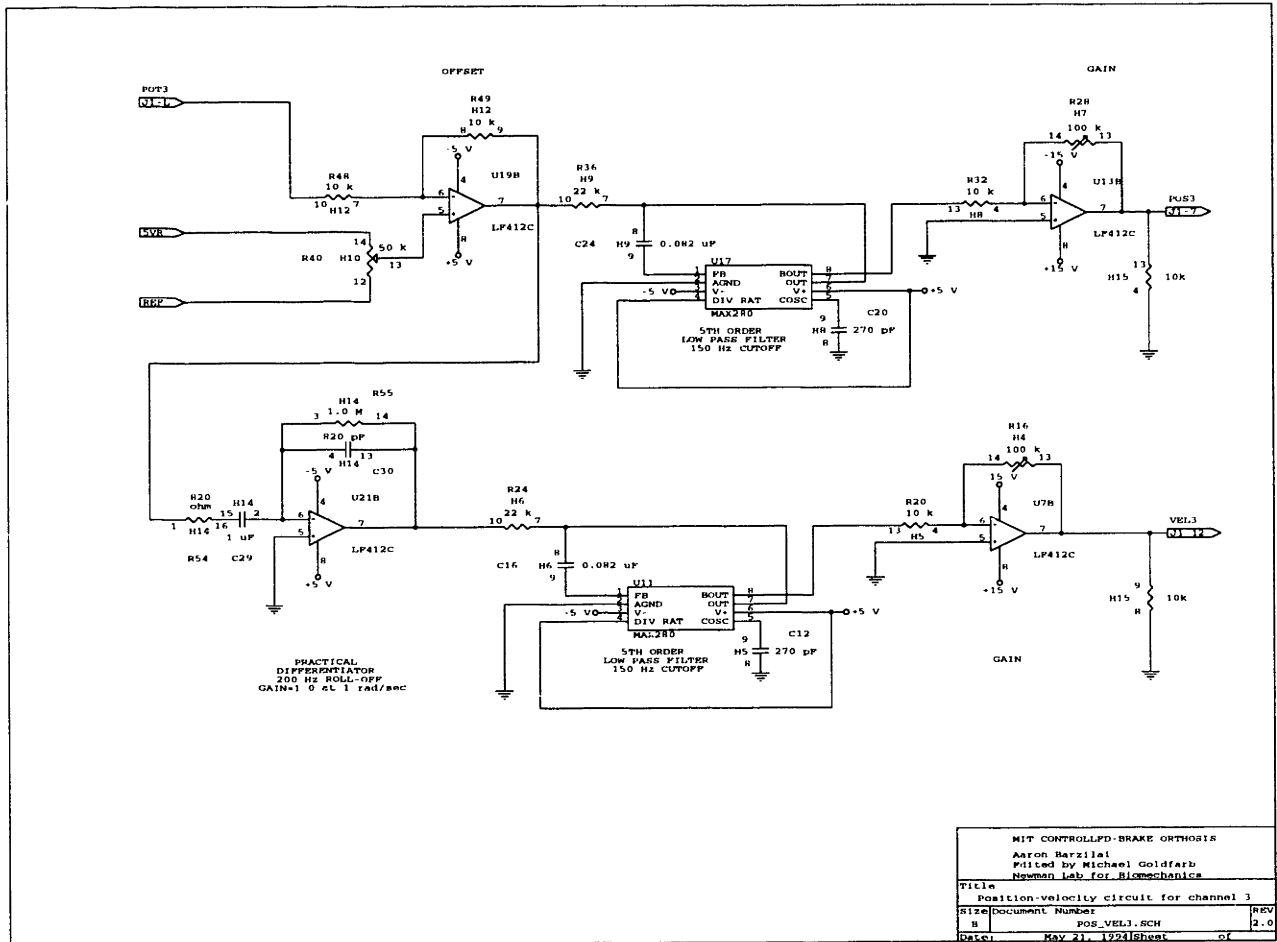
Figure B-6: Channel 3 joint angle and velocity signal processing. The joint angle processing includes an offset stage, a low-pass anti-aliasing filter with a 150 Hz cutoff, and an adjustable gain stage. The velocity segment includes a practical differentiator, a low-pass anti-aliasing filter, and a gain stage.

163
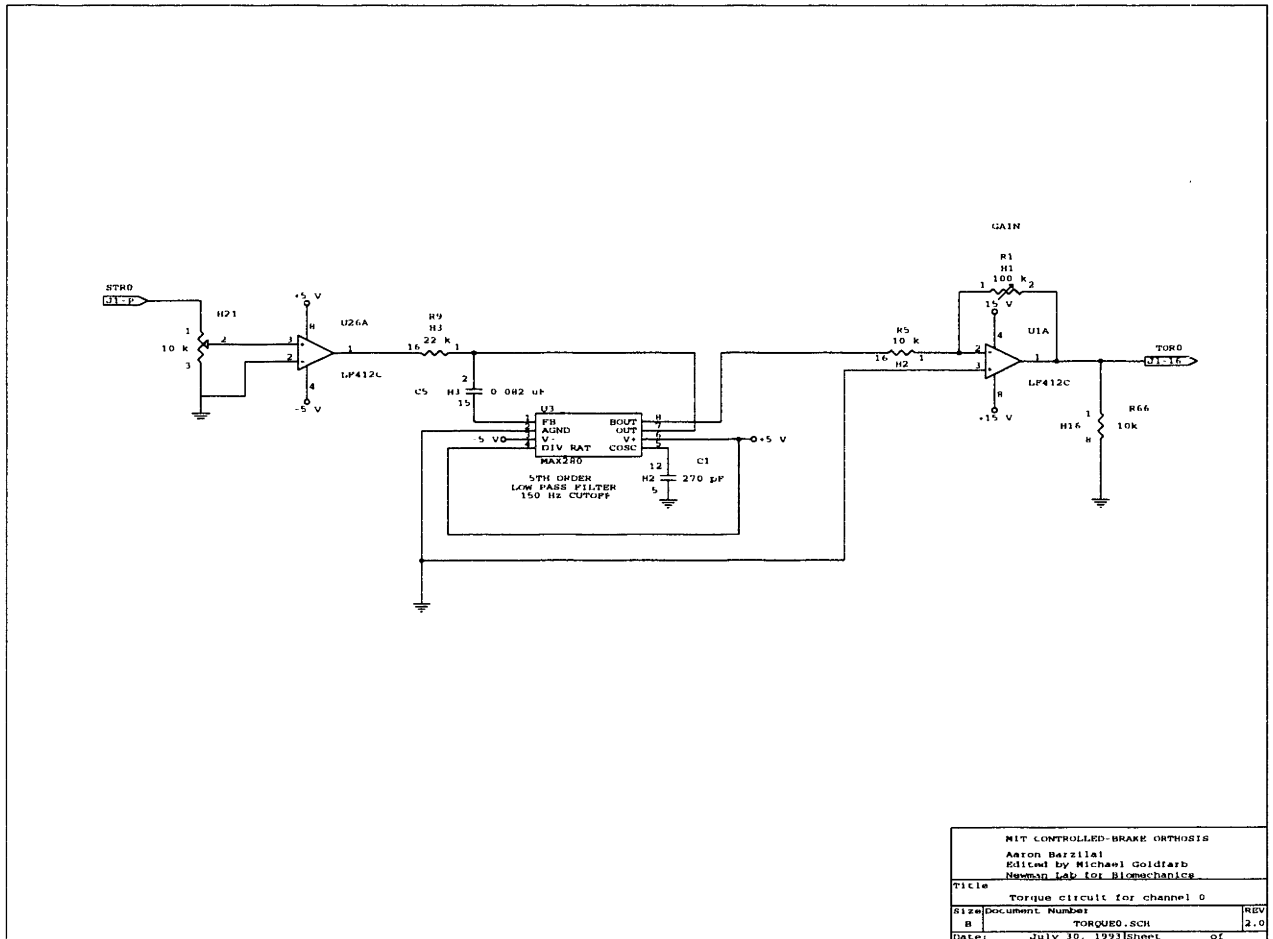
Figure B-7: Channel 0 joint torque signal processing. The torque signal is sent through the brace umbilical at a voltage level between +15V and -15V to maximize the signal-to-noise ratio, then attenuated for the low pass filters, since the CMOS filters can only accomodate between +5V and -5V. The torque signal processing includes an initial gain stage (located in the joint electronics of the brace and not shown in this schematic), an attenuation, a low-pass anti-aliasing filter with a 150 Hz cutoff, and an adjustable gain stage.

164
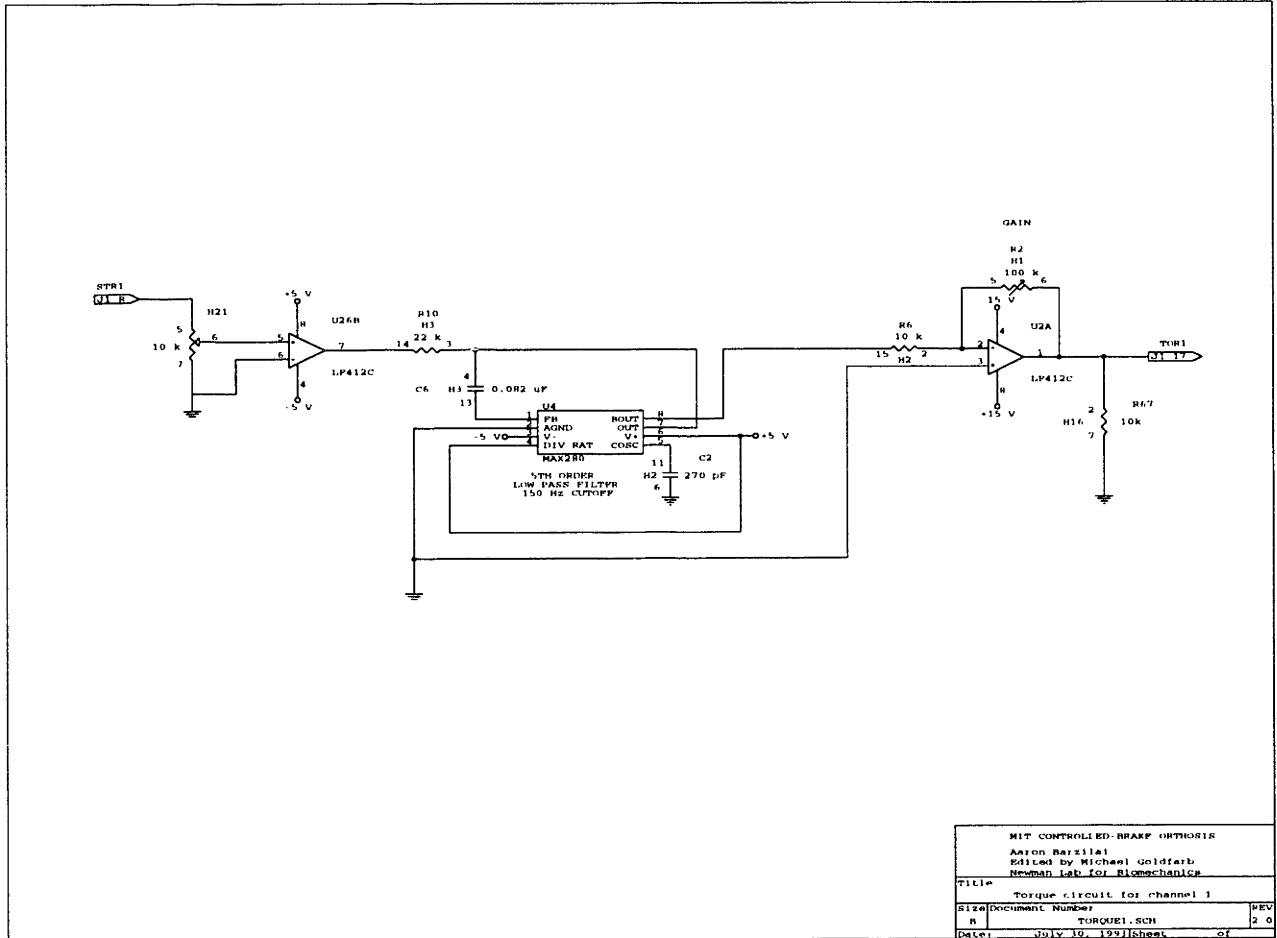
Figure B-8: Channel 1 joint torque signal processing. The torque signal is sent through the brace umbilical at a voltage level between +15V and -15V to maximize the signal-to-noise ratio, then attenuated for the low pass filters, since the CMOS filters can only accomodate between +5V and -5V. The torque signal processing includes an initial gain stage (located in the joint electronics of the brace and not shown in this schematic), an attenuation, a low-pass anti-aliasing filter with a 150 Hz cutoff, and an adjustable gain stage.
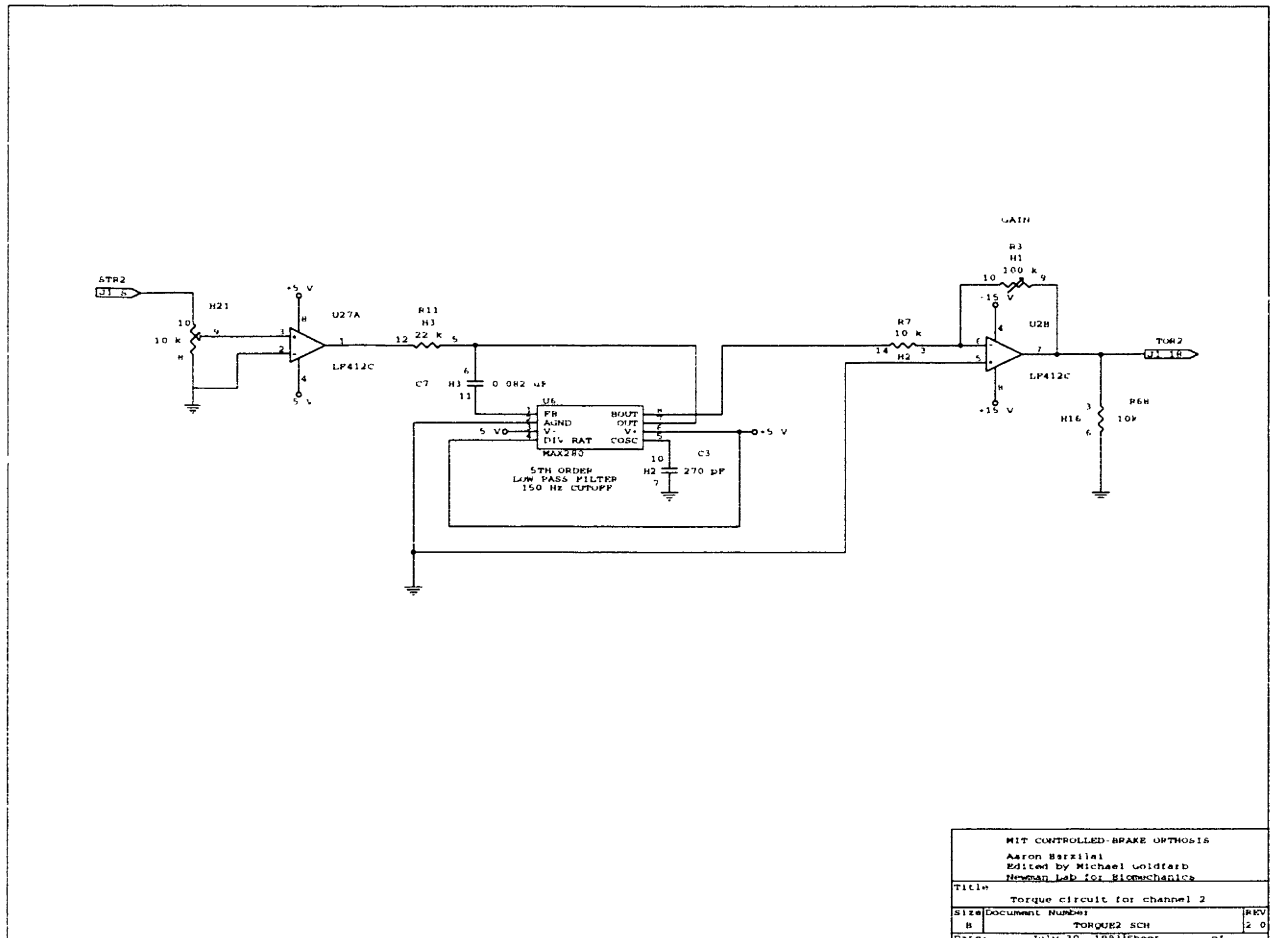
Figure B-9: Channel 2 joint torque signal processing. The torque signal is sent through the brace umbilical at a voltage level between +15V and -15V to maximize the signal-to-noise ratio, then attenuated for the low pass filters, since the CMOS filters can only accomodate between +5V and -5V. The torque signal processing includes an initial gain stage (located in the joint electronics of the brace and not shown in this schematic), an attenuation, a low-pass anti-aliasing filter with a 150 Hz cutoff, and an adjustable gain stage.
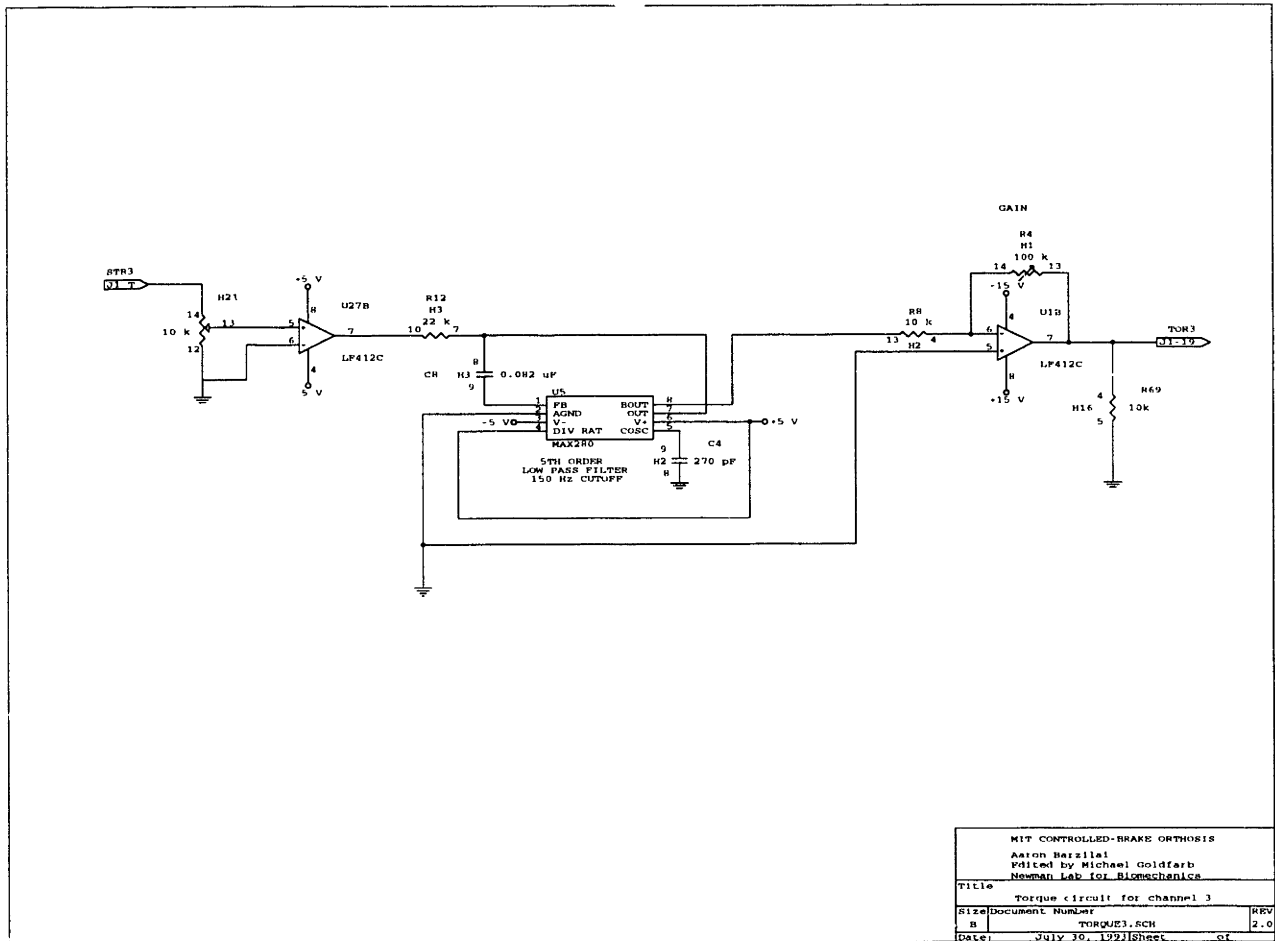
Figure B-10: Channel 3 joint torque signal processing. The torque signal is sent through the brace umbilical at a voltage level between +15V and -15V to maximize the signal-to-noise ratio, then attenuated for the low pass filters, since the CMOS filters can only accomodate between +5V and -5V. The torque signal processing includes an initial gain stage (located in the joint electronics of the brace and not shown in this schematic), an attenuation, a low-pass anti-aliasing filter with a 150 Hz cutoff, and an adjustable gain stage.
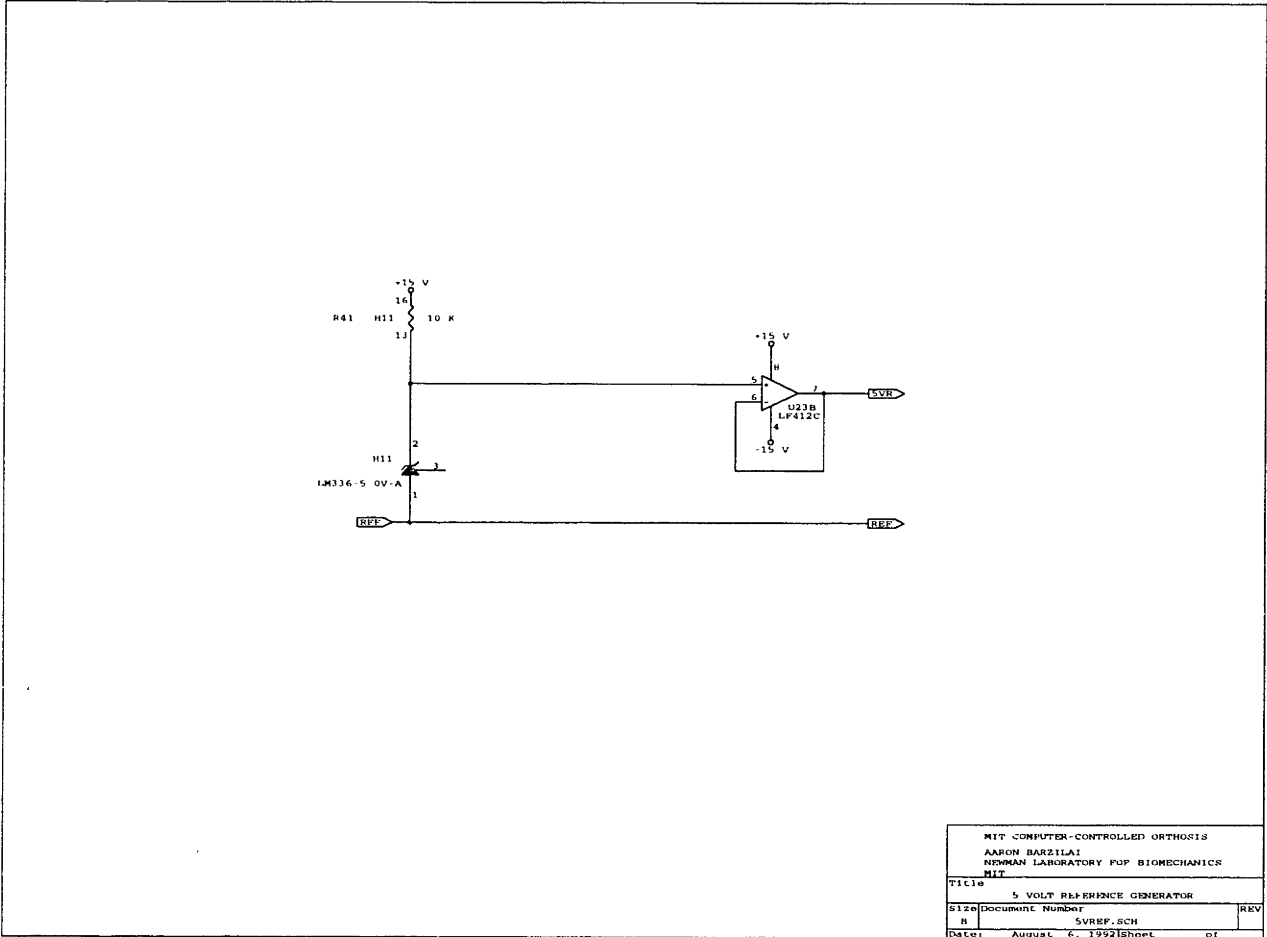
Figure B-11: Circuit to provide +5V reference voltage for all sensor signals.
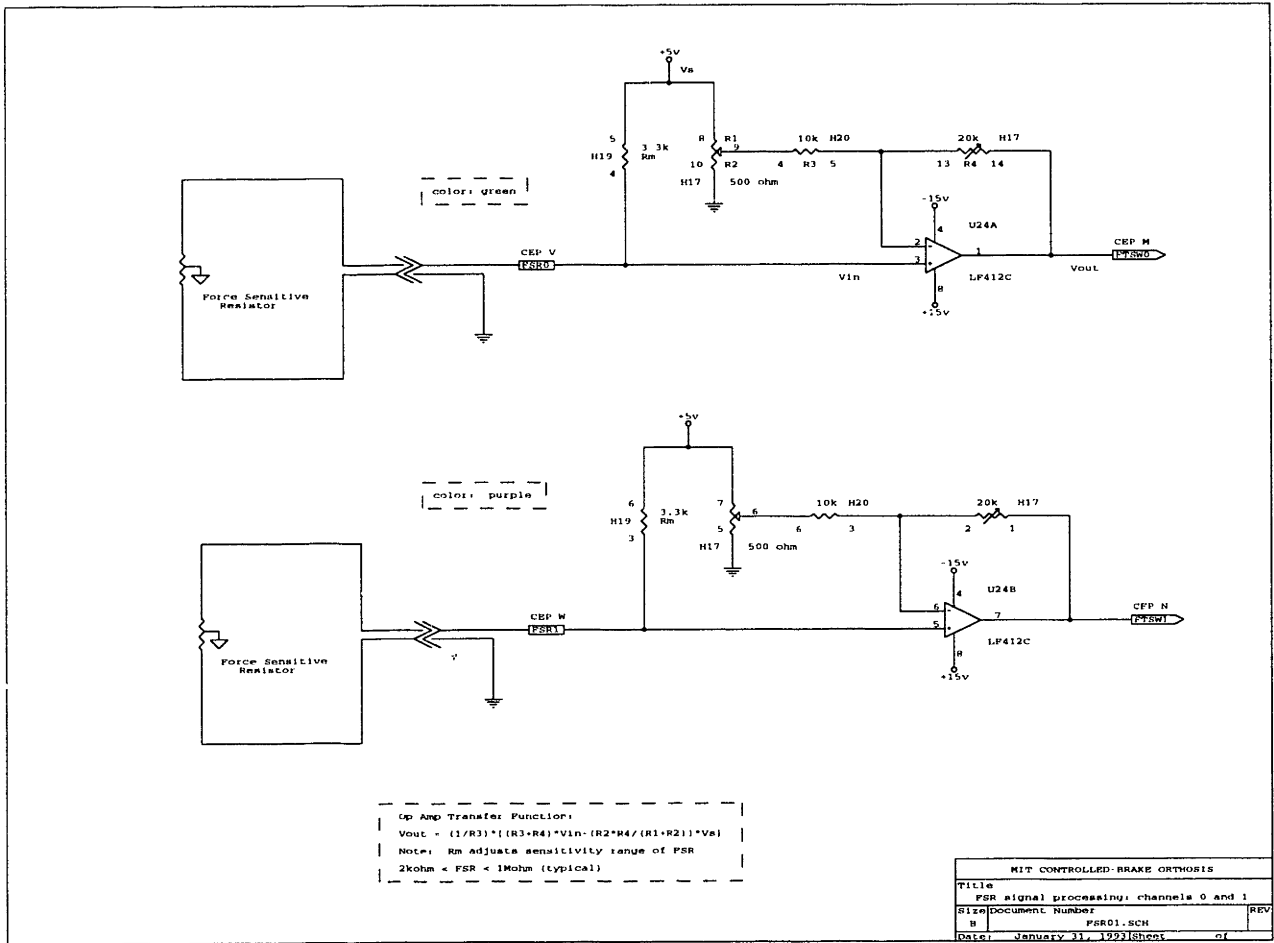
Figure B-12: Circuit for Interlink Electronics Force Sensitive Resistors (FSR) for channels 0 and 1. These circuits are currently wired, but FSR's are not presently implemented on the CBO.
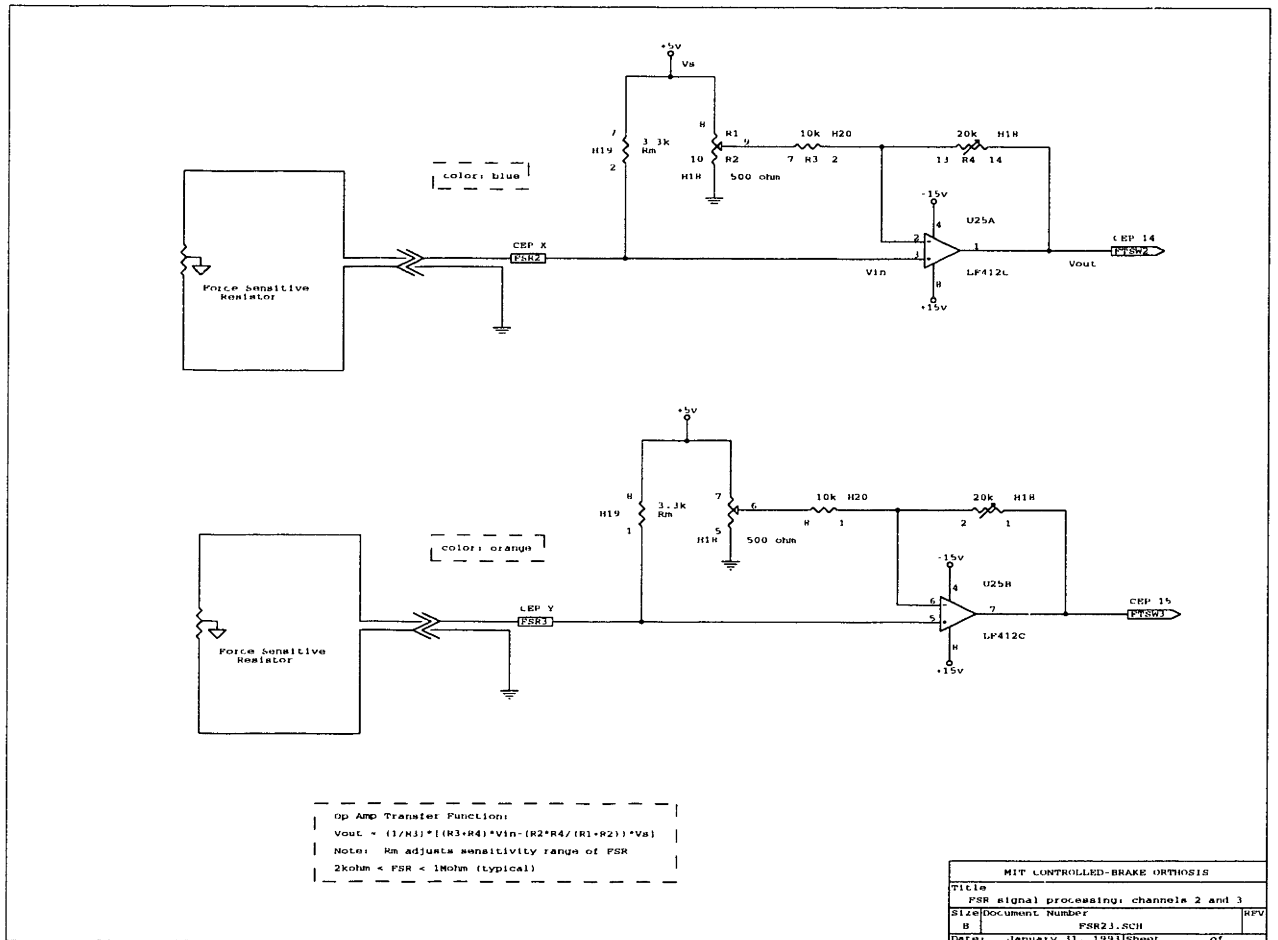
Figure B-13: Circuit for Interlink Electronics Force Sensitive Resistors (FSR) for channels 2 and 3. These circuits are currently wired, but FSR's are not presently implemented on the CBO.
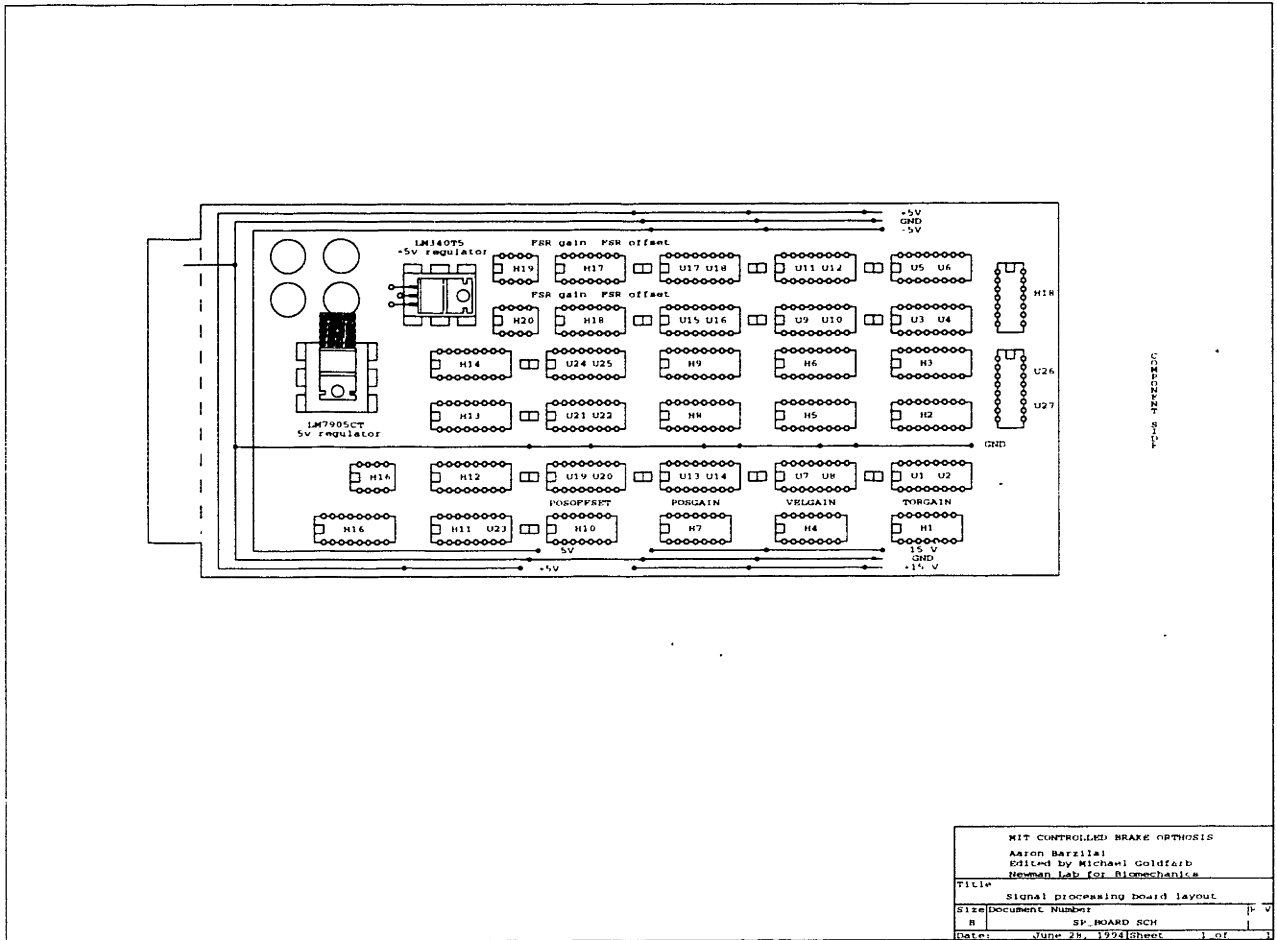
Figure B-14: Signal processing board.

B.1.2 Magnetic Particle Brake Servo-amplifiers
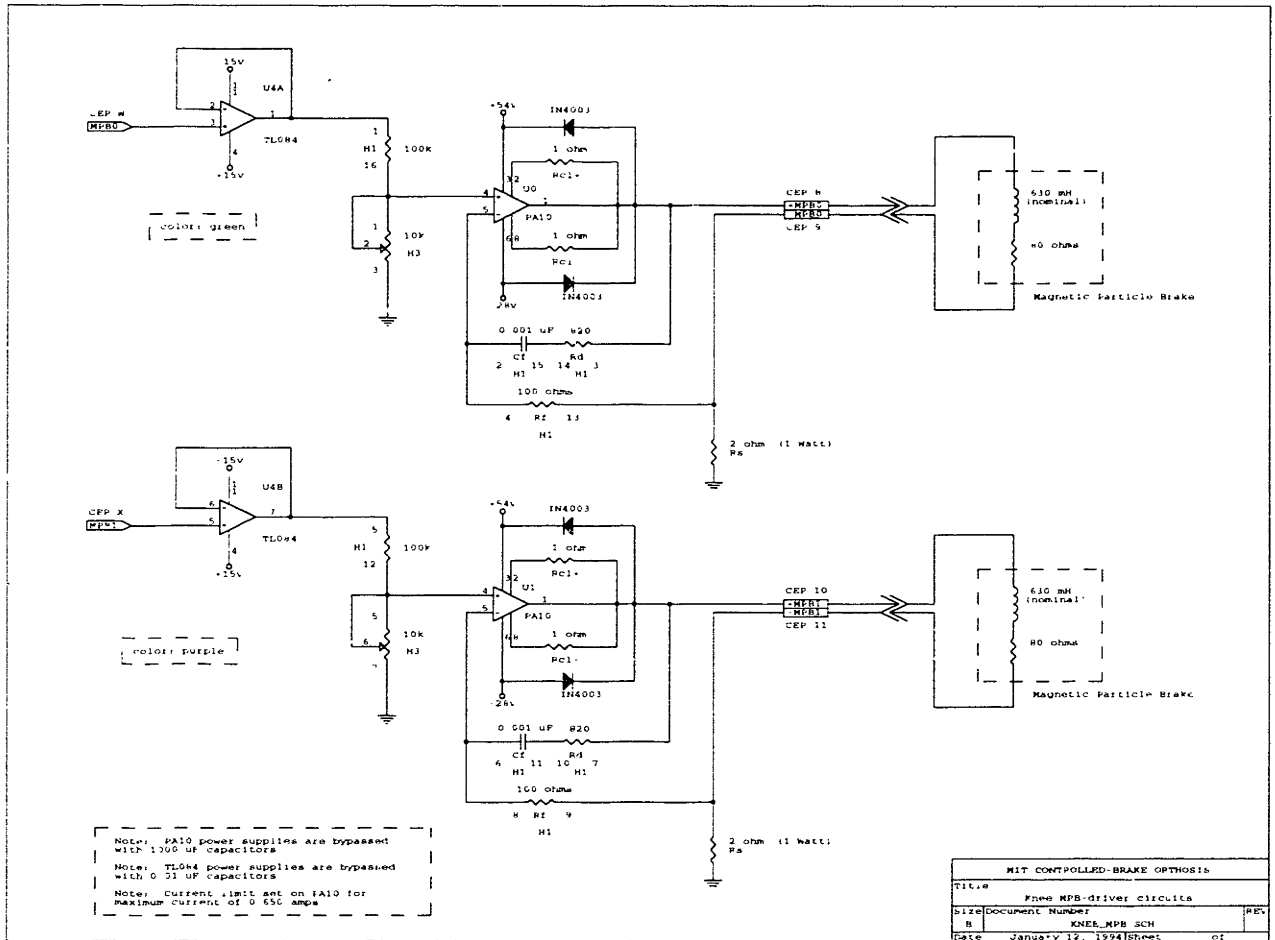
Figure B-15: Servo-amplifiers for the right and left knee magnetic particle brakes (channels 0 and 1, respectively). The voltage-to-current converters are based on Apex PA10 power amplifiers. The resistors and capacitor in the feedback path act to stabilize the closed-loop system.
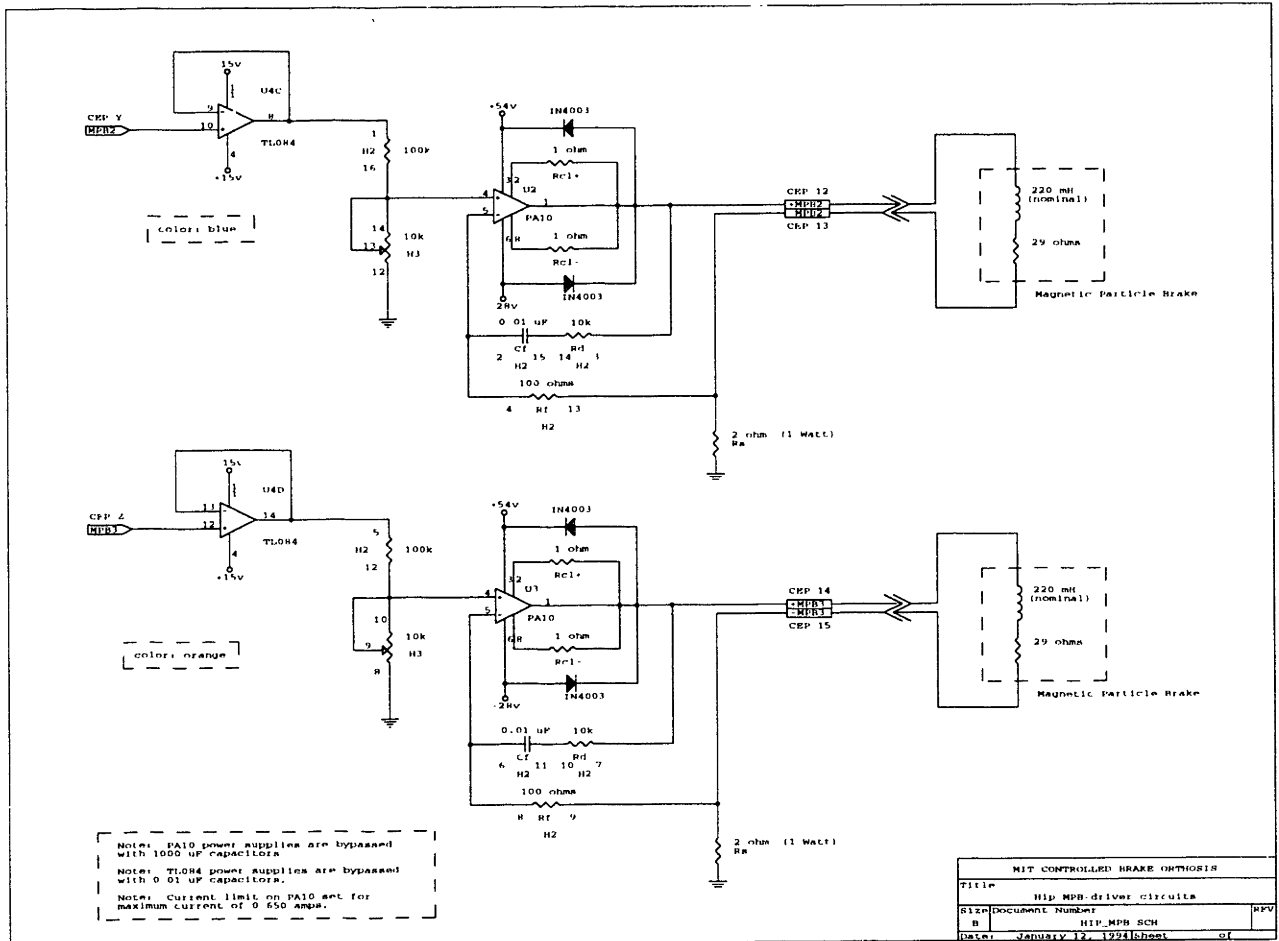
Figure B-16: Servo-amplifiers for the right and left hip magnetic particle brakes (channels 2 and 3, respectively). The voltage-to-current converters are based on Apex PA10 power amplifiers. The resistors and capacitor in the feedback path act to stabilize the closed-loop system.

173
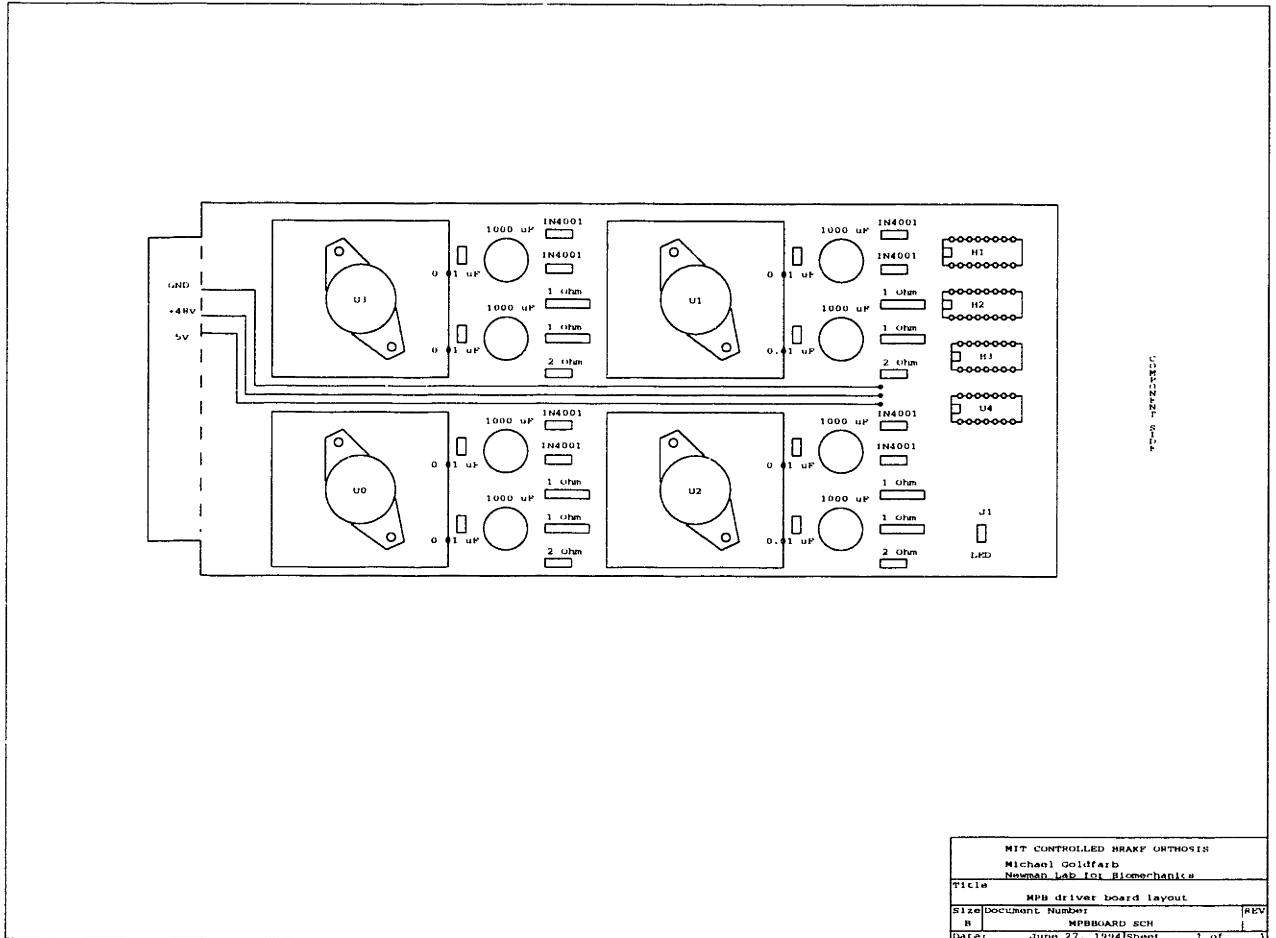
Figure B-17: Magnetic particle brake servo-amplifier board.

B.1.3 Connections

Figure B-18: Schematic of brace electronics input/output connections.
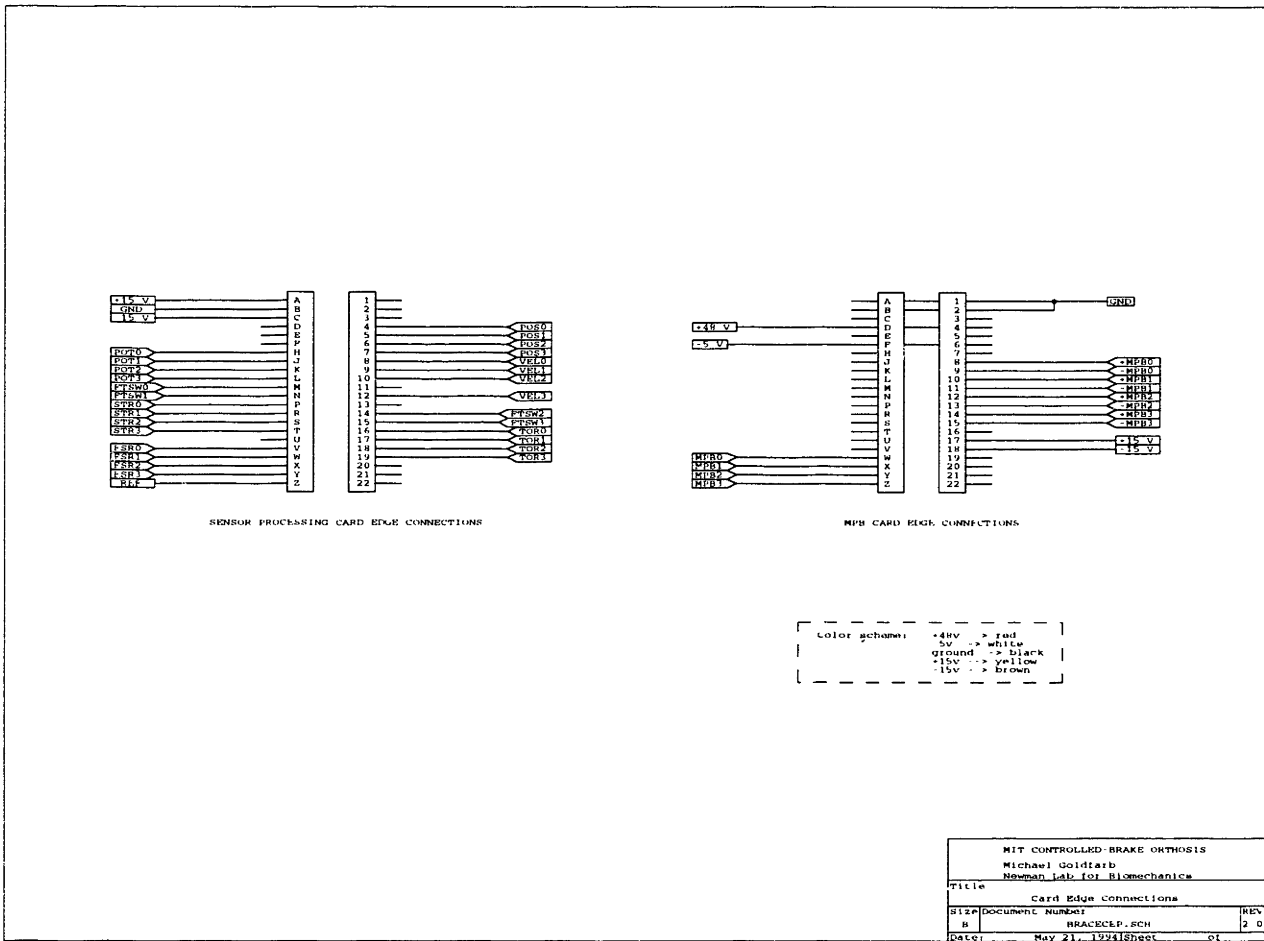
Figure B-19: Schematic of card edge connector pin assignments.

B.2 Parts List

B.2.1 Card Rack and Case

Item (Mfr Part No.)	Description	Quantity	Distributor (Dstr Part No.)
Hammond RCBS Rack Case		1	Newark (50F8488)
Vector Card Cage (CCK14F190)		1	Newark (51F3497)
Vector Card Guides (CG2-95P)		1	Newark (98F2284)
Vector Cards (3662-2)		3	Newark (38F1105)
Vector Card Edge Connectors (R644-3)		3	Newark (38F1140)

B.2.2 Case Components and Power Supplies

Item (Mfr Part No.)	Description	Quantity	Distributor (Dstr Part No.)
Power One +48V Supply (HD48-3-A)	positive rail for particle brake servoamps	1	Pioneer (HD48-3-A)
Power One +24V Supply (HB24-1.2-A)	negative rail for particle brake servoamps	1	Pioneer (HB24-1.2-A)
Power One +/-15V Supply (HBB15-1.5-A)	supply for IC's	1	Pioneer (HBB15-1.5-A)
Micro Fan (2408NL-04W-B30)	12V DC electric fan	1	Newark (50F5382)
green LED	panel mount	1	Digi-Key (L10005-ND)
DPDT rocker switch	panel mount	1	Digi-Key (SW307-ND)
37-pin female, panel mount, solder-tail D-connector	connector for Metrabyte DDA-06 card	1	Digi-Key (137F-ND)
37-pin male, panel mount, solder-tail D-connector	connector for stimulator	1	Digi-Key (137M-ND)
25-pin female, panel mount, solder-tail D-connector	connector for sensor umbilical	1	Digi-Key (125F-ND)
9-pin female, panel mount, solder-tail D-connector	connector for particle brake umbilical	1	Digi-Key (109F-ND)
50-pin, panel mount, flat cable connector	connector for Analog Devices RTI-815 card	1	Digi-Key (MPL50G-ND)
820 ohm resistor	for LED circuit	1	Digi-Key (820Q)
jack screw kit	mounting hardware for connectors	1	Digi-Key (7233K-ND)

B.2.3 Signal Processing Board

Item (Mfr Part No.)	Description	Quantity	Distributor (Dstr Part No.)
Maxim 280ACPA	Butterworth 5-pole low pass filter	12	Allied (MAX280ACPA)
National LF412CN	dual op amp	13	Digi-Key (LF412CN)
National LM340T-5	+5V regulator	1	Digi-Key (LM340T-5)
National LM7905CT	-5V regulator	1	Digi-Key (LM7905CT)
National LM336Z-5.0	+5V reference	1	Digi-Key (LM336Z-5.0)
10 Kohm resistor	for LM336Z-5.0	1	Digi-Key (10KQ)
10 Kohm trimpots		4	Digi-Key (3299W-103-ND)
50 Kohm trimpots		4	Digi-Key (3299W-503-ND)
100 Kohm trimpots		12	Digi-Key (3299W-104-ND)
22 Kohm resistor		12	Digi-Key (22KQ)
10 Kohm resistor		32	Digi-Key (10KQ)
820 ohm resistor		4	Digi-Key (820Q)
470 Kohm resistor		2	Digi-Key (470KQ)
1.0 Mohm resistor		2	Digi-Key (1MQ)
100 uF electrolytic capacitors		4	Digi-Key (P6227)
0.082 uF non-polarized capacitors		12	Digi-Key (EF1823)
1.0 uF non-polarized capacitors		4	Digi-Key (EF1105)
270 pF capacitors		12	Digi-Key (P4029)
820 pF capacitors		2	Digi-Key (P4184)
1500 pF capacitors		2	Digi-Key (P4187)
0.01 uF capacitors	power supply bypass capacitors	30	Digi-Key (P4300)

B.2.4 MPB Servoamp Board

Item (Mfr Part No.)	Description	Quantity	Distributor (Dstr Part No.)
Apex PA10	power op amp	4	Apex (PA10)
PA10 heat sink		4	Apex (HS02)
PA10 socket		4	Apex (MS03)
PA10 thermal washers		4	Apex (TW03)
Texas Instruments TL084CJ	quad op amp	1	Allied (TL084CJ)
2 ohm, 1 watt resistor		4	Digi-Key (SC1A2.0-ND)
2 ohm, 1/2 watt resistor		8	Digi-Key (2.0H)
10 Kohm trimpots		4	Digi-Key (3299W-103-ND)
10 Kohm resistor		2	Digi-Key (10KQ)
100 Kohm resistor		4	Digi-Key (100KQ)
100 ohm resistor		4	Digi-Key (100Q)
820 ohm resistor		2	Digi-Key (820Q)
0.01 uF capacitors		10	Digi-Key (P4300)
0.001 uF capacitors		2	Digi-Key (DH102)
1000 uF, 63V electrolytic capacitors		4	Digi-Key (P6287)
1000 uF, 50V electrolytic capacitors		4	Digi-Key (P6272)
IN4003 diodes		8	Digi-Key (IN4003)

B.2.5 Joint PC Boards

Item (Mfr Part No.)	Description	Quantity	Distributor (Dstr Part No.)
Analog Devices AD620AN	instrumentation amp	4	Allied (AD620AN)
National LF412CN	dual op amp	4	Digi-Key (LF412CN)
National LM336Z-5.0	+5V reference	4	Digi-Key (LM336Z-5.0)
10 Kohm resistor	for LM336Z-5.0	4	Digi-Key (10KQ)
22 Kohm resistor		4	Digi-Key (22KQ)
49.9 1% ohm resistor		2	Digi-Key (49.9XQ)
100 1% ohm resistor		2	Digi-Key (100XQ)
50 Kohm 1/4" trimpots		4	Digi-Key (3266X-503-ND)
6 pin connector sockets		1	Digi-Key (A3015-ND)
connector header		1	Digi-Key (S1082-36)
connector contacts		1	Digi-Key (A3003-ND)

B.2.6 Force Sensitive Resistive Circuits

Item (Mfr Part No.)	Description	Quantity	Distributor (Dstr Part No.)
National LF412CN	dual op amp	2	Digi-Key (LF412CN)
10 Kohm resistor		4	Digi-Key (10KQ)
3.3 Kohm resistor		4	Digi-Key (3.3KQ)
20 Kohm trimpots		4	Digi-Key (3299W-203-ND)
500 ohm trimpots		4	Digi-Key (3299W-501-ND)

B.2.7 Miscellaneous Parts

Item (Mfr Part No.)	Description	Quantity	Distributor (Dstr Part No.)
8 pin wire wrap socket		3	Digi-Key (ED4308)
14 pin wire wrap socket		9	Digi-Key (ED4314)
16 pin wire wrap socket		26	Digi-Key (ED4316)
8 pin socket labels		29	Jameco (8ID)
14 pin socket labels		9	Newark (46F5166)
16 pin socket labels		12	Newark (46F5167)
16 pin socket headers		12	Newark (44F5151)
T44 pins			Newark (38F1329)

B.3 Component Characterization

B.3.1 Servoamplifiers

Channel 0 Servoamplifier Responses
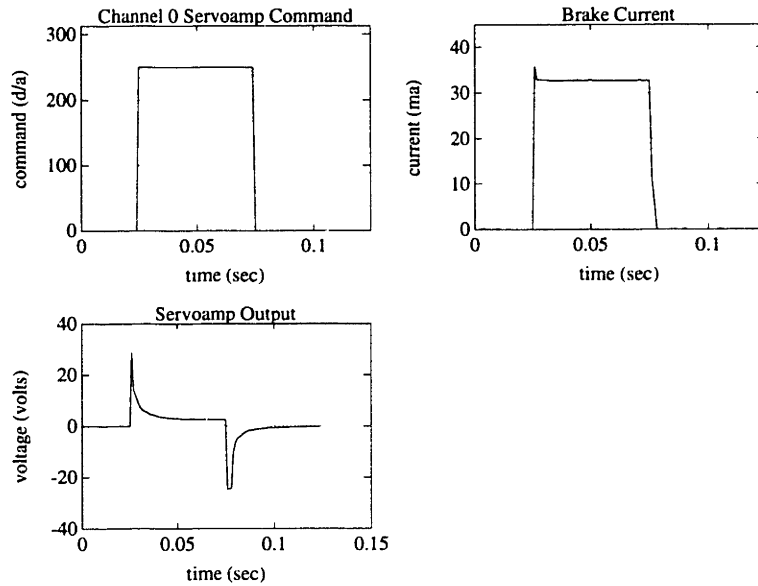
Figure B-20: Step response of the channel 0 (right knee) servoamplifier for a step input of 250 D/A units.
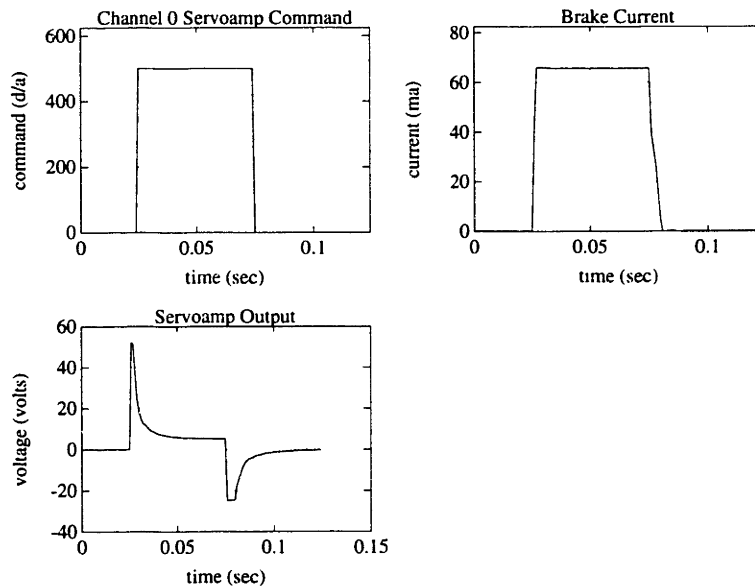
Figure B-21: Step response of the channel 0 (right knee) servoamplifier for a step input of 500 D/A units.
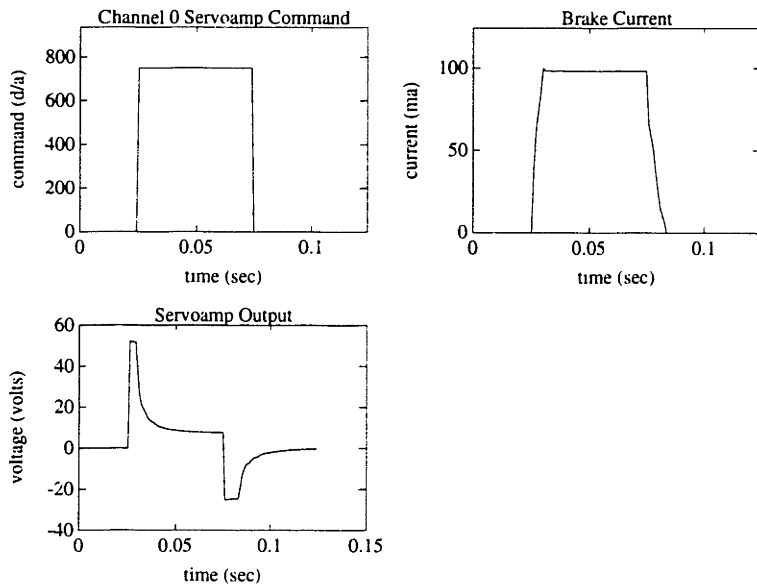
Figure B-22: Step response of the channel 0 (right knee) servoamplifier for a step input of 750 D/A units.
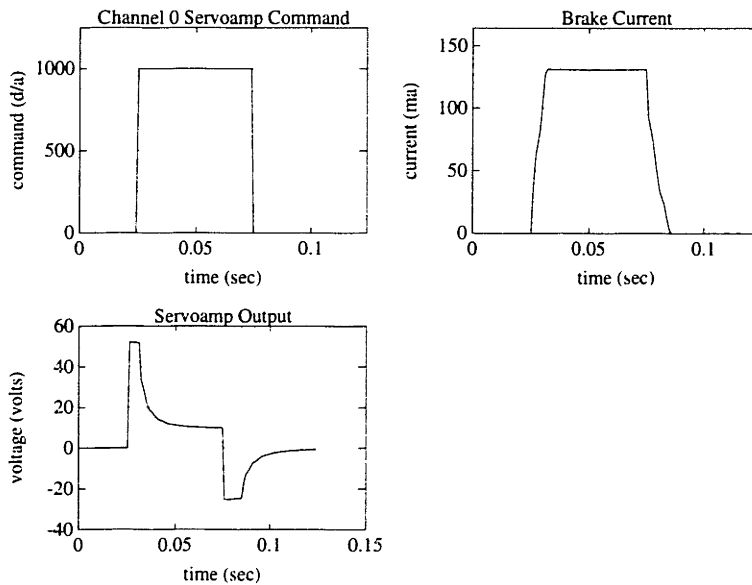
Figure B-23: Step response of the channel 0 (right knee) servoamplifier for a step input of 1000 D/A units.
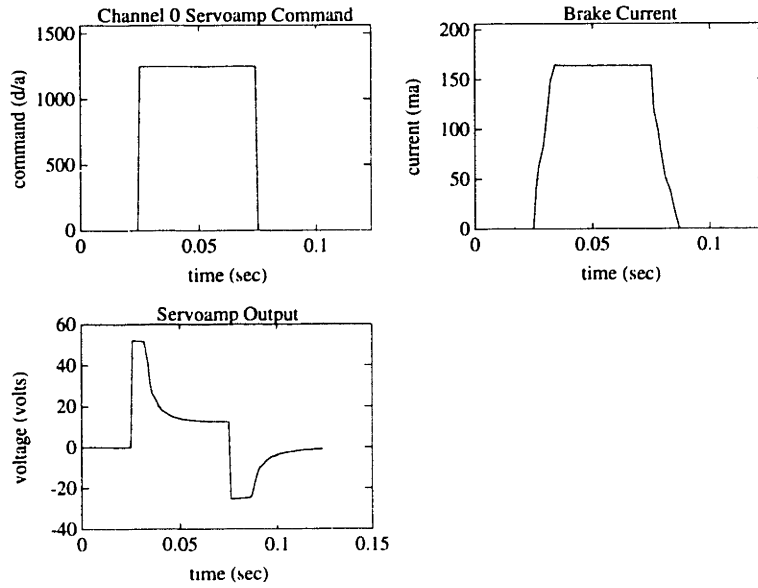
Figure B-24: Step response of the channel 0 (right knee) servoamplifier for a step input of 1250 D/A units.
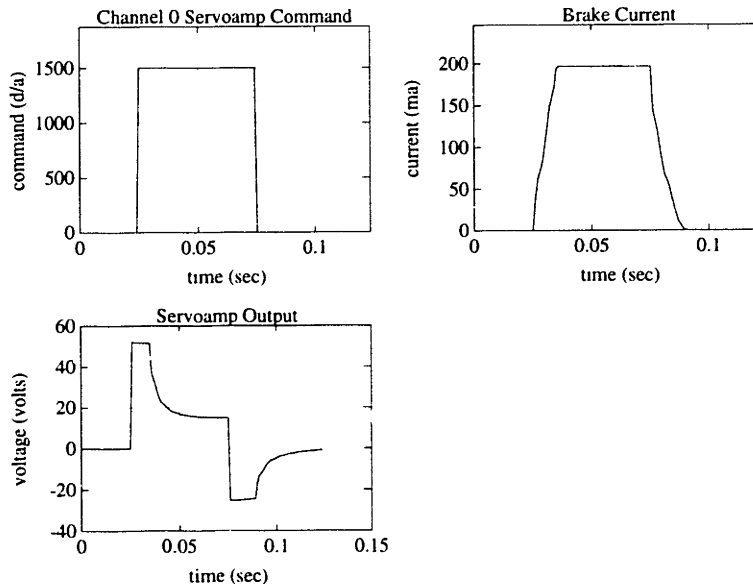
Figure B-25: Step response of the channel 0 (right knee) servoamplifier for a step input of 1500 D/A units.
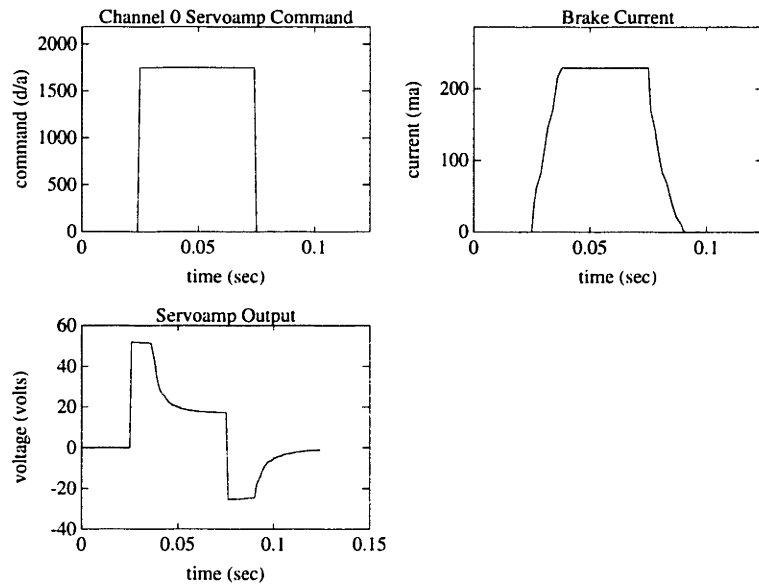
Figure B-26: Step response of the channel 0 (right knee) servoamplifier for a step input of 1750 D/A units.
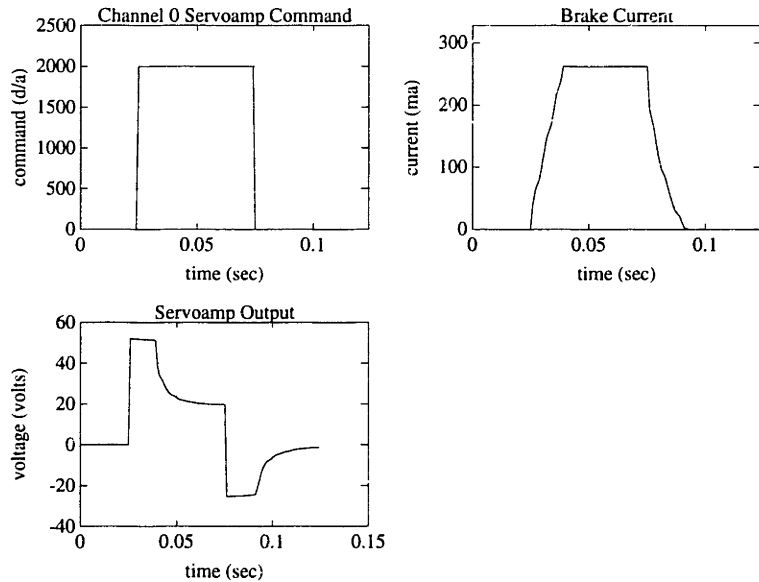
Figure B-27: Step response of the channel 0 (right knee) servoamplifier for a step input of 2000 D/A units.

Channel 1 Servoamplifier Responses
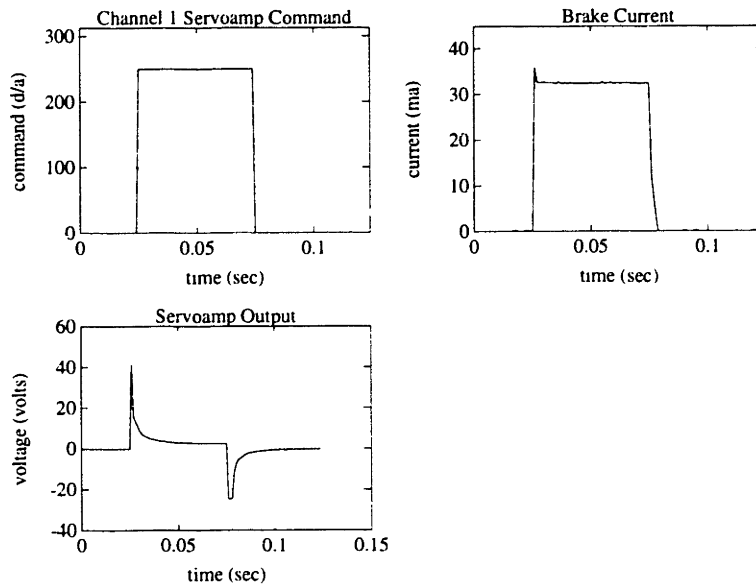
Figure B-28: Step response of the channel 1 (left knee) servoamplifier for a step input of 250 D/A units.
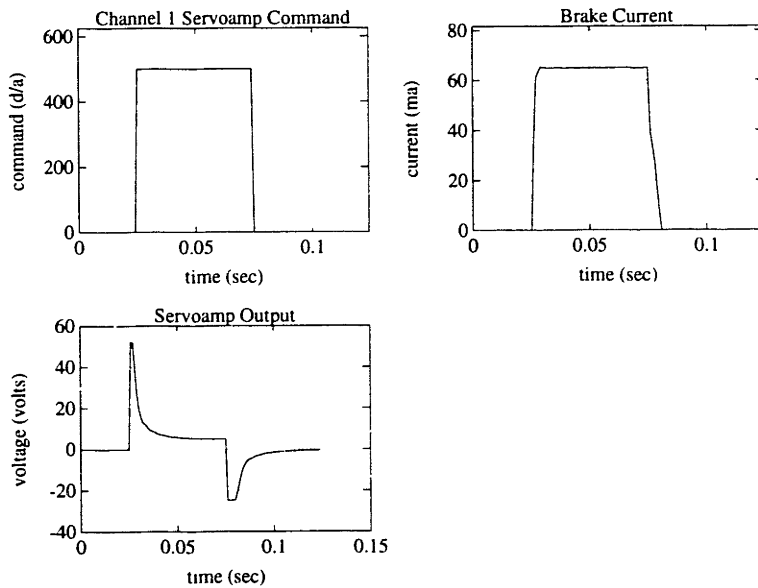
Figure B-29: Step response of the channel 1 (left knee) servoamplifier for a step input of 500 D/A units.
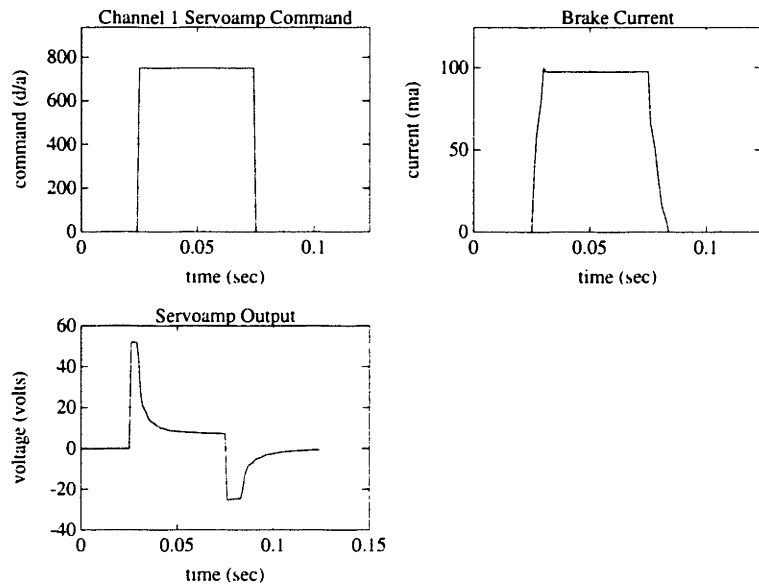
Figure B-30: Step response of the channel 1 (left knee) servoamplifier for a step input of 750 D/A units.
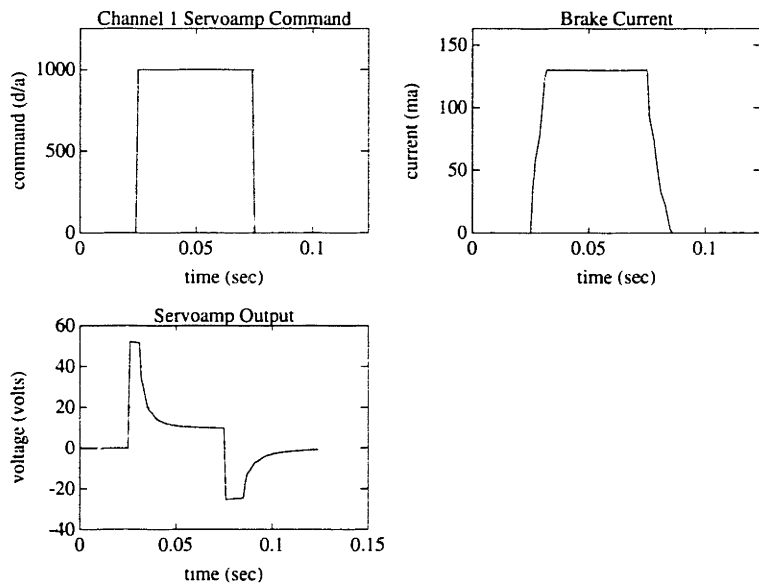
Figure B-31: Step response of the channel 1 (left knee) servoamplifier for a step input of 1000 D/A units.

188
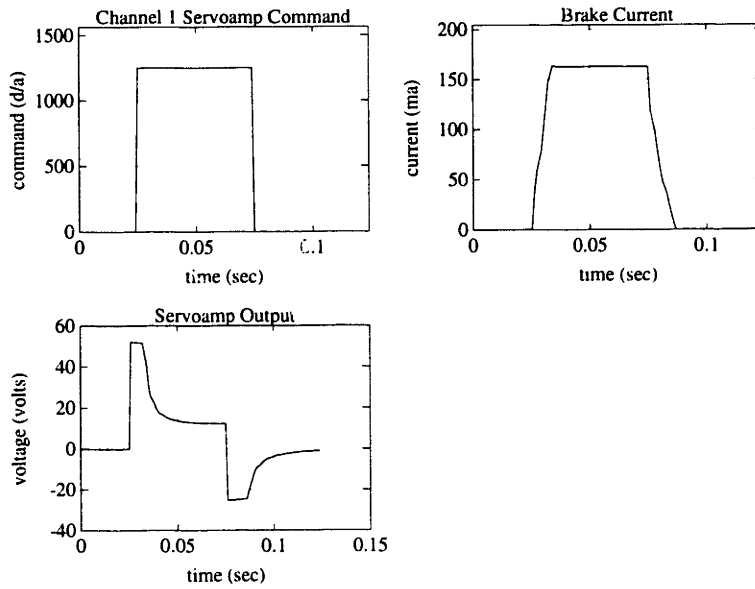
Figure B-32: Step response of the channel 1 (left knee) servoamplifier for a step input of 1250 D/A units.
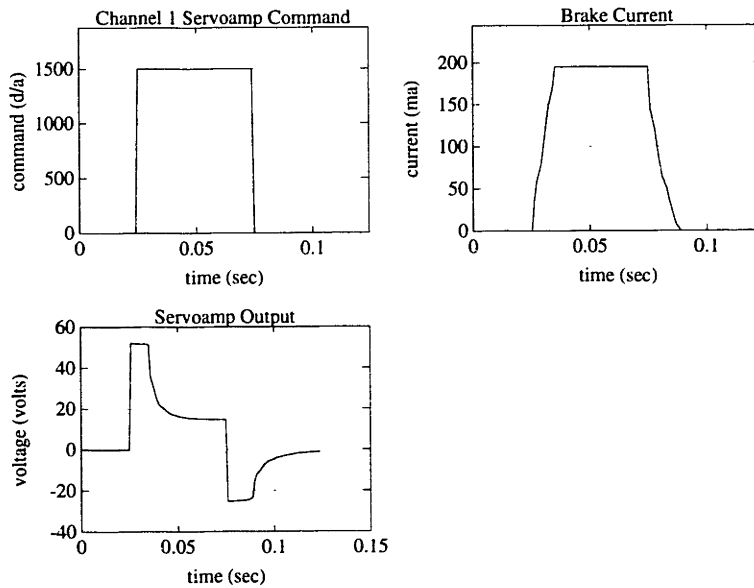
Figure B-33: Step response of the channel 1 (left knee) servoamplifier for a step input of 1500 D/A units.
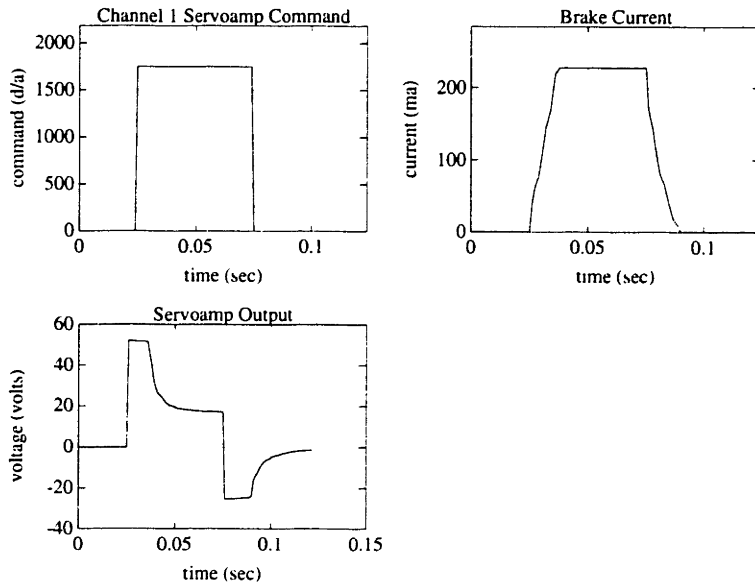
Figure B-34: Step response of the channel 1 (left knee) servoamplifier for a step input of 1750 D/A units.
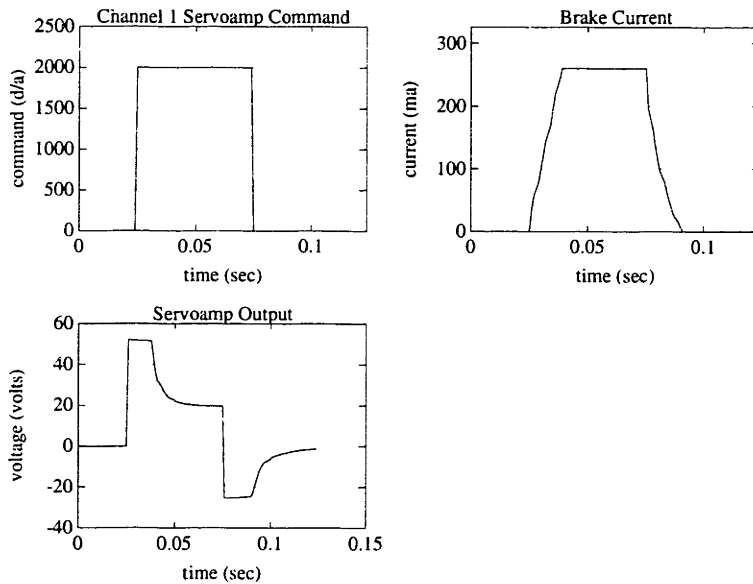
Figure B-35: Step response of the channel 1 (left knee) servoamplifier for a step input of 2000 D/A units.

Channel 2 Servoamplifier Responses
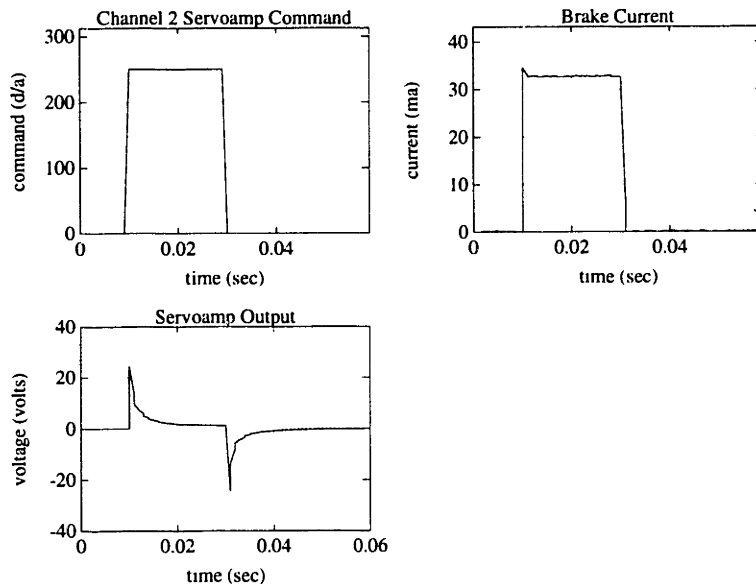
Figure B-36: Step response of the channel 2 (right hip) servoamplifier for a step input of 250 D/A units.
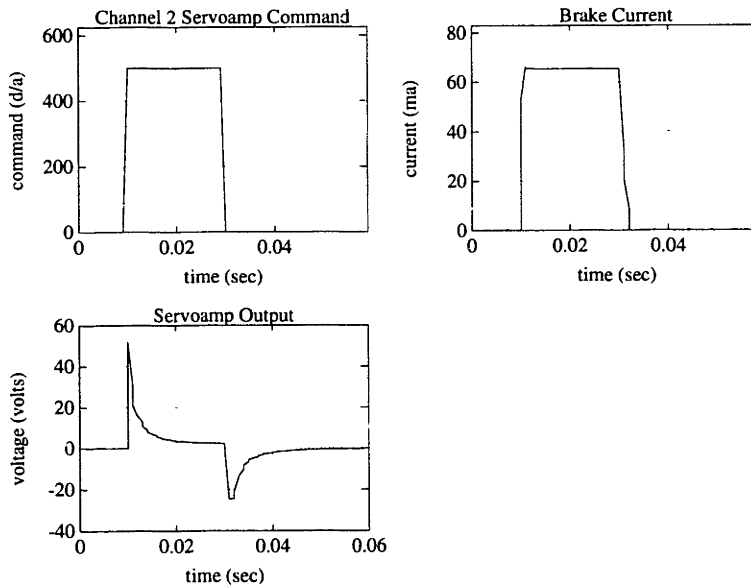
Figure B-37: Step response of the channel 2 (right hip) servoamplifier for a step input of 500 D/A units.
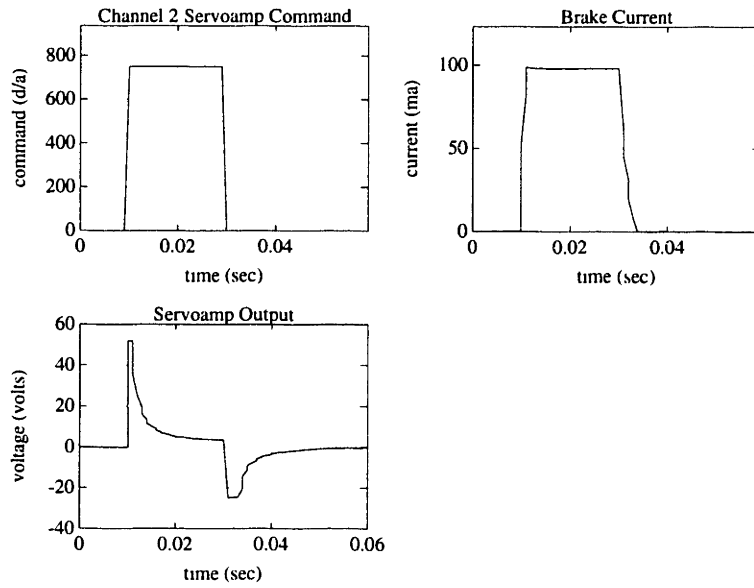
Figure B-38: Step response of the channel 2 (right hip) servoamplifier for a step input of 750 D/A units.
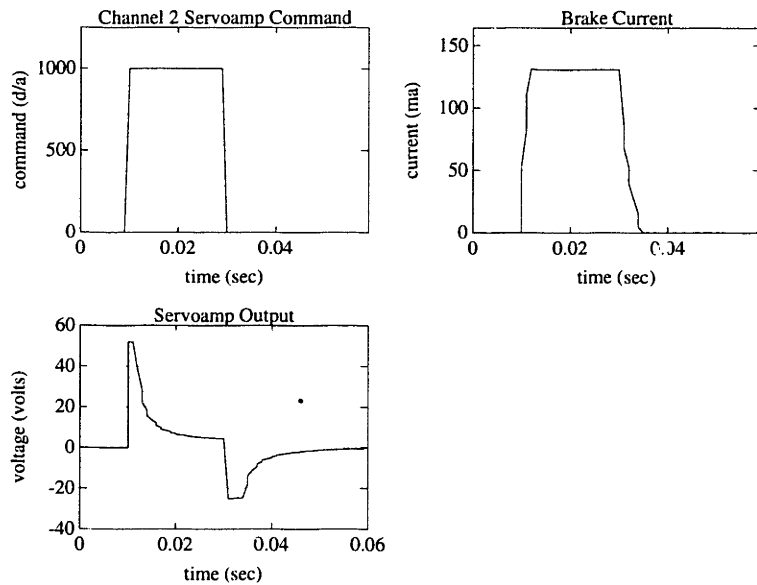
Figure B-39: Step response of the channel 2 (right hip) servoamplifier for a step input of 1000 D/A units.
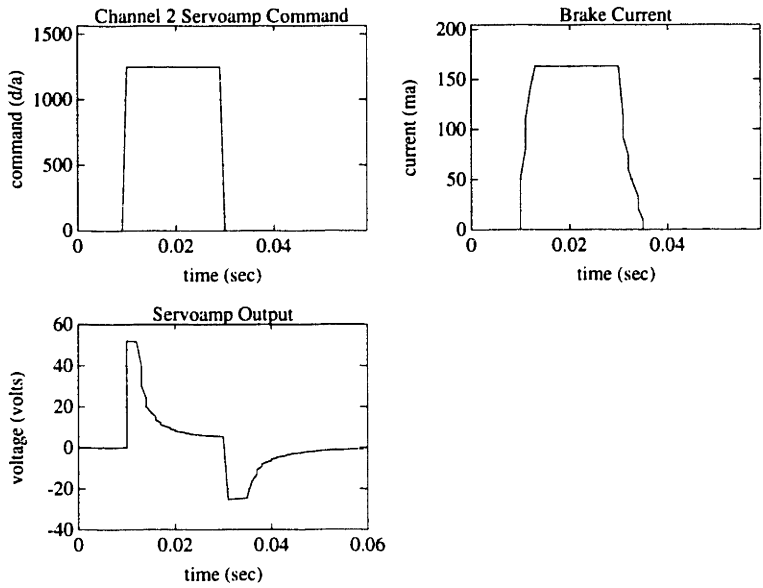
Figure B-40: Step response of the channel 2 (right hip) servoamplifier for a step input of 1250 D/A units.
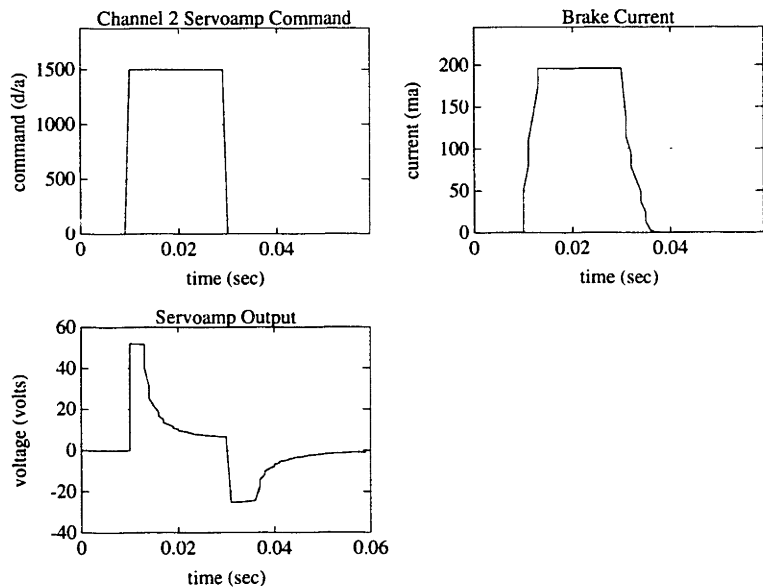
Figure B-41: Step response of the channel 2 (right hip) servoamplifier for a step input of 1500 D/A units.
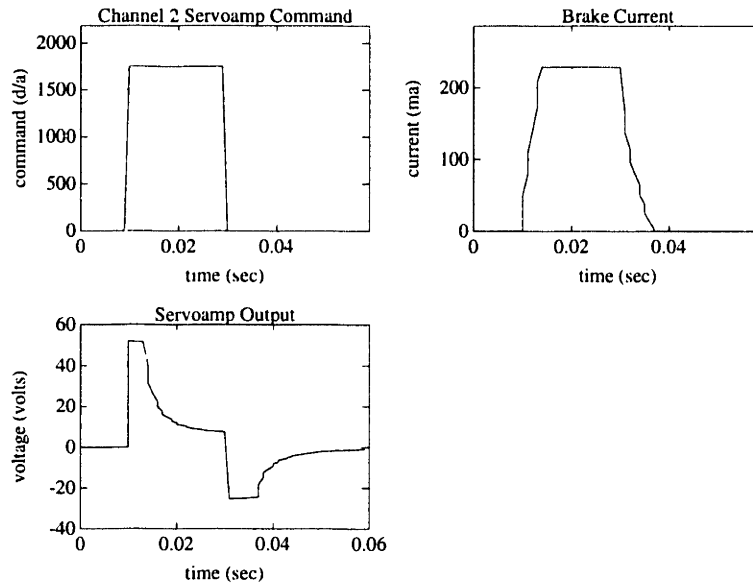
Figure B-42: Step response of the channel 2 (right hip) servoamplifier for a step input of 1750 D/A units.
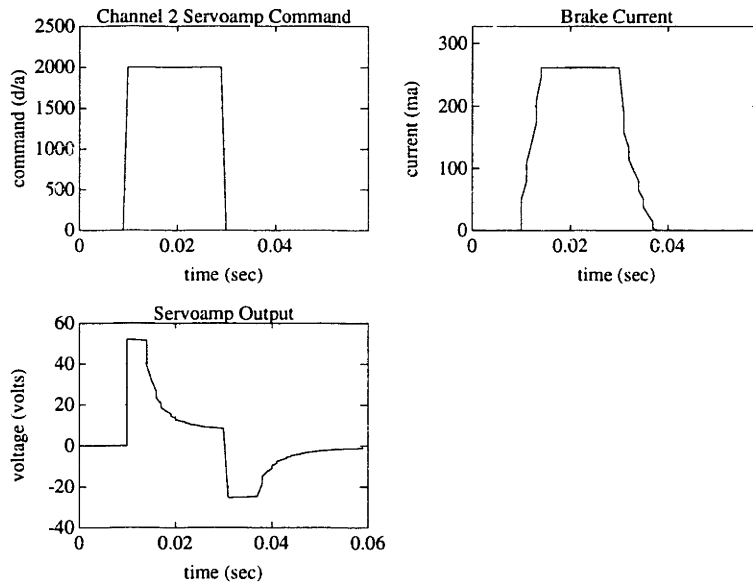
Figure B-43: Step response of the channel 2 (right hip) servoamplifier for a step input of 2000 D/A units.

Channel 3 Servoamplifier Responses
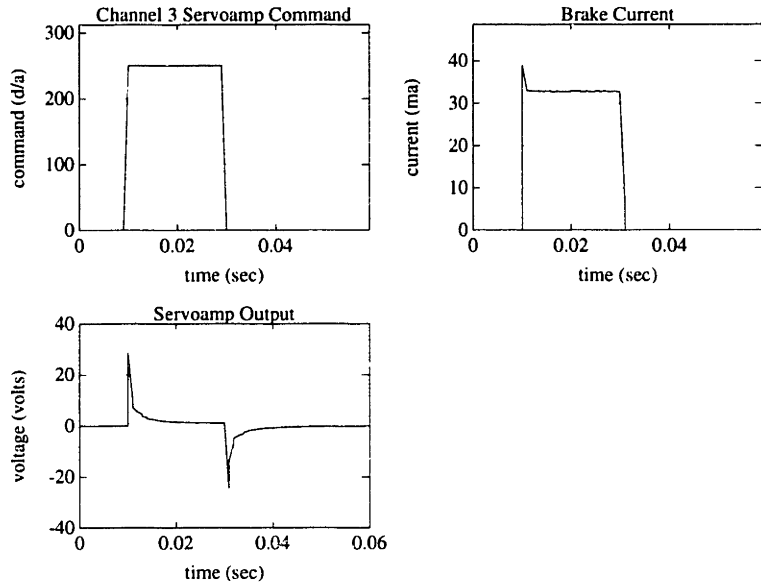
Figure B-44: Step response of the channel 3 (left hip) servoamplifier for a step input of 250 D/A units.
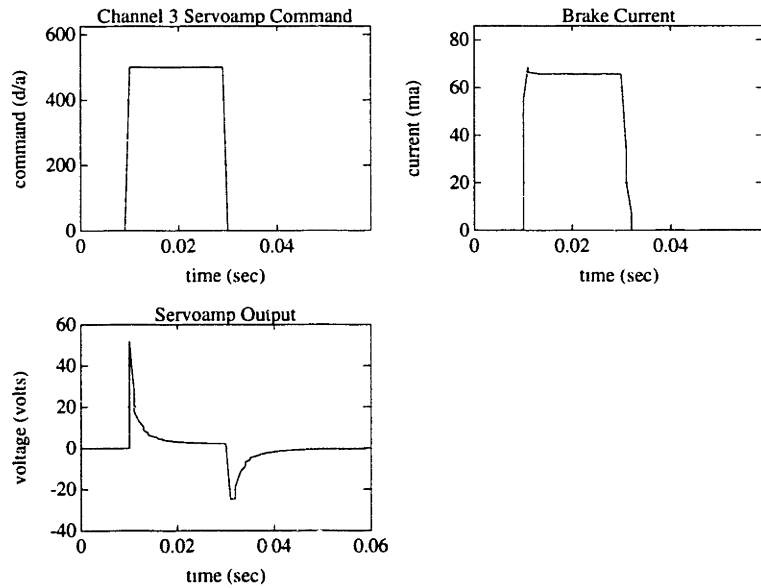
Figure B-45: Step response of the channel 3 (left hip) servoamplifier for a step input of 500 D/A units.
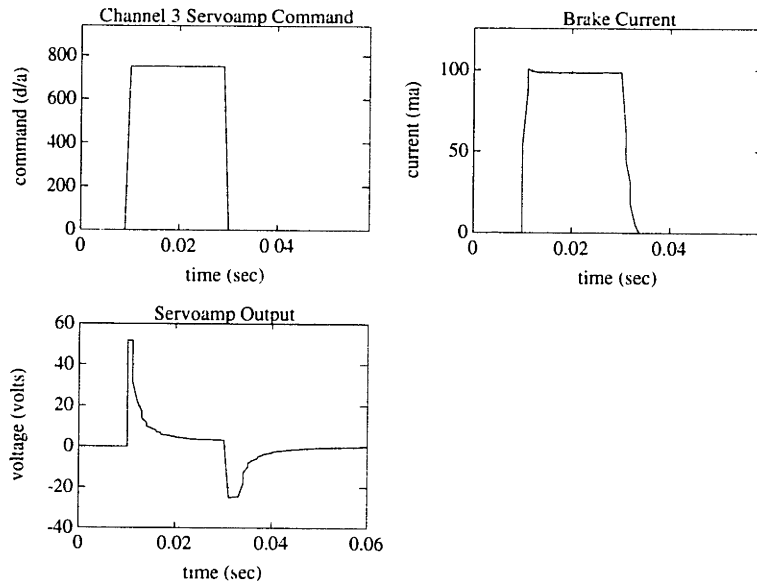
Figure B-46: Step response of the channel 3 (left hip) servoamplifier for a step input of 750 D/A units.
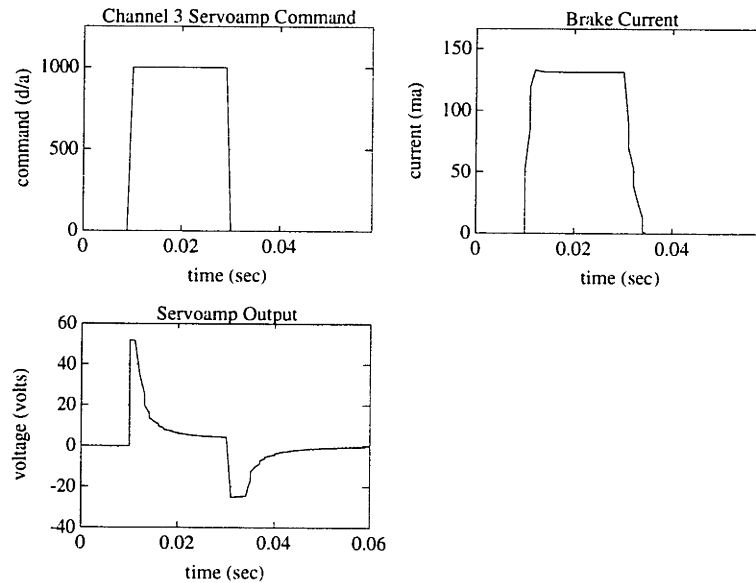
Figure B-47: Step response of the channel 3 (left hip) servoamplifier for a step input of 1000 D/A units.

196
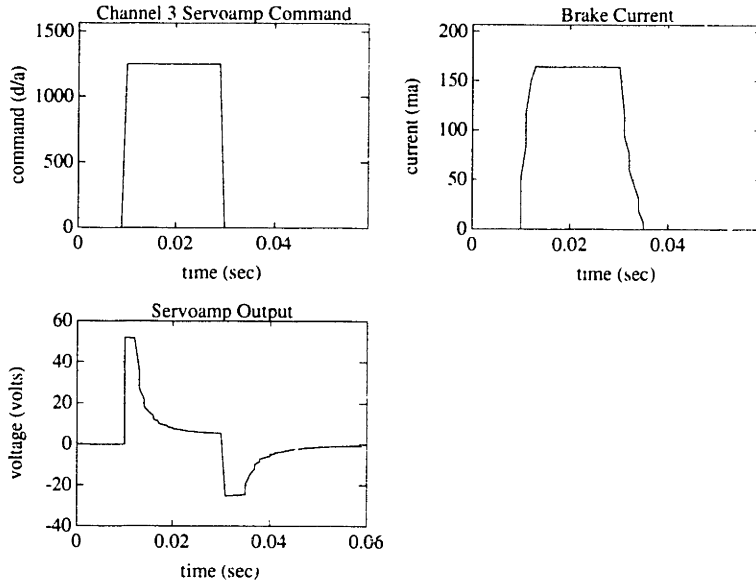
Figure B-48: Step response of the channel 3 (left hip) servoamplifier for a step input of 1250 D/A units.
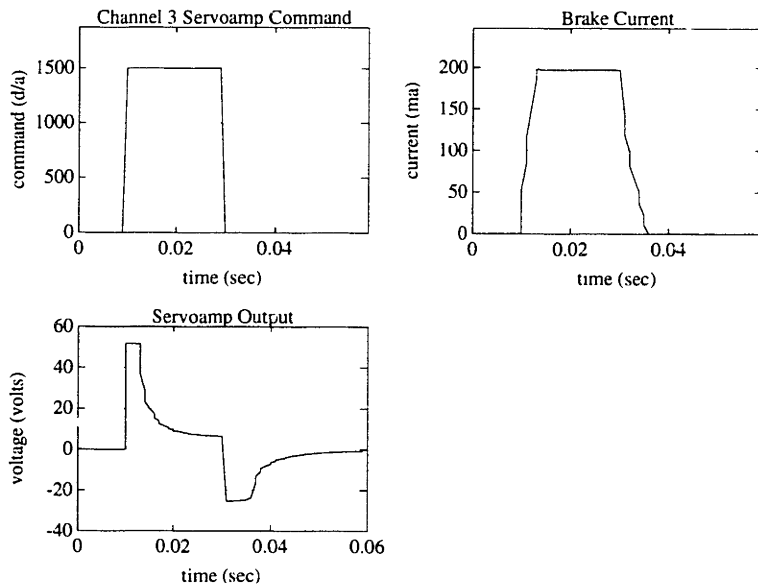
Figure B-49: Step response of the channel 3 (left hip) servoamplifier for a step input of 1500 D/A units.

197
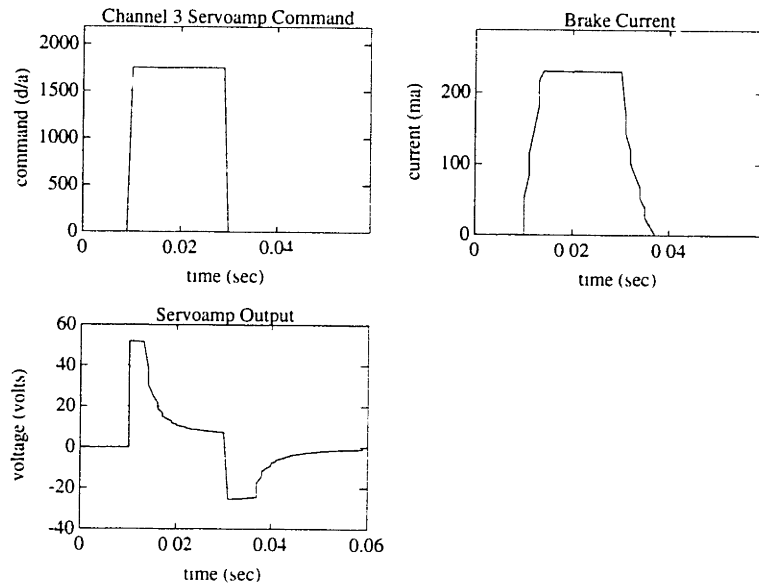
Figure B-50: Step response of the channel 3 (left hip) servoamplifier for a step input of 1750 D/A units.
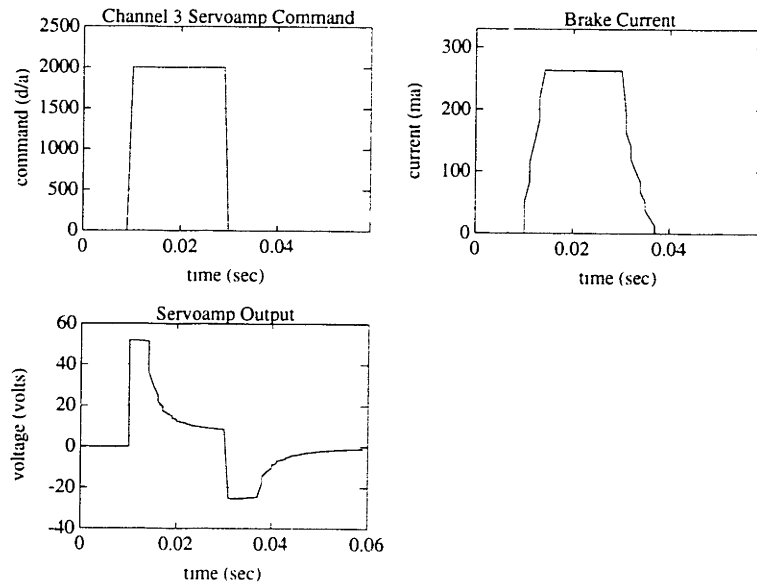
Figure B-51: Step response of the channel 3 (left hip) servoamplifier for a step input of 2000 D/A units.

B.3.2 Anti-aliasing Filter Frequency Responses

Theoretical and Empirical Frequency Response of Channel 0 Filter with fc = 150 Hz
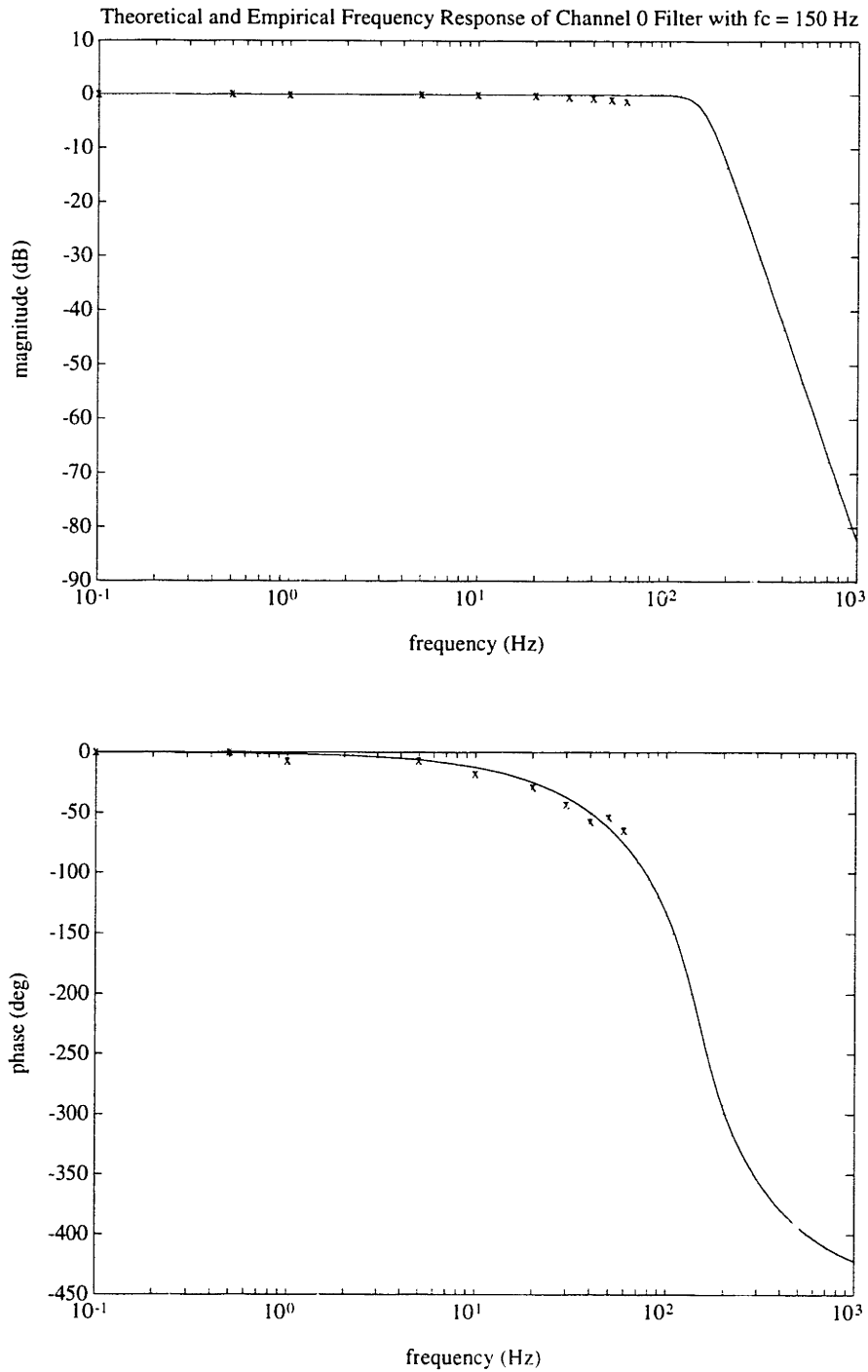
Figure B-52: Theoretical (line) and measured (x-mark's) frequency response of the channel 0 (right knee position) 5th order Butterworth low pass anti-aliasing filter.
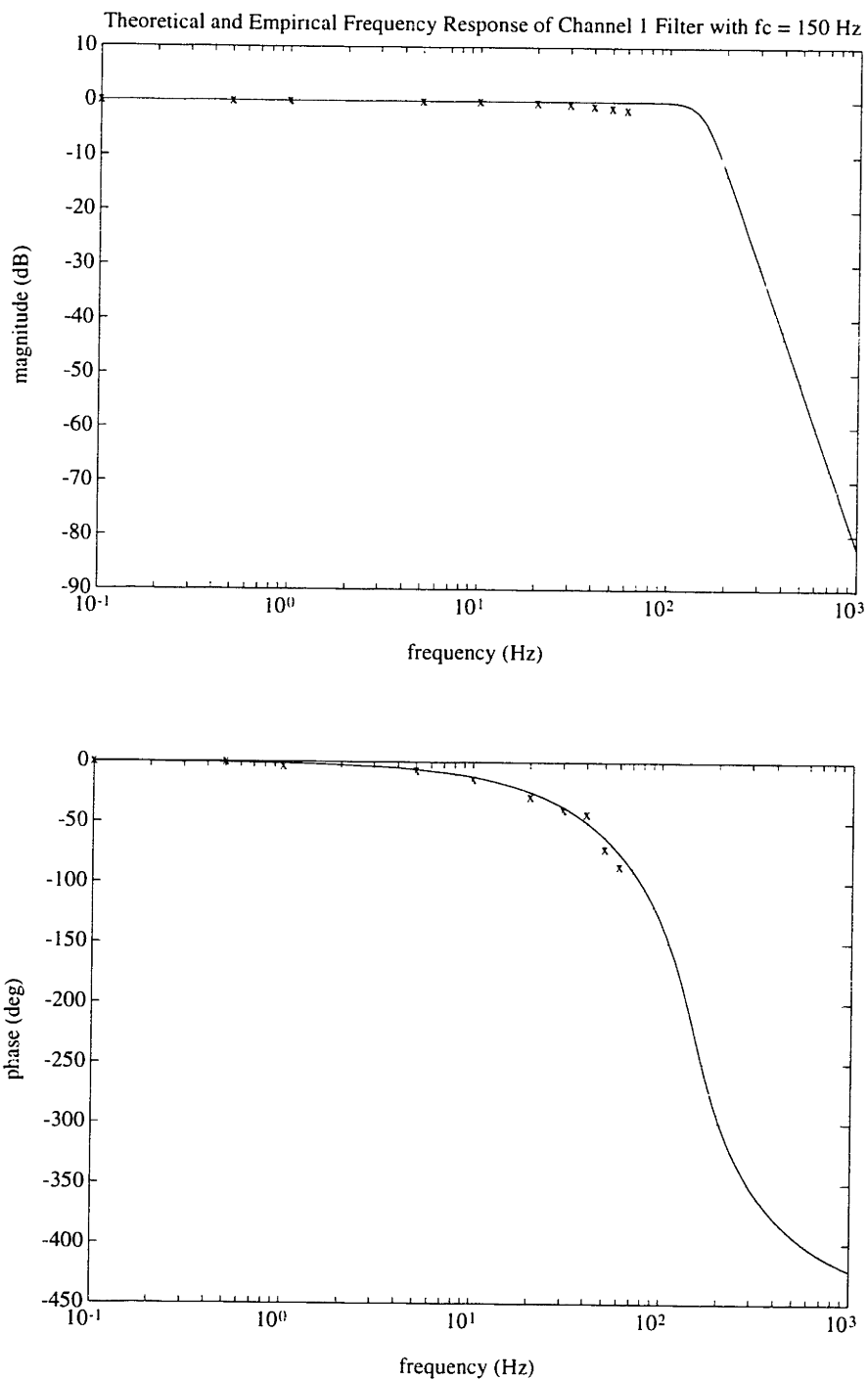
Figure B-53: Theoretical (line) and measured (x-mark's) frequency response of the channel 1 (left knee position) 5th order Butterworth low pass anti-aliasing filter.

200
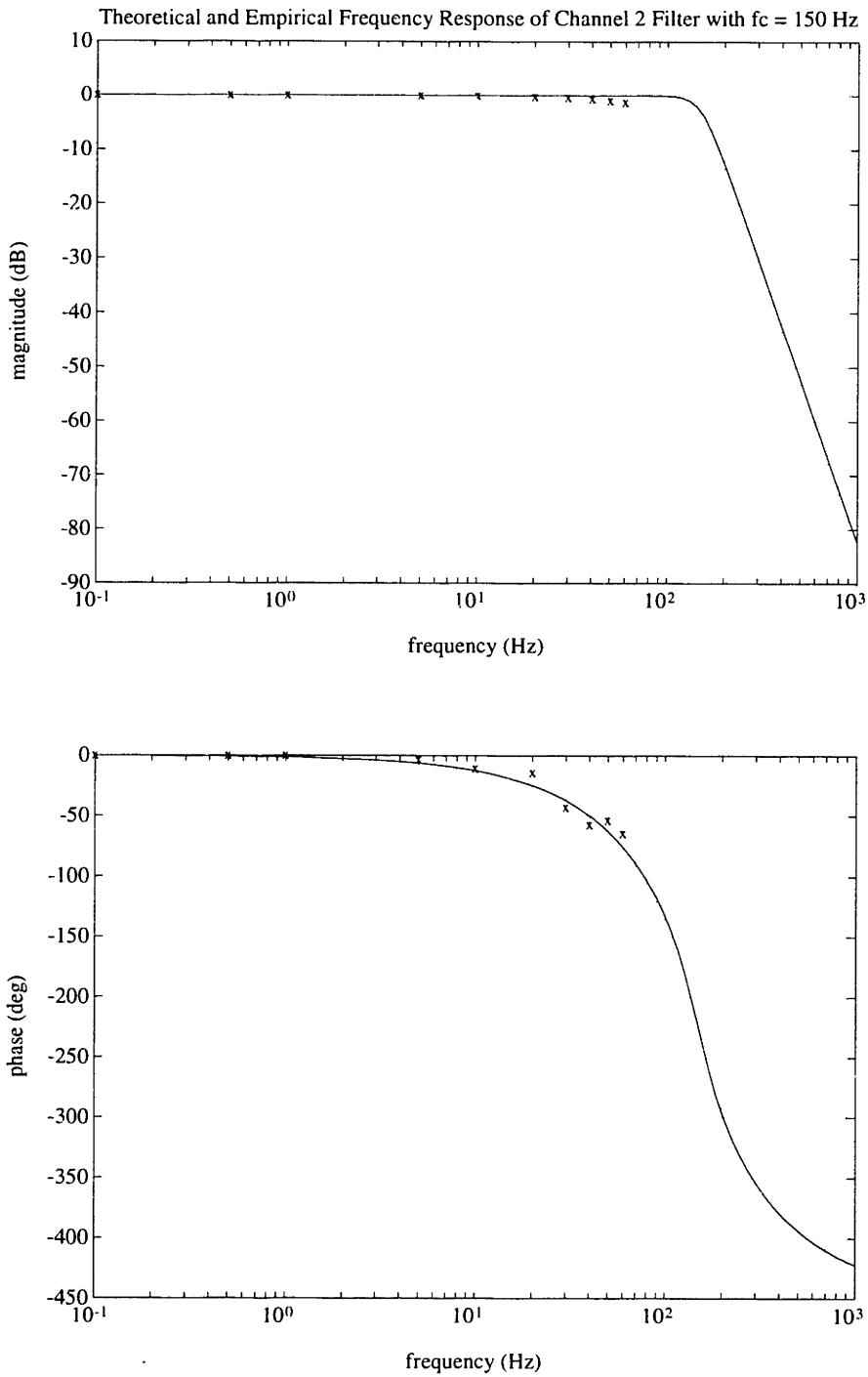
Figure B-54: Theoretical (line) and measured (x-mark's) frequency response of the channel 2 (right hip position) 5th order Butterworth low pass anti-aliasing filter.
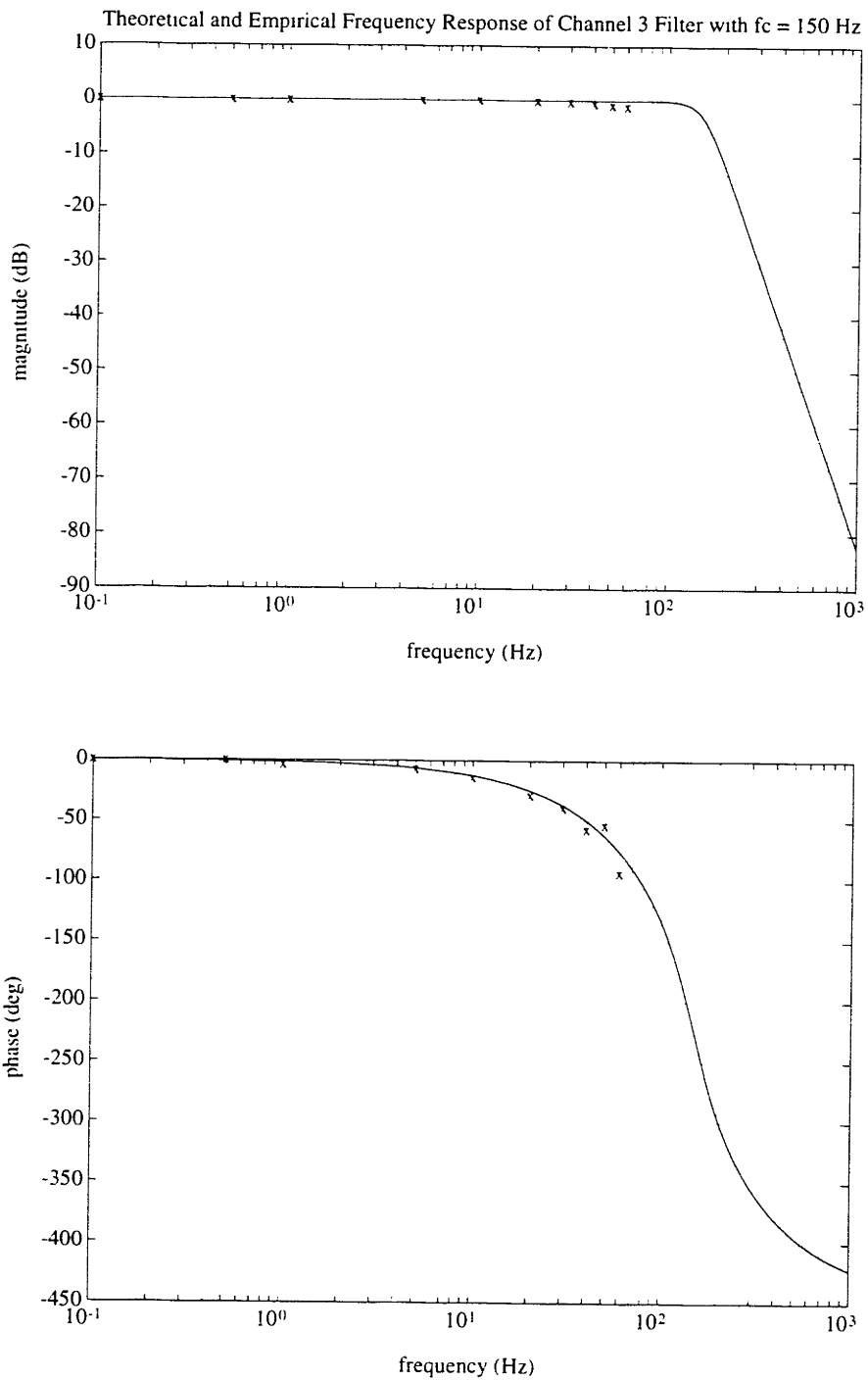
Figure B-55: Theoretical (line) and measured (x-mark's) frequency response of the channel 3 (left hip position) 5th order Butterworth low pass anti-aliasing filter.
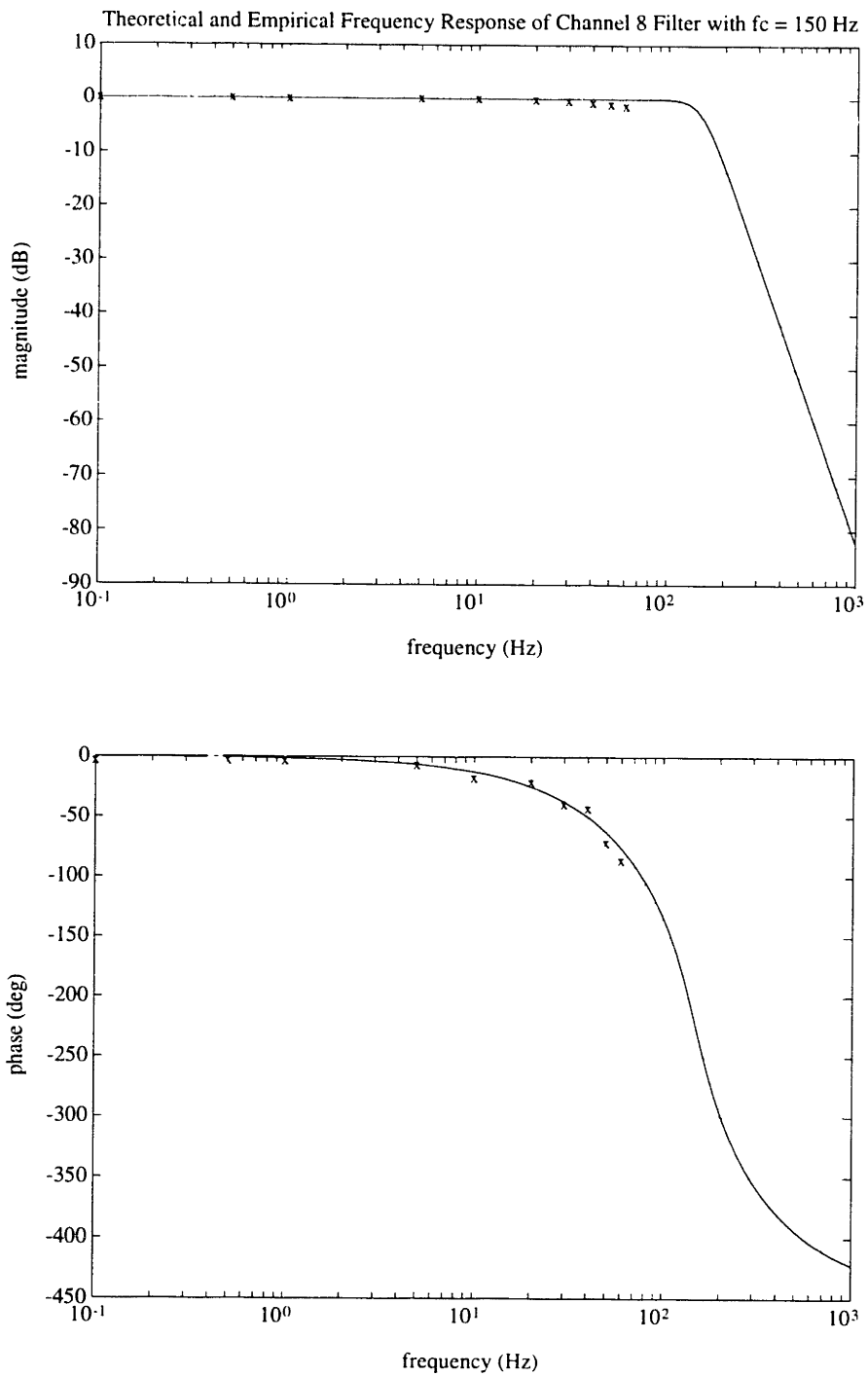
Figure B-56: Theoretical (line) and measured (x-mark's) frequency response of the channel 8 (right knee torque) 5th order Butterworth low pass anti-aliasing filter.
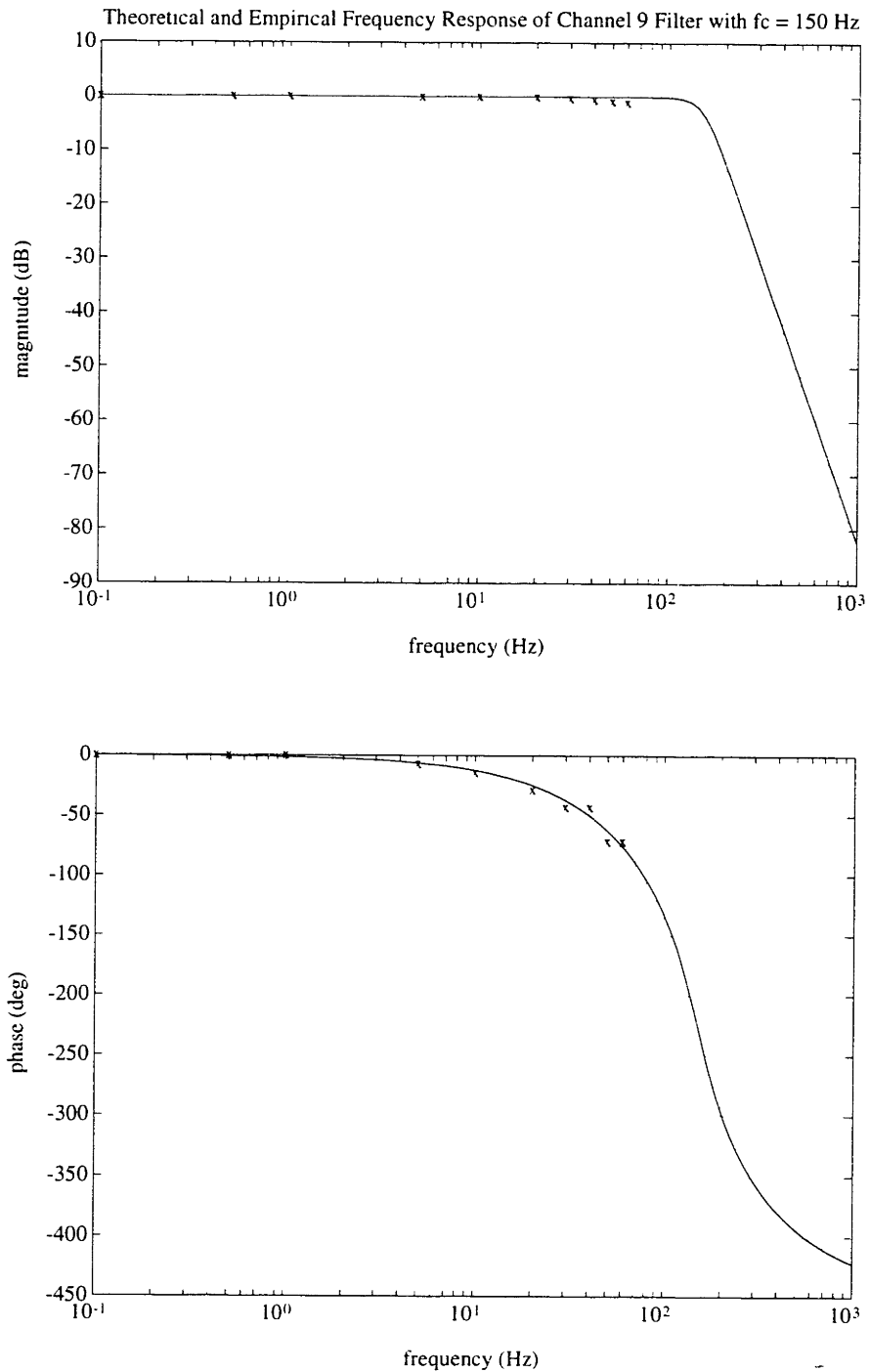
Figure B-57: Theoretical (line) and measured (x-mark's) frequency response of the channel 9 (left knee torque) 5th order Butterworth low pass anti-aliasing filter.

204
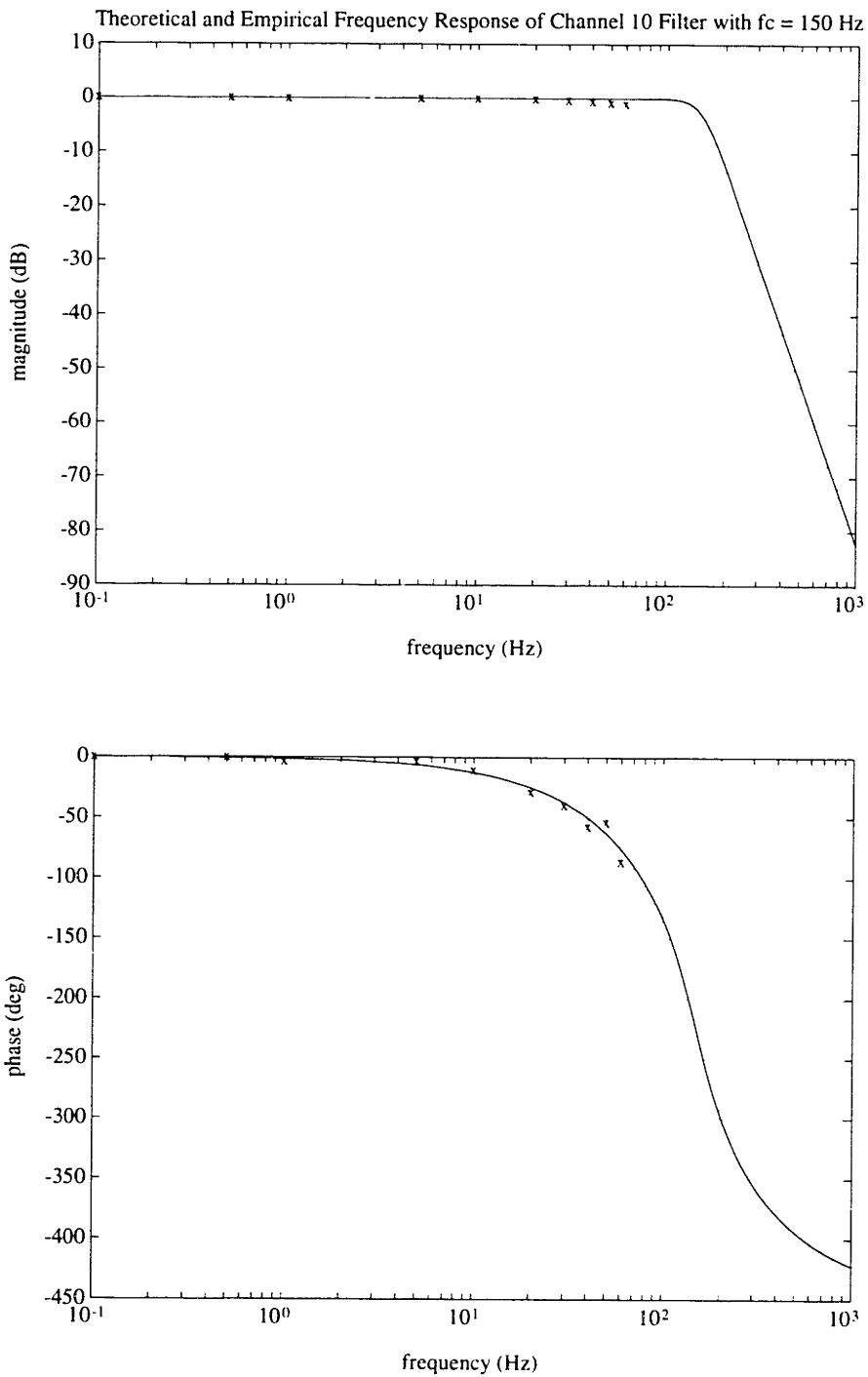
Figure B-58: Theoretical (line) and measured (x-mark's) frequency response of the channel 10 (right hip torque) 5th order Butterworth low pass anti-aliasing filter.
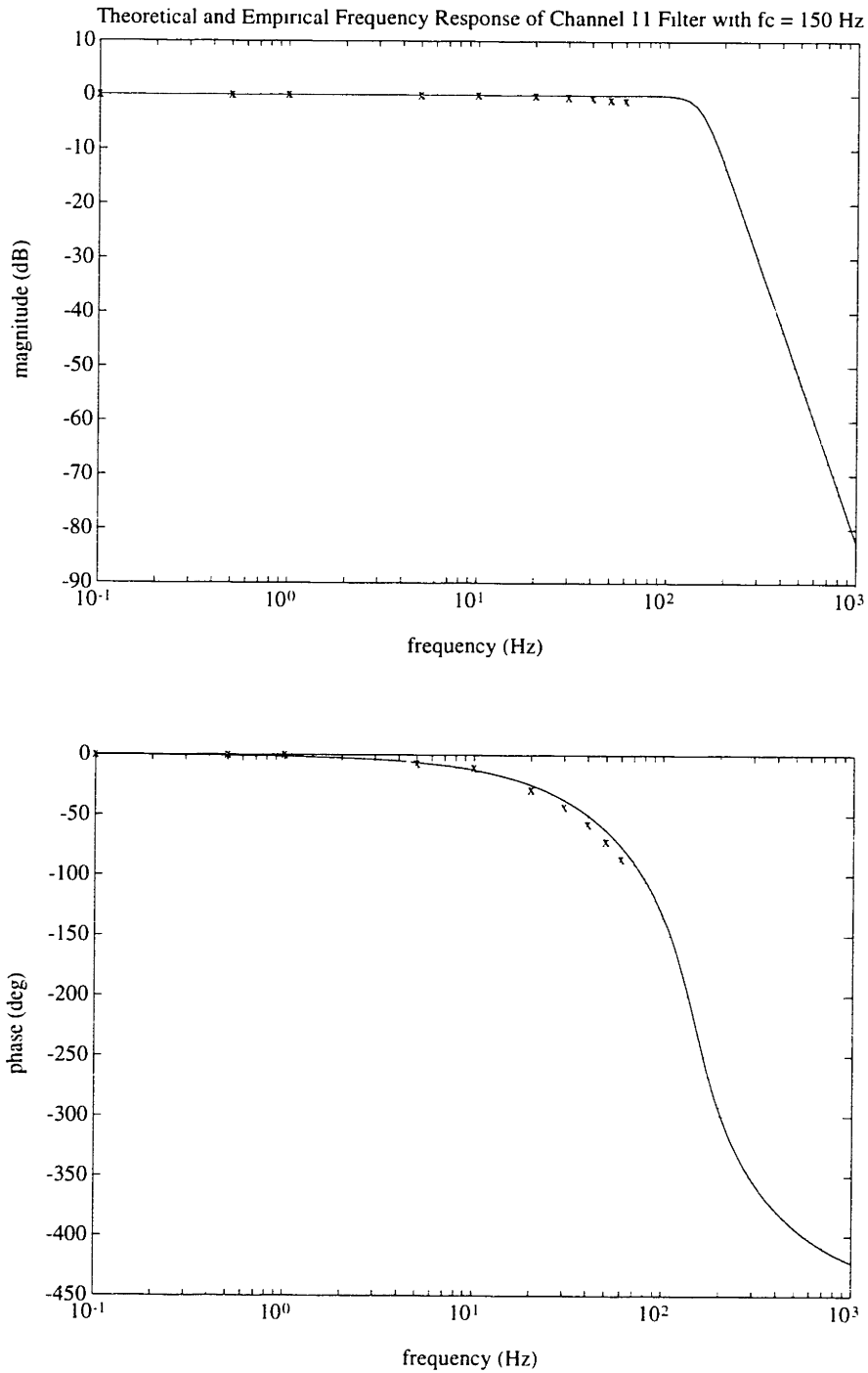
Figure B-59: Theoretical (line) and measured (x-mark's) frequency response of the channel 11 (left hip torque) 5th order Butterworth low pass anti-aliasing filter.

B.3.3 Analog Differentiator Frequency Responses
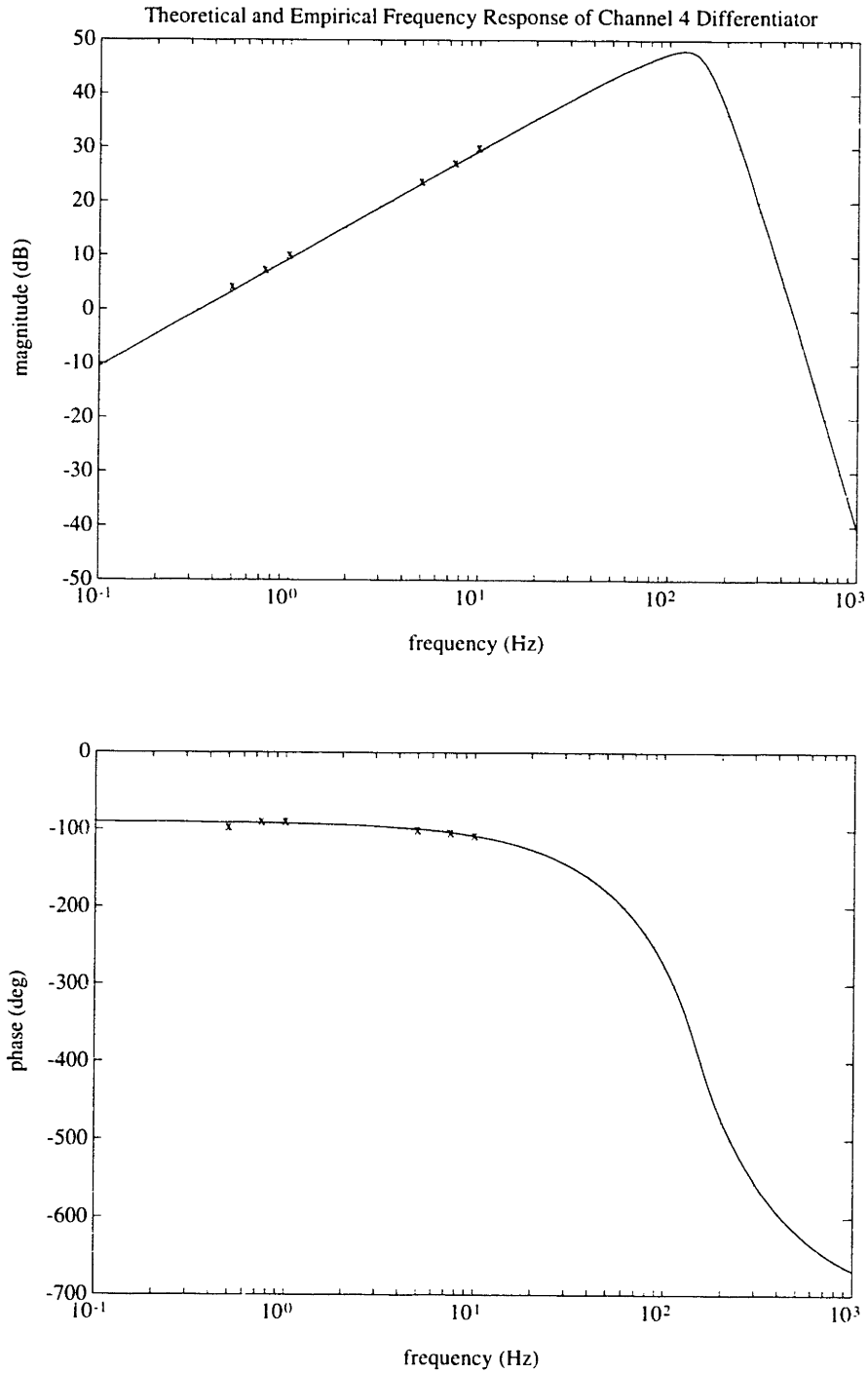
Figure B-60: Theoretical (line) and measured (x-mark's) frequency response of the channel 4 (right knee velocity) practical differentiator. The differentiator consists of an ideal differentiator in series with a 7th order low pass filter.
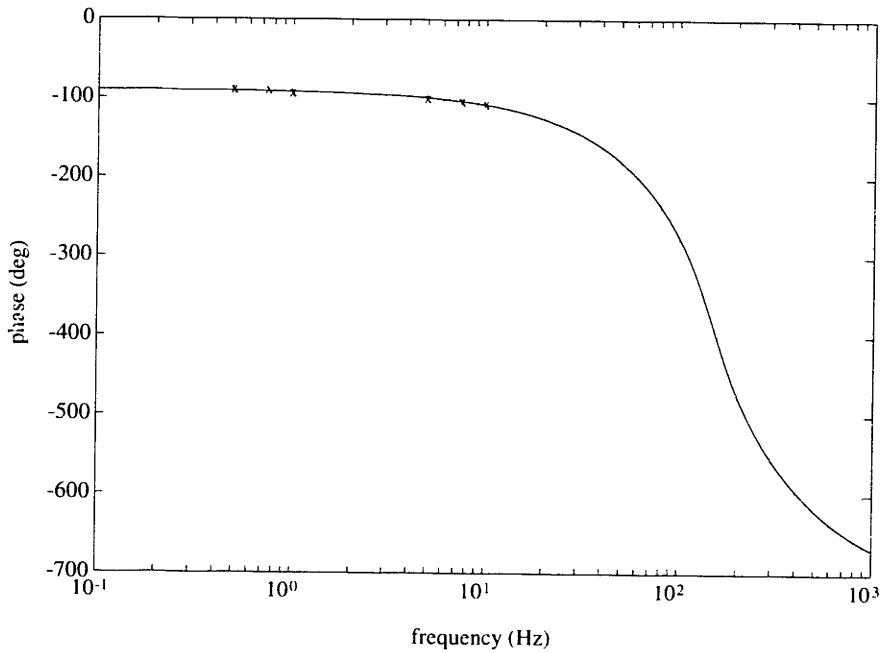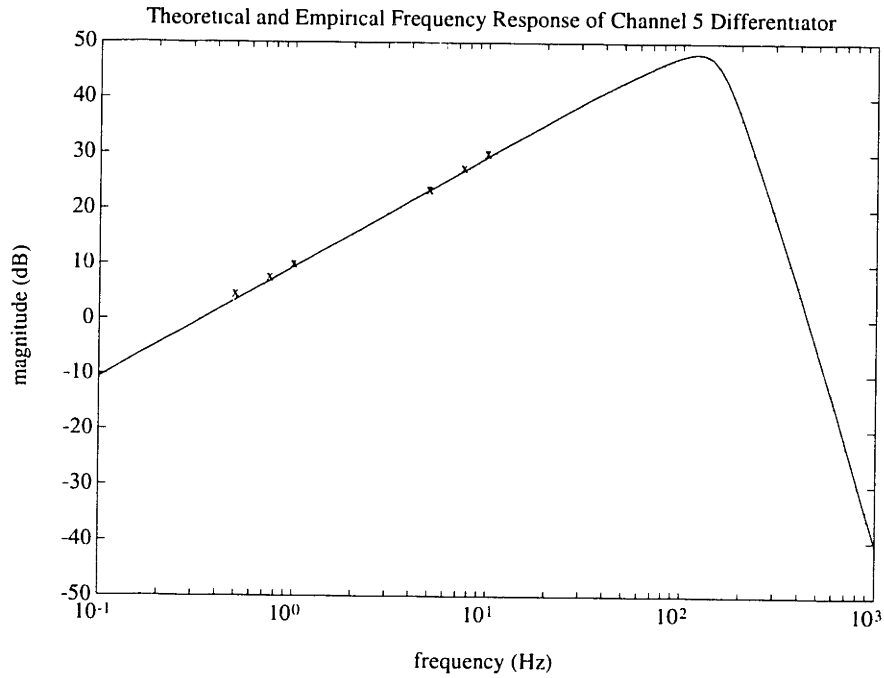
Figure B-61: Theoretical (line) and measured (x-mark's) frequency response of the channel 5 (left knee velocity) practical differentiator. The differentiator consists of an ideal differentiator in series with a 7th order low pass filter.

208
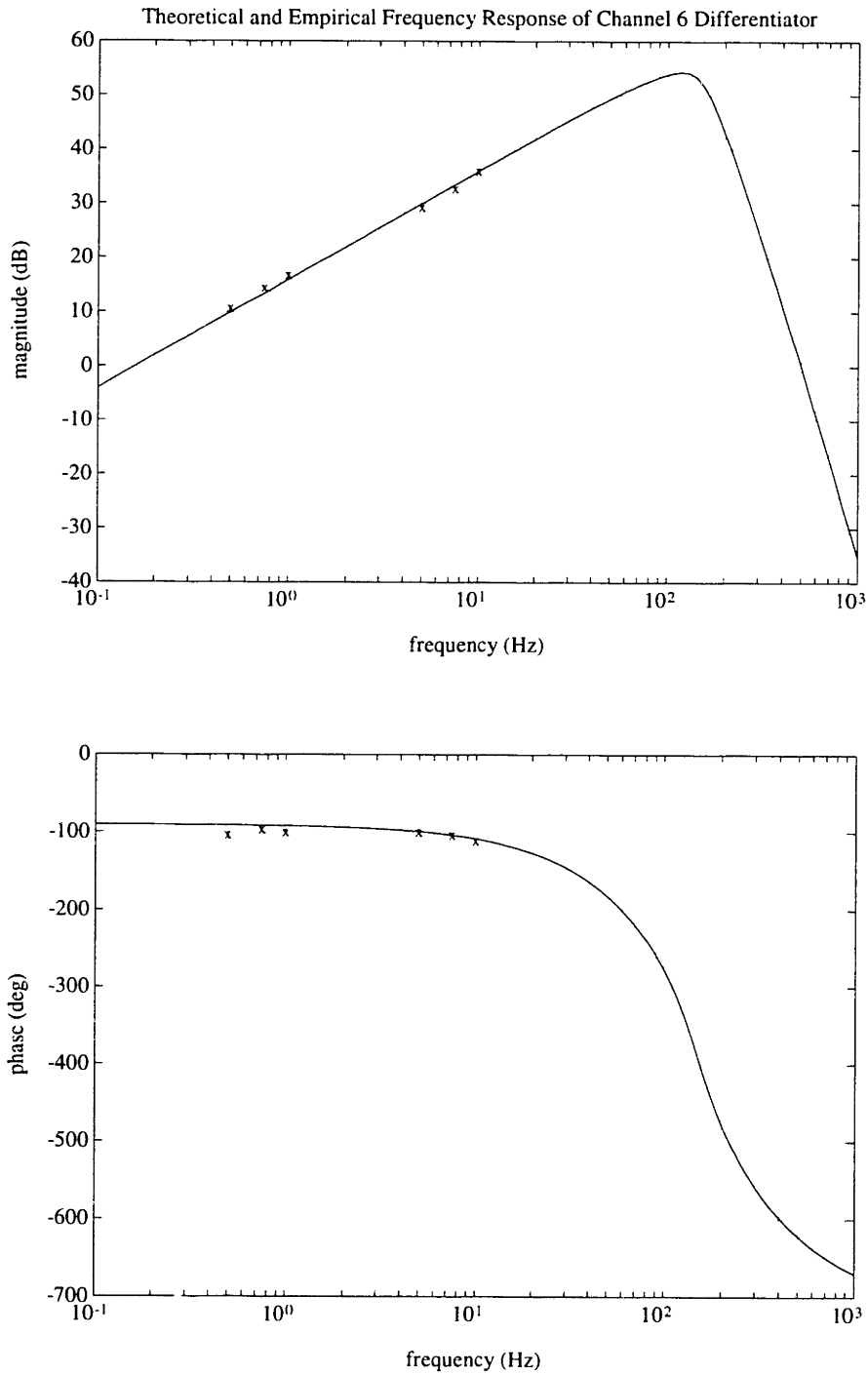
Figure B-62: Theoretical (line) and measured (x-mark's) frequency response of the channel 6 (right hip velocity) practical differentiator. The differentiator consists of an ideal differentiator in series with a 7th order low pass filter.
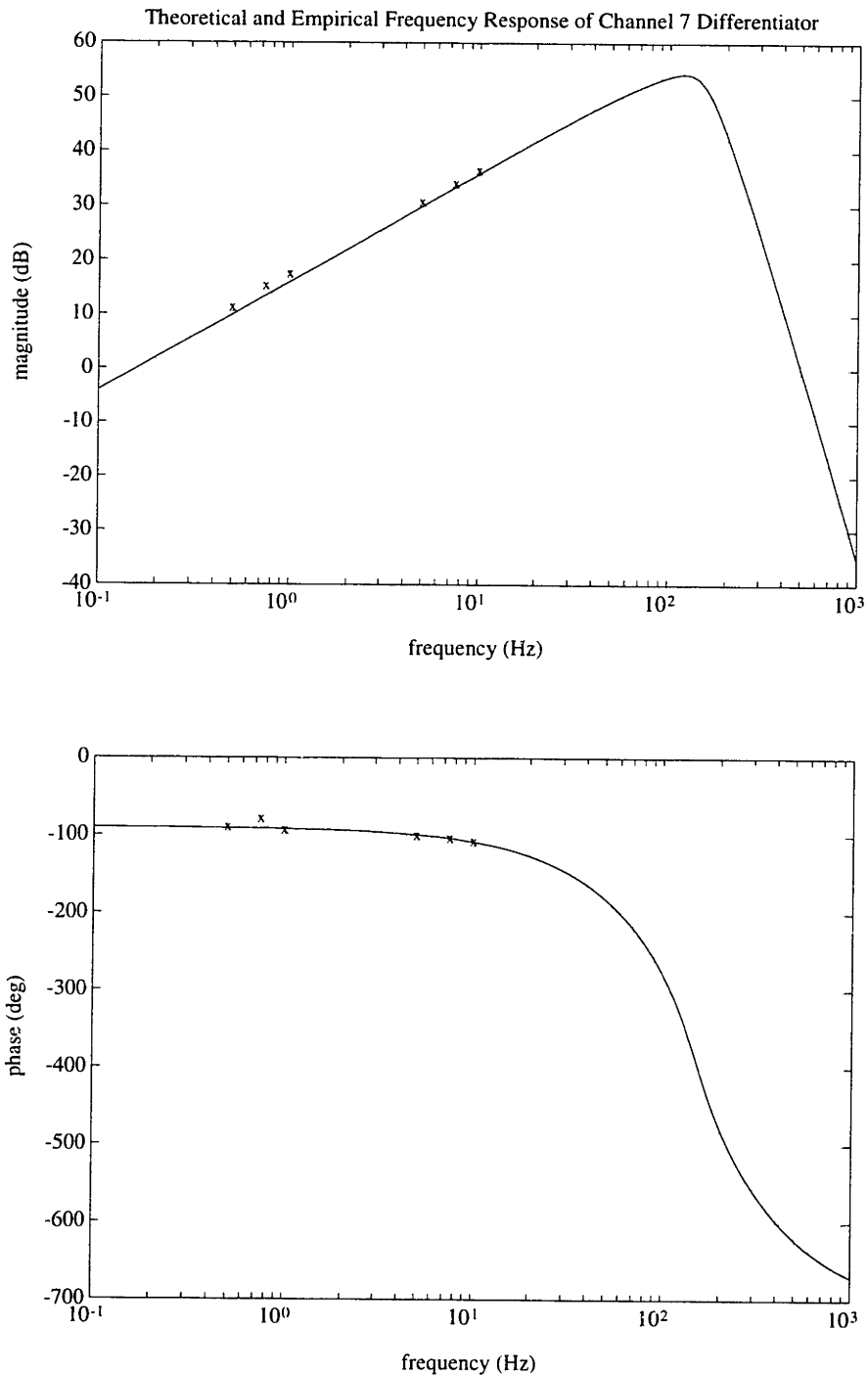
Figure B-63: Theoretical (line) and measured (x-mark's) frequency response of the channel 7 (left hip velocity) practical differentiator. The differentiator consists of an ideal differentiator in series with a 7th order low pass filter.

210

B.4 Sensor Calibrations

Each of the following plots contain the equation of a line that was fit to the output of the respective sensor in a least squares fashion. The coefficient of determination, which is also given, provides a measure of how well this line describes the sensor output. The coefficient is defined as:

$$r^2 = \frac{\sum_{i=1}^n (\hat{y}_i - \bar{y})^2}{\sum_{i=1}^n (y_i - \bar{y})^2} \tag{B.1}$$

where y_i are the data points, $\hat{y}_i$ are the points as given by the least squares fit, and $\bar{y}$ is the mean of the data points.

B.4.1 Position Sensor Calibrations
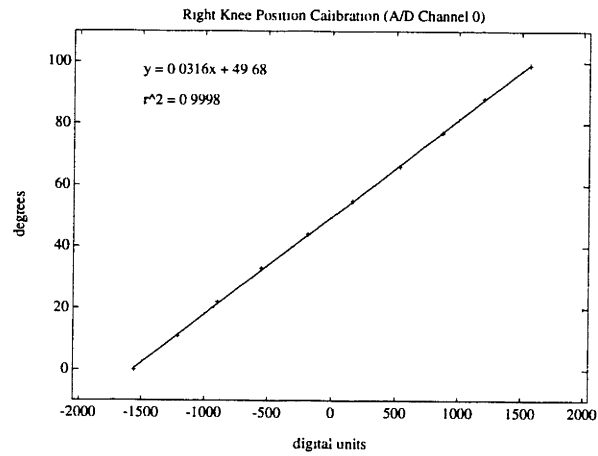
Figure B-64: Calibration of channel 0 (right knee position) sensor.
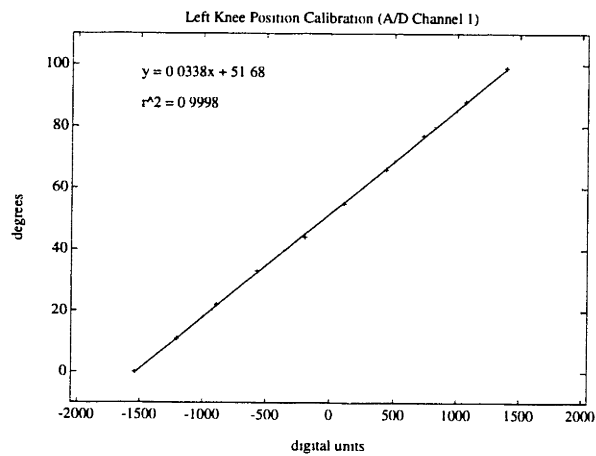
Figure B-65: Calibration of channel 1 (left knee position) sensor.
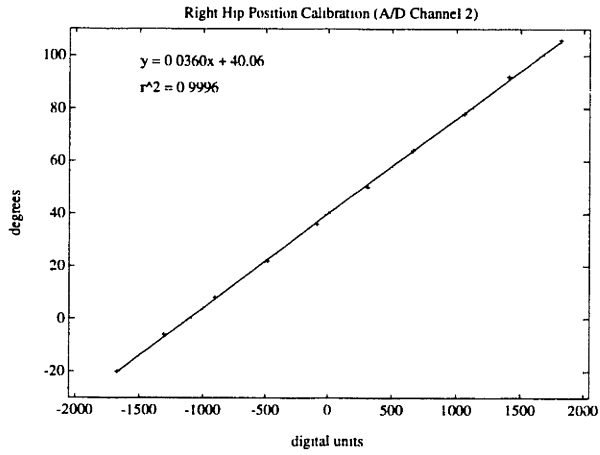
Figure B-66: Calibration of channel 2 (right hip position) sensor.
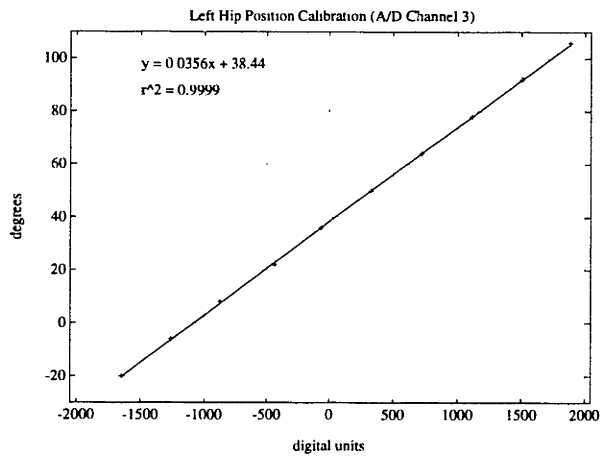
Figure B-67: Calibration of channel 3 (left hip position) sensor.

B.4.2 Velocity Sensor Calibrations
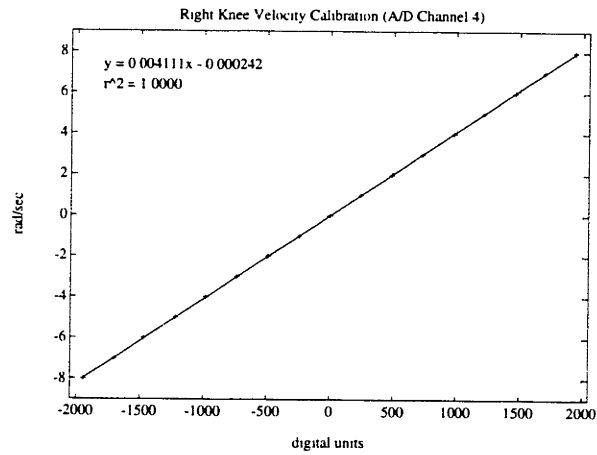
Figure B-68: Calibration of channel 4 (right knee velocity) sensor.
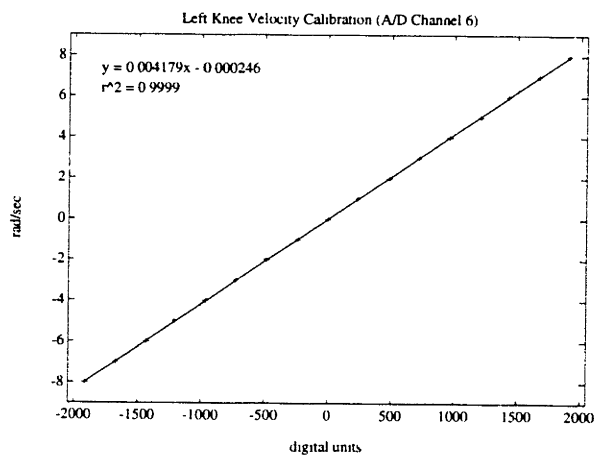
Figure B-69: Calibration of channel 5 (left knee velocity) sensor.
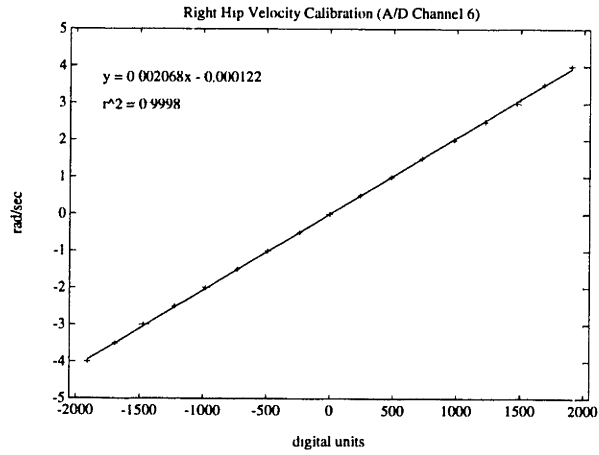
Figure B-70: Calibration of channel 6 (right hip velocity) sensor.
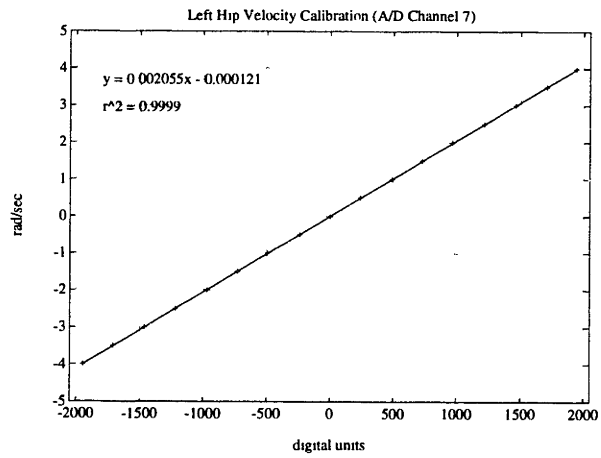
Figure B-71: Calibration of channel 7 (left hip velocity) sensor.

B.4.3 Torque Sensor Calibrations
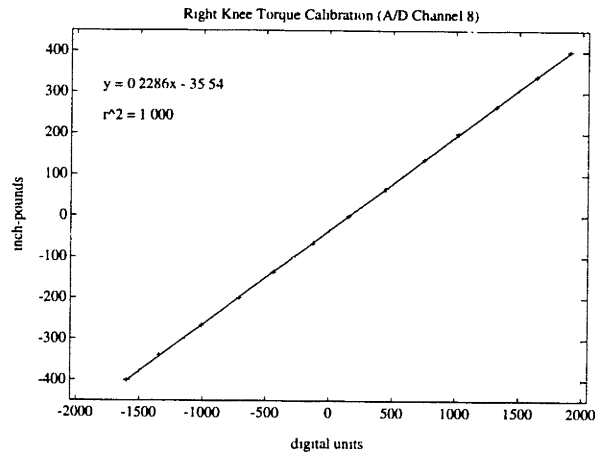
Figure B-72: Calibration of channel 8 (right knee torque) sensor.
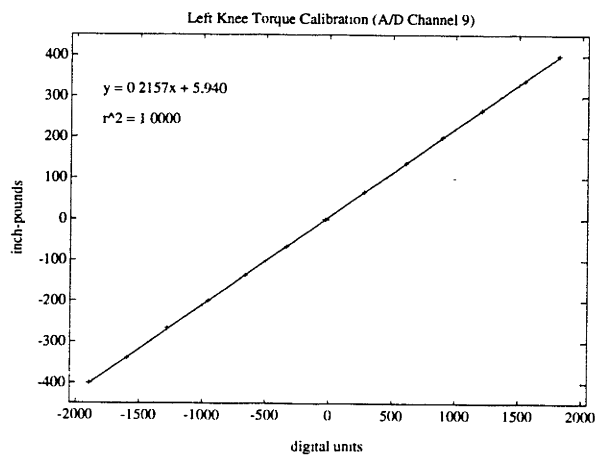
Figure B-73: Calibration of channel 9 (left knee torque) sensor.

216
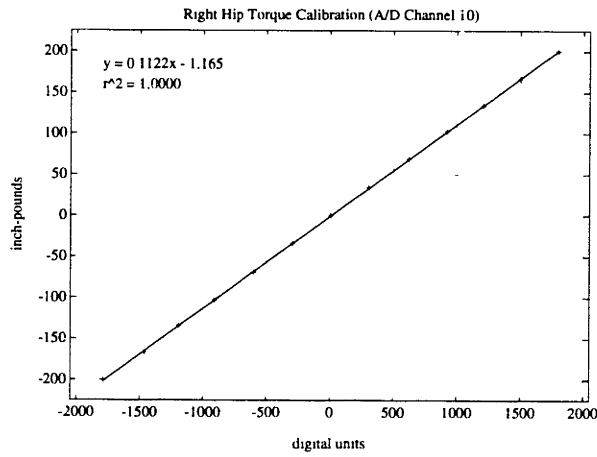
Figure B-74: Calibration of channel 10 (right hip torque) sensor.
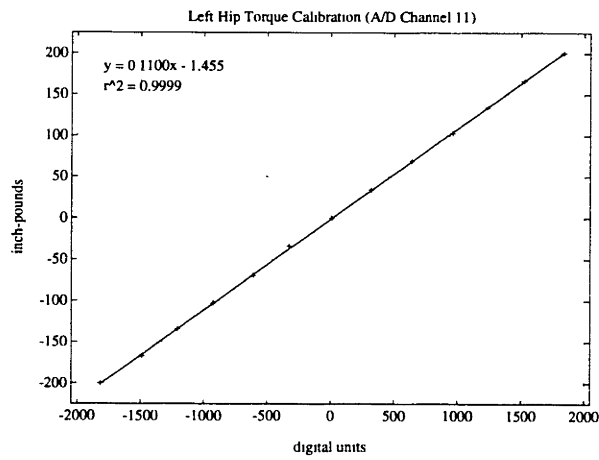
Figure B-75: Calibration of channel 11 (left hip torque) sensor.

217

Appendix C

Stimulator Documentation

C.1 Stimulator Schematics

C.1.1 Digital Stage
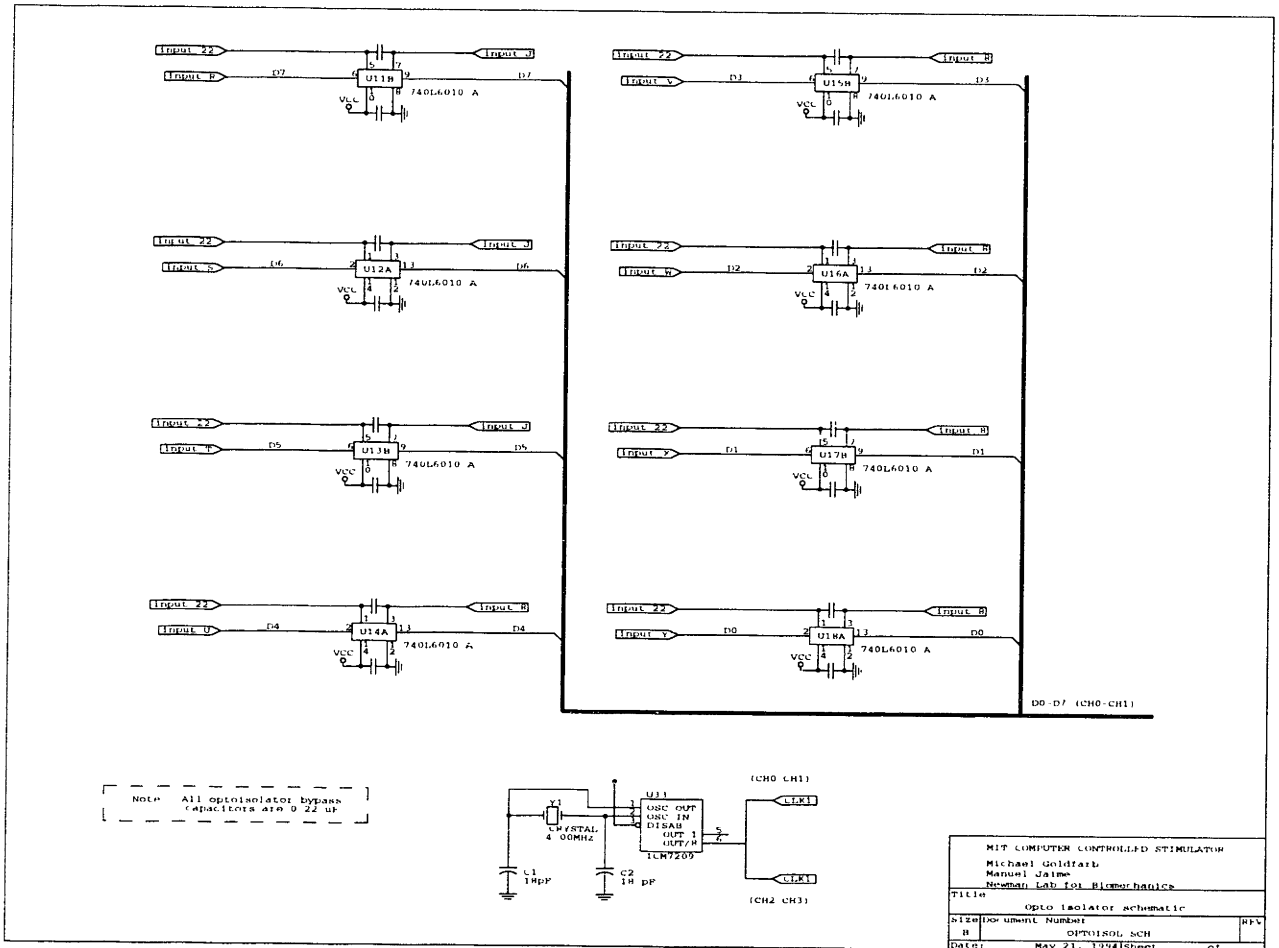
Figure C-1: Schematic of optoisolator circuit for transmitting digital information from the computer to the stimulator. The optoisolators electrically isolate the stimulator power from the computer power so that the subject is isolated from the eletrical power of the wall. The eight lines consitute the digital word that is used to load the D/A converters and the counters that determine the pulse amplitude and width, respectively.
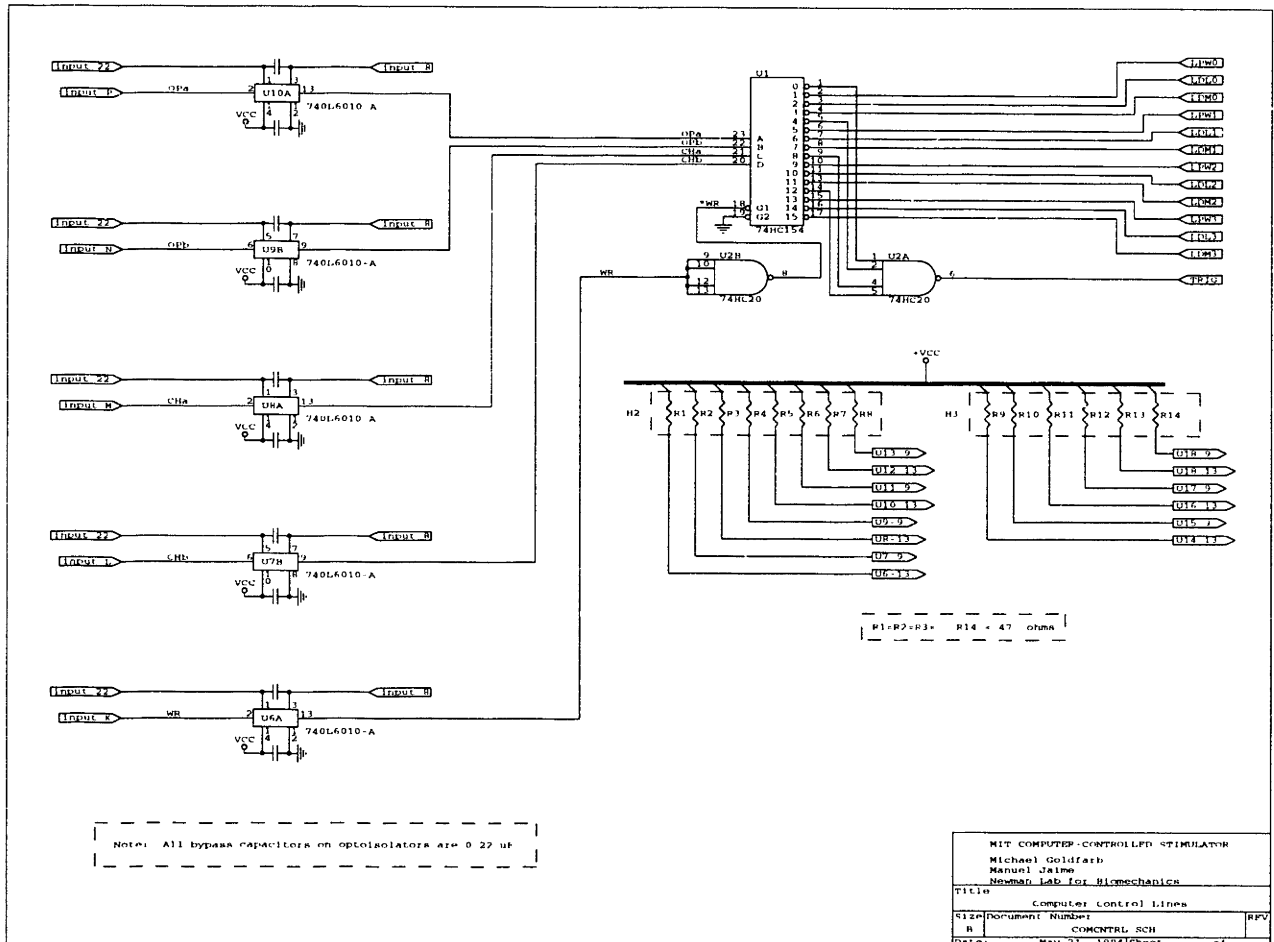
Figure C-2: Schematic of optoisolator circuit for transmitting digital information from the computer to the stimulator. The optoisolators electrically isolate the stimulator power from the computer power so that the subject is isolated from the eletrical power of the wall. Four of the digital lines provide control of the demultiplexer for directing the data bits. The fifth digital line is the trigger for releasing the stimulation pulse.
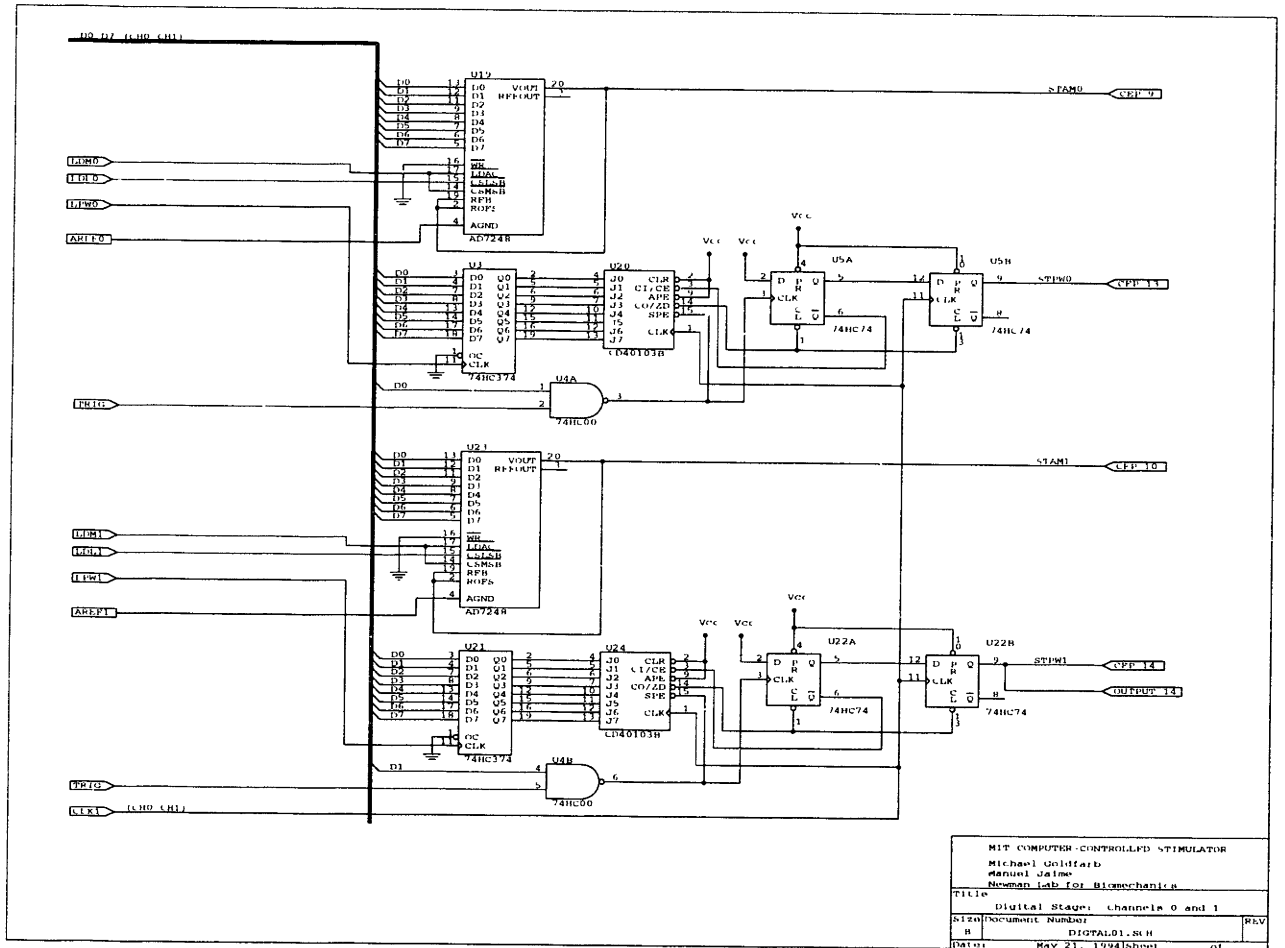
Figure C-3: Schematic of pulse amplitude and width circuits for stimulation channels 0 and 1. Information is supplied by the eight data lines from the computer. The data lines are directed by the control lines from the demultiplexer. The twelve-bit D/A converters are loaded in an eight+four serial manner.
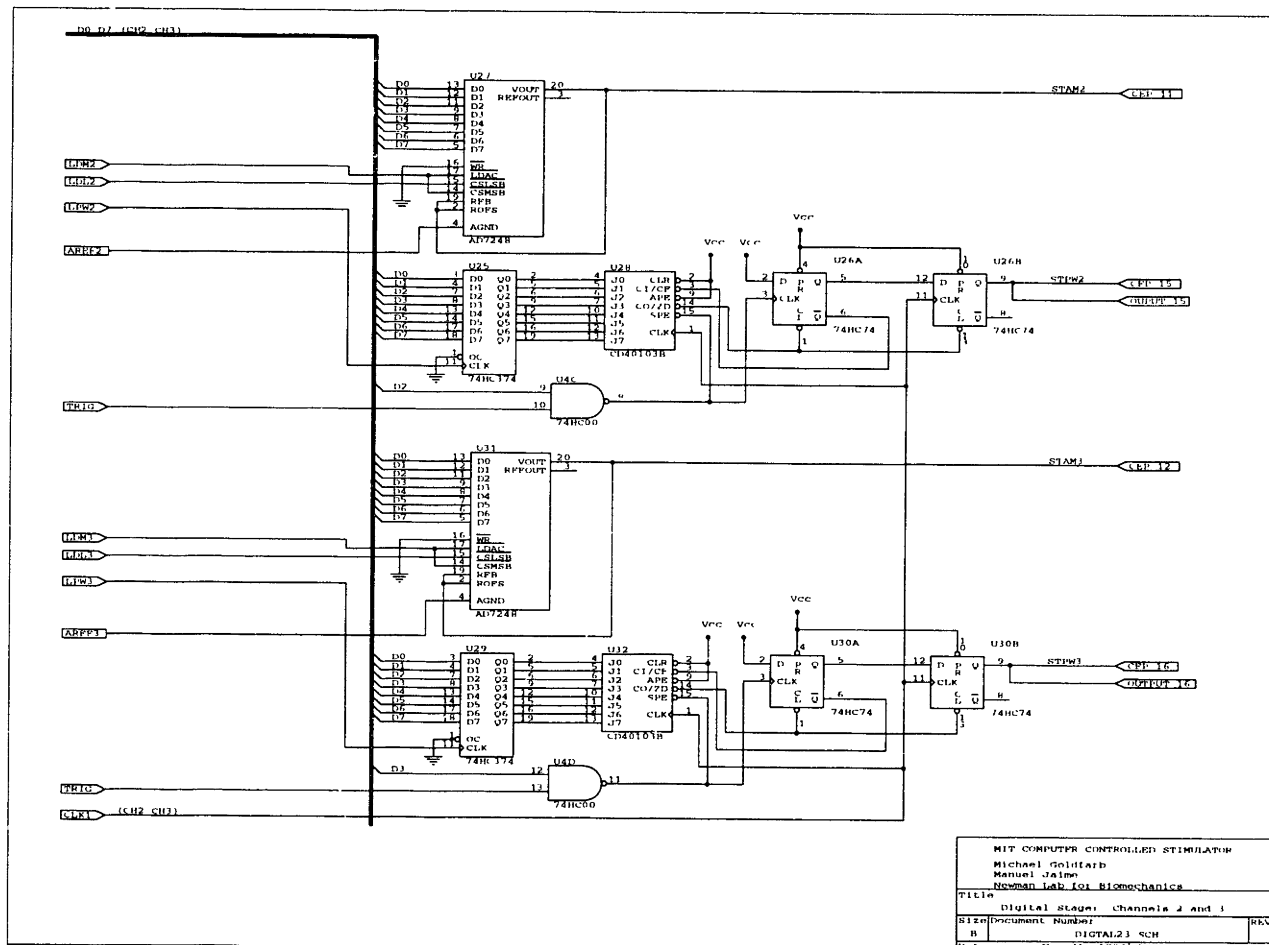
Figure C-4: Schematic of pulse amplitude and width circuits for stimulation channels 2 and 3. Information is supplied by the eight data lines from the computer. The data lines are directed by the control lines from the demultiplexer. The twelve-bit D/A converters are loaded in an eight+four serial manner.
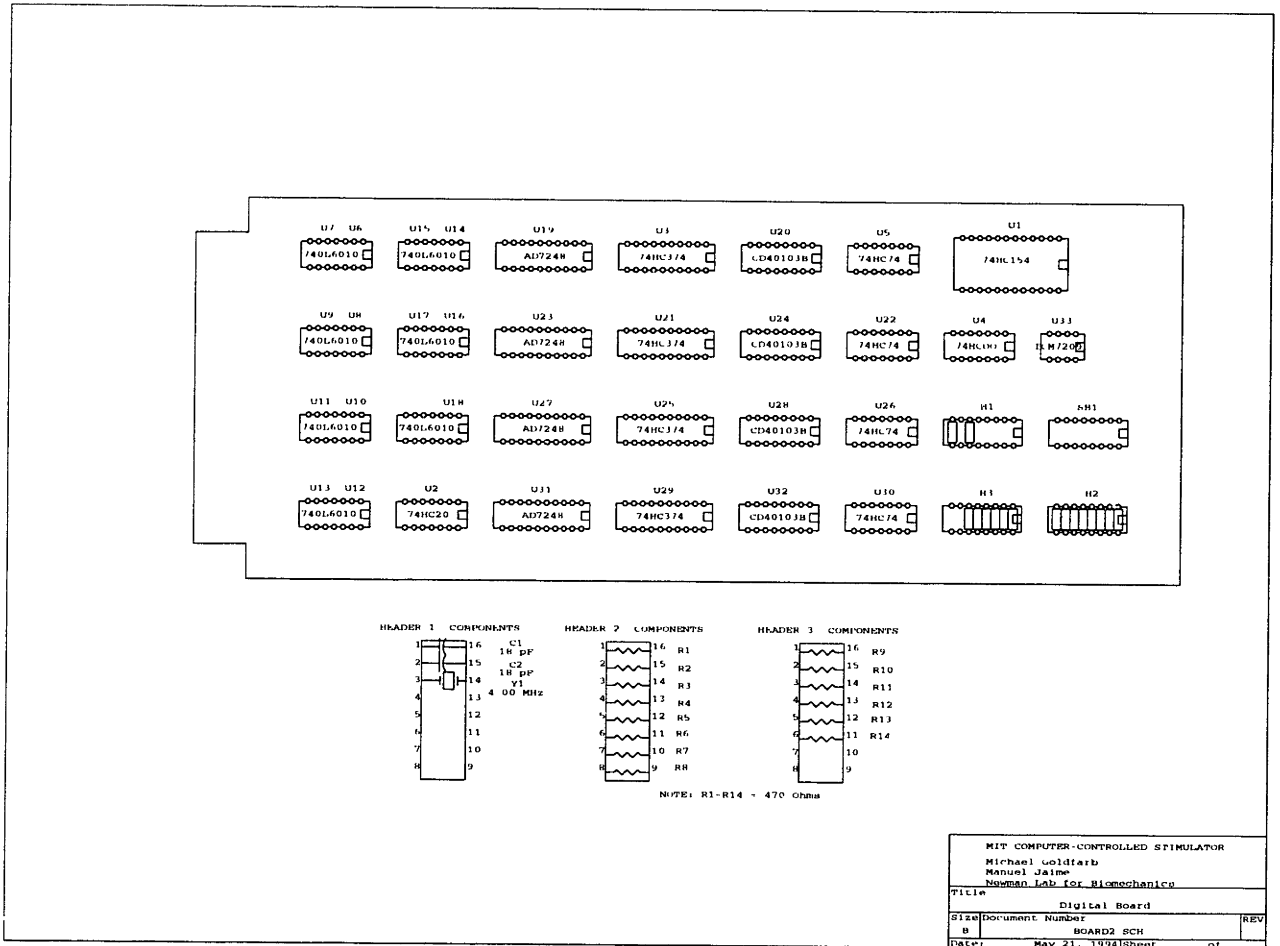
Figure C-5: Layout of the digital board.

C.1.2 Analog Stage
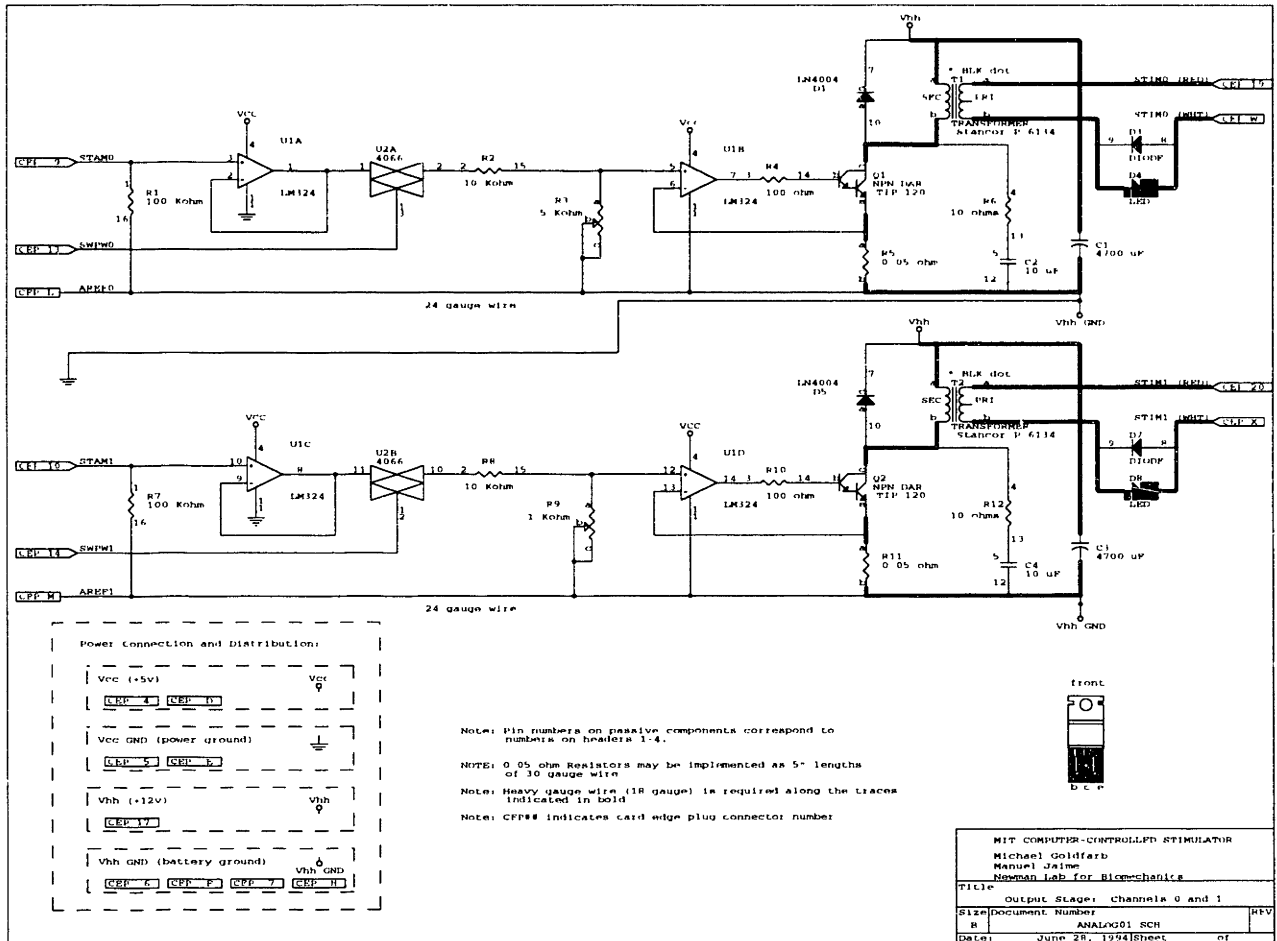
Figure C-6: Schematic of stimulation output stage for channels 0 and 1. Stimulation amplitude and pulse width information are supplied by the digital stage.

225
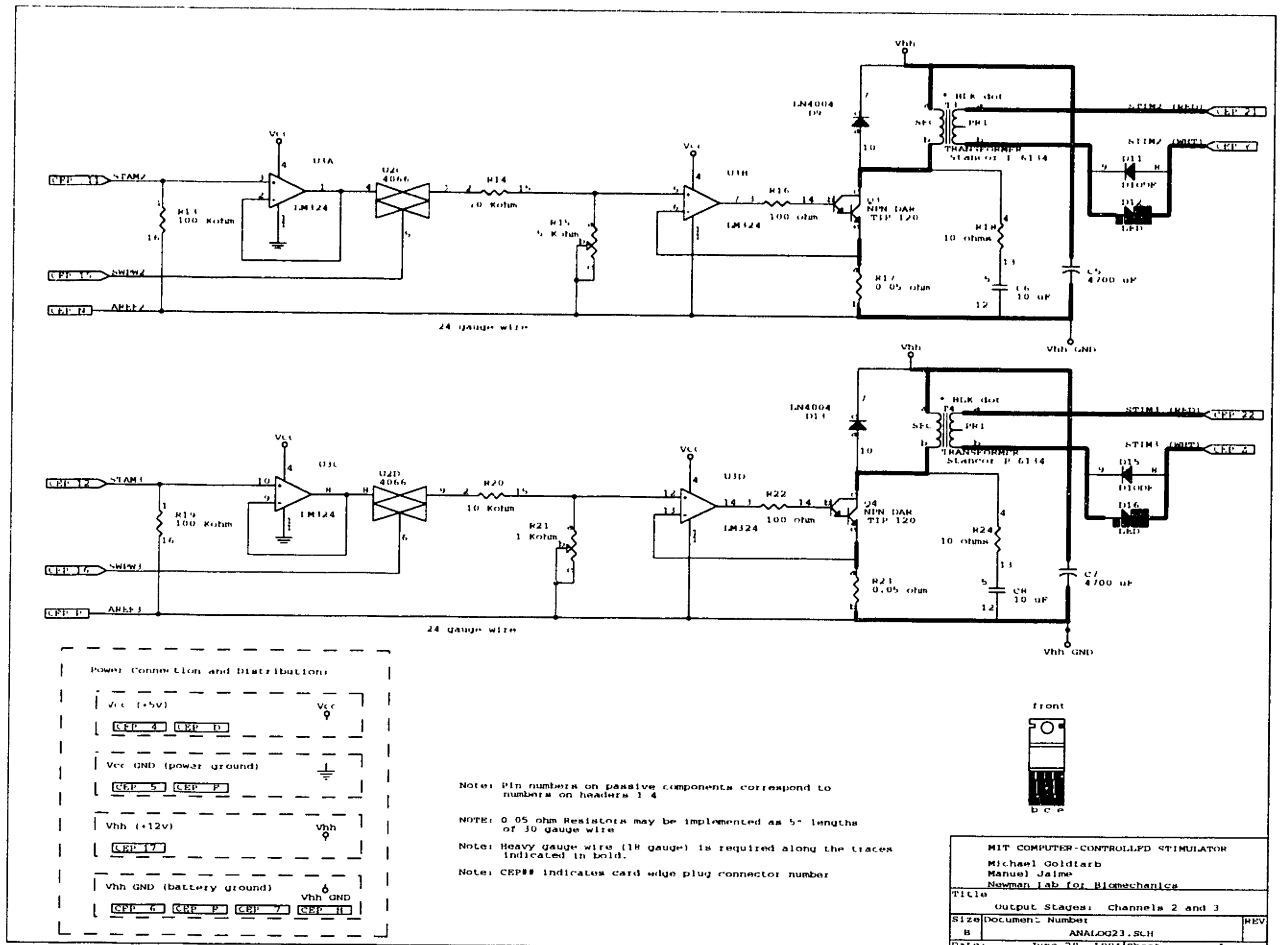
Figure C-7: Schematic of stimulation output stage for channels 2 and 3. Stimulation amplitude and pulse width information are supplied by the digital stage.
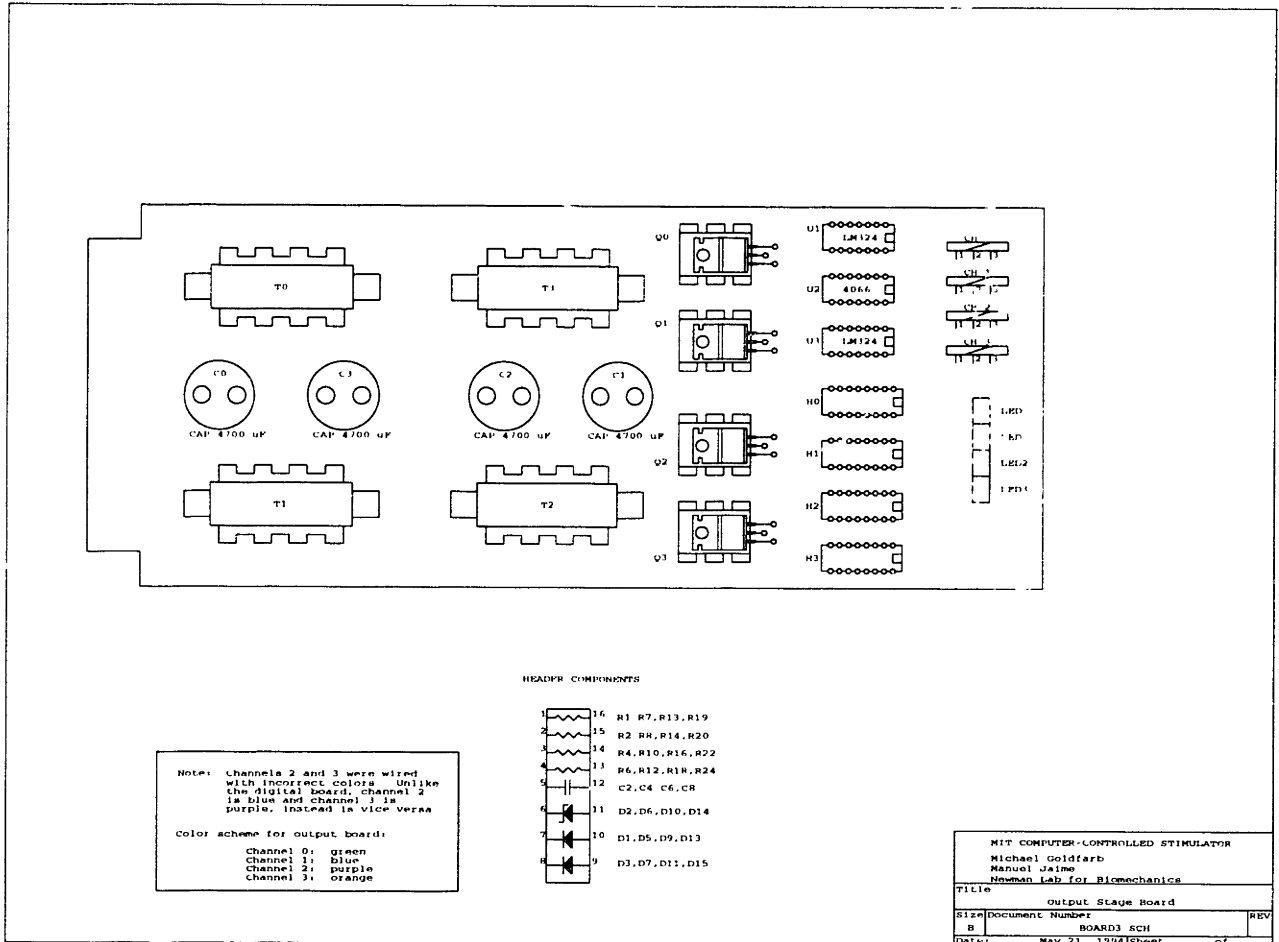
Figure C-8: Layout of the analog (output stage) board.

C.1.3 Power Board
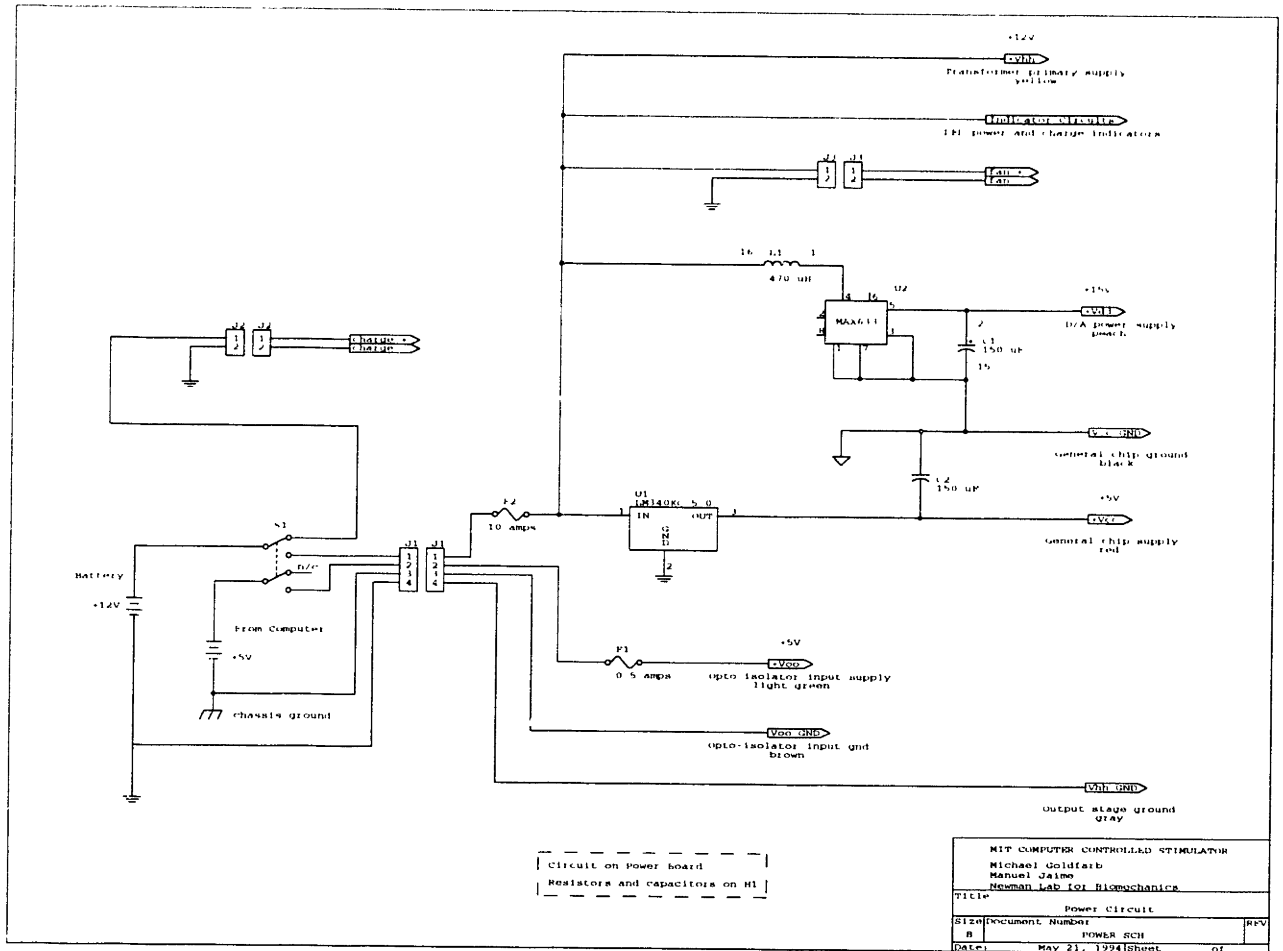
Figure C-9: Schematic of power regulation circuit.
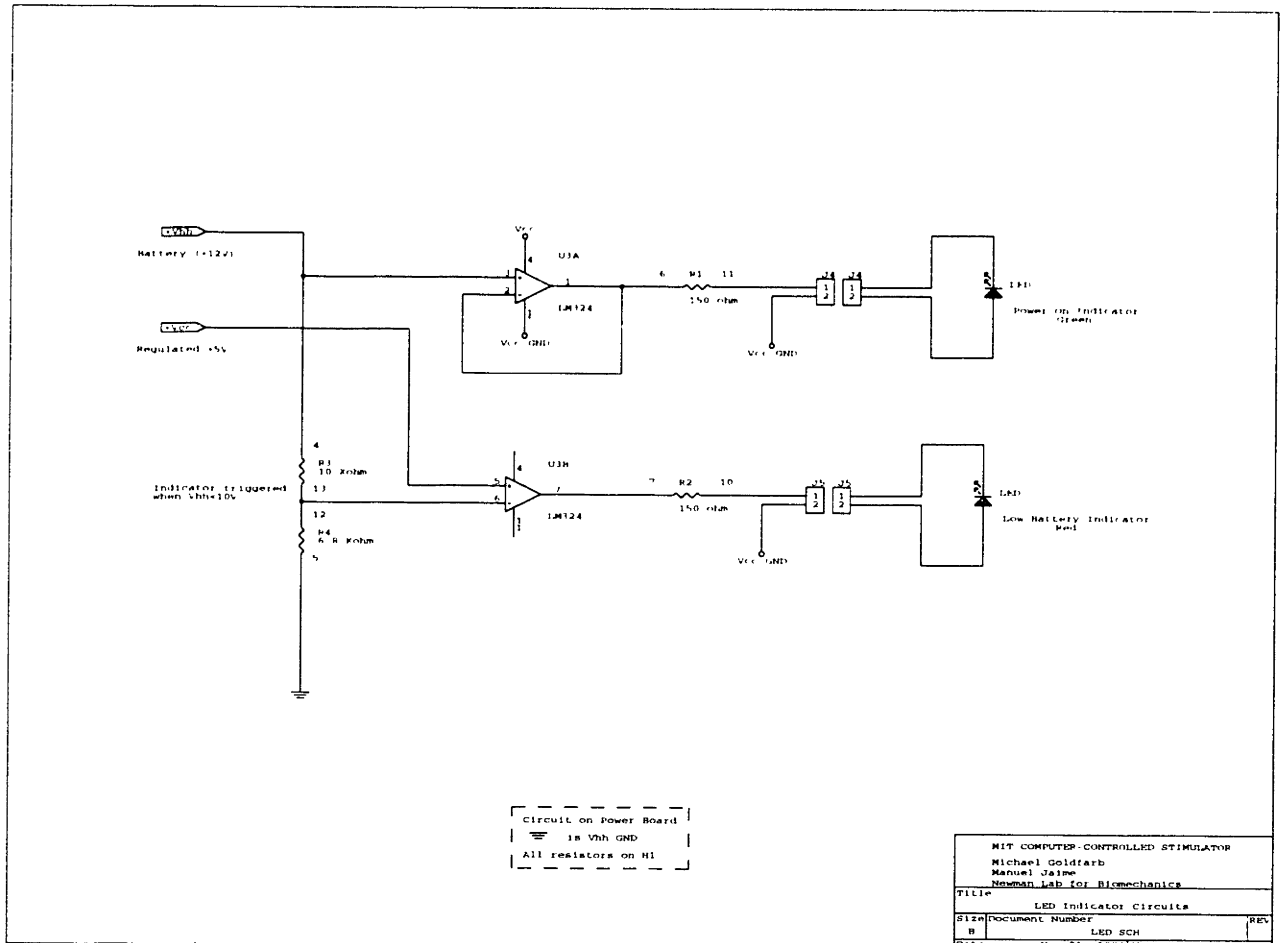
Figure C-10: Schematic of power and battery charge LED indicator circuits.

Figure C-11: Layout of power and I/O board.

C.1.4 Connections
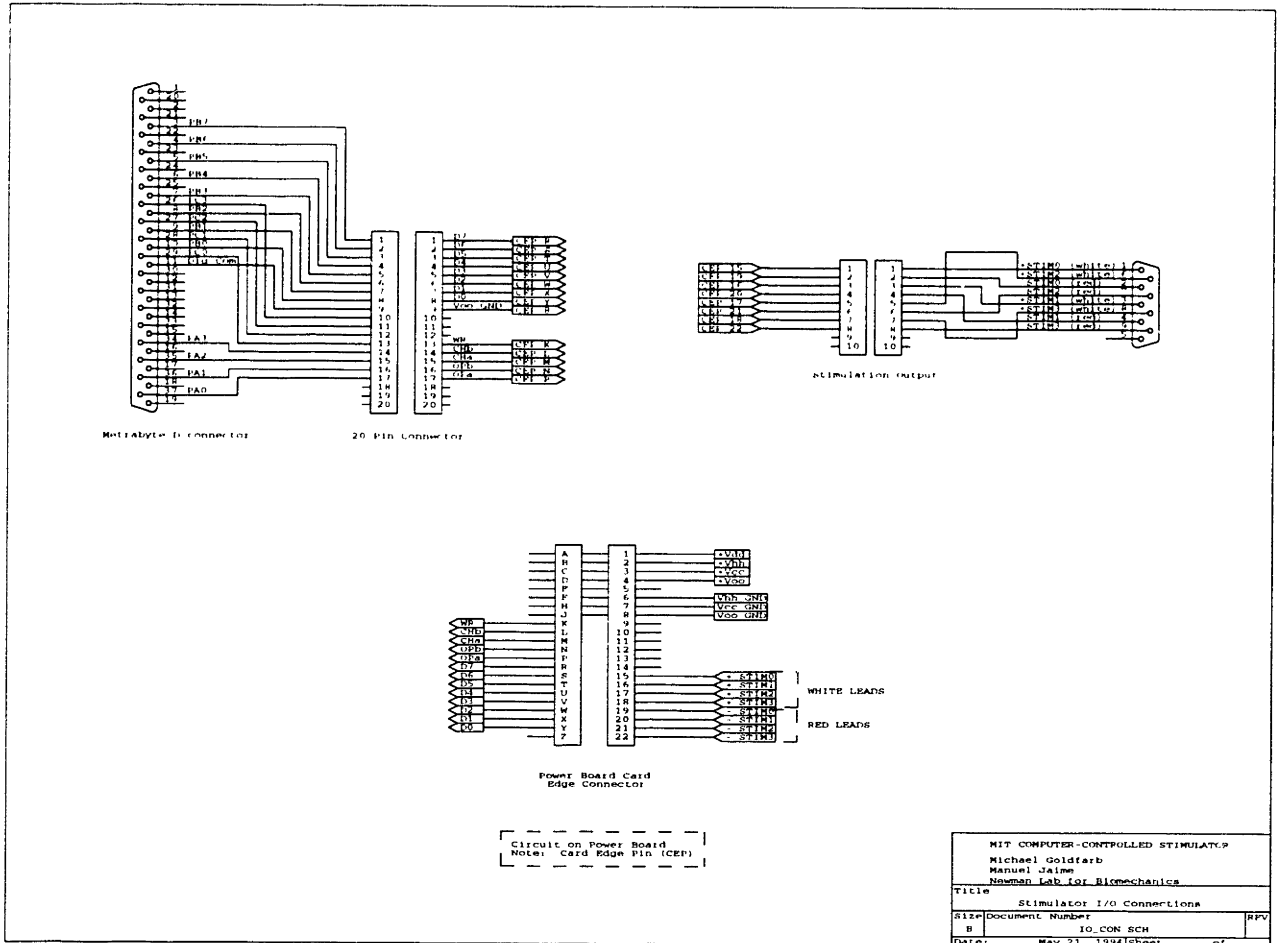
Figure C-12: Schematic of stimulator input/output connections.
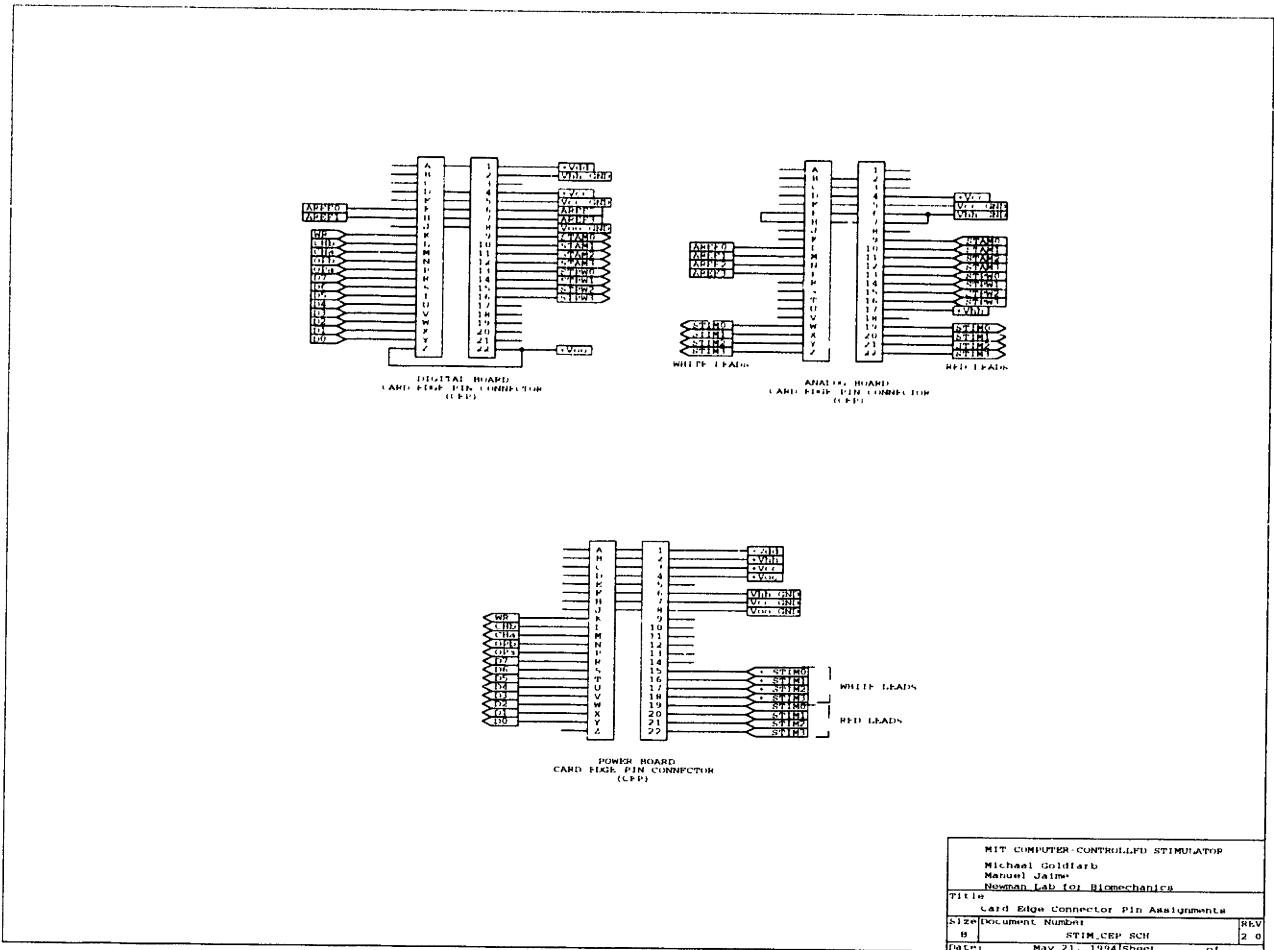
Figure C-13: Schematic of card edge connector pin assignments.

C.2 Stimulator Parts List

C.2.1 Card Rack and Case

Item (Mfr Part No.)	Description	Quantity	Distributor (Dstr Part No.)
Hammond RCBS Rack Case		1	Newark (50F8488)
Vector Card Cage (CCK14F190)		1	Newark (51F3497)
Vector Card Guides (CG2-95P)		1	Newark (98F2284)
Vector Cards (3662-2)		3	Newark (38F1105)
Vector Card Edge Connectors (R644-3)		3	Newark (38F1140)

C.2.2 Case Components and Connectors

Item (Mfr Part No.)	Description	Quantity	Distributor (Dstr Part No.)
Micro Fan (2408NL-04W-B30)	12V DC electric fan	1	Newark (50F5382)
red LED	panel mount	1	Digi-Key (L10001-ND)
green LED	panel mount	1	Digi-Key (L10005-ND)
yellow LED	panel mount	4	Digi-Key (L10007-ND)
DPDT rocker switch	panel mount	1	Digi-Key (SW307-ND)
3-contact male connector	connector for +5V from computer	1	Digi-Key (A1400)
3-contact female connector	connector for +5V from computer	1	Digi-Key (A1401)
pin contacts	connector for +5V from computer	10	Digi-Key (A1436-ND)
pin contacts	connector for +5V from computer	10	Digi-Key (A1437-ND)
2-contact Jones plug	connector for recharger	1	Digi-Key (CJ102P-ND)
2-contact Jones socket	connector for recharger	1	Digi-Key (CJ302S-ND)
20-pin ribbon cable header	connector for digital input	1	Digi-Key (CKR20T-ND)
20-pin wire wrap card connector	connector for digital input	1	Digi-Key (CKA20G-ND)
37-pin female, panel mount, solder-tail D-connector	connector for digital input	1	Digi-Key (137F-ND)
10-pin ribbon cable header	connector for stimulation output	1	Digi-Key (CKR10T-ND)
10-pin wire wrap card connector	connector for stimulation output	1	Digi-Key (CKA10G-ND)
9-pin female, panel mount, solder-tail D-connector	connector for stimulation output	1	Digi-Key (109F-ND)

C.2.3 Power and I/O Board

Item (Mfr Part No.)	Description	Quantity	Distributor (Dstr Part No.)
Maxim 633ACPA	12V to 15V converter	1	Maxim 633ACPA (samples)
National LM340KC-5.0	+5V regulator	1	Digi-Key (LMKC340-5)
National LM324J	quad op-amp	1	Digi-Key (LM324N)
150 uF capacitors		2	Digi-Key (P5732)
470 uH inductor		1	Newark (44F4247)
150 ohm resistor		2	Digi-Key (150Q)
10 Kohm resistor		1	Digi-Key (10KQ)
6.8 Kohm resistor		1	Digi-Key (6.8KQ)
4 contact terminal block	for power lines	1	Newark (46F862)
0.5 amp fuse		1	Digi-Key (F602-ND)
fuse holder		1	Digi-Key (3536K-ND)
voltage regulator socket		1	Digi-Key (4600K-ND)
mica insulation insert	for voltage regulator	1	Digi-Key (4662K-ND)
heat sink	for voltage regulator	1	Digi-Key (HS-140)

C.2.4 Digital Board

Item (Mfr Part No.)	Description	Quantity	Distributor (Dstr Part No.)
National 74HC154N	4 to 16 line decoder	1	Digi-Key (MM74HC154N)
Harris ICM7209	clock	1	Newark (ICM7209IPA)
Texas Instruments 74HC00N	quad 2-input NAND gate	1	Newark (MM74CH74AN)
National 74HC74AN	dual flip-flop	4	Digi-Key (MM74HC74AN)
Harris CD40103BEX	timer	4	Newark (CD40103BEX)
National 74HC374N	octal filp-flop	4	Digi-Key (MM74HC374N)
Analog Devices AD7248JN	12-bit (8+4) D/A converter	4	Newark (AD7248JN)
National 74HC20N	dual 4-input NAND gate	1	Digi-Key (MM74HC20N)
Quality Technology 74OL6010	optoisolators	13	Digi-Key (74OL6010GI)
4.00 MHz crystal		1	Digi-Key (X006)
470 ohm resistor	for optoisolators	13	Digi-Key (470Q)
20 pF capacitor	for clock chip	2	Digi-Key (P4448)
0.1 uF tantalum capacitors	for despiking power supplies	20	Digi-Key (P2053)
0.22 uF tantalum capacitors	for optoisolators	26	Digi-Key (P2055)

C.2.5 Analog Board

Item (Mfr Part No.)	Description	Quantity	Distributor (Dstr Part No.)
National LM324N	quad op-amp	2	Digi-Key (LM324N)
National CD4066BCN	quad analog switch	1	Digi-Key (CD4066BCN)
TIP 120	NPN Darlington transistors	4	Digi-Key (TIP120PH-ND)
heat sinks	for TIP 120's	4	Newark (58F1360)
1N4004 diodes		8	Digi-Key (1N4004GI)
Stancor P-6134 transformers		4	Gerber (P-6134)
4700 uF electrolytic capacitors		4	Digi-Key (P6246)
1 Kohm trimpots		4	Digi-Key (3009P-102-ND)
100 ohm resistors		4	Digi-Key (100Q)
10 Kohm resistors		4	Digi-Key (10KQ)
10 ohm resistors		4	Digi-Key (10Q)
10 uF capacitors		4	Digi-Key (P2065)

C.2.6 Miscellaneous Parts

Item (Mfr Part No.)	Description	Quantity	Distributor (Dstr Part No.)
Panasonic 12V, 6.5 A-hr lead acid battery		1	Digi-Key (P173)
Xenotronics recharger	Xenotronics, Valencia, CA	1	(8101D1208AN)
8 pin wire wrap socket		1	Digi-Key (ED4308)
14 pin wire wrap socket		17	Digi-Key (ED4314)
16 pin wire wrap socket		12	Digi-Key (ED4316)
20 pin wire wrap socket		8	Digi-Key (ED4320)
24 pin wire wrap socket		1	Digi-Key (ED4324)
8 pin socket labels		1	Jameco (8ID)
14 pin socket labels		17	Newark (46F5166)
16 pin socket labels		12	Newark (46F5167)
20 pin socket labels		8	Newark (46F5169)
24 pin socket labels		1	Newark (46F5171)
16 pin socket headers		8	Newark (44F5151)
miniature board connector sockets	for LED connections	1	Digi-Key (A3011-ND)
miniature board connector header	for LED connections	1	Digi-Key (S1082-36)
miniature board connector contacts	for LED connections	1	Digi-Key (A3003-ND)
T44 pins			Newark (38F1329)

Appendix D

CBO Documentation

D.1 Brace Parts List

Description	Quantity	Manufacturer (Mfr Part No.)	Telephone
Hip joint particle brakes	2	Force Limited (B20SF14). Coil resistance is 30 Ohms. Brakes produce approximately 16 in-lbs torque @ 400 ma	(310) 392-3021
Knee joint particle brakes	2	Force Limited (B20SF15). Coil resistance is 81 Ohms. Brakes produce approximately 32 in-lbs torque @ 450 ma	(310) 392-3021
Hip gear and pinion	2	ASI Technologies. Uncut gear has 64 teeth, 3.56 inch O.D., and 0.472 inch face. Pinion has four teeth.	(215) 674-8910
Knee gear and pinion	2	ASI Technologies. Uncut gear has 64 teeth, 4.40 inch O.D., and 0.631 inch face. Pinion has four teeth.	(215) 674-8910

Description	Quantity	Manufacturer (Mfr Part No.)	Telephone
Potentiometers	4	Midori America (CP-2FK)	(714) 449–0997
Strain gages	16	Micro Measurements (EA-13-125PC-350-E)	(919) 365–3800
Pinion bearings	8	FAG (618/8)	(203) 327–1960
Hip gear radial bearings	2	Furon Dixon (Rulon FCJ 16-F20-0.470)	(401) 253–2000
Knee gear radial bearings	2	Furon Dixon (Rulon FCJ 16-F20-0.630)	(401) 253–2000
Brace/gear link radial bearings	2	Furon Dixon (Rulon FCJ 16-F20-0.246)	(401) 253–2000
Gear thrust bearings	8	Torrington (NTA-1625)	(404) 696–7400
Gear thrust washers	16	Torrington (TRA-1625)	(404) 696–7400
Ab/adduction linkage radial bearings (1/4" ID, 3/8" OD)	12	Rexnord (701-0004-012)	(708) 969–8752
Ab/adduction linkage thrust bearings (1/4" ID, 5/8" OD)	12	Rexnord (G10, one face TFE)	(708) 969–8752
Hip cross bar	1	Tioga Prestige II handlebar with 6 degree bend (Nashbar TG-HB)	(800) 627–4227
Ankle-foot orthoses	1 of each	AliMed (6604, 6605, 6606, 6607)	(800) 225–2610
Hip MPB/pinion shaft coupling	2	W.M. Berg (CS-51)	(516) 599–5010
Knee MPB/pinion shaft coupling	2	W.M. Berg (CS-52)	(516) 599–5010
Large diameter chromoly tubing		Aircraft Spruce (03-01700)	(800) 824–1930
Small diameter chromoly tubing		Aircraft Spruce (03-00500)	(800) 824–1930

Description	Quantity	Manufacturer (Mfr Part No.)	Telephone
Sensor umbilical	100 ft	Belden (9637)	(317) 983-5200
MPB umbilical	100 ft	Belden (9455)	(317) 983-5200
Brace harness wire	200 ft	Belden (9986)	(317) 983-5200
Sensor umbilical connectors	1 of each	Amp (Digi-Key A1369-ND, A1378-ND)	(800) 344-4539
MPB umbilical connectors	1 of each	Amp (Digi-Key A1369-ND, A1371-ND)	(800) 344-4539
Sensor umbilical cable clamps	2	Amp (Digi-Key A1332-ND)	(800) 344-4539
MPB umbilical cable clamps	2	Amp (Digi-Key A1330-ND)	(800) 344-4539
Contacts for umbilical connectors	40 of each	Amp (Digi-Key A1008-ND, A1009-ND)	(800) 344-4539
Female harness connectors	8	Amp (Ampmodu MTE: 103945-4)	(800) 522-6752
Male harness connectors (need 8 for each set of brace links)	8	Amp (Ampmodu MTE: 103957-4)	(800) 522-6752
PC board kit	1 of each	All Electronics (TTS-5, ER-3, ER-18, PCB-33)	(800) 826-5432

D.2 Joint Torque Calculations

Maximum joint torque specifications for the CBO prototype were derived based on three desired capabilities. The orthosis should (1) be able to provide the dissipative torques observed in normal gait, (2) be capable of locking a joint against a stimulated muscle contraction, and (3) implement a controlled stand-to-sit maneuver without the aid of muscle activation.

D.2.1 Dissipative Torques during Able-bodied Gait

- Maximum dissipative knee torque is approximately 0.3 Nm/kg body weight [105]. For a body mass of 80 kg, the maximum dissipative knee torque is 24 Nm (210 in-lbs).

- Maximum dissipative hip torque is approximately 0.4 Nm/kg body weight [105]. For a body mass of 80 kg, the maximum dissipative knee torque is 32 Nm (285 in-lbs).

D.2.2 Locking Against a Stimulation Contraction

- Maximum knee torque from quadricep stimulation is approximately 50 Nm (445 ft-lbs)

- Torques produced by flexion withdrawal reflex are not well known.

D.2.3 Controlled Stand-to-Sit Maneuver

Assumptions:

- quasi-static

- subject does not use arms

- head, arms and trunk weight weight 45 kg (100 lbs) and are the only significant load

- center of gravity (CG) vector passes through midpoint of foot and through midpoint of thigh

242
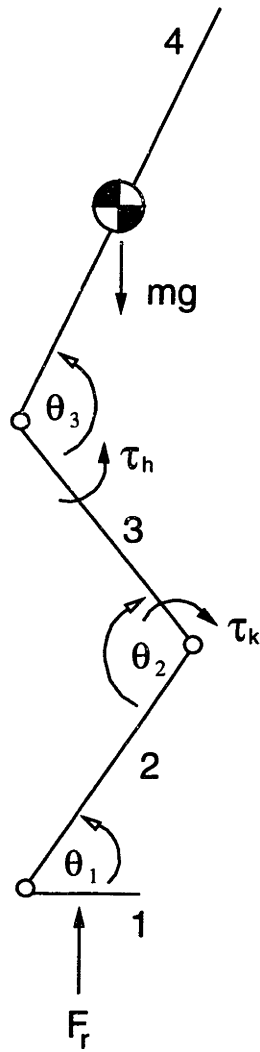
Figure D-1: Free body diagram for controlled stand-to-sit calculation.

- foot length l_1 is 20 cm (8 in)

- shank length l_2 is 46 cm (18 in)

- thigh length l_3 is 46 cm (18 in)

- head/trunk length l_4 is 77 cm (30 in)

Constraint Equations:

(1) CG passes through midpoint of foot

$$-\frac{l_1}{2} + l_2 \cos\theta_1 - l_3 \cos\theta_2 - \theta_1 + \frac{l_4}{2} \cos\theta_3 - \theta_2 + \theta_1 = 0 \qquad (D.1)$$

(2) CG passes through midpoint of thigh

$$-\frac{l_1}{2} + l_2 \cos\theta_1 - l_3 \cos\theta_2 - \theta_1 = 0 \qquad (D.2)$$

Torque Equations:

(1) knee torque

$$\tau_k = -\frac{mg}{2} \left[-\frac{l_1}{2} + l_2 \cos\theta_1 \right] \qquad (D.3)$$

(2) hip torque

$$\tau_h = \frac{mg}{2} \left[l_3 \cos\theta_2 - \theta_1 + \frac{l_4}{2} \cos\theta_3 - \theta_2 + \theta_1 \right] \qquad (D.4)$$

Solution:

Assuming each leg takes half the total load

$$\tau_{k_{max}} = \tau_{h_{max}} = 25 \text{ Nm (220 in-lbs)} \qquad (D.5)$$

which occurs at $\theta_1 = 45°$, $\theta_2 = 60°$, and $\theta_3 = 70°$.
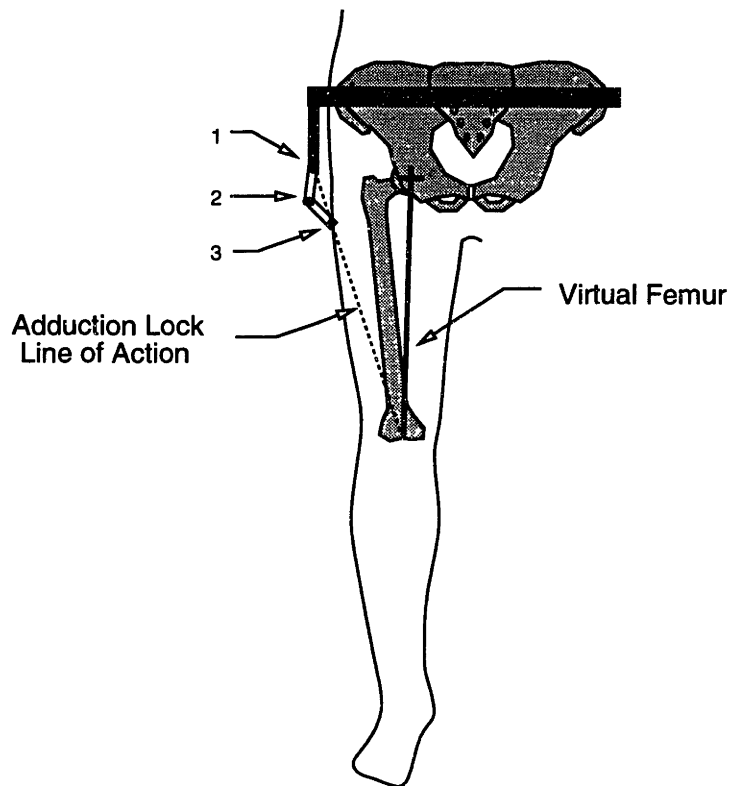
Figure D-2: Diagram of hip adduction lock.

D.3 Hip Adduction Lock

Figure D-2 illustrates the hip adduction lock. The hip abduction and adduction degree of freedom is accomodated by a three degree of freedom linkage as shown. All three linkage degrees of freedom are revolute joints, which are labelled in the figure as joints 1, 2, and 3. Though not shown in the figure, joint 2 contains an adjustable lock that, once engaged, prevents the segment 1–3 from increasing in length.

Assuming a good coupling with the skeleton, a rigid member extending from joint 1 to the inferior end of the femur (represented in the figure by the dashed line) would prevent further hip adduction. Since the line of action of this member passes through joints 1 and 3, these joints need not sustain a moment. Hip adduction can therefore be effectively implemented by locking only the middle of the three revolute joints.

D.4 CBO Machine Drawings

All machine drawings included in this appendix have been reduced to 50 percent of their original size.
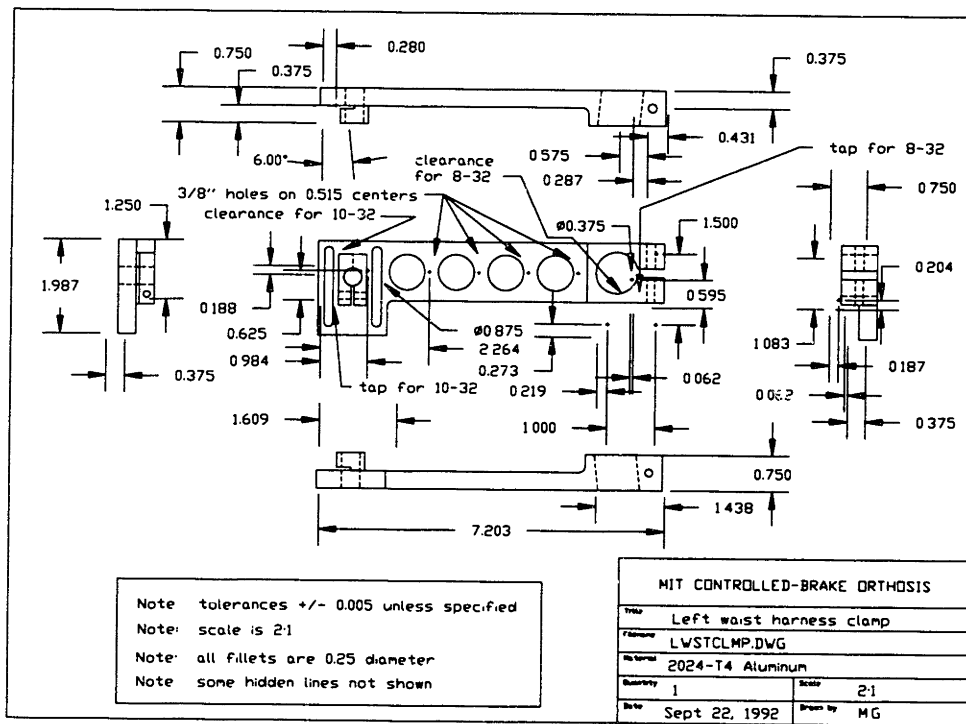
Figure D-3: Left waist clamp.

Figure D-4: Right waist clamp.

Figure D-5: Detail of right waist clamp (drawing 1 of 3).
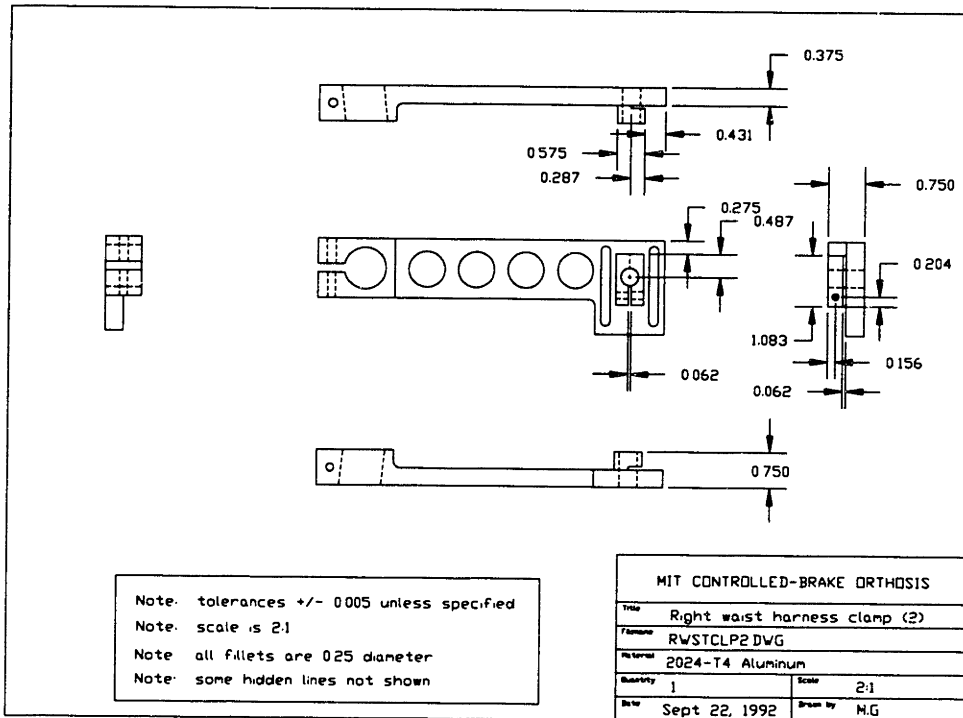
Figure D-6: Detail of right waist clamp (drawing 2 of 3).
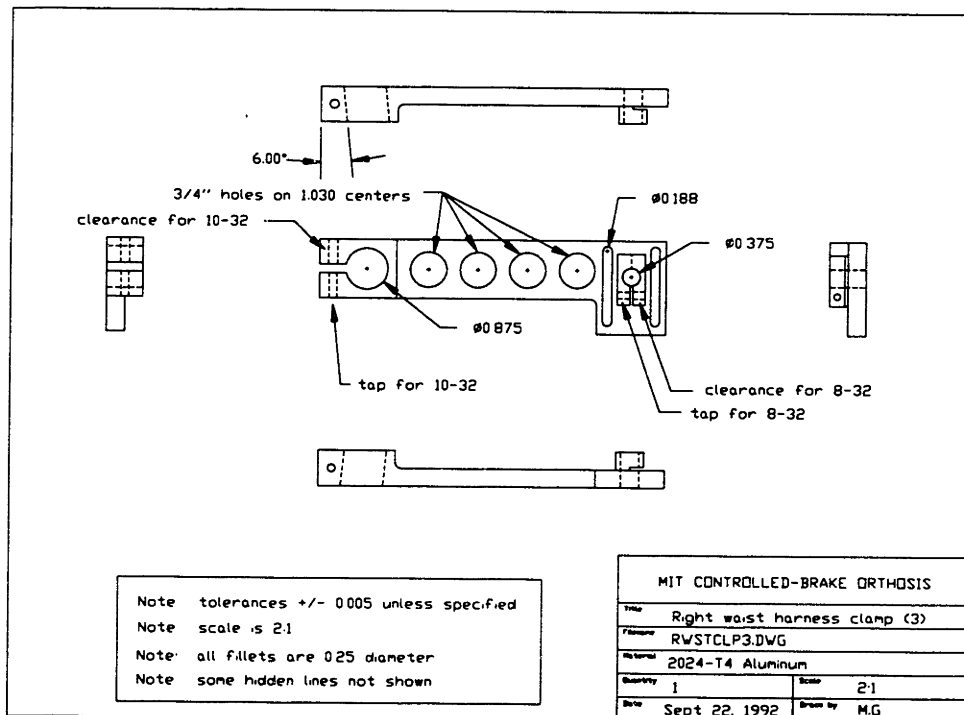
Figure D-7: Detail of right waist clamp (drawing 3 of 3).
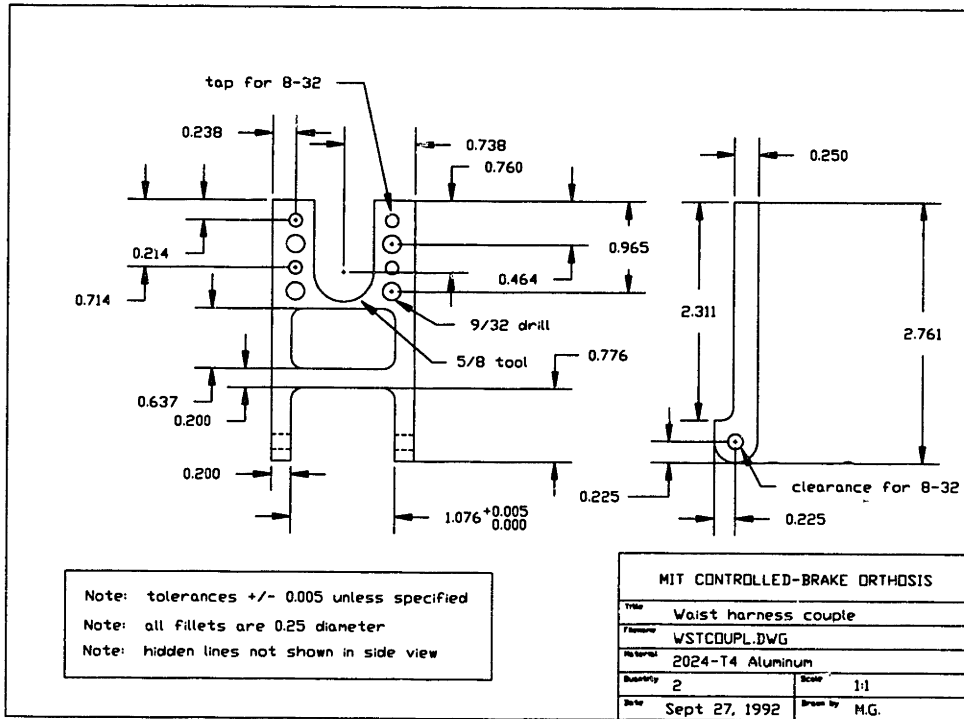
Figure D-8: Link that couples waist clamp to hip joint.
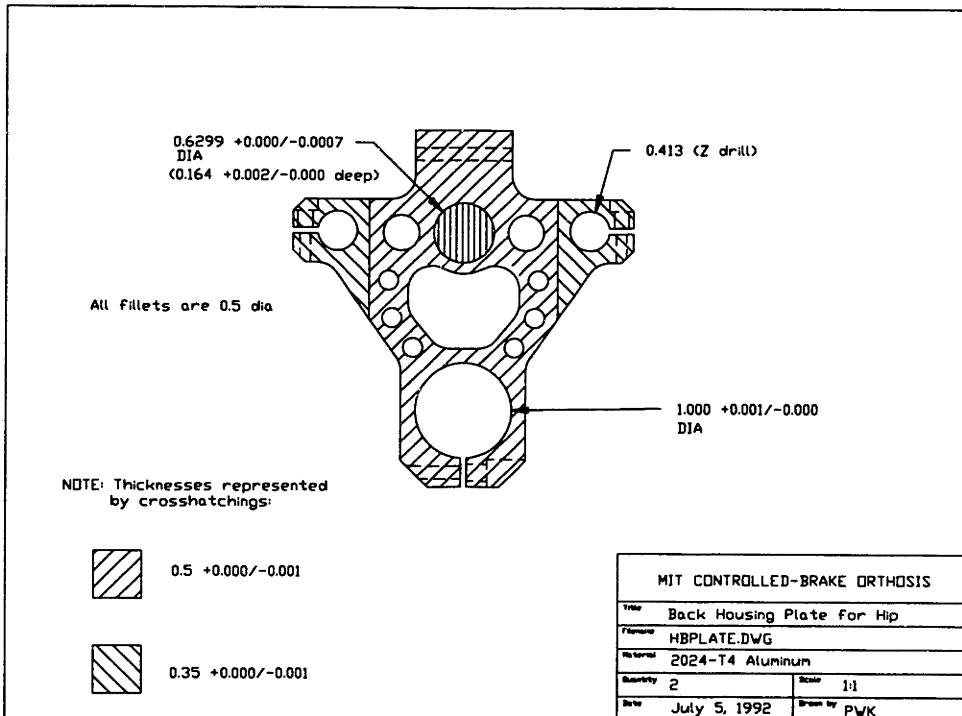
Figure D-9: Back plate of hip gear housing (drawing 1 of 2).
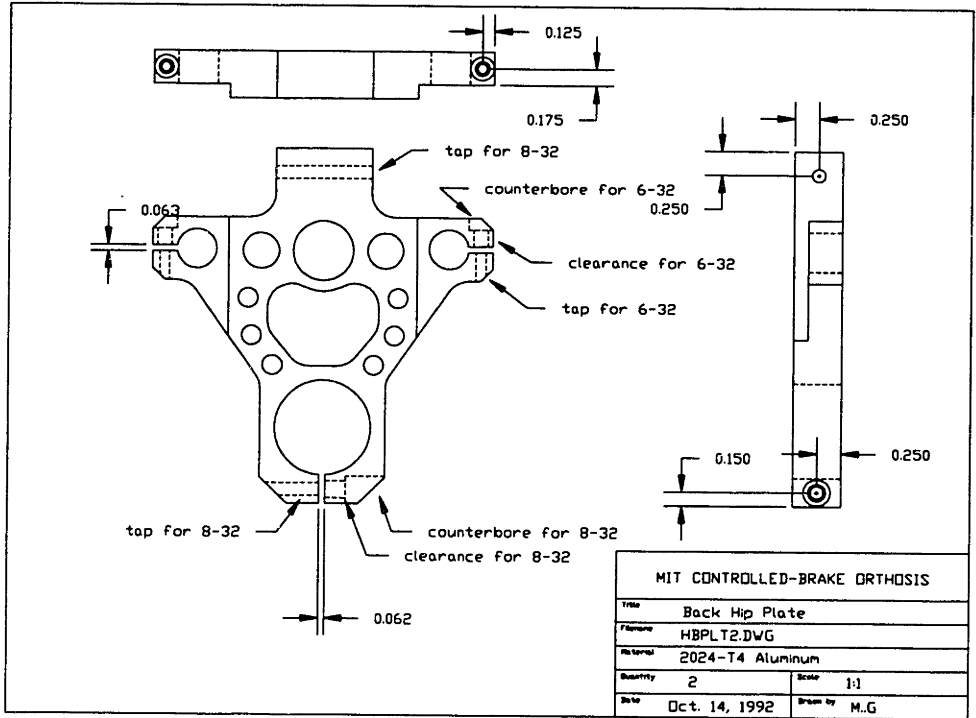
Figure D-10: Back plate of hip gear housing (drawing 2 of 2).
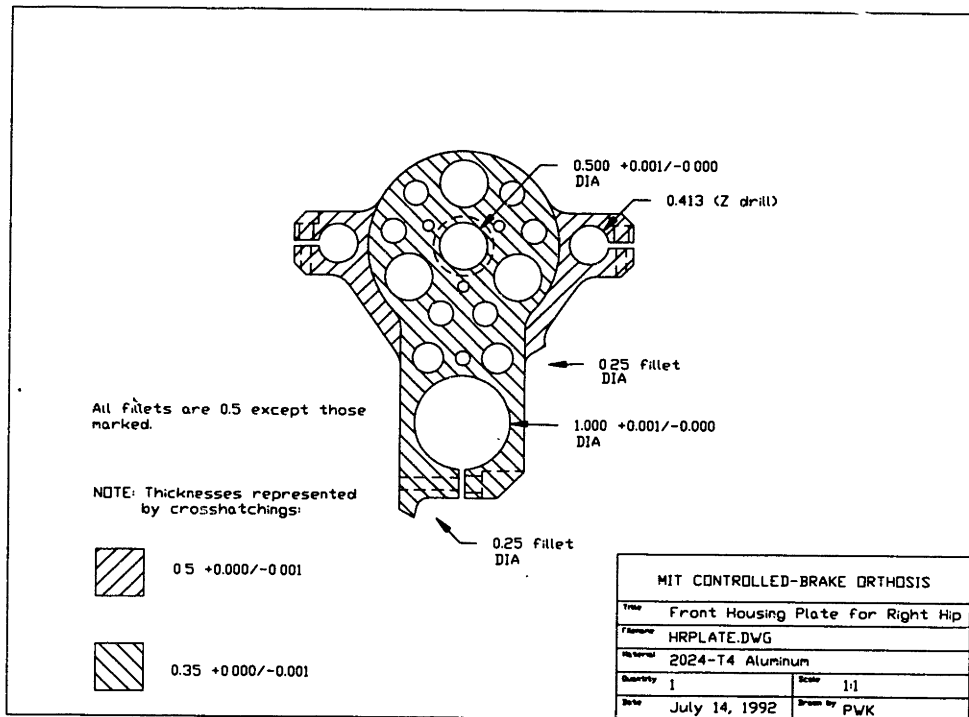
Figure D-11: Front plate for right hip gear housing (drawing 1 of 2).
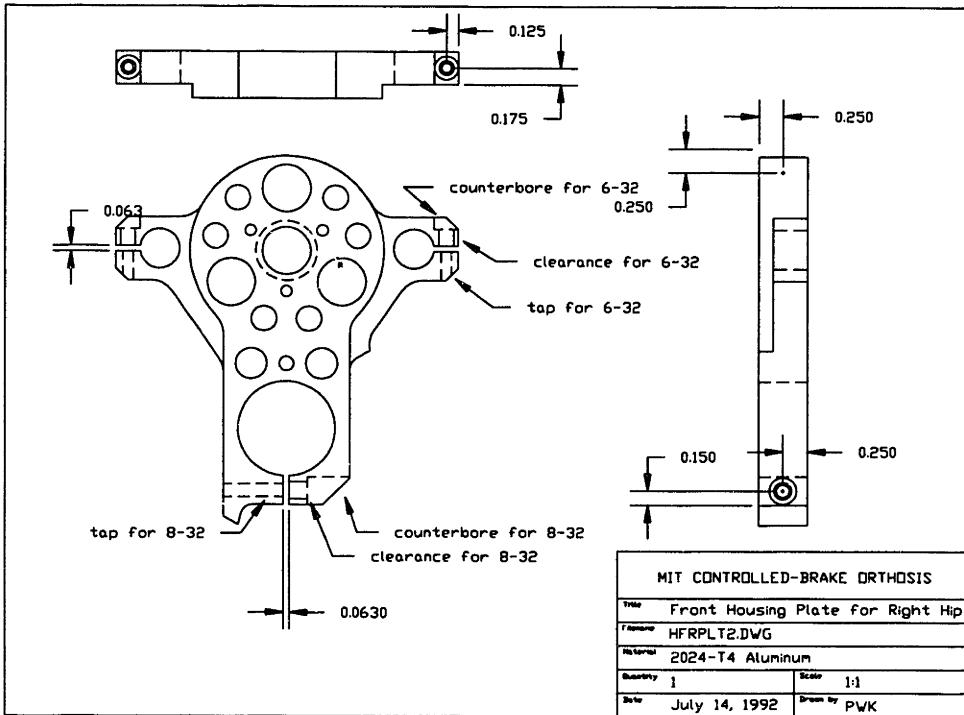
Figure D-12: Front plate for right hip gear housing (drawing 2 of 2).
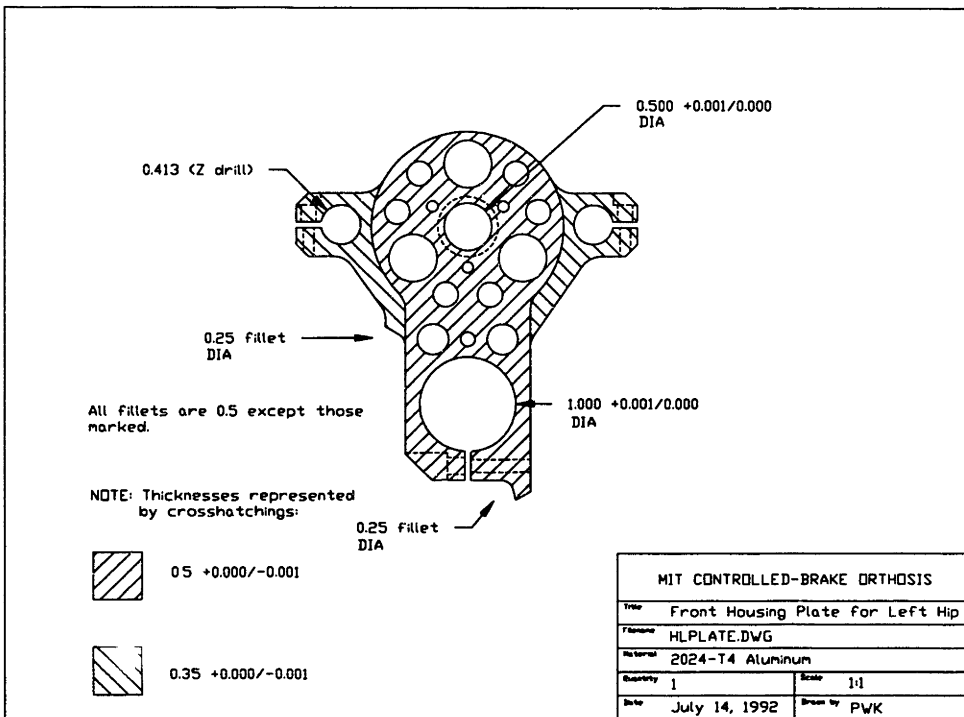
Figure D-13: Front plate for left hip gear housing.

251

Ø0.8780 0.0000/-0.0005   Ø0.9980 0.0000/-0.0005   1.991 0.000/-0.005

Note: pots have 0.8765 O.D.

Note: hard-coat anodizing adds
       0.001U +/-0.0001 to surface

MIT CONTROLLED-BRAKE ORTHOSIS

Title	Hip Gear Shaft		
Filename	HSHAFT.DWG		
Material	2024-T4 Aluminum		
Quantity	2	Scale	1:1
Date	August 8, 1992	Drawn by	M.G.
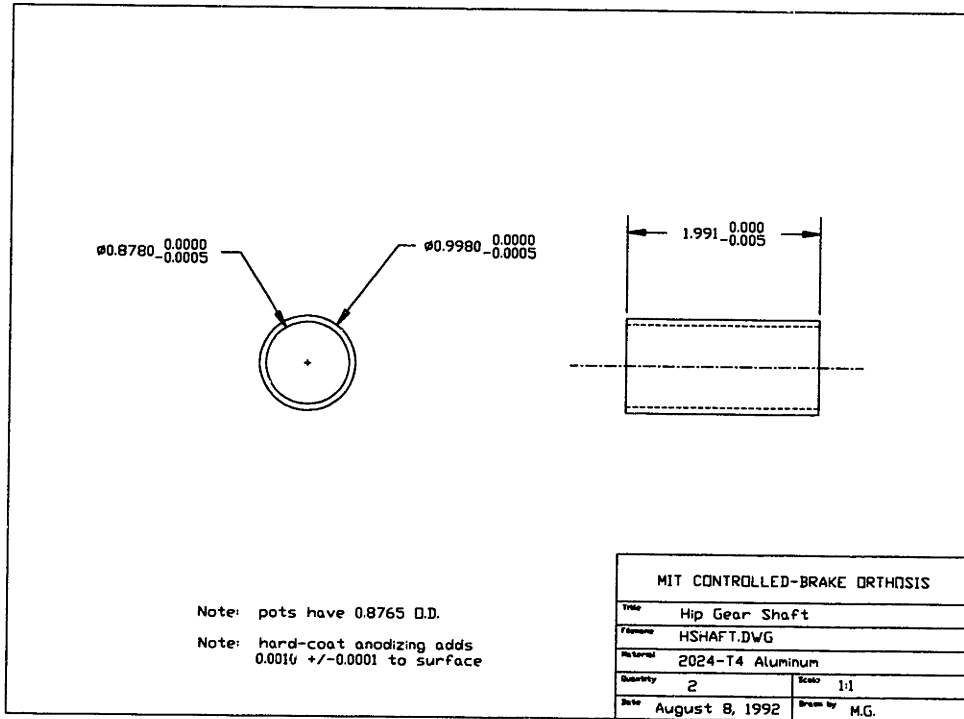
Figure D-14: Hip gear shaft.

Ø0.188±0.005   Ø0.412 0.000/-0.002   1.839 0.000/-0.005

MIT CONTROLLED-BRAKE ORTHOSIS

Title	Hip Housing Stand-off		
Filename	HSTNDOFF.DWG		
Material	2024-T4 Aluminum		
Quantity	4	Scale	1:1
Date	August 8, 1992	Drawn by	M.G.
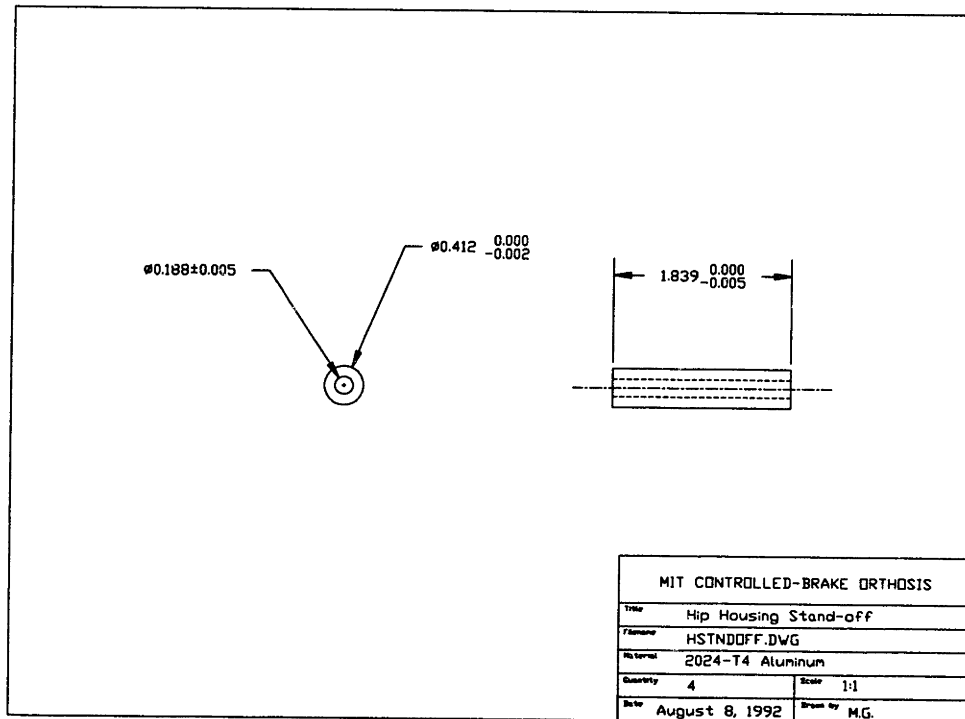
Figure D-15: Stand-offs for hip gear housing.
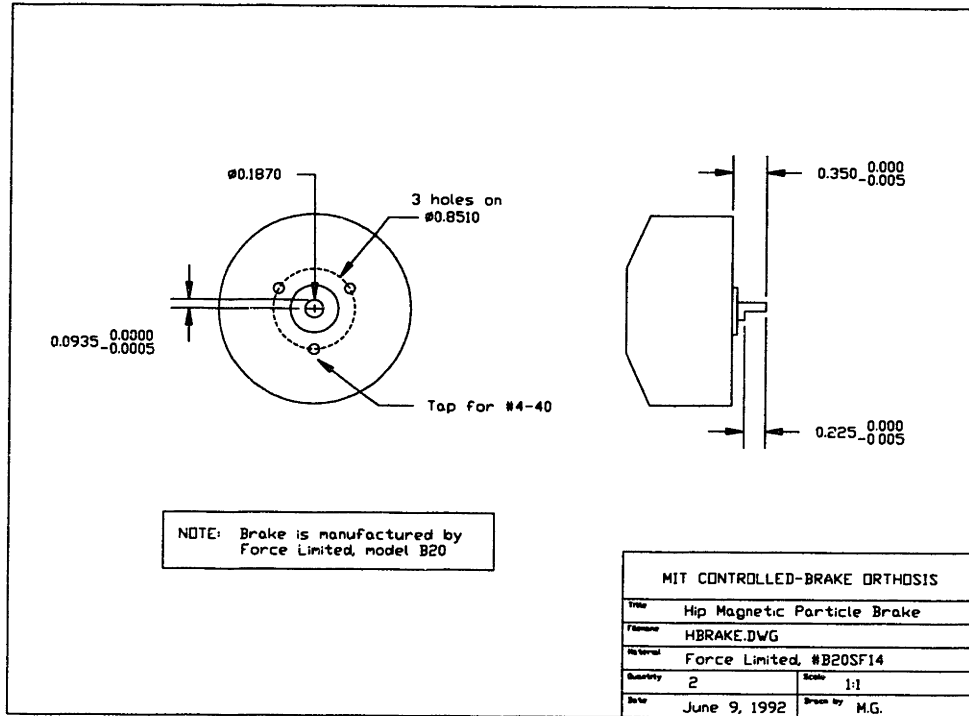
Figure D-16: Mounting configuration of hip magnetic particle brakes.
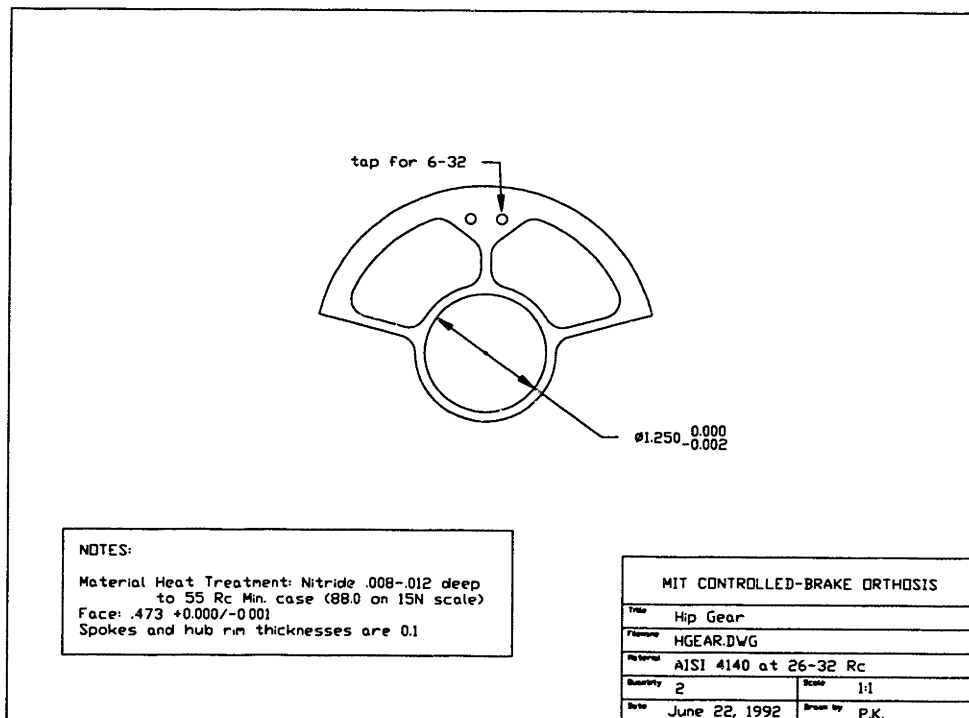
Figure D-17: Modification of Evoloid hip gears.

253
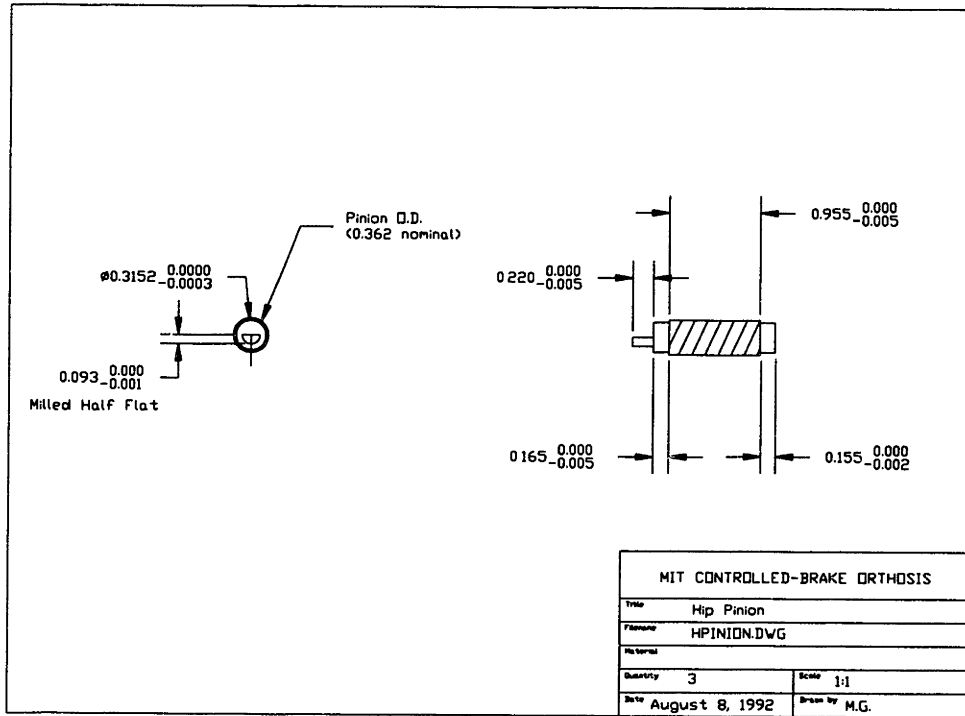
Figure D-18: Modification of Evoloid hip pinions.
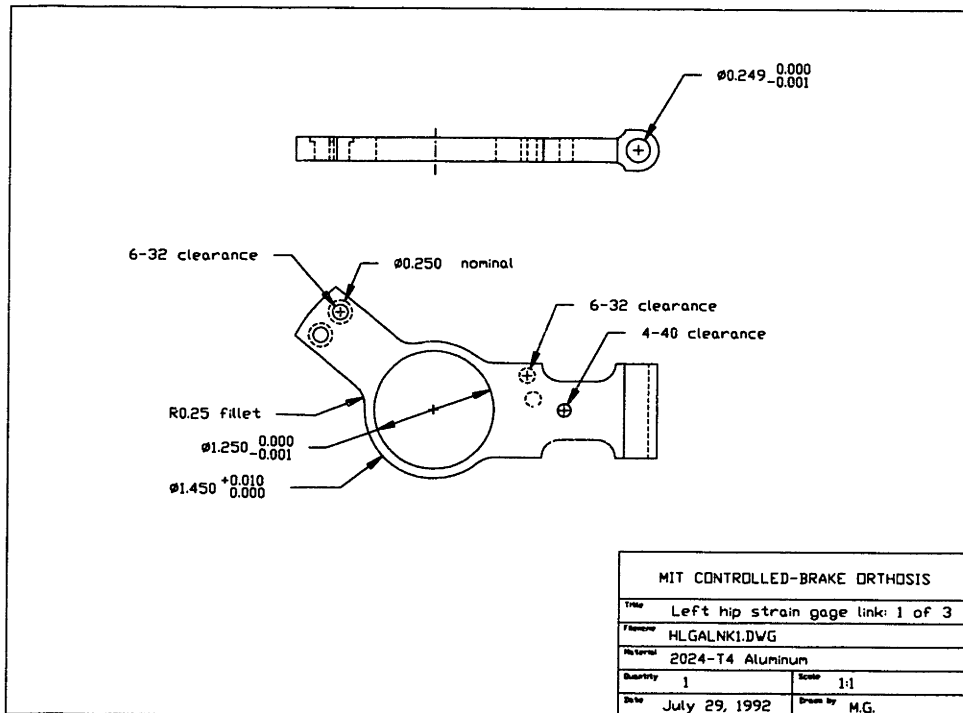
Figure D-19: Link that couples left hip gear to the brace (drawing 1 of 3).
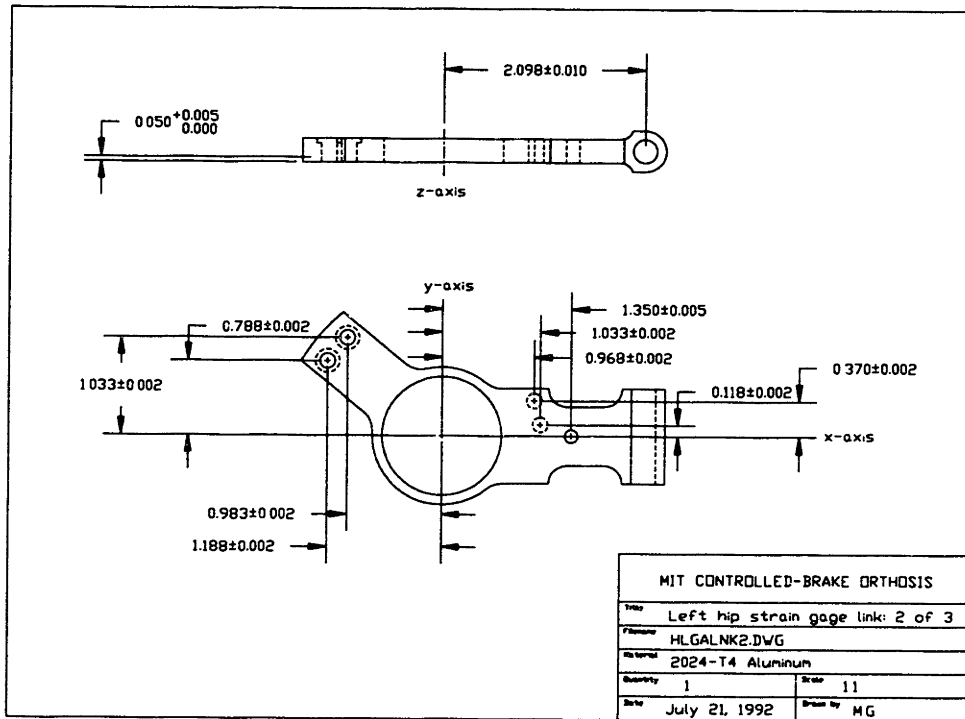
Figure D-20: Link that couples left hip gear to the brace (drawing 2 of 3).
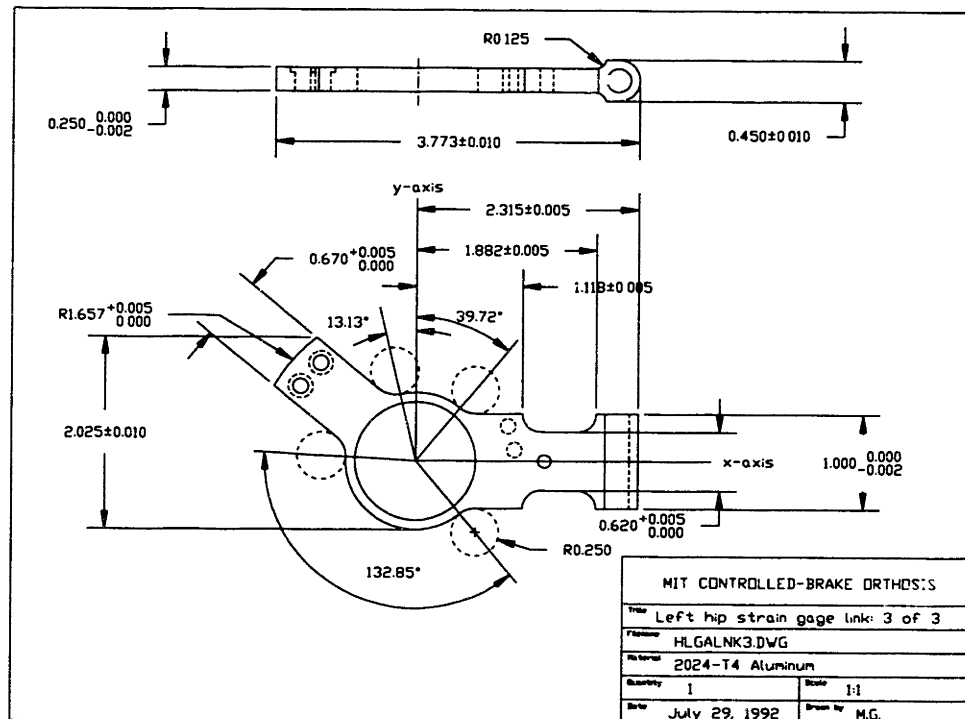
Figure D-21: Link that couples left hip gear to the brace (drawing 3 of 3).
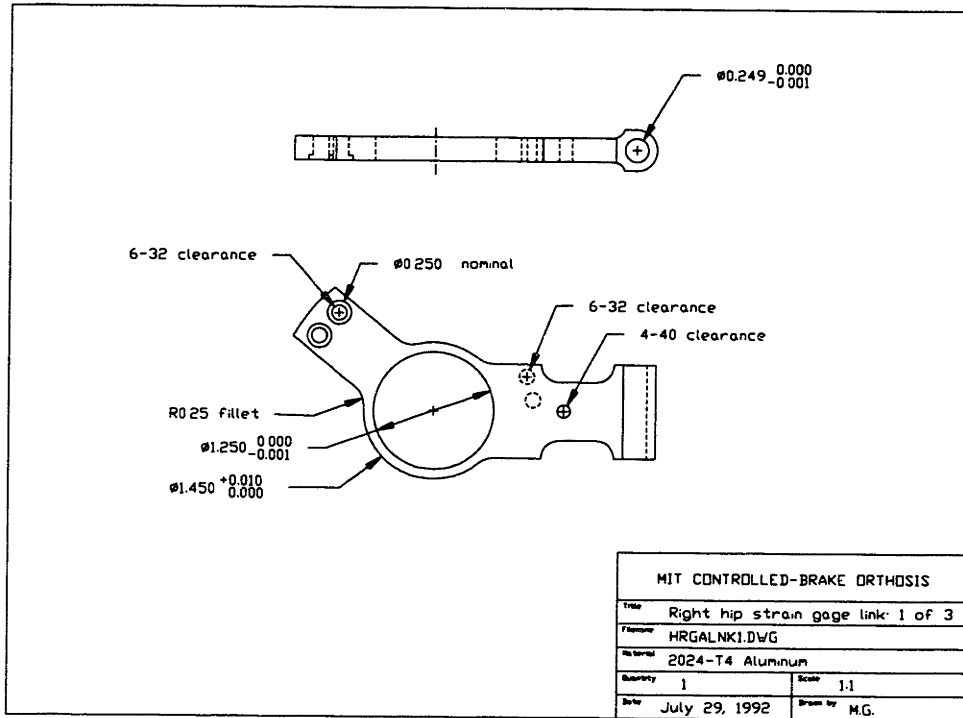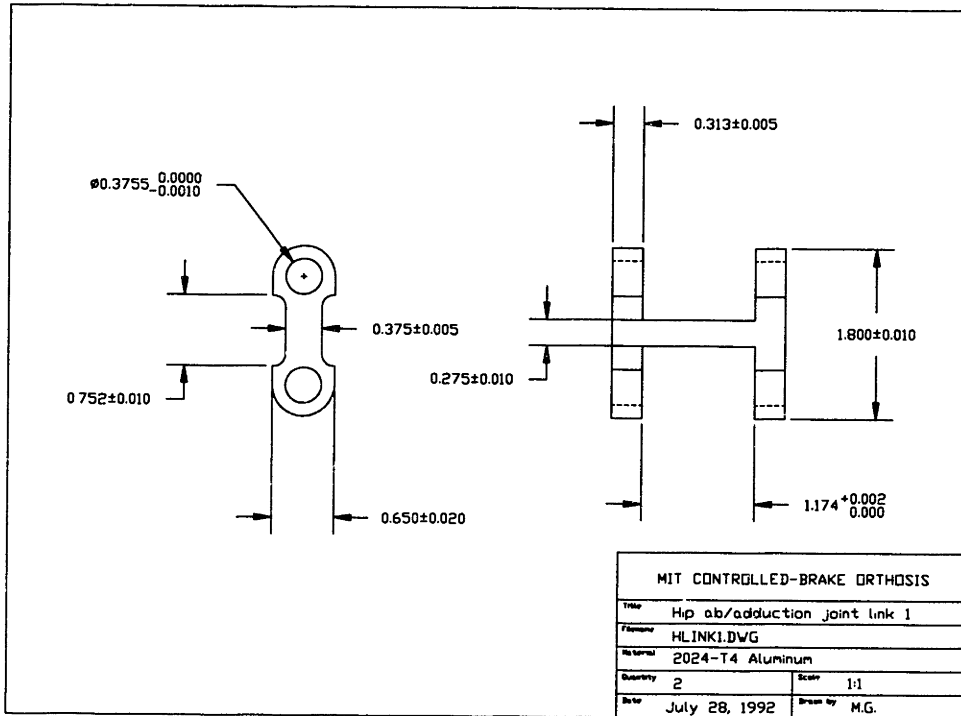
Figure D-22: Link that couples right hip gear to the brace (drawing 1 of 3).
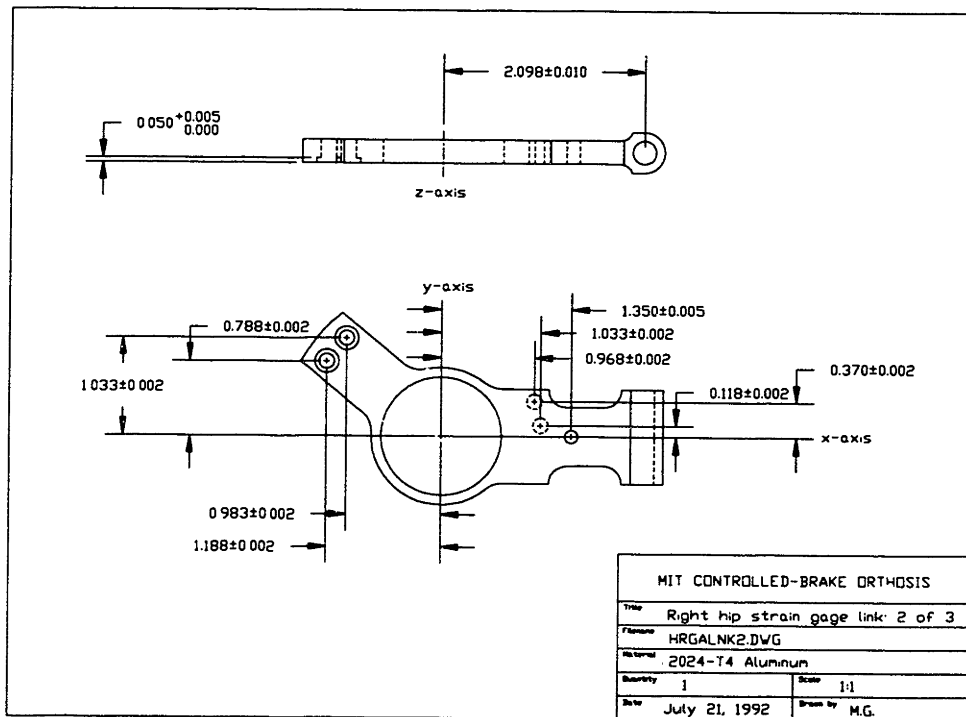
Figure D-23: Link that couples right hip gear to the brace (drawing 2 of 3).
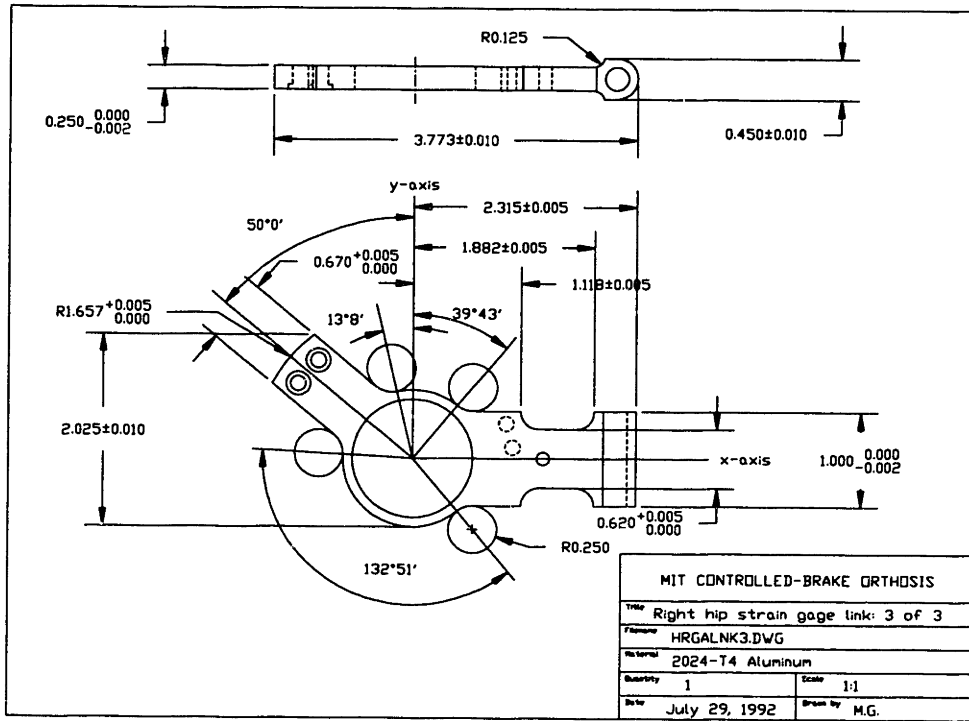
Figure D-24: Link that couples right hip gear to the brace (drawing 3 of 3).
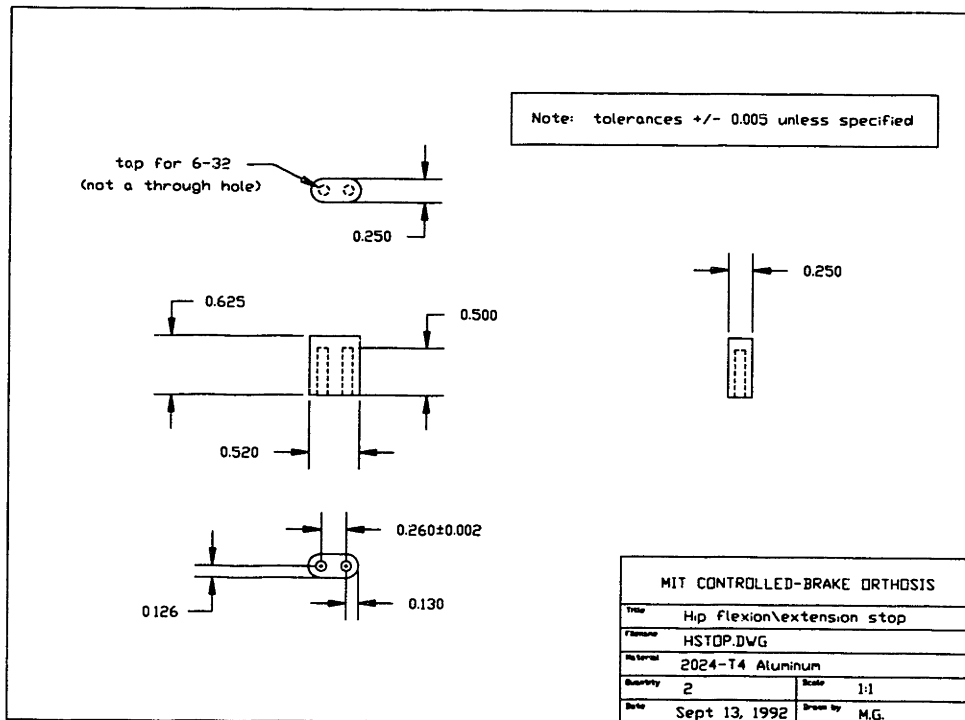
Figure D-25: Motion stop of hip joint.

Figure D-26: Upper link of hip ab/adduction linkage.
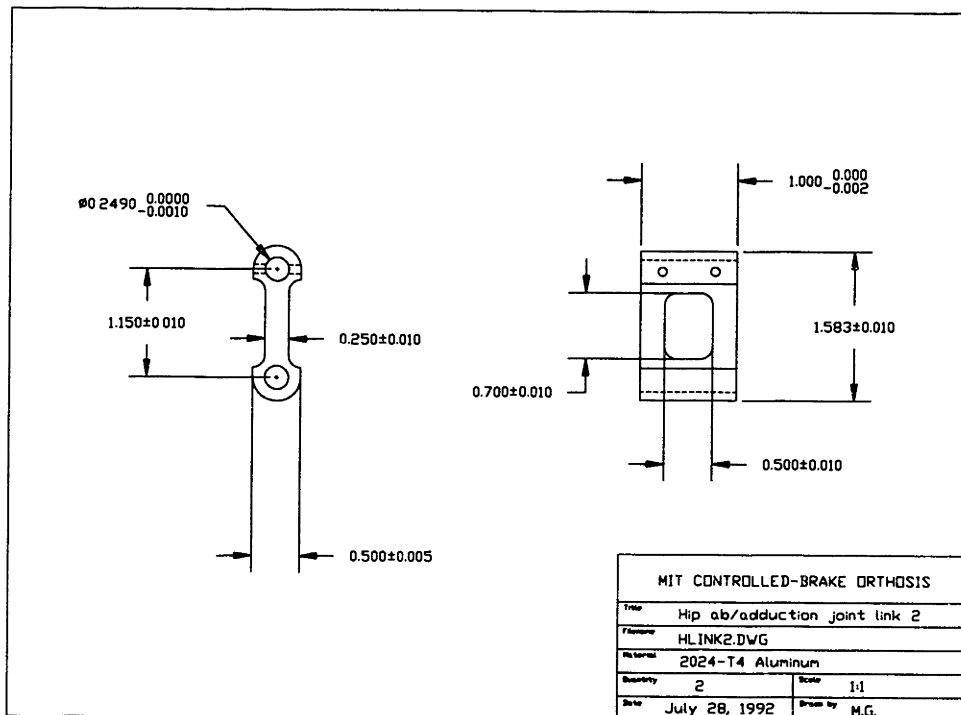
Figure D-27: Middle link of hip ab/adduction linkage.

258
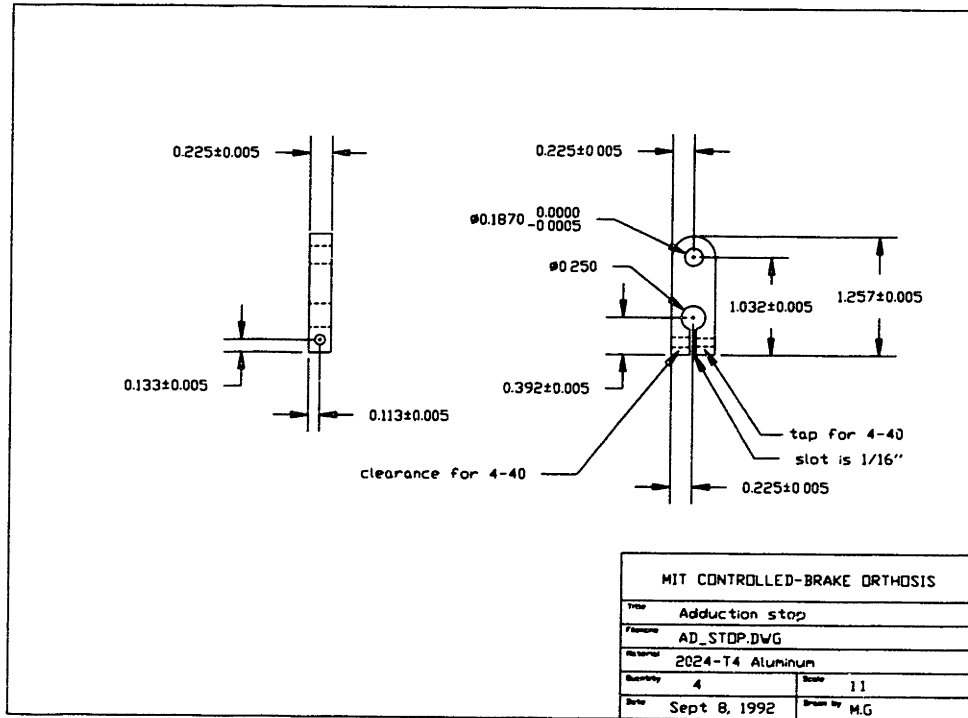
Figure D-28: Adjustable lock for the hip ab/adduction linkage.
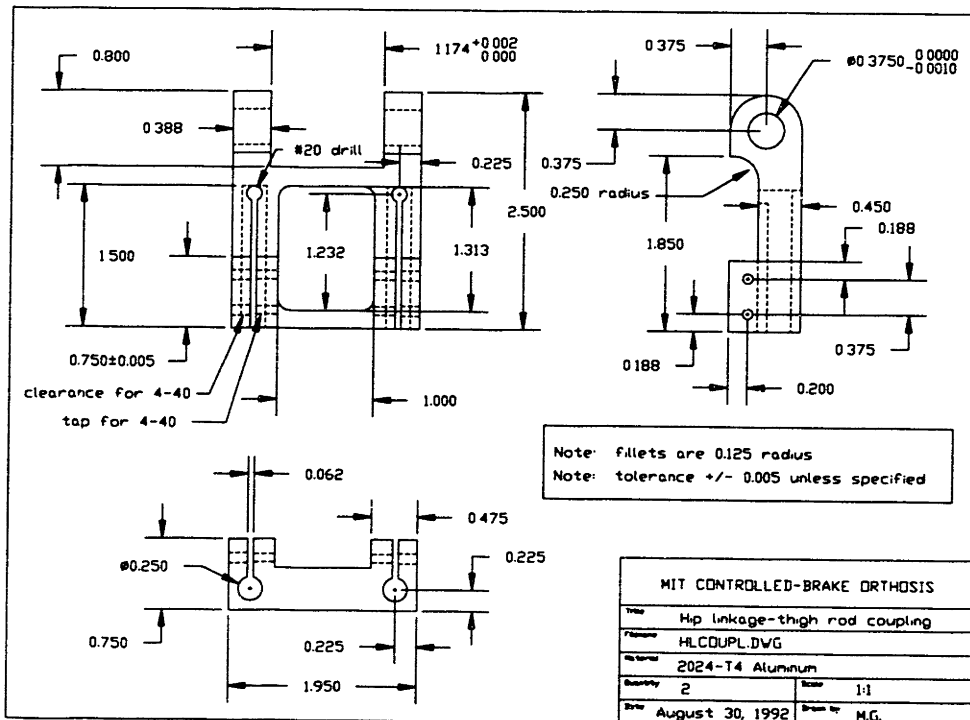
Figure D-29: Lower link of hip ab/adduction linkage.

259
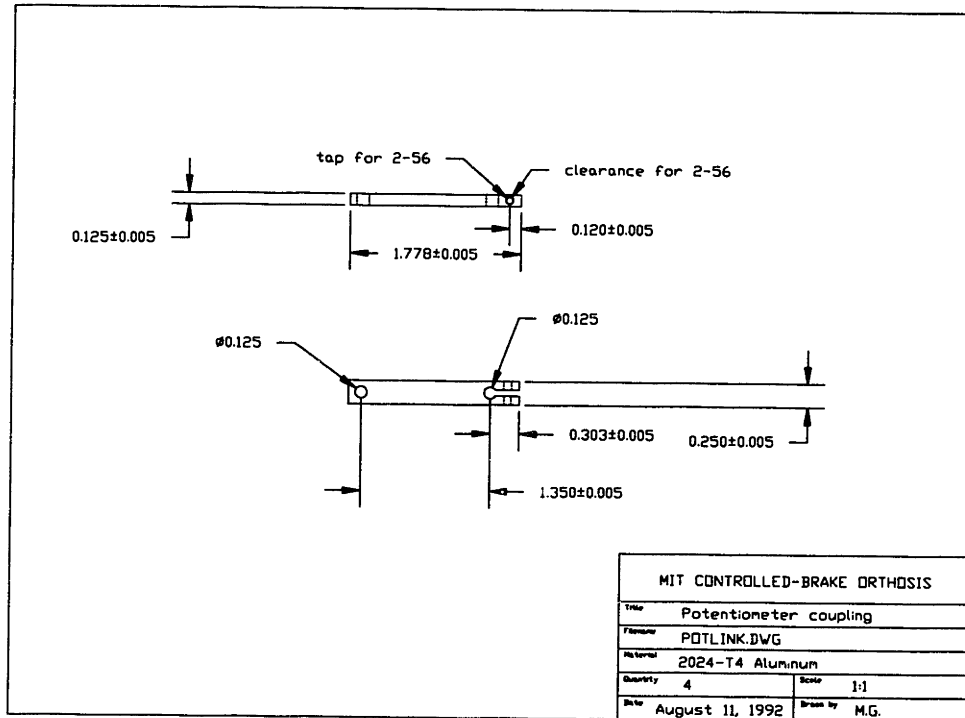
Figure D-30: Link for coupling brace to potentiometer.
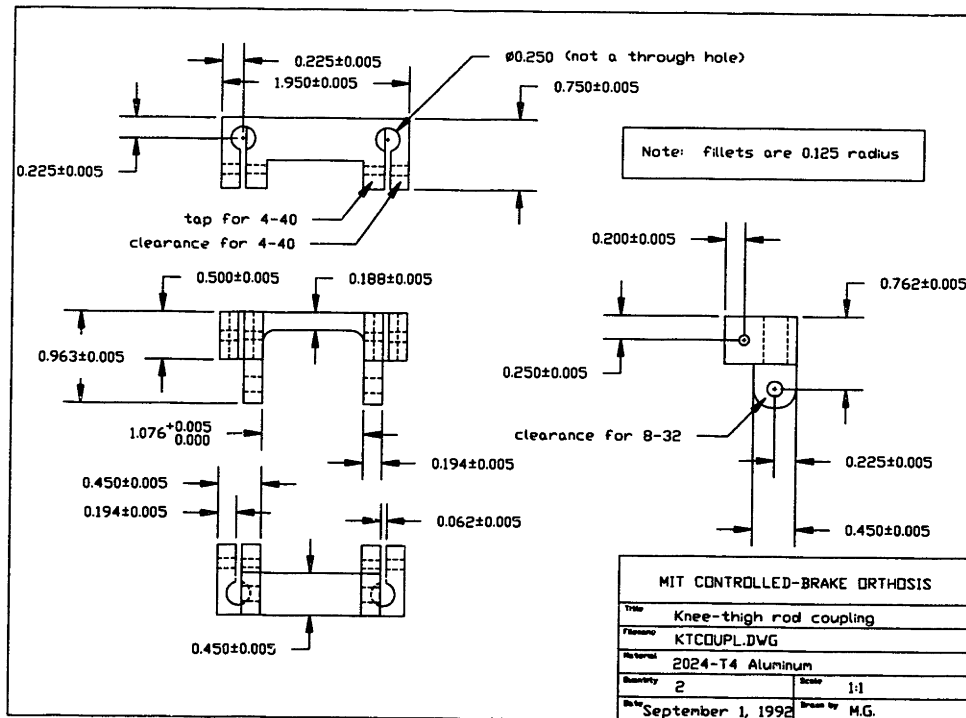
Figure D-31: Link that couples knee joint to thigh segment of brace.
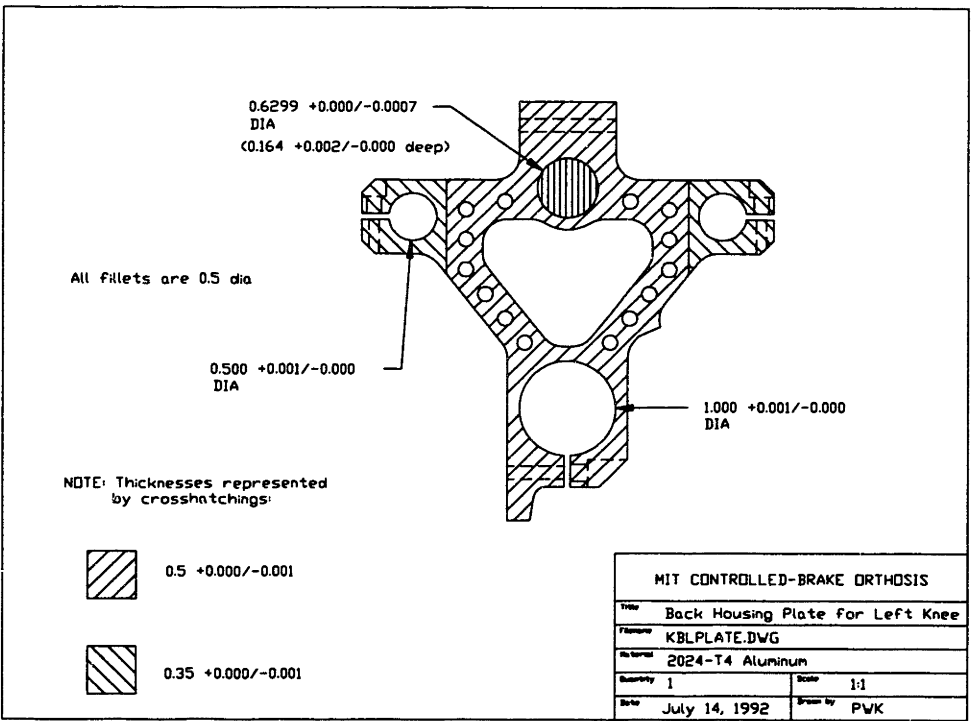
260
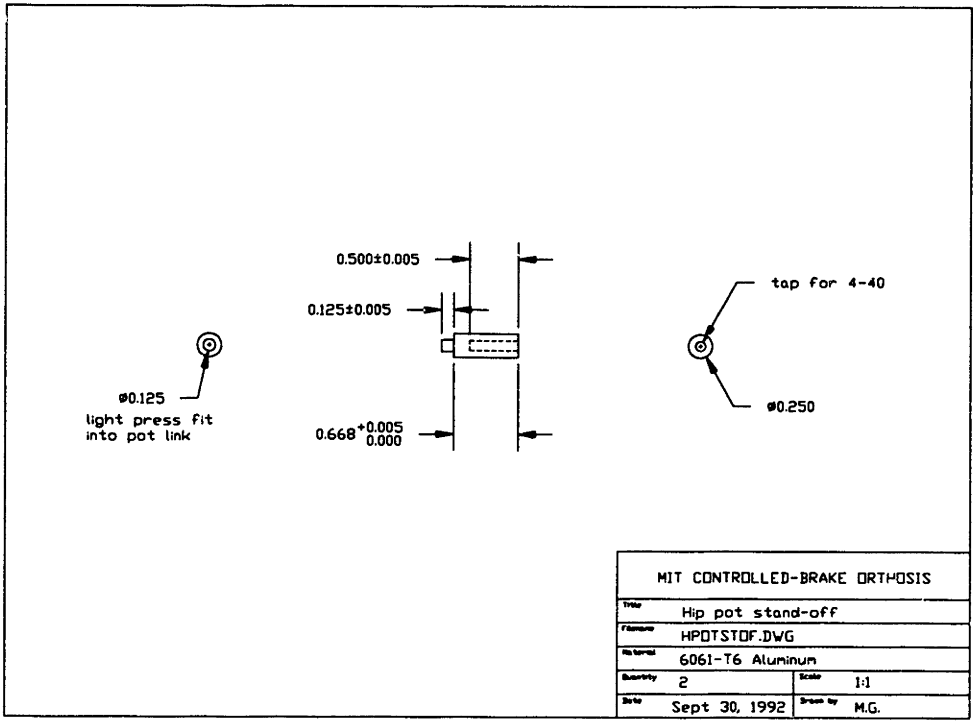
Figure D-32: Stand-off for hip potentiometer coupling.

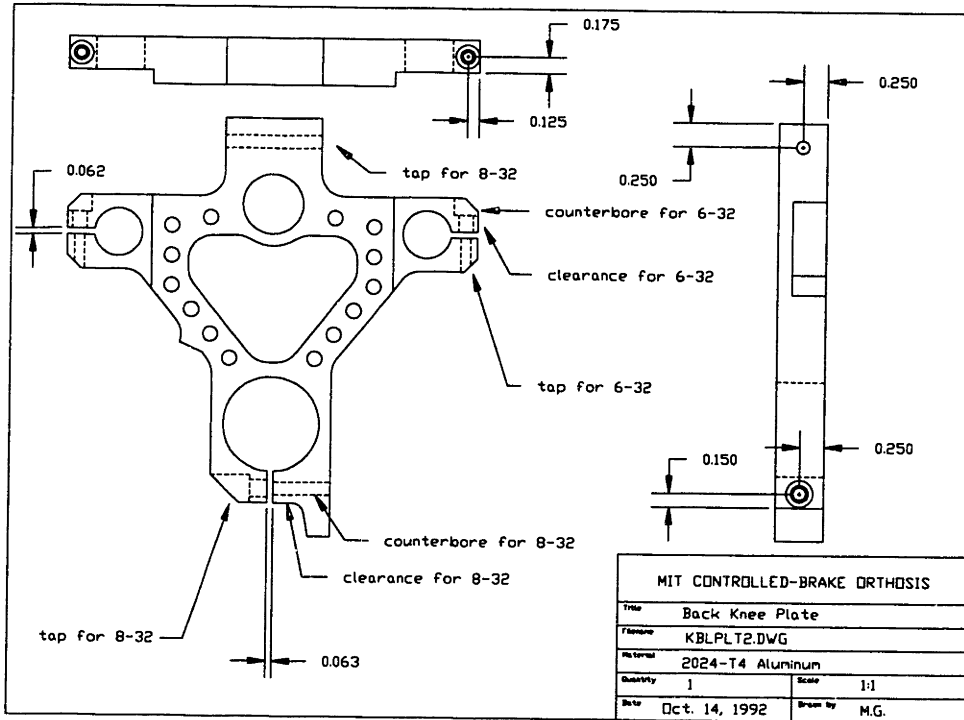Figure D-33: Back plate for left knee gear housing (drawing 1 of 2).

0.175

0.125

0.250

0.062

tap for 8-32

0.250

counterbore for 6-32

clearance for 6-32

tap for 6-32

0.150

0.250

counterbore for 8-32

clearance for 8-32

tap for 8-32

0.063

MIT CONTROLLED-BRAKE ORTHOSIS		
Title	Back Knee Plate	
Filename	KBLPLT2.DWG	
Material	2024-T4 Aluminum	
Quantity 1	Scale	1:1
Date Oct. 14, 1992	Drawn by	M.G.

Figure D-34: Back plate for left knee gear housing (drawing 2 of 2).

0.6299 +0.000/-0.0007
DIA
(0.164 +0.002/-0.000 deep)

All fillets are 0.5 dia

0.500 +0.001/-0.000
DIA

1.000 +0.001/-0.000
DIA

NOTE: Thicknesses represented
by crosshatchings·

0.5 +0.000/-0.001

0.35 +0.000/-0.001

MIT CONTROLLED-BRAKE ORTHOSIS		
Title	Back Housing Plate for Right Knee	
Filename	KBRPLATE.DWG	
Material	2024-T4 Aluminum	
Quantity 1	Scale	1:1
Date July 14, 1992	Drawn by	Peter Kassakian
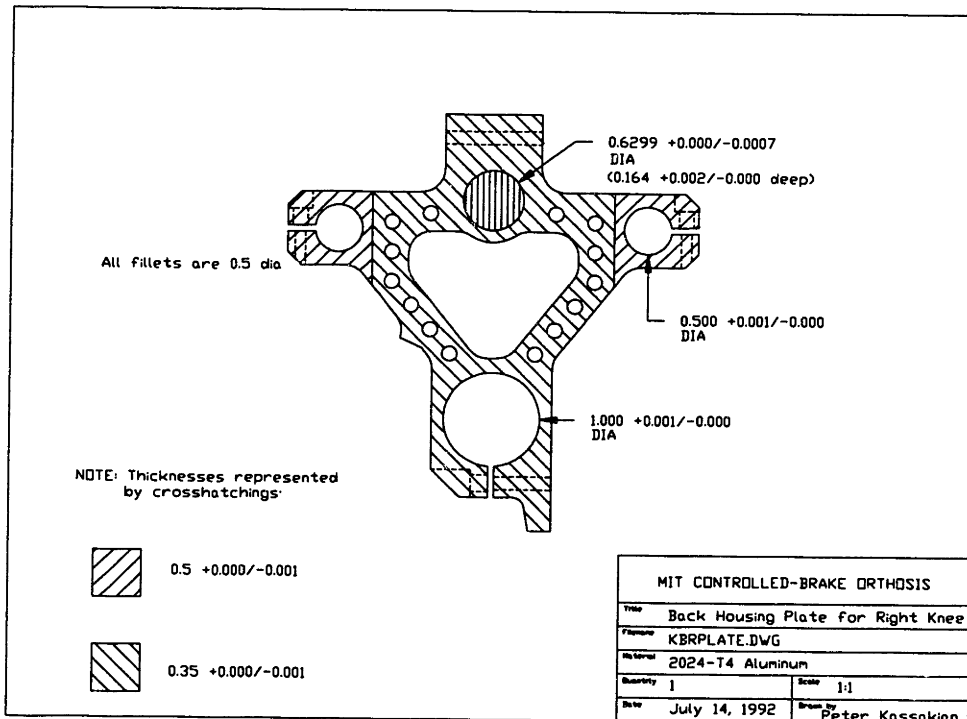
Figure D-35: Back plate for right knee gear housing (drawing 1 of 2).
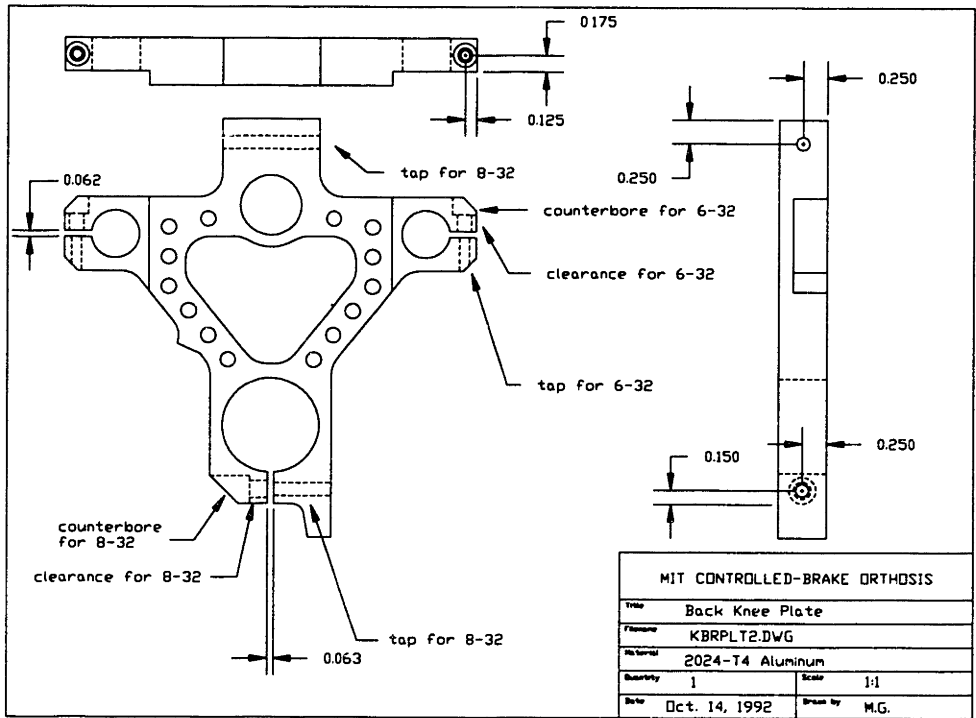
262

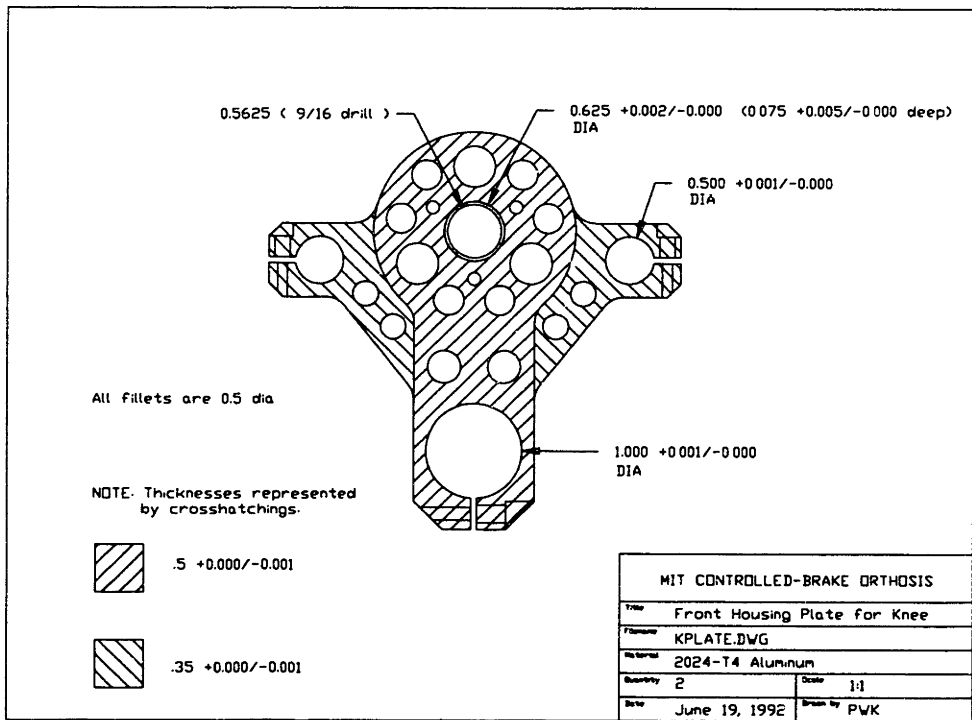Figure D-36: Back plate for right knee gear housing (drawing 2 of 2).

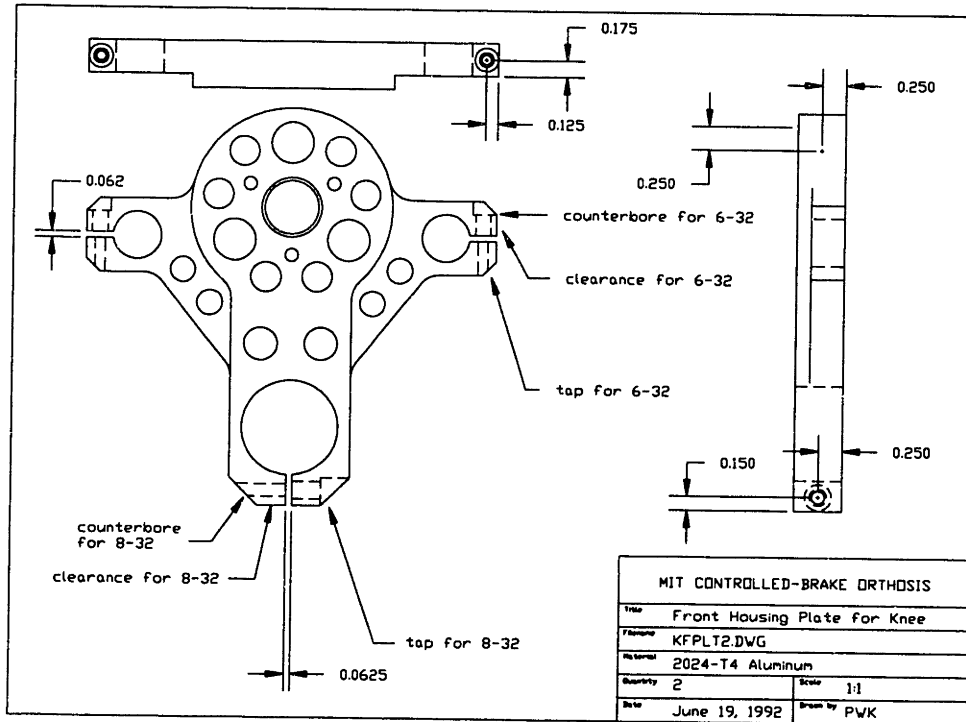Figure D-37: Front plate for knee gear housing (drawing 1 of 2).

263

Figure D-38: Front plate for knee gear housing (drawing 2 of 2).
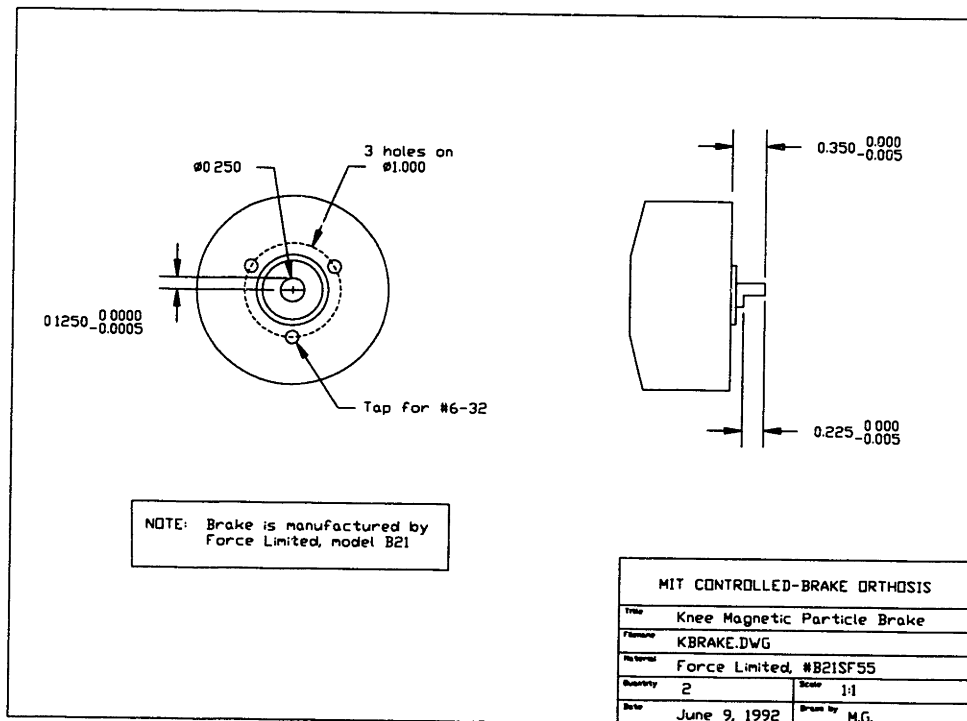

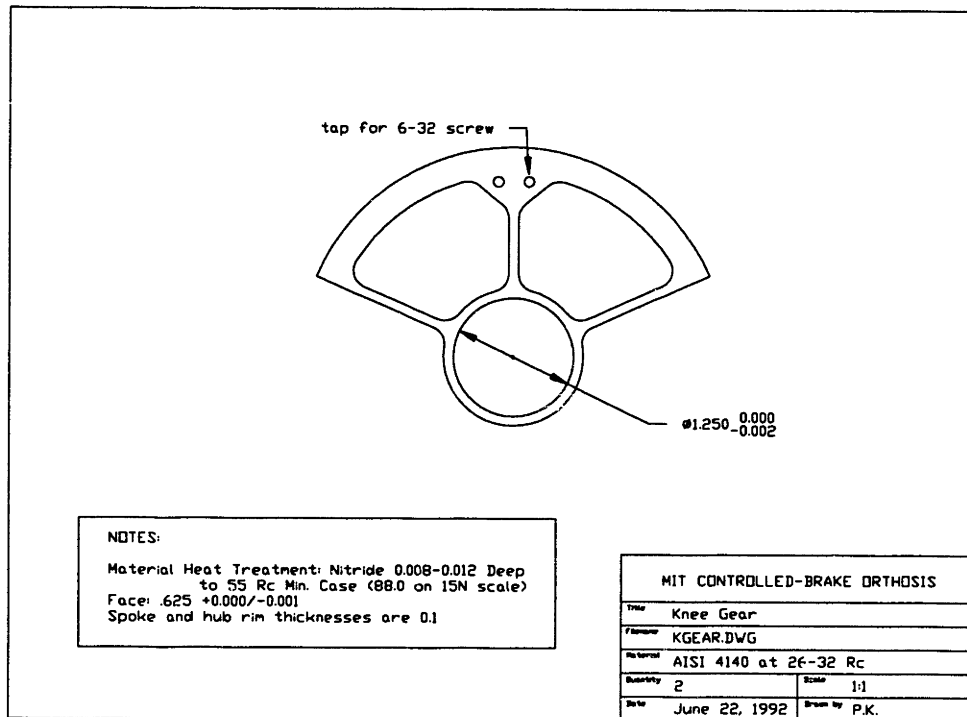Figure D-39: Mounting configuration of knee magnetic particle brakes.

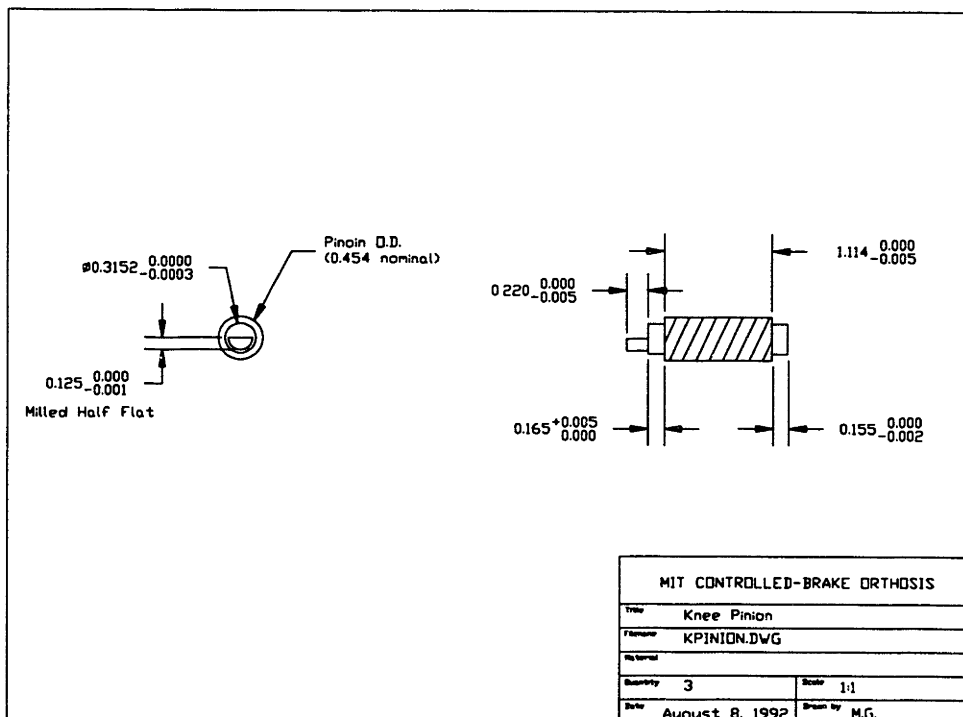Figure D-40: Modification of Evoloid knee gears.

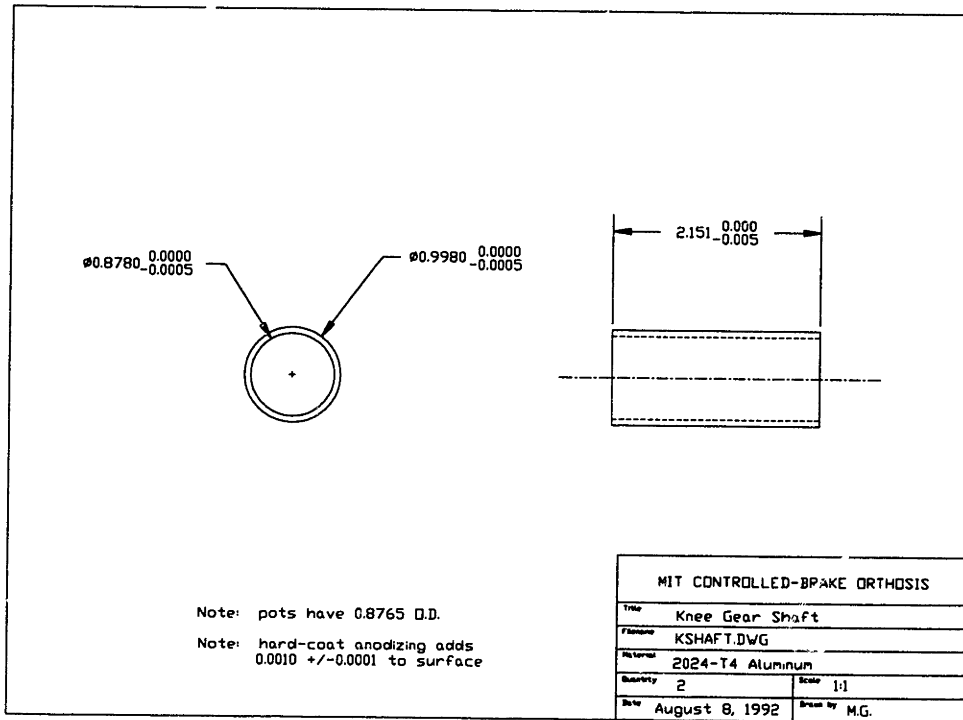
Figure D-41: Modification of Evoloid knee pinions.

ø0.8780 $^{0.0000}_{-0.0005}$ ø0.9980 $^{0.0000}_{-0.0005}$

2.151 $^{0.000}_{-0.005}$

Note: pots have 0.8765 O.D.

Note: hard-coat anodizing adds
         0.0010 +/-0.0001 to surface

MIT CONTROLLED-BRAKE ORTHOSIS

Title	Knee Gear Shaft	
Filename	KSHAFT.DWG	
Material	2024-T4 Aluminum	
Quantity	2	Scale 1:1
Date	August 8, 1992	Drawn by M.G.

Figure D-42: Knee gear shaft.

ø0.250±0.005   ø0.499 $^{0.000}_{-0.002}$

1.999 $^{0.000}_{-0.005}$

MIT CONTROLLED-BRAKE ORTHOSIS

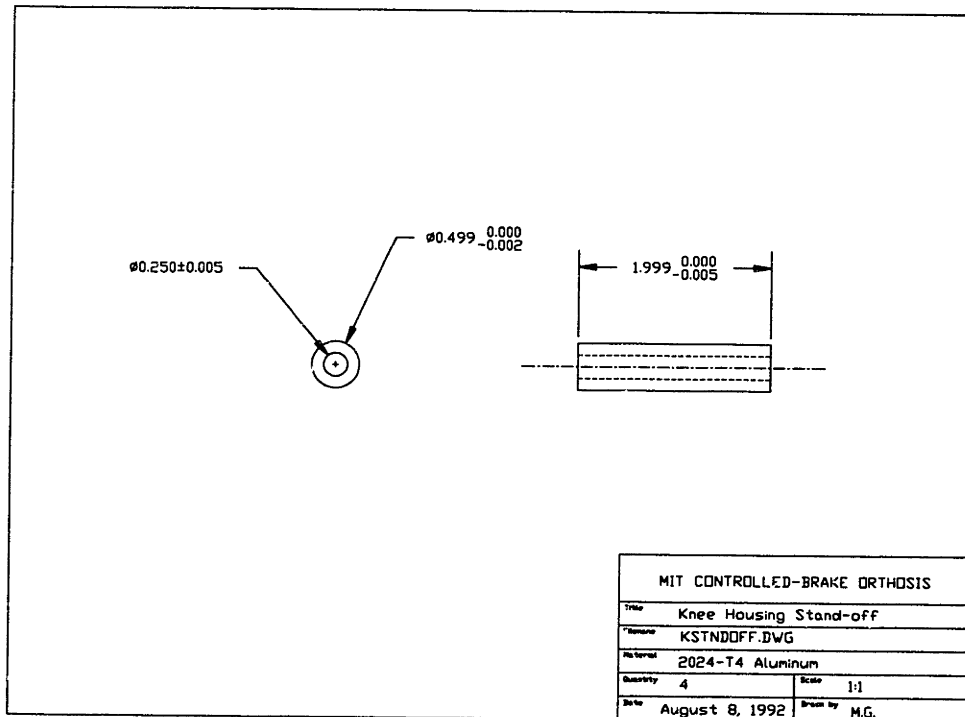| Title	Knee Housing Stand-off	
Filename	KSTNDOFF.DWG	
Material	2024-T4 Aluminum	
Quantity	4	Scale 1:1
Date	August 8, 1992	Drawn by M.G.

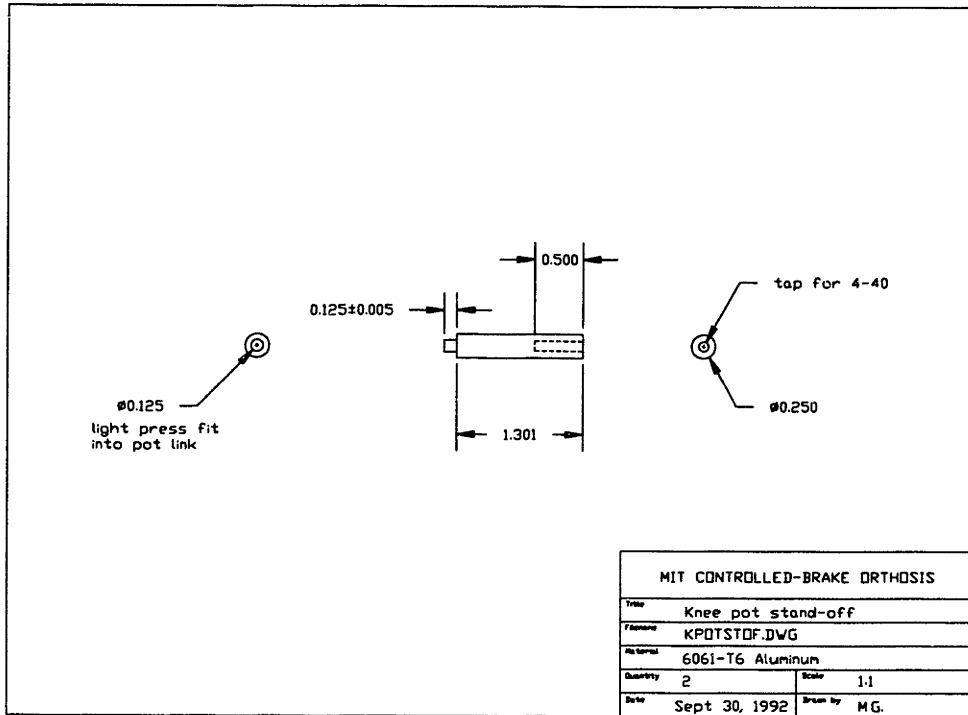Figure D-43: Stand-offs for knee gear housing.

266

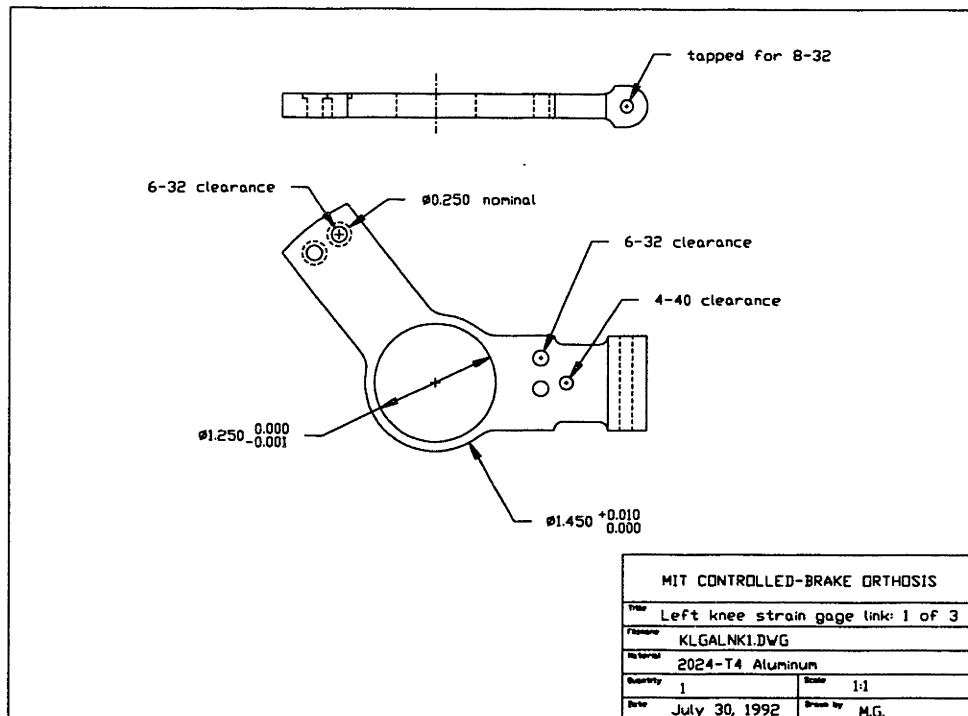Figure D-44: Stand-off for knee potentiometer coupling.

Figure D-45: Link that couples left knee gear to the brace (drawing 1 of 3).
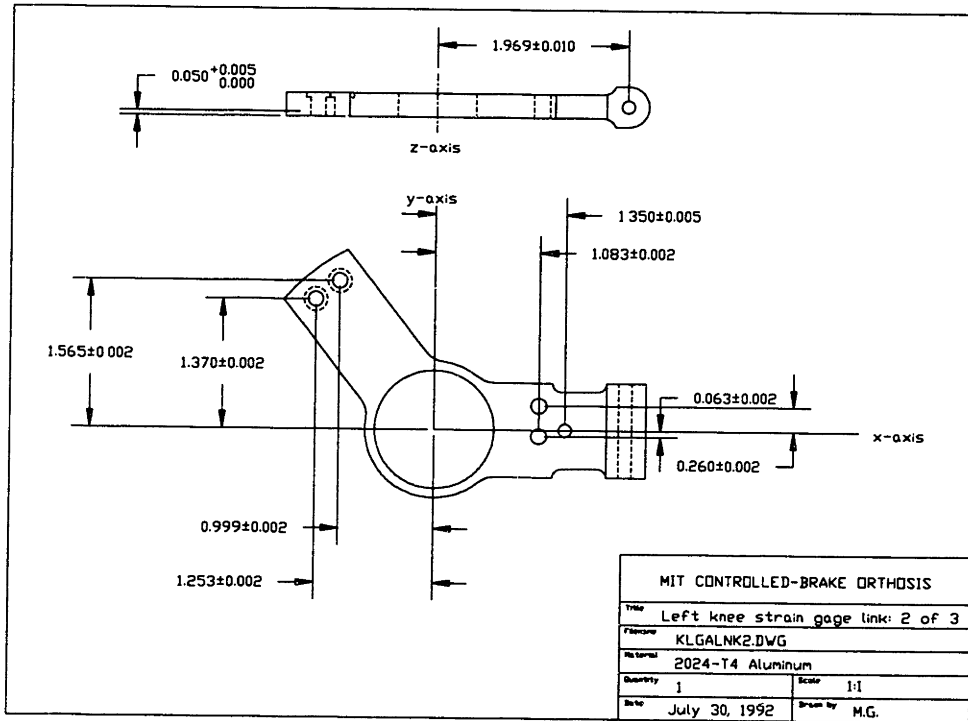
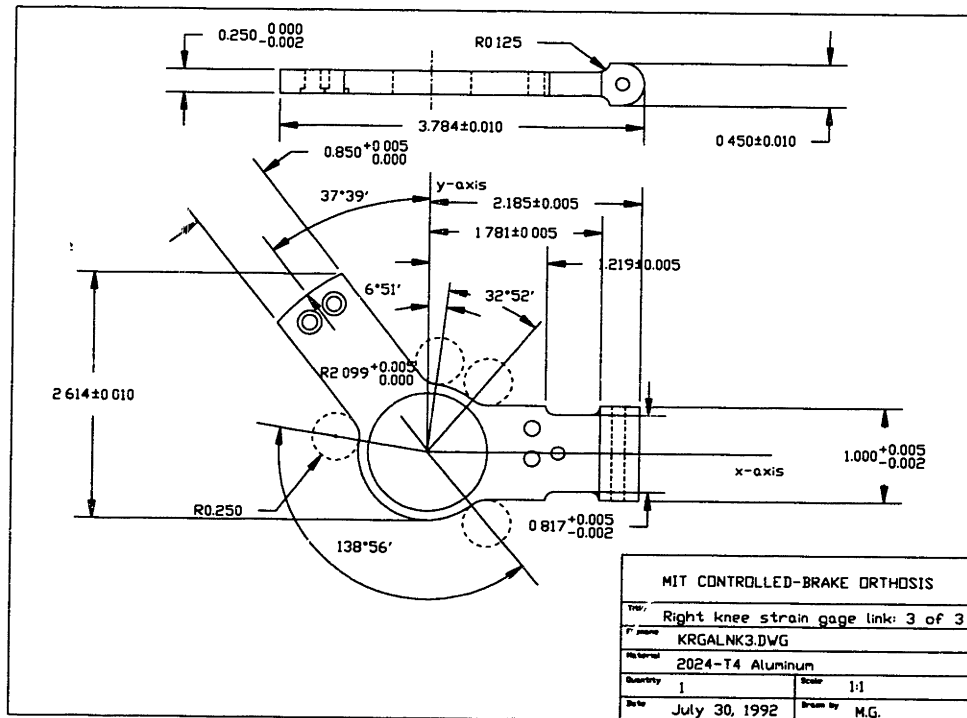Figure D-46: Link that couples left knee gear to the brace (drawing 2 of 3).

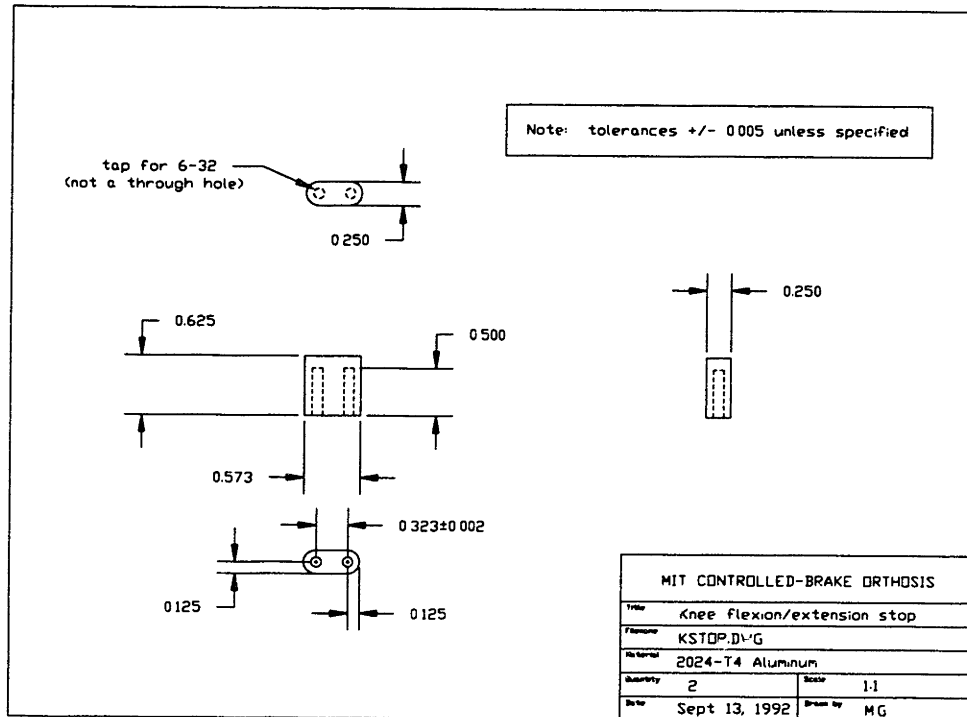Figure D-47: Link that couples right knee gear to the brace (drawing 3 of 3).
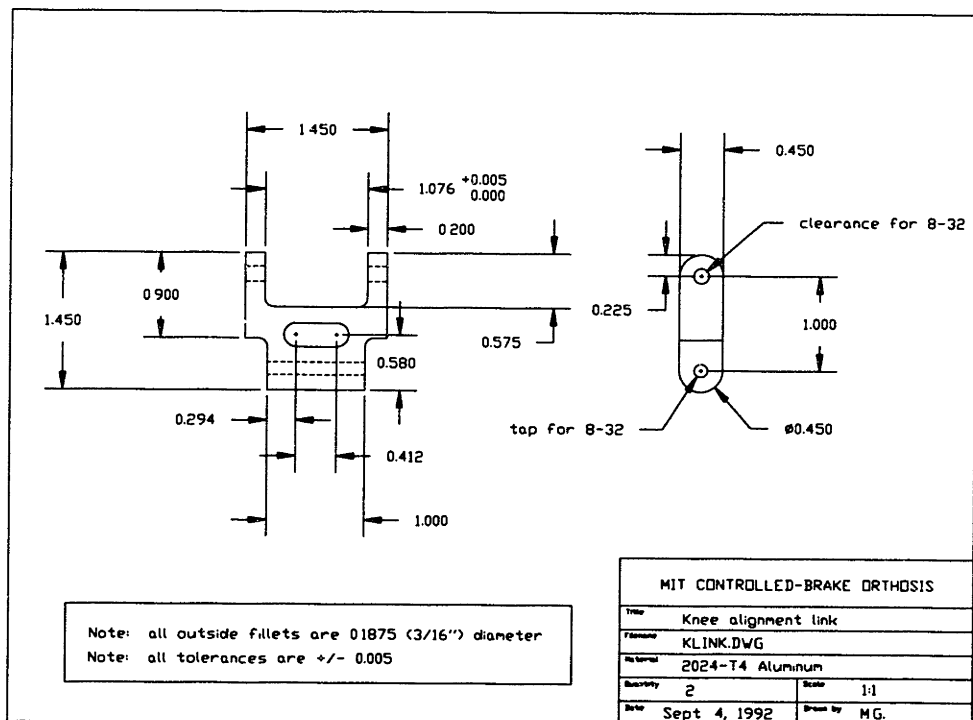
268

Figure D-48: Motion stop of knee joint.
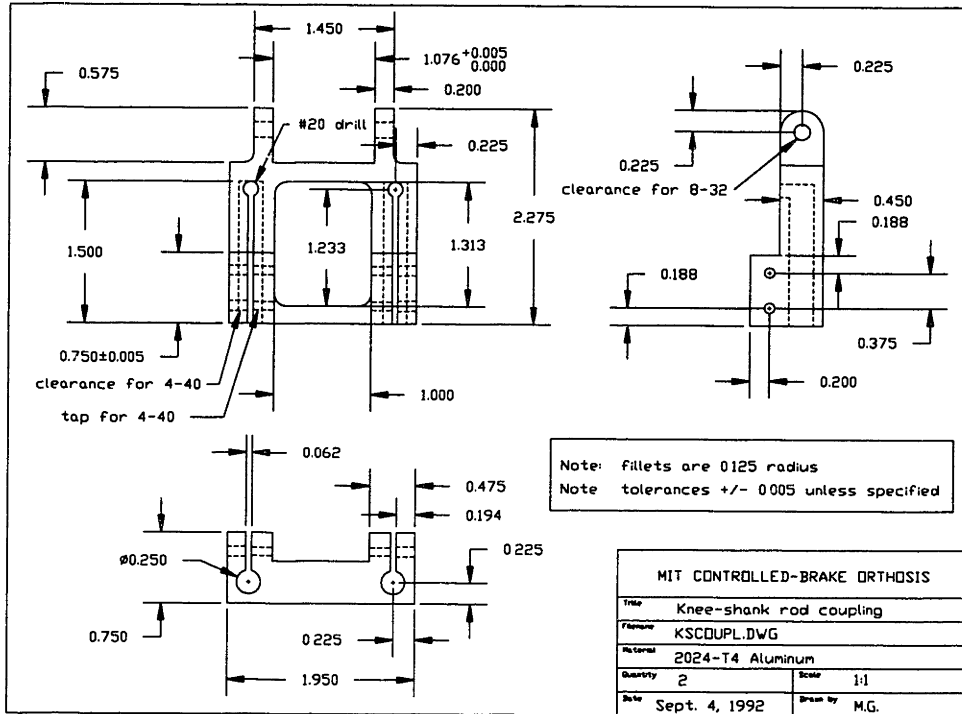

Figure D-49: Link that couples knee gear link to the brace.

269

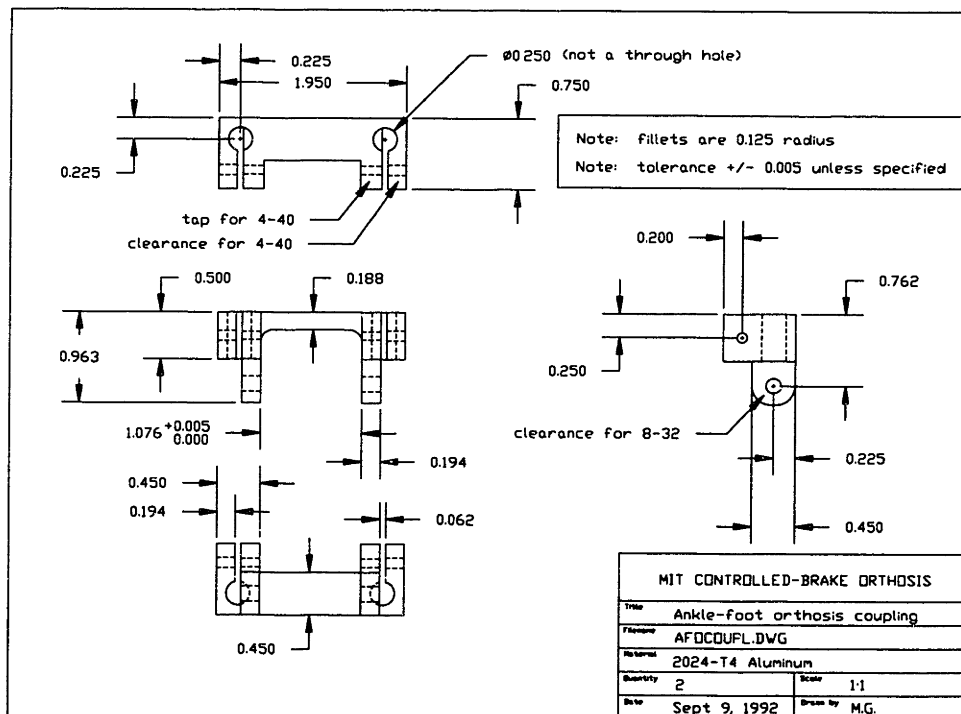**Figure D-50: Link that couples knee segment to shank segment.**

Note: fillets are 0.125 radius
Note tolerances +/- 0.005 unless specified

MIT CONTROLLED-BRAKE ORTHOSIS

Title	Knee-shank rod coupling
Filename	KSCOUPL.DWG
Material	2024-T4 Aluminum
Quantity	2	Scale	1:1
Date	Sept. 4, 1992	Drawn by	M.G.

Figure D-51: Bracket for attaching AFO link to brace.

Note: fillets are 0.125 radius
Note: tolerance +/- 0.005 unless specified

MIT CONTROLLED-BRAKE ORTHOSIS

Title	Ankle-foot orthosis coupling
Filename	AFOCOUPL.DWG
Material	2024-T4 Aluminum
Quantity	2	Scale	1:1
Date	Sept 9, 1992	Drawn by	M.G.

270
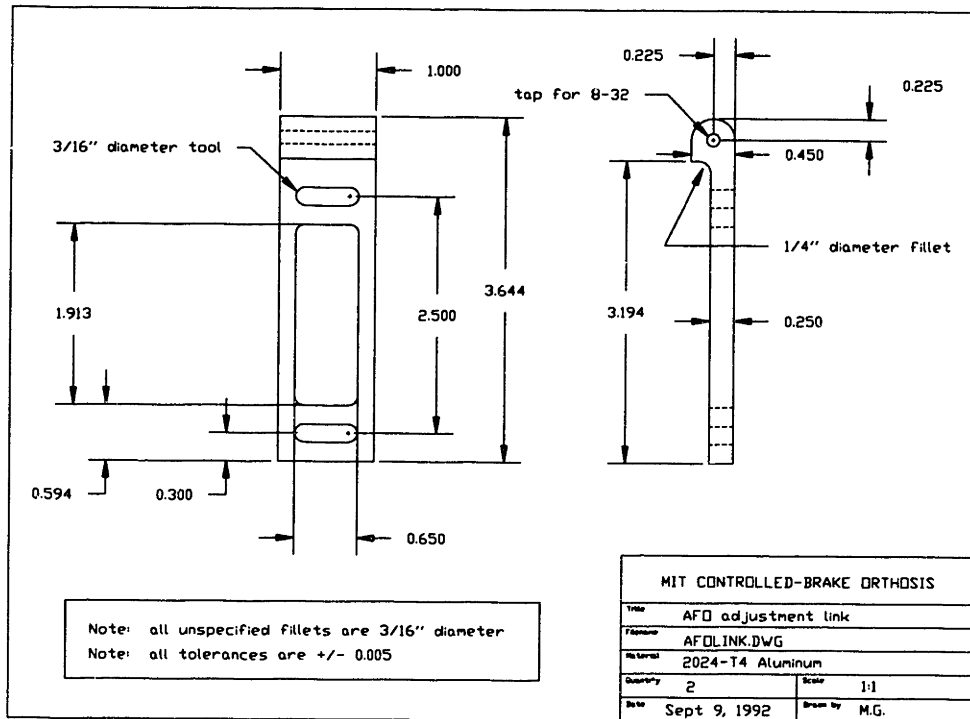
Figure D-52: Bracket for attaching AFO to AFO link.
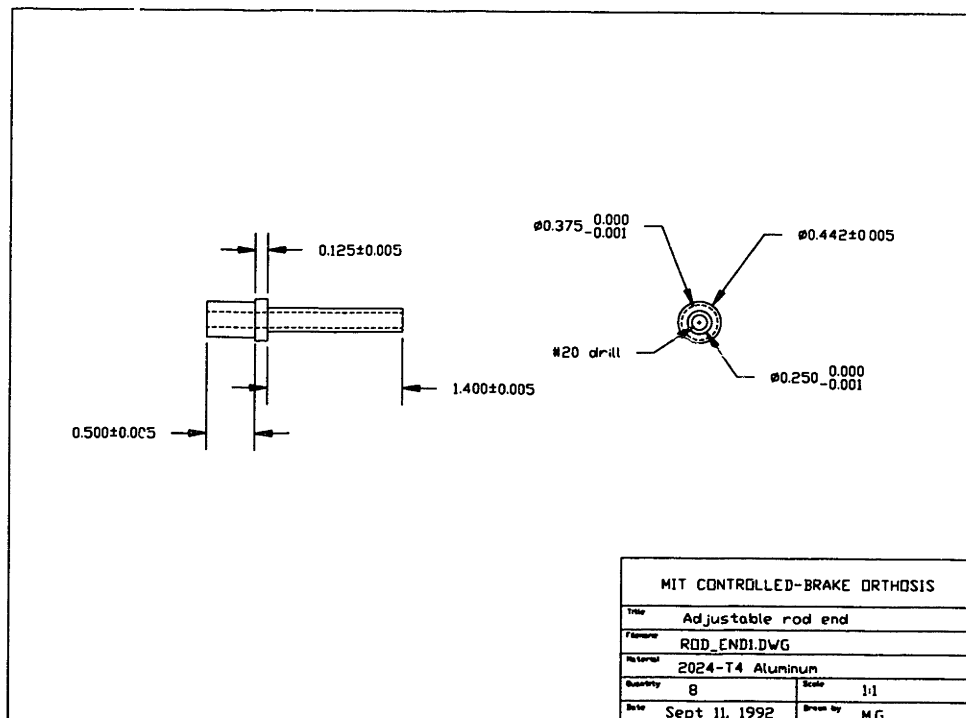
Figure D-53: Brace link rod tip (adjustable end).

271

0.125±0.005

0.500±0.005

0.500±0.005

∅0.375 0.000 -0.001

∅0.442±0.005

#20 drill

∅0.250 0.000 -0.001

MIT CONTROLLED-BRAKE ORTHOSIS

Title	Fixed rod end		
Filename	ROD_END2.DWG		
Material	2024-T4 Aluminum		
Quantity	8	Scale	1:1
Date	Sept 11, 1992	Drawn by	M.G.
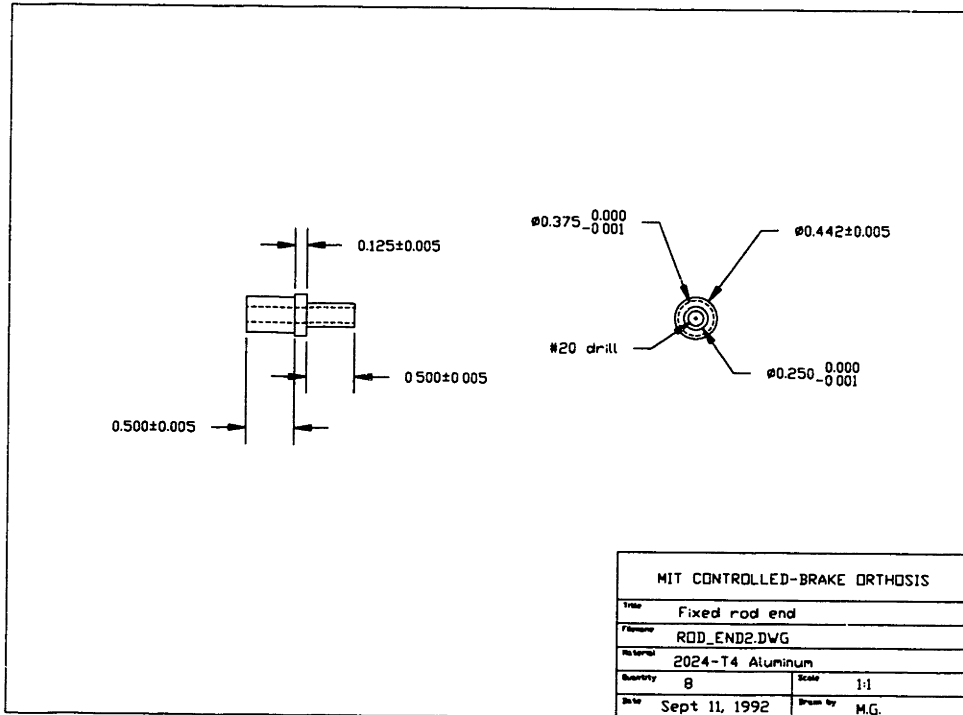
Figure D-54: Brace link rod tip (fixed end).

2.192

0.346

0.345

29/64 drill

3/16" tool

0.450

0.225

0.500

0.846

Note: tolerances +/- 0.005 unless specified

MIT CONTROLLED-BRAKE ORTHOSIS

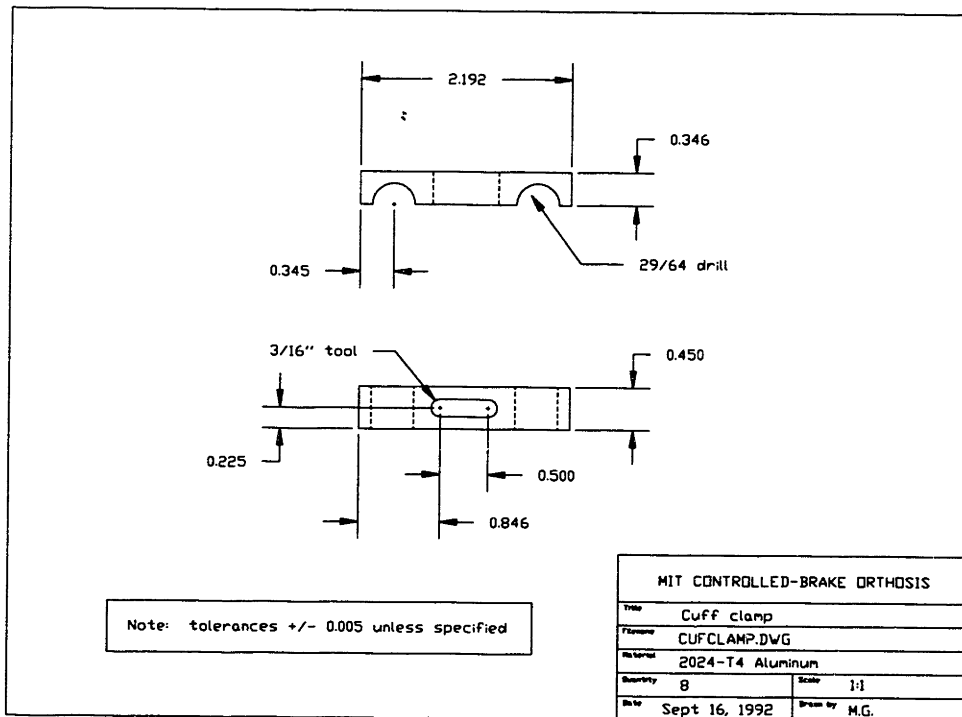| Title	Cuff clamp		
Filename	CUFCLAMP.DWG		
Material	2024-T4 Aluminum		
Quantity	8	Scale	1:1
Date	Sept 16, 1992	Drawn by	M.G.

Figure D-55: Clamps for attaching leg cuffs to brace.